Development of an External Ultrasonic Sensor Technique to Measure Interface Conditions in Metal Rolling

The University Of Sheffield.

Adeyemi Gbenga Joshua

The Department of Mechanical Engineering

This dissertation is submitted for the degree of Doctor of Philosophy

December 2017

Abstract

Metal rolling is by friction which develops at metal-to-roll interfaces during the rolling process. But, friction at the metal-to-roll interface during the metal rolling process can cause roll surface damage if not controlled. Over time, friction results in downtime and repair of the mill. Therefore, lubrication is essential to control the metal-to-roll interface coefficient of friction. It is important to understand the conditions at the metal-to-roll interface to minimize energy loss and improve the strip surface finish.

In this work, a new method for measurement of metal-to-roll interface conditions, based on the reflection of ultrasound, is evaluated during the cold metal rolling operation. The method is a pitch-catch sensor layout arrangement. Here, a piezoelectric element generates an ultrasonic pulse which is transmitted to the metal-to-roll contact interface. This method is non-invasive to both roll and strip during the process.

The wave reflection from the metal-to-roll interface is received by a second transducer. The amplitude of the reflected waves is processed in the frequency domain. The reflection coefficient values are used to study the metal-to-roll interface conditions at different rolling parameters like, roll speeds and rolling loads. The results show that the reflection coefficient increases with increasing roll speed. This is because of reduction in the roll-bite contact area or increase in the frictional resistance of interface during the roll speed increment. However, the reflection coefficient decreases with increasing rolling load due to either increase in the roll-bite contact area or pressure.

The reflection coefficient determines the oil film thickness formation at the metal-to-roll interface. In-addition, the Time-of-Flight of the reflected wave obtained from this technique is used to estimate strip thickness and roll-bite length during the rolling process. The oil film thickness in the range of 1.25μm to 3.05μm was measured during the rolling process. The film thickness increases with increasing roll speed and reduces with increasing rolling load. The roll-bite value of 5.5mm was measured during the process.

The results from this study show that this ultrasonic technique can measure the metal-to-roll interface conditions (roll-bite, oil film and strip thickness) during the rolling process. This ultrasonic technique has the advantage of minor roll modification. Additionally, the

experimental roll condition values obtained from the ultrasonic reflection method agree with theoretical values. The technique shows promising results as a research tool, and with further development, could be used for lubricant monitoring. Also, it can be utilized in the control system of a working mill for reduction of friction losses in the metal rolling process.

Acknowledgements

Praises to Almighty God for his abundant grace, blesses, wisdom, knowledge and understanding given to me to finish the research.

I would like to thank the encouragement, inspiration, and support provided by my supervisors throughout the duration of this project. I appreciate my first supervisor, Doctor Christophe Pinna for his assistance, advice, and support from the beginning of this project. Special thanks go to Professor Rob Dwyer-Joyce for his patience and invaluable help throughout of this program; I appreciate all his invested time and ideas in the supervision of my thesis and for his readiness for scientific discussion. Thanks also to Doctor Matt Marshall for his input and good scientific advice that are for the benefit of this project. I am very grateful to David Butcher for his technical assistance and the nice time we were working together.

Much gratitude to the Tertiary Education Trust Fund (TETFund), Nigeria for their financial assistance and providing the scholarship scheme that funded my PhD; this program would not have been possible without their support. I also wish to appreciate the Ekiti State University Management Members for their financial assistance, encouragement and for the opportunity given to me to do my PhD in one of the world renowned universities. Many thanks go to the staff of the Faculty of Engineering, Ekiti State University, particularly the Department of Mechanical Engineering, for their understanding during the program. I would like to thank Professor S. B. Adeyemo and Professor Aribisala Olugbenga James for their advice during the period of this project.

Millions of thanks go to my family, mainly my wife Feyisayo Kemisola Adeyemi and my children, for their understanding, help, and patience, for the period of being away from them. Thanks to my friend and my brother Doctor Temitope Stephen for his assistance at the early stage and throughout this project. My thanks also go to Sia Kemoh and her children for their moral support all the time during this study.

I would also like to acknowledge the Leonardo Centre for Tribology Group for the excellent working atmosphere and for their useful suggestions at various stages of this project provided. I would like to thank Robin Mills, Andy Hunter, Xiangwei Li, and Thomas Holdich

for their hospitality and for providing useful attentions, discussions, and suggestions throughout this project. I also thank the English Language Teaching Centre, University of Sheffield for helping improve my writing.

Finally, I would like to appreciate my friends, both home and abroad; Ogunjemilusi D.K., Omojola Jola, and Peter for their support throughout this program. Many thanks to my colleagues from Nigeria in University of Sheffield: Benjamin Oluwadare David Akindele, Julius Abere, Alhaji Lawal Abdulqadir, Ayotunde Ojo, and Oku Nyong for their support and assistance during this work.

Contents

List of Figures

List of Tables

Nomenclature

Symbols	Meaning	Units
F_N	Applied load	N
η	Viscosity	Pas
V_r	Roll speed	m/sec
R_o	Roll radius	m/sec
h_o	Inlet oil film thickness	µm
t_o, t_f	Initial and finial strip thickness	mm
μ	Coefficient of friction	-
τ	Shear stress	N/m^2
f	Ultrasonic frequency	MHz
R	Reflection coefficient	-
K	Stiffness	GPa/µm
ω	Angular frequency	rad/sec
Z	Acoustic impendence	kg/m^2s
β	Bulk of modulus	GPa
ToF	Time-of-flight	µsec
ρ	Density	kg/m^3
C	Speed of sound	m/Sec
E	Young's modulus	Pa
A_O	Amplitude of signal	mV
L_O	Roll length	mm
$Sin\theta_r$	Reflection angle	Degree
$Sin\theta_i$	Incidence angle	Degree
C_I	Speed of sound of material 1	m/sec
C_r	Speed of sound of material 2	m/sec
d_c	Diameter of the piezo-element	mm
v	Poisson's ratio	-
R'	Roll deflection	mm

σ	Stress	N/m2
$\boldsymbol{\gamma}$	Viscosity pressure coefficient	GPa^{-1}
P	Contact pressure	Pa
$\sigma *$	Lambda ratio	-
V_O	Initial strip speed	mm/sec
V_f	Initial strip speed	mm/sec
F_r	Frictional force	N
F_y	Normal load	N
F_t	Tangential force	N
l_P	Length of contact	mm
b_O	Initial strip breath	mm
b_f	Final strip breath	mm
T	Torque	kw
ε	Strain	mμ
α	Contact angle	Degree
θ	Neutral angle	Degree
R_{q1}	Quadratic roughness of the strip	mμ
R_{q2}	Quadratic roughness of the roll	mμ

Chapter 1

Introduction

Metal forming is a tribological procedure that consists of reducing a metal thickness to a particular required level. Metal forming includes various metal reducing processes such as rolling of metal, metal extrusion, tube and wire drawing processes [1]. Metal rolling is one of the most valuable metals manufacturing processes and it plays a significant role in the modern world. The production of sheet metal from the slab is often done by metal rolling processes [2]. In 2015, it was reported that the production of steel increased from 189 to 1665 million tonnes between 1950 and 2014. It was stated that 50% of steel production is consumed annually by the housing and construction sectors. It was also projected that the demand for steel will be 1.5 times higher than the present requirement in the year 2050 as a result of population growth [3].

Metal rolling is used by many industrial sectors for goods' production globally [4]. Previous research studies have been conducted to measure the oil film thickness within the metal-to-roll interface during the cold metal rolling process. However, there is significant paucity in the development of measurement techniques in metal rolling processes. The remainder of this chapter states the problem on which this thesis focuses, in addition to outlining the aim and research objectives together with an overview of the thesis layout. It concludes with a discussion of knowledge gaps, which the research study expects to fill.

1.1 Statement of the Problem

This research addresses the planning and process of improving metal forming operations to deliver excellent products. The research concentrates on cold metal rolling and its operational process only. During cold metal rolling, the friction force that develops at the metal-to-roll contact, grasps and drags the strip through the roll-bite. Therefore, the rapid changes of friction value at the roll-bite have a significant effect on the metal rolling process. Yingian [5] noted that for a successful rolling operation, the friction force of the roll-bite must not be less than one half value of the roll contact angle. He also explained that there

must not be an excessive increase of the friction force at the metal-to-roll interface, to avoid increases in the roll force. Furthermore, the friction force must be sufficient to maintain good rolling process efficiency [6, 7]. In the past two decades, investigation of friction at the roll-bite has been paid more attention by other scholars due to its importance in steel production processes.

The metal forming industry has long been known for cutting-edge research on the steel rolling process. Additionally, the continual upgrade of measurement techniques has stimulated operational performance. Despite the economic importance of the metal forming industry, literature reviews have not highlighted any improvement in film thickness measurement at the roll-bite through the ultrasonic measuring technique. Lubricants are applied to separate the roll and workpiece surfaces by the fluid film formed at their interface during the rolling process. The thickness of the oil formed at the metal-to-roll interface provides control information on friction conditions during the rolling process.

The coefficient of friction value of the roll and a strip surface depends on the quantity of oil that is drawn into the roll-bite, together with rolling conditions. Metal cold rolling generally takes place within a mixed lubrication regime. As such, there will be a formation of pressurized oil thickness within the roll-to-strip interface to separate them. If the lubricant thickness within the interface is known, then the friction force is easily determined. However, an oil film at the roll-bite is needed to control the friction strength at the metal-to-roll interface. This will be required to reduce the amount of energy wasted during the metal rolling process. Therefore, a good quality of surface finish product will be obtained [6, 8].

The harsh nature of cold rolling makes implementing sensors in industrial applications difficult. Additionally, any modification of the roll has the potential to negatively affect the rolling process. This makes instrumentation of cold rolling mills difficult. This research study develops a non-invasive and no need for an embedded plug to measure the oil film at the metal-to-roll interface and strip thickness by using ultrasound. This method is based on the external arrangement of the longitudinal and shear wave sensors, mounted on both sides of the roll. These sensors are used to generate an ultrasonic wave, which is transmitted through the roll to the metal-to-roll interface. When ultrasound waves travel through materials, some proportions of the waves are transmitted whilst the rest is reflected back from the interface of the materials. Therefore, the reflection coefficient obtained from the

reflected wave can be used to monitor the roll-bite and to measure the film thickness at the metal-to-roll interface during the rolling process

1.2 Aim and Objectives

The aim of this study is to develop a non-invasive and non-damaging ultrasonic method to measure deformation and interface conditions in metal rolling. This technique is based on rigorous analysis of the reflection coefficient of the ultrasonic signal obtained from the surfaces of the rolled material and the rolling parameters employed.

To achieve this aim, the following objectives are considered:

- To investigate the approaches for ultrasonic measurement that does not require major modification of the mill roll.
- To build the new external ultrasonic measuring device with longitudinal and shear wave sensors on the roll.
- To apply a mathematical model of the oblique reflection of the ultrasonic signals to study the roll-to-strip interface;
- To measure the strip thickness at both stationary and dynamic modes;
- To measure the oil film thickness at the roll-bite interface during the cold metal rolling process with the new device mentioned above;
- To investigate the effect of rolling parameters (rolling load and roll speed) on the formation of oil film thickness at the roll-bite surfaces during the cold rolling process.
- To measure the roll-bite length during the rolling process

1.3 Thesis Layout

The chapters of this thesis follow a logical sequence to reflect the overall aim of the project.

Chapter 1 describes the problem, states the aim of the project and provides an outline of its research objectives. The thesis layout and the knowledge gaps which this research study seeks to fill are explained in the first chapter.

Chapter 2 briefly introduces the basics of metal forming such as bulk and sheet metal forming processes. Additionally, the chapter focuses on the analyses of metal rolling processes together with their diverse properties. The methods of measuring the friction

force of the roll-bite during the cold metal rolling are illustrated. The lubricant effects on the coefficient of friction at the metal-to-roll interface during the metal cold rolling process are also discussed. Similarly, the lubricant properties and oil film thickness formation at the metal-to-metal interface during the cold metal rolling are reviewed. Finally, the chapter examines the limitations of existing experimental procedures for determining the oil film thicknesses during cold metal rolling. The measurement of oil film thickness with an internal ultrasonic technique at the roll-bite during the rolling process is also discussed.

Chapter 3 offers a comprehensive review of the ultrasonic principles in engineering applications, modes of wave propagation and types of ultrasonic wave propagation. Additionally, reflection capturing techniques are discussed within this chapter. The measurement of oil film thickness with ultrasonic methods in the mixed lubrication regime is reviewed.

Chapter 4 describes the justification of the optimum external ultrasonic sensor arrangement, carried out with the oblique and normal incidence reflection layouts to study the metal-to-roll interface. Shear and longitudinal wave sensors were used to perform various tests with both of the aforementioned ultrasonically measured techniques in this section. The results obtained from each technique are analysed.

Chapter 5 elucidates the implementation procedure of the ultrasonic reflection layout method on a pilot mill metal roll, discovered as an optimum arrangement in Chapter 4. Strip thickness measurement was carried out both in stationary and dynamic (rolling) positions.

Chapter 6 describes the modelling and experimental procedure of the reflection coefficients from the two measuring techniques discussed in Chapter 4. The reflection coefficient and the stiffnesses obtained from the modelling and experimental processes of both measuring techniques are evaluated using a comparative analytical technique. This is done to validate the calculating parameters employed in the oblique reflection measuring method before applying to the measurement film thickness in Chapter 7.

Chapter 7 describes the measurement of oil film thickness at the metal-to-roll interface. Additionally, the measurement of oil film thicknesses has been conducted under different applied deformation loads. The effects of roll speed on the oil film thickness formation

during the rolling operation is also investigated and explained in this chapter. All these research activities were successfully conducted following the validation of the measurement technique undertaken in Chapter 6.

Chapter 8 discusses the overall implications of the research project, draws some important conclusions and details suggestions for future studies.

1.4 Contribution to Knowledge

The novelty of the research within this thesis is developing and implementing a new experimental procedure with an external sensor arrangement on a pilot mill to measure metal-to-roll interface conditions during the cold metal rolling. The oblique reflection measurement technique based on active piezoelectric sensors has been mounted on the roll and fixed to the pilot mill. Therefore, the following points can be drawn as its contribution to knowledge:

- Design and implementation of ultrasonic oblique reflection measurement layout technique on a pilot mill;
- Reflection coefficient at metal-to-roll interface having been tested with models developed by Pialucha [9] at 0^{o} and 19^{o} angles of incidence. The measured reflection coefficient was validated by the experimental result;
- The designed layout technique was used to measure oil film thickness at roll-bite, and the experiment was conducted under two different rolling loads and roll speed respectively. The experimental oil film thickness values obtained were used to verify the mixed lubrication regime at roll-bite at various applied loads;
- The layout was used to measure the roll-bite length at the strip-to-roll interface;
- This layout was also used to measure strip thicknesses at both stationary and dynamic modes.

Chapter 2

Metal Rolling Background

This chapter introduces the basics of metal forming and the current methods of measuring friction force of the roll-bite during cold metal rolling. The lubricant and other rolling parameters' effect on the coefficient friction at the metal-to-roll interface during metal cold rolling process are discussed. The chapter also explains the measurement of oil film thickness with an internal ultrasonic technique at the roll-bite during a rolling process. The chapter concludes by discussing the limitations of existing experimental procedures for determining the ultrasonic instrumentation during cold metal rolling.

.

2.0 Introduction

2.1 Metal Forming Processes

Metal forming is a tribological procedure that involves transforming the solid material (metal) from one shape into another. The transformation process can either be the reduction in thickness, shape or both in the material. Metal forming is a wide-ranging metal deformation processing that includes various metal manufacturing processes. It is characterized by the plastic deformation of the involved material into a required shape or size. Metal forming can be classified into two broad groups as shown in Figure 2-1; bulk-forming processes and sheet-forming processes [10].

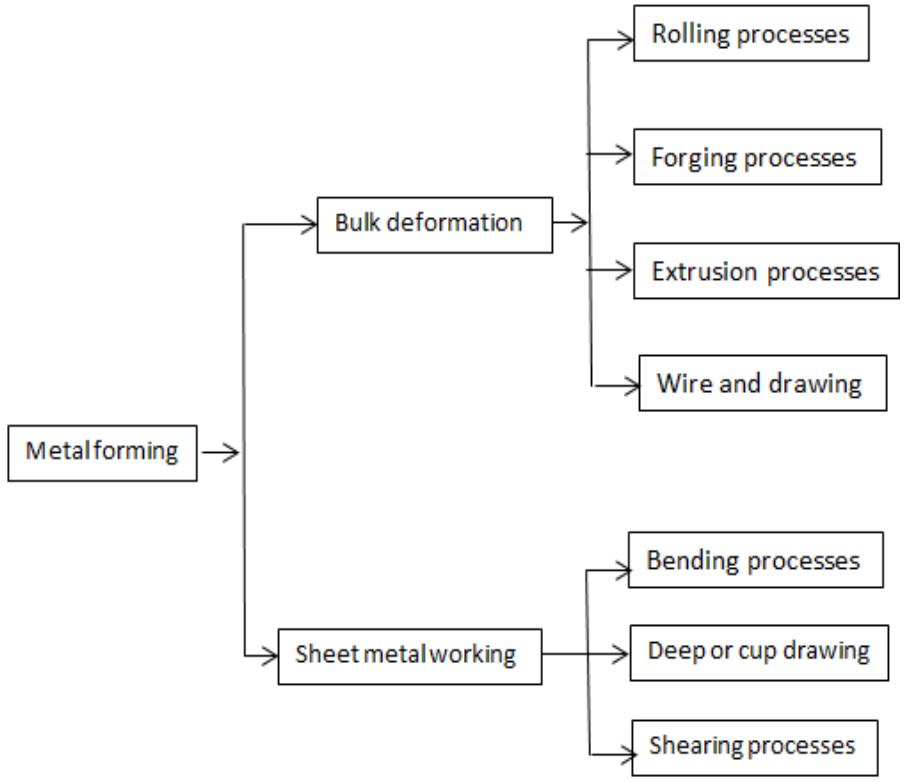

Figure 2-1: Groups of metal forming process

The classification of the metal forming process is based on the working surface area to the volume ratio of the material involved. With bulk forming, the contact tools have a low surface covered area compared with the volume of the work done on the material involved. Sheet metal forming is the opposite, being processed with the larger surface area contact of the tools to the small volume of the material.

2.1.1 Metal Rolling Process

Metal rolling is a tribological process consisting of the continuous squeeze of a flat metal to reduce its cross section to the required level. This process is one of the most valuable metal manufacturing techniques in the modern world [11].

In the metal rolling process, the surfaces of the rolling material and the rolls are usually in contact, and friction between them has an important influence on the operation [12]. During the rolling process, the frictional force that develops at the metal-to-roll contact grips and keeps dragging the strip through the roll-bite, as shown in Figure 2-2.

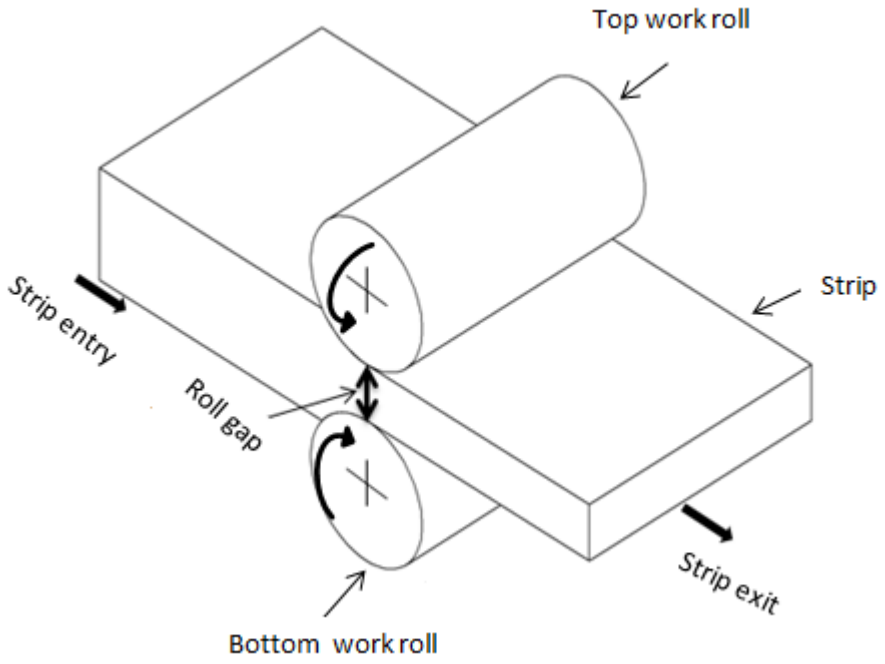

Figure 2-2: Schematic diagram of the strip rolling process

The strip with a large thickness enters the roll gap at the entrance plane of the roll contact. The strip passes through the roll gap and leaves the outlet zone with a reduced thickness strip (Figure 2-2). However, these rapid changes in friction value at the roll bite have a serious effect on the metal rolling process and friction force effects have great significance throughout deformation processes.

2.1.2 Rolling Mill Design

A rolling mill is a machine that consists of a set of rolls mounted on casings established as a stand for the rolls. The stands are constituted to produce different kinds of mill layouts for

particular functions, by removing and replacing the rolls. Additionally, rolling mill consists of an adjusting screw to control the roll gap, a pair of the rolls, and a pair of stand that fixed with roll. It also consists of housing, bearing, motor, gear box, connecting shaft, switch buttons, and speed control.

2.1.2.1 Types of Rolling Mills

There are many common types of rolling mill arrangements available in industry, which are selected based on the size of the material, type of rolling (hot or cold) and mechanical property of the material (hardness). Common types of rolling mills are shown in Figure 2-3 (a- e) [10, 13]

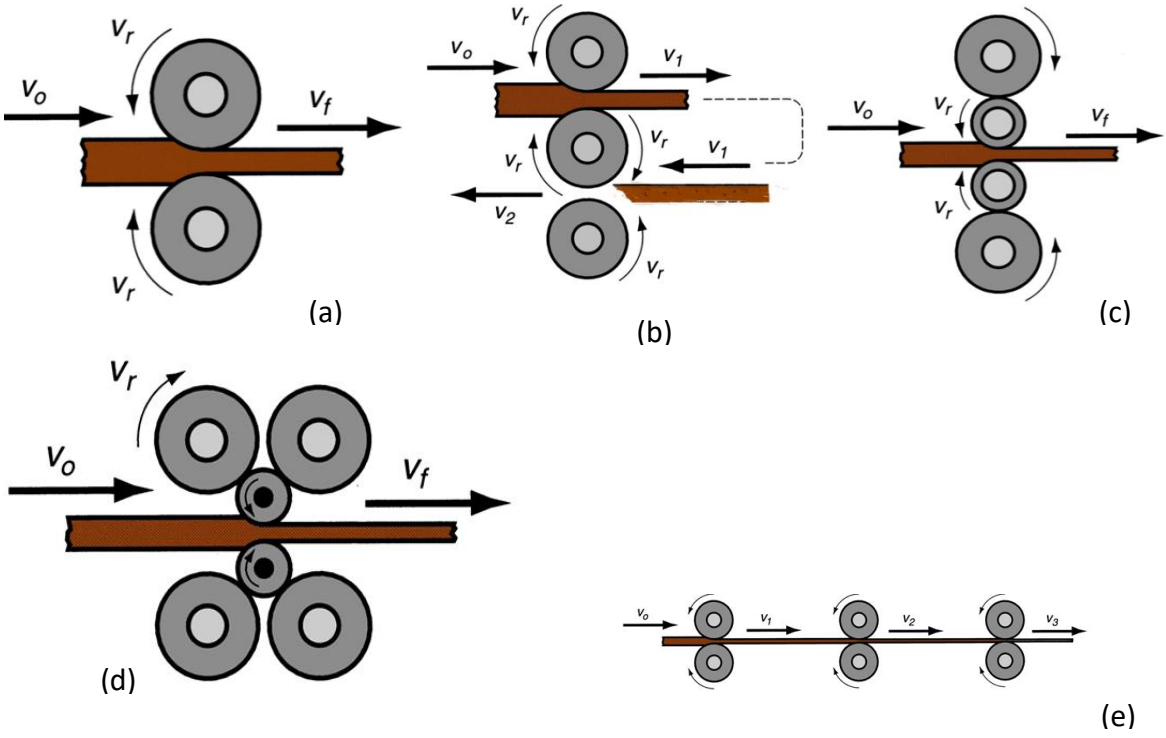

Figure 2-3: Configuration of (a) Two-High (b) Three-High (c) Four-High (d) Cluster (e) Tandem rolling mills

2.1.2.2 Two-High Rolling Mill

The two-high rolling mill consists of a pair of horizontal rolls arranged one above the other, as shown in Figure 2-3a. The metal reduction takes place by feeding the material into the gap between the adjacent rolls, as indicated above. The two adjacent rolls of the mill rotate

in the forward direction (non-reversing), while some are capable of turning backward and forward (reversing).

2.1.2.3 Three-High Rolling Mill

The three adjacent rolls are arranged vertically, one above the other, in the three-high rolling mill, as indicated in Figure 2-3b. This mill consists of three different rolls (upper, middle and lower) driven by different electric motors. These rolls are arranged so that a series of metal reductions can take place without the need to change the direction of the rotating rolls. During the rolling process, steel is rolled backward between the middle and bottom rolls and forward between the middle and top rolls respectively. The directions of rotation of the rolls in three-high mills are not reversed as in the two-high rolling mill. The three-high rolls rotates in both directions continuously, as demonstrated by the dotted line in Figure 2-3b.

2.1.2.4 Four-High Rolling Mill

Figure 2-3c shows the arrangement of the four-high rolling mill. This contains two small-diameter rolls that are reinforced by another two backup larger-diameter rolls. The two small-diameter rolls are less strong and rigid compared with backup rolls during the metal rolling process. They are called work rolls in this roll arrangement. These two small rolls are used to reduce metal deflection during the rolling process. The two large-diameter rolls are used to give support to the work rolls during the rolling process. Four-high stands can work in both directions. The metal can be passed backward and forward between the same rolls, as illustrated in a two-high mill.

2.1.2.5 Cluster Mill

The cluster mill (Figure 2-3d) consists of small diameter work rolls supported by two or more backing rolls. The two pairs of backup rolls, which are much larger and stronger than the working rolls are placed on the two small operating work rolls to prevent their alteration during the rolling process. This type of roll arrangement allows the smaller working rolls to be used perfectly despite their low strength and rigidity.

2.1.2.6 Tandem Rolling Mill

This is an arrangement of the rolls in a sequential series of stands with different rolling gaps for metal reduction, as shown in Figure 2-3 (e). The tandem rolling mill consists of a continuous long bar mill of several independent roll stands. Each roll stand has its own motor, the speed of which can be easily changed independently of the others.

This type of mill is differentiated by the different sizes of the roll gaps, which start from the largest to the smallest roll gap respectively. It operates in a continuous manner as shown in Figure 2-3 (e). However, as the rolling of the metal continues, the mechanical properties of the material are changed. This change occurs sequentially along the process by decreasing metal diameters, increasing surface hardness and decreasing yield strength.

2.1.3 Types of Metal Rolling

Metal rolling process can be classified into two broad categories by the metal geometry or the actual working temperature.

2.1.3.1 By Geometry of the Material

This is the process by which the rolling of the metal is classified in accordance with its profile, such as a flat and curved shape. Shape metal rolling, is a bulk metal forming operation where the high thickness metal square cross-section will be formed into a shape, such as an I-beam, as indicated in Figure 2-4a. While the flat metal rolling is the process of reducing the rectangular thickness cross-section of metal into sheet or plate, as shown in Figure 2-4b. In flat metal rolling, the final product is either called a strip, with a thickness less than 5mm, or plate when the thickness exceeds 5mm. It belongs to the sheet metal forming group.

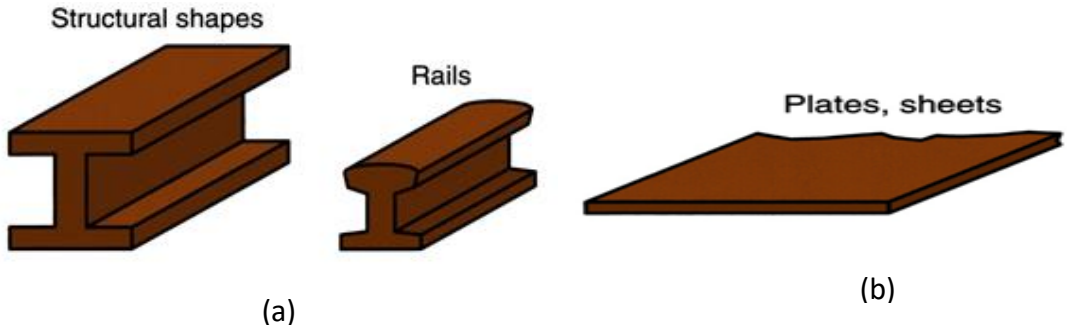

Figure 2-4: Samples of (a) shape and (b) sheet or plate metal rolling [11]

2.1.3.2 Material Working Temperature

The difference between hot and cold rolling depends on the working temperature of the material. If this is above its recrystallization temperature, the process is called hot rolling. Rolling of the metal from room temperature up to recrystallization temperature is referred to as cold rolling. Recrystallization temperature is the temperature at which distorted grains of the crystal structure are replaced by a new grain. The recrystallization temperature varies with the properties of the material.

2.1.3.2.1 Hot Rolling

This is the process of rolling metal through the elastic to a plastic state above the material recrystallization temperature. It is most commonly used when a large percentage of the metal deformation is required. The advantages and disadvantages of this process are listed in Table 2-1.

Table 2-1: Advantages and disadvantages of hot rolling process

Advantages	Disadvantages
No stain hardening of the working material during the process.	The phase of the material changes in the process.
Brittle material can be easily worked on without distortion.	Poor surface finish due to the formation of scale on the material surface.
Little rolling force is required.	Difficulties in achieving accurate dimensions of the product after the operation.
Low rolling capacity of the pilot mill is needed.	Hard to operate due to the high heat involved.
Holes, porosity, and cracks within the working material are welded together during the operation.	Deterioration of the metal roll life span.

2.1.3.2.2 Cold Rolling

This is the process of rolling metal to a plastic state, below the crystallization temperature. Cold rolling is suitable for the production of finished sheet and plate standard. Table 2-2 shows the advantages and disadvantages of the cold rolling process.

Table 2-2: Advantages and disadvantages of the cold rolling process

Advantages	Disadvantages
Improves the material strength and hardness.	High rolling force required.
No changes of phase involved.	High rolling pilot mill capacity is needed.
Good product surface finishing.	Lack of good control of the frictional force that can increase the damage of roll and product surfaces
No decarburization or oxidation of the material properties.	

2.2 Mechanics of Metal Rolling

2.2.1 Calculation of the Neutral Plane

During the metal rolling process, each metal roll is powered by a motor connected through the shaft. The relative velocity of the roll and the strip changes with the aid of the connected motor during the rolling process. The schematic diagram of the rolls at neutral mode is shown in Figure 2-5. Therefore, the neutral plane is a middle point between the entry and exit zone where the strip parameters (speed and rolling force) are equal to the roll parameters (speed and the friction force) [14]. These parameters are acting opposites of each other, as shown in Figure 2-5.

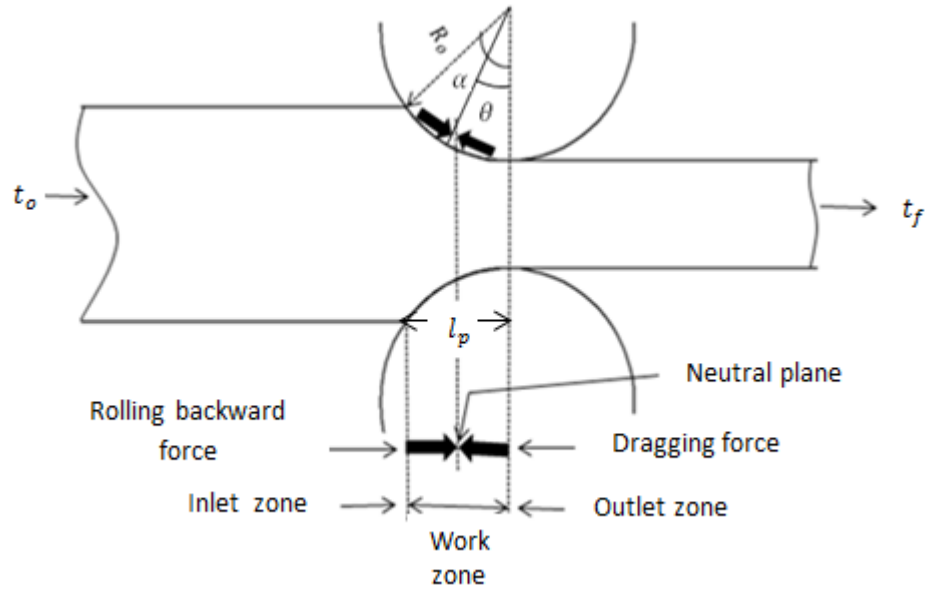

Figure 2-5: Neutral plane at metal-to-roll interface

The location of the neutral angle indicated in Figure 2-5 is defined as [5] :

$$\theta = \frac{\alpha}{2} - \frac{1}{\mu}\frac{\alpha^2}{2} \qquad 2\text{-}1$$

While α is the roll contact angle, the roll radius and metal-to-roll contact length (Fig. 2-5) relations are expressed as follows:

$$Sin\,\alpha = \frac{l_p}{R_o} \qquad 2\text{-}2$$

R_o is the radius of the roll, while l_p is length of contact of the roll-to-metal interface and defined [12] as:

$$l_p = \sqrt{R_o \Delta t} \qquad 2\text{-}3$$

Δt is changes in strip thickness during the rolling process (i.e. $t_o - t_f$), t_o and t_f are initial and final strip thicknesses.

Therefore, $Sin\,\alpha = \frac{\sqrt{R_o \Delta t}}{R_o}$, and it simplified and redefined as follows:

$$\sin \alpha = \sqrt{\frac{\Delta t}{R_o}} \qquad 2\text{-}4$$

Therefore, if $\sqrt{\frac{\Delta t}{R_o}}$ is substituted for α in equation 2-1, then the neutral angle (Figure 2-5) can be obtained in terms of the rolling parameters if the coefficient of friction is given as:

$$\theta = \sqrt{\frac{\Delta t}{4R_o}} - \frac{1}{\mu}\frac{\Delta t}{4R_o} \qquad 2\text{-}5$$

Moreover, μ is coefficient of friction develops at metal-to-roll interface during the rolling process and is expressed [5] as follows:

$$\mu = \frac{F_r}{F_N} \qquad 2\text{-}6$$

F_N is the rolling force while the F_r is the friction force respectively.

2.2.2 Determination of Roll Pressure and Torque in Metal Rolling

The approximate mechanical analysis of the strip rolling process has been discussed in Section 2.2.1. The deformation zone in the cold metal rolling process is very complex and broad, during which the material usually undergoes strain hardness as it is out of the rolls. The deformation of the roll geometry zone was analysed by equation 2-7 to obtain the rolling force under the following assumptions [15]:

- That the material undergoes strain plane process;
- That the width of the material remains the same;
- That the friction coefficient is constant along the roll-bite length;
- That the materials undergo plastic deformation.

The direction of the rolling force and applied torque along the roll-bite during the strip deformation is shown in Figure 2-6.

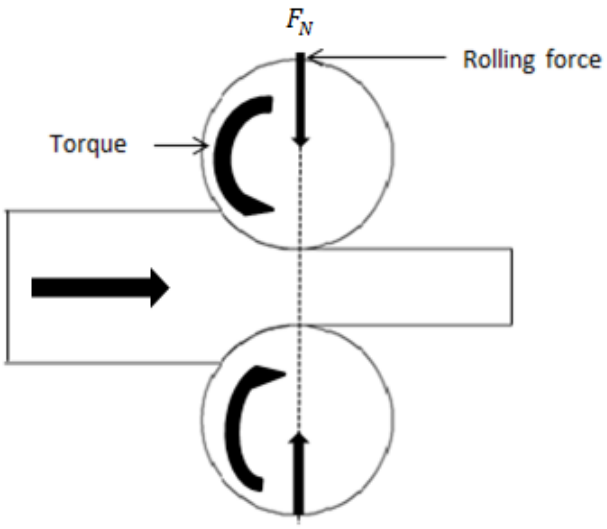

Figure 2-6: Rolling force and applied torque during cold rolling

Rolling forces are applied in both directions to reduce the material's thickness. This required rolling force is estimated [16] as follows:

$$F_N = 1.2 l_p b_o Y_{avg} \qquad 2\text{-}7$$

F_N is rolling force, b_o = is the strip's width. lp is the roll-bite length has been defined in equation 2-3 as follows:

$$lp = \sqrt{R_o \Delta t}$$

Y_{avg} = is an average true stress of the material and is expressed as follows:

$$Y_{avg} = \frac{K\, e^n}{1+n} \qquad 2\text{-}8$$

While *K* and *n* are the strength coefficient and strain hardness exponent respectively. These are constant properties to calculate the average stress of the rolling material during the deformation processing. The *K* and *n* values rolling materials are shown in Table 2-3.

Table 2-3: Values of the parameters (*K* and n) for different materials at room temperature [17]

Materials		*K* (MPa)	*n*
Aluminium	1100-O	180	0.20
	2024-T	690	0.16
	6061-O	205	0.20
	6061-T6	410	0.05
	7075-O	400	0.17
Brass	70 -30, annealed	900	0.49
	85-15, cold-rolled	580	0.34
	Cobalt-based alloy, heat-treated	2070	0.50
	Copper, annealed	315	0.54
Steel	Low-C annealed	530	0.26
	4135 annealed	1015	0.17
	4135 cold-rolled	1100	0.14
	4340 annealed	640	0.15
	304 stainless, annealed	1275	0.45
	410 stainless, annealed	960	0.10

With the knowledge of the rolling load, the required rolling power can be calculated as follows:

$$Power = F_N \frac{l_p}{2} \frac{2\pi N}{60000} \qquad 2\text{-}9$$

While the *N* is angular roll speed (rpm) and the unit of the power is defined as Kw [13].

2.2.3 Determination of Roll Deflection

During the metal rolling process, the forces generated are transmitted to the strip through the roll. The rolls tend to bend along the contact length, which leads to the separation of the roll and strip interface during the rolling process. This separation is caused by the reactions between the strip and roll. Therefore, the rolls flatten at the contact, as shown in Figure 2-7 leading to the increased radius curvature of the roll from R_o to R'_o. The metal roll deflection is due to the elastic behaviour of the rolls during the rolling process as shown in Figure 2.7.

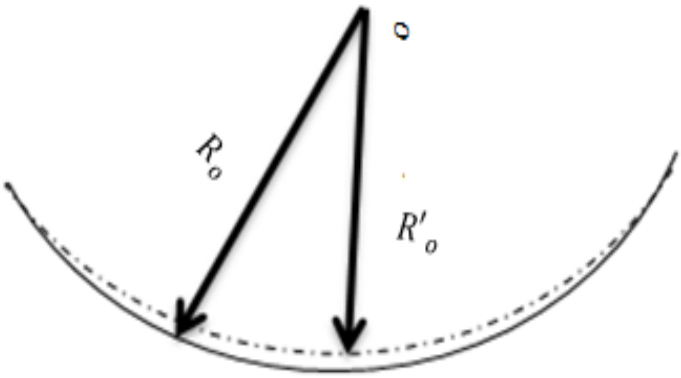

Figure 2-7: Schematic diagram of the deformed roll.

This is due to the increased reduction of the roll radius during the elastic behavior of the roll when it engages with the strip during the deformation process. The roll flatness' is defined [15] as:

$$R'_o = R_o\left[1 + \frac{CF_N}{(\Delta t)}\right] \qquad 2\text{-}10$$

R'_o is deformed roll radius, R_o is non-deformed roll radius, F_N is rolling force and Δt is changes in strip thickness. While C is the constant parameter of the rolling material that is defined as:

$$C = 16\frac{(1-\nu^2)}{\pi E} = 2.16 \times 10^{-11}\text{Pa}^{-1} \qquad 2\text{-}11$$

ν Is the steel Poisson's ratio, while E is the steel Youngs modulus respectively.

2.3 Friction in Metal Rolling

Friction force developed during the metal cold rolling process has been problematic. This is due to the high resistance load and more power being required in the rolling process, leading to heat generation at the roll-bite. Therefore, the proper lubricant film thickness at the roll-bite, during the rolling process, is necessary for the separation of the interface [18].

The damaging consequences of the friction force of the roll-bite during metal rolling have long been recognized. Research [5, 19, 20] has clearly shown that the friction force plays a significant role in the resultant thickness of various strips subjected to different experimental investigations. The friction force developed at the metal-to-roll interface contributes to the high level of coefficient of friction at the interface during the process. This

is caused by the contact peaks form the two surfaces. The low coefficient friction contact takes place due to the hydrodynamic pressure of the oil at asperities valleys of the surfaces [21, 22]. The asperity flattening process depends on the loads on the asperity tops and in the valleys. Other rolling parameters, such as rolling speed, material hardness and the geometrical conditions of the strip and roll (roll diameter, strip thickness and reduction), are also essential.

In metal deformation theory and practice, the coefficient of friction and resistance to deformation in the roll-bite process has been considered. The coefficient of friction at the roll-bite has been shown to depend on the condition of rolls and strip surfaces, the viscosity and volume of lubricant used [23].

2.3.1 Measurement of Friction

In metal rolling, friction is associated with high pressures, and develops naturally during the deformation process. In addition, frictional stress and normal pressure go together at the metal-to-roll interface during the rolling process. Due to the harsh environment at the interface, it has been problematic to determine the correct value of normal pressure and friction during the metal rolling process [24]. Friction force has been one of the major factors influencing the accuracy of the coefficient of friction in cold rolling. The coefficient of friction at the roll - bite is defined as the ratio of the interface frictional stress to the normal pressure. Therefore, the coefficient of friction at the roll-to-metal interface is determined by the amount of normal pressure and frictional stress developed during the deformation process. The developed coefficient of friction contributes to the surface quality of the product generated during the rolling process. Therefore, the actual correct value of the friction force to determine the accurate value of the coefficient of friction at the roll-bite is essential. The coefficient of friction is necessary for cold metal rolling process. Its excess developing at the roll-bite during the rolling process has been the most significant problem with the rolling process. However, the nature of friction at the metal-to-roll interface is not yet understood.

Different measures have been adopted by researchers to determine the value of normal pressure and friction force required for the metal rolling process [25]. These include direct and indirect frictional force measurement systems during the rolling process. In the direct

system, a pin is inserted radially in the work roll of a rolling mill, which has been pressed down upon a load cell mounted within the roll [26]. The indirect method is the process of measuring the required parameters to determine interface coefficient of friction at the roll-bite, with the aid of other measurement techniques such as strip making and the Laser Doppler method [19].

2.3.1.1 Direct Measurement System

The direct measurement method in metal rolling was the process of inserting a sensor on the work roll [26] for the measurement of normal and friction forces at the interface between roll and strip. This sensor consisted of a pin mounted directly on a load cell before being fixed into the body of the roll. The displacement of the pin plunger by the normal pressure developed at the roll-to-metal interface was displayed by the load cell monitor device and recorded for further uses. The disadvantage of this device was that it could not measure frictional forces.

The technique saw additional development into another sensor by Rooyen and Backofen [27]. This consisted of two pins mounted within the holes of the work roll. The first pin was radially inserted, the second inserted at an angle to the first. Both forces acting along the axis of each pin were measured by the strain gauge mounted on each pin during the rolling process. The radial pin measured the normal pressure while the oblique pin measured both normal and frictional forces. The value of the coefficient of frictions at the roll interface was calculated by the ratio of the forces and radial directions. This coefficient of friction at the roll-to-metal value was obtained with the following formula:

$$\mu = \left(\frac{P_1}{P_2} - 1\right) tan\, \emptyset \qquad 2\text{-}12$$

While P_1, is normal pressure and P_2, is an oblique pressure pin.

Lenard [28], furthered this technique, by varying the location angles of the pins on the roll. The major disadvantage of this design is the traces of the pin marks on the surface of the rolled strip and the pin bending as it slides across the strip surface during the rolling process.

MacGregor and Palme [29] designed a cantilever pin sensor due to the disadvantage of the technique developed by Siebel and Lueg. This sensor was successfully used to measure

frictional force. The tip of the sensor was in contact with the workpiece surface while the main body of the sensor was inserted within the roll. The normal and frictional forces at the surfaces of the roll and strip were measured by the strain gauge mounted on the pin. The obtained data were used to determine the coefficient of friction developed during the rolling process. There was no sliding movement of the pin during the rolling process. This technique, used by Wilson et al. [30], to verify the performance of the capstan friction simulator.

Jeswiet et al. [31] employed the capstan simulator to determine the average coefficient of friction of sheet metal forming and found it to be accurate. However, it was noted that the normal pressures obtained from the capstan simulator were very low with the low rolling condition when compared with high rolling. This was due to the extrusion of material into the gap around the pin surface at high normal pressure. The sensor was found to leave a mark on the strip and stop operating properly at the moment the extrusion occurred.

Moore et al. [32], designed a diaphragm sensor consisting of strain gauges inserted on a thin layer of the roll, adjacent to the strip surface. The sensor was designed with two strain gauges to measure in vertical and horizontal directions during the process. During the test, normal load was first applied, followed by the shear load. The sensor was subjected to cycles at the rate of 1Hz and 30 seconds for each applied load and the strains' values were recorded. They were employed to measure the normal and frictional forces at the metal-to-roll interface during the rolling process. The magnitude of both forces was resolved with the aid of the strain gauges arranged in the direction of the frictional forces. In the case of normal loading, both strain gauges measured the same strain values of normal pressure and frictional forces. These are expressed as follows:

$$\varepsilon_1 = \varepsilon_2 = \varepsilon_N \qquad 2\text{-}13$$

The measurement of the strain gauges was different once the frictional forces were not equal. The changes in measured strain were equal and opposite in direction. The measured strain values are expressed as follows:

$$\varepsilon_1 = \varepsilon_N + \varepsilon_F$$

$$\varepsilon_2 = \varepsilon_N - \varepsilon_F \quad \text{2-14}$$

ε_1 and ε_2 are normal and frictional forces while the ε_N and ε_F are the strain of normal and frictional force readings. This sensor was used to eliminate the strip extrusion problem that occurred due to the gap around the surface of the pin inside the sensor. However, the results obtained showed the same trend as another method but it was difficult to identify the normal pressure from the frictional stress. Furthermore the thin layer surface of the sensor collapsed when high loads were applied.

Yajure [33], developed a sealed cantilever pin to avoid the extrusion of the strip into the gap around the sensor tip surface during the rolling process. This device was installed 1.5 mm below the surface of the roll, it consists of a square pin was inserted into a round hole of a square post; large clearance was made around the pin for the purpose of high rolling pressure. Collapse of the die around the tip was still experienced during the rolling process. However, the device gave a clear signal during the rolling process.

Henningsen et al. [34], designed a portal frame sensor device that contained two strain gauges mounted on to the two vertical beams of the frame. These strain gauges measure deflections of the two beams separated during the rolling process. The signals obtained from these two strain gauges were used to show the value of frictional force in the rolling direction.

This sensor was used successfully to conduct various tests on a pilot mill during the metal rolling process. The sensor is strong and can withstand the high pressure that occurs during the rolling process. However, the device is not capable of measuring the frictional force in the transverse rolling direction. Additionally, it had the imprinted mark of the pin left on the surface of the material after the rolling.

2.3.1.2 Indirect Measurement System

An indirect method for the coefficient of friction is the process of determining the coefficients of friction through the value of the parameters obtained from the measurement techniques employed. The most common techniques for the measurement of these parameters are strip mark and Laser Doppler methods.

The strip mark layout technique is the process of measuring the forward slip movement of the strip in respect of the roll rotation. Both roll and strip will rotate simultaneously, then the mark on the roll will be imprinted on the surface of the strip during the rolling process. Lenard [25] employed this technique to obtain the parameters for the determination of coefficient of friction at the roll-bite during the cold rolling process. Figure 2-8 shows the line l_1 sited between marks A and B within the roll surface. The machine was operated and the strip passed through the roll gap. The line l_2 was l_1 noted to have duplicated onto the surface of the rolled strip after the rolling operation.

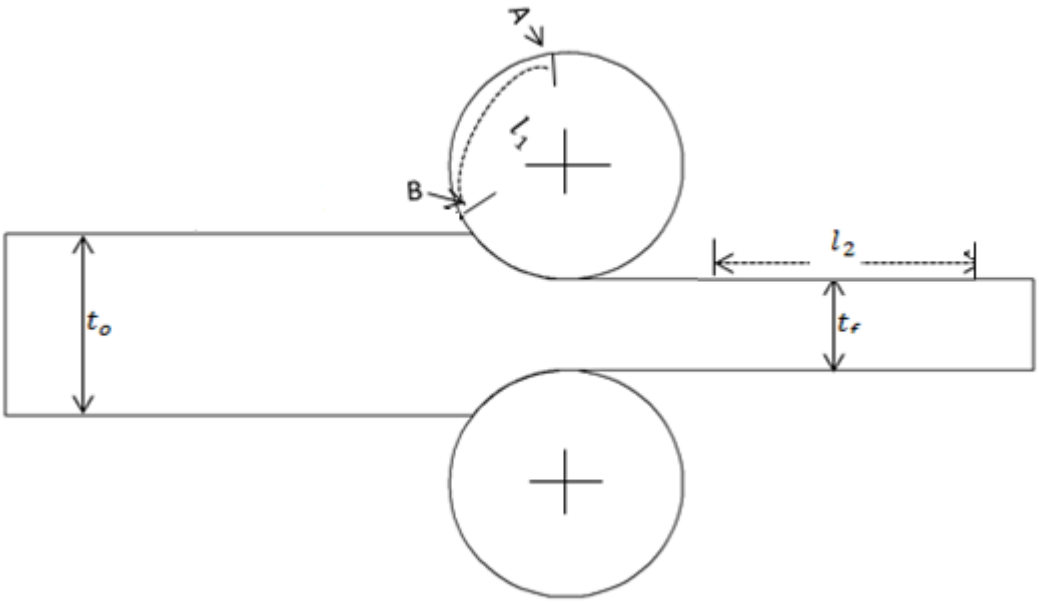

Figure 2-8: Schematic diagram of roll with mark layout technique [35]

Figure 2-9 shows the line l_2 on the strip surface, which was the imprinted of the mark l_1, that had initially been printed onto the surface of the roll before the strip was rolled.

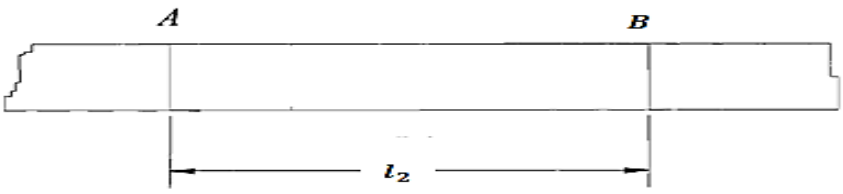

Figure 2-9: Imprint lines after rolling process

This mark illustrates the elongation length of the strip that underwent the rolling process. These two marks were used to determine the average forward slip of the rolled material and were expressed as follows:

$$S_f = \frac{(l_2 - l_1)}{l_1} \qquad 2\text{-}15$$

while S_f, is the forward slip to be calculated, l_1 is the distance between the scratched lines on the roll's circumference. The l_2 is the distance of the imprinted lines on the strip's surface after one revolution turn of the roll. The coefficient of friction can finally be calculated from the forward slip values obtained in equation 2-15 with the combination of equations in 2-16 shown below.

$$\mu = \frac{t_o - t_f}{2\sqrt{R'(t_o - t_f) - 4\sqrt{S_f R' t_f}}} \qquad 2\text{-}16$$

The value for the variable R' the roll deflection has been already defined in equation 2-10. Therefore, Lenard concluded that the coefficient of friction obtained was decreasing as the rolling speed increased, which was almost of the same trend as the theoretical prediction.

Liu [5], employed Laser Doppler probes to obtain both roll and strip velocity during the metal rolling process for the determination of the coefficient of friction at the roll-bite during the rolling process. As shown in Figure 2-10, one Laser probe was mounted in the front of the upper roll to measure the roll speed and another was sited on one side of the pilot mill to detect the speed of the strip.

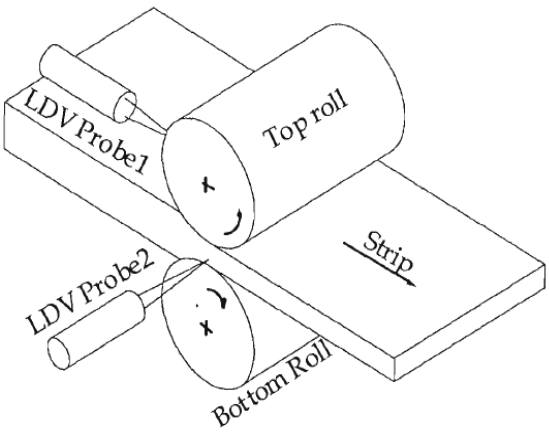

Figure 2-10: schematic diagram of a Laser Doppler measuring method [5]

The forward slip value obtained is proportional to the difference of the existing strip velocity V_2, and rolls velocity U_r. The strip and the rolls velocities are related as:

$$S_f = \frac{V_2 - U_r}{U_r} \qquad 2\text{-}17$$

The value of the coefficient of friction at the roll-bite was calculated from the forward slip values obtained in equation 2-16 with the combination of equations 2-17 respectively. The value of the coefficient of friction obtained was almost the same trend as per the theoretical prediction.

The summary of the coefficient of friction measurement techniques reviewed with the years of the research and name of the authors, are presented in Table 2-4.

Table 2-4: Coefficient of friction measurement reviewed techniques

Authors/Date	Method	Limitation of method
Lueg, E.S. (1933) [26]	Sensor pin	Not able to measure frictional force
Rooyen Backonfen (1957) [30]	Two sensor pins at angle	Traces of the pins mark the surface of measured material.
Lenard, J.G (2000) [28]	Two sensors pins at various angles	Traces of the pins mark the surface of measured material
MacGregor and Palme (1948) [29]	Cantilever pin sensor	Traces of the pins mark the surface of measured material
Jeswiet et al (2001) [31]	Capstan simulator device	Extrusion of the strip into the gap around the sensor tip surface
Moore et al (2002) [32]	Diaphragm sensor device	Collapsing of the thin layer of the sensor.
Yajure et al (2002) [33]	Sealed cantilever pin device	Collapsing of the thin layer of the sensor.
Henningsen et al (2006) [34]	Portal frame sensor	Not capable of measurement of frictional force in the transverse rolling direction

Furthermore, all the results reported from the various experimental procedures for the measurement of the coefficient of friction reviewed above section are reliable. Although, these techniques are good and straightforward to understand, none have links with the application of the ultrasonic measuring technique either directly or indirectly for the measurement of the coefficient of friction and its variables. Additionally, these are invasive methods requiring embedded plugs in the roll, which is dangerous for both roll and strip surfaces during the rolling process. The extrusion of the material into the gap around the surface pin during the rolling process is another problem of these techniques. Finally, the

surface of the sensor installed into a roll does collapse at high pressure during the rolling process, due to the thin layer of the sensor on the roll body during the installation [36].

2.4 Metal Rolling Lubricant

In the metal rolling process, the lubricant is the fluid substance applied to separate the roll from the metal surface during the rolling operation. Lubrication is the process or method of applying the lubricant to the rolling surface and has a significant influence on the roll durability and its load capacity. In the metal forming process an emulsion is usually applied to avoid direct contact of roll and strip and to reduce damage to the strip surface. Additionally, the oil cools the roll-bite, protects strip and roll from corrosion and maintains the interface temperature from surface damage [37]. If the lubricant film fails, the friction force at metal-to-roll can increase and damage the interface.

In addition, the oil film thickness, formed in the two contact zones, is sustained by the oil pressure developed within the roll and strip together with the strip contacts of the two bodies. This is referred to as the mixed lubrication regime where the two surfaces are partially separated by asperity contact of materials and pressurised lubrication oil within the surface valleys. Lubrication is very important in controlling the surface interactions between the rolls and the strip during the rolling process. The tool (roll) and the workpiece (strip) surface interaction at the wet interface is shown in Figure 2-11 (a). The two surfaces consist of a major contact and a minor contact of the asperity of both surfaces. Furthermore, minor-pores are created by the valleys on both surfaces and a convex hull, which develops as a result of the pressure on both surfaces. These minor pores fill with oil during the rolling operation. The closest contact with the asperities of the two surfaces is presented in Figure 2-11 (b).

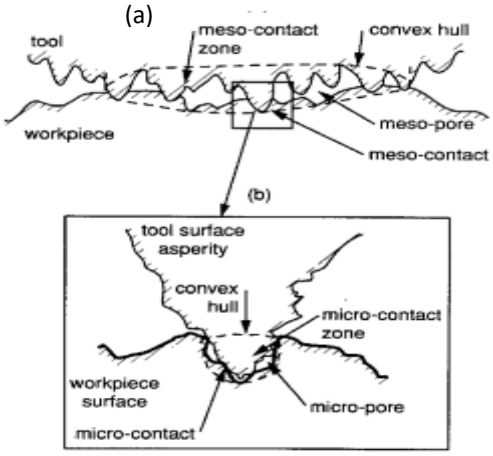

Figure 2-11 Schematic diagram of two contact surfaces

This interaction needs four conditions to be satisfied in order to create an adequate lubricated contact. First, enough lubricant must be made available at the entry zone of the roll-bite. The lubricant must then be entrapped, that is, the oil droplets must be captured and drawn into the metal-to-roll contact zone. The emulsion must be spread through the contact uniformly and cover the contact surfaces of the two materials. Finally, the lubricant must then flow through the work to the exit zone [38]. Some of the primary functions of the lubricant at the metal-to-roll interface during the rolling operation are itemised and shown in Figure 2-12.

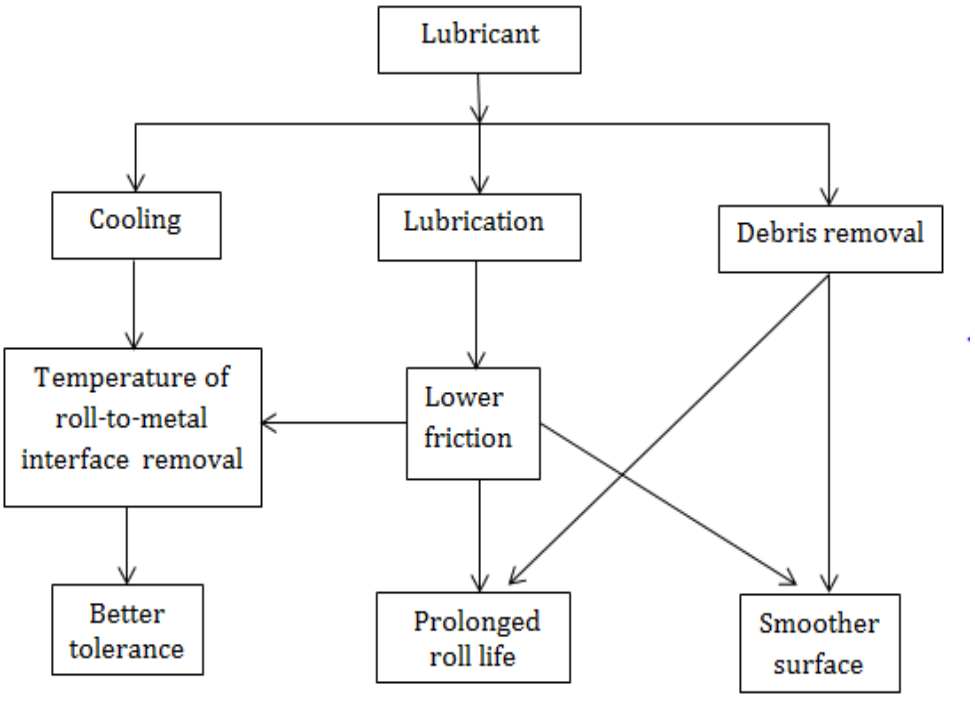

Figure 2-12: Functions of the lubricant [39]

The applied lubricant during the cold rolling of steel strip, needs to have the above detailed functional properties, in order to create good lubricating conditions, and acceptable surfaces with efficient cooling during the rolling interaction (Figure 2-11).

The film thickness of the lubricant formed at the roll to metal contact interface depends on the lubricant's physical properties such as density and viscosity. Furthermore, rolling speed, load, and roll-to-metal interface roughness are important in determining the amount of the lubricant film thickness formed during the rolling process. The quality of the product surface and the roll-to-metal surface protection from wear depends on the integrity and thickness of the lubricant formed at the roll-bite [23].

Azushima [40], investigated the effects of rolling speed on the formation of coefficient of friction during the rolling process. His results show that the higher the rolling speed, the lower the rolling pressure, and the thicker the film of oil formed at the roll-to-metal interface. This is due to the increasing frictional resistance within the layer of lubricant that causes an increase in the separation of the interface in order to accommodate more oil.

Similarly, Button [41], explains the variation of pressure and the formation of oil film thicknesses at the inlet and work zone during the cold rolling of an aluminium strip. The result shows that these differences are also strongly influenced by the rolling conditions such as the lubricant viscosity and percentage reduction of the strip in the value of the formed coefficient of friction.

2.4.1 Lubricant Properties

In metal rolling, lubricant properties have a significant effect on performance during the rolling process. As previously explained, a lubricant with good properties is expected to provide a small separation at the metal-to-roll interface during the rolling to avoid the total direct contact of the surfaces. In addition, this provides support for enough coefficient of friction for a smooth rolling process [42]. The good performance of the lubricant functions, listed in Figure 2-12, all depend on the properties of the lubricant applied. Furthermore, the oil film thickness obtained at the roll-bite during the rolling operation depends on lubricant properties (density, bulk modulus and viscosity), the rolls and strip geometric features, and

some of the rolling conditions (load and speed). The lubricating properties that are relevant for the fluid used in this research are itemized and explained in sub-sections 2.4.1.1 below.

2.4.1.1 Viscosity

Viscosity is a lubricant property having a significant effect on the lubricant's internal resistance to flow. Generally, viscosity is necessary for the lubrication and a suitable amount is required for the best performance of the oil. The first explanation of viscosity was given by Isaac Newton in relation to the combination of piston and oil and closed cylinder, as shown in Figure 2-13.

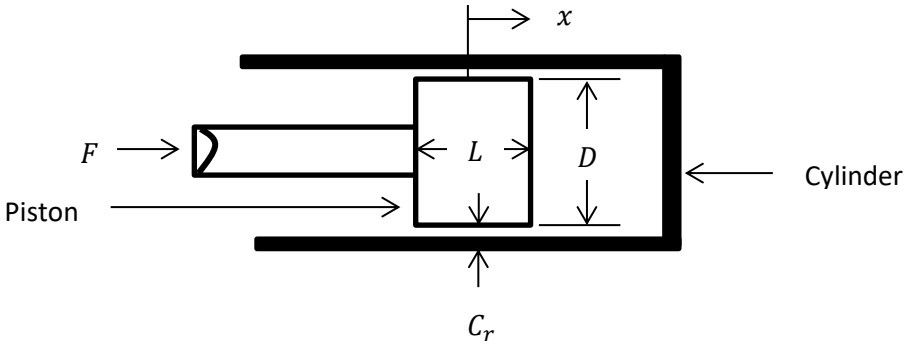

Figure 2-13: Illustration of viscosity with piston and cylinder

C_r is the radial clearance between the piston and the cylinder, L and D are the piston length and diameter, x is the distance moved by the piston while F is the force applied to the piston. The force applied to cause the relative motion of the piston was measured by the fluid resistance to shear, which is directly proportional to the contact area and to the velocity of the piston [43]. It is also indirectly proportional to the oil film thickness. Therefore,

$$F = \frac{\pi DL\mu}{C_r}\frac{\partial x}{\partial t} \qquad 2\text{-}18$$

μ is oil viscosity, πDL (A) is the contact area. Normally, the lubricant film is expected to be thick enough and be able to separate the metal-to-roll interface, but not so thick to the extent of creating additional force (F) to overcome the shear rate of the lubricant during the rolling process [44].

2.4.1.1.1 Types of Viscosity

The lubricant viscosity is classified according to its measurement technique, which are Dynamic (Absolute) Viscosity and Kinematic Viscosity.

2.4.1.1.1.1 Dynamic (Absolute) Viscosity

Dynamic Viscosity is defined as the measurement of resistance of the fluid to flow under the deformation or applied load. This viscosity is defined by [45] as:

$$\eta = \frac{\frac{F_r}{A}}{\frac{V_o}{h_m}} = \frac{\tau}{\gamma} \qquad 2\text{-}19$$

while τ and γ denote shear stress and shear strain rate. F_r and A are the friction force and the lubricated contact area. Finally, V_o and h_m are surface velocity and film thickness respectively. This dynamic viscosity is normally measured in Centipoise (cP). 1 cP = mPa.s.

2.4.1.1.1.2 Kinematic Viscosity

Kinematic Viscosity is generally known as the measurement of the resistance of a fluid to flow under the forces of gravity. It is also defined as the ratio of the dynamic viscosity to its density and expressed as follows:

$$\eta_k = \frac{\eta}{\rho} \qquad 2\text{-}20$$

While ρ is the density of the fluid and η is the dynamic viscosity respectively. This type of viscosity is mostly quoted in data sheets at 40°C and 100°C; it is generally measured in centistokes unit (mm^2/s in SI unit). In addition, temperature and pressure have a major effect on lubricant viscosity properties, but this effect will be discussed within the bulk modulus oil property section.

2.4.1.2 Bulk modulus

The bulk modulus is a property of fluids which expresses the change in volume of the fluid due to the external pressure applied [46]. The numerical change in the volume of fluid during the applied external force depends on the operation conditions, the amount of air present in the system and how the pressure is applied. Therefore, the following operating conditions: oil pressure and temperature, closeness and the rigidity of the surfaces and the

content of air at the interface, influence the change in the bulk modulus of the fluid during the operation [47].

To understand the meaning of the bulk modulus of fluid and how it was derived the equation of state for fluids must be known. This is defined as a function relating density, pressure and temperature of a fluid together. Due to the small change in fluid density to the change of pressure and temperature, these three variables can be approximately related using Taylor's series [43]. Therefore,

$$\rho = \rho_O + \left(\frac{\partial \rho}{\partial P}\right)_T (P - P_O) + \left(\frac{\partial \rho}{\partial T}\right)_P (T - T_O) \quad 2\text{-}21$$

While equation 2-21 is simplified further for clarification and re-defined as follows:

$$\rho = \rho_o \left[1 + \frac{1}{\beta}(P - P_O) - \alpha(T - T_O)\right] \quad 2\text{-}22$$

ρ, P and T are the initial fluid density, pressure and temperature while ρ_o, P_O and T_O are final fluid density, pressure and temperature respectively.

Also,

$$\beta = \rho_o \left(\frac{\partial P}{\partial \rho}\right)_T \quad 2\text{-}23$$

And

$$\alpha = -\frac{1}{\rho_O}\left(\frac{\partial \rho}{\partial T}\right)_P \quad 2\text{-}24$$

As shown in equation 2-23, the density increases as the pressure increases with the decrease in temperature. This is because the density is mass divided by volume. β and α were re-defined in terms of volume and expressed as follows:

$$\beta = -V_o \left(\frac{\partial P}{\partial V}\right)_T \quad 2\text{-}25$$

$$\alpha = \frac{1}{V_o}\left(\frac{\partial V}{\partial T}\right)_P \quad 2\text{-}26$$

While V and V_o are the total and the initial volume of the fluid, β is the change in pressure divided by the change in volume at a constant temperature and is known as bulk modulus of

the fluid. α is referred to as the cubical expansion coefficient, which is the fractional change in volume due to a change in temperature.

There are various types of bulk modulus, which are only specific to their own applicable conditions. These have been widely used in textbooks:

- Isothermal secant bulk modulus
- Isothermal tangent bulk modulus

Furthermore, Figure 2-14 shows the relationship between the change in fluid pressure and the change in volume of the fluid at a constant temperature. The above mentioned types of the bulk modulus are indicated in Figure 2-14 below, but are fully explained in the next sub-sections.

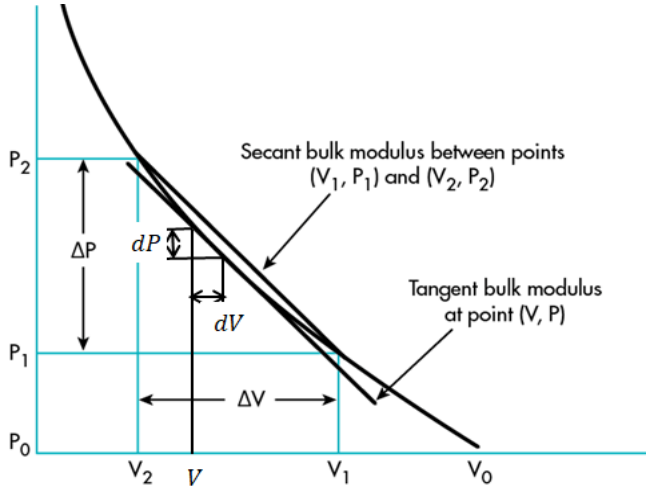

Figure 2-14: Determination of the value of bulk modulus of applied oil [45]

2.4.1.2.1 Isothermal Secant Bulk Modulus

Isothermal secant bulk modulus is expressed as product of the original volume V_O and the slope of the line drawn from the original to any specified point on the plot of the pressure versus specific volume. This method is suitable for large pressure changes. This is referred to as the isothermal secant bulk modulus if the process undergoes a change in pressure at a constant temperature. The above expression is defined as follows [46]:

$$B_s = V_O\left(\frac{P_2-P_1}{V_1-V_2}\right) \qquad 2\text{-}27$$

Therefore, B_s is the isothermal secant bulk modulus, P_1 is the final fluid pressure, P_2 Is the initial fluid pressure, V_1 and , V_2 are the initial and final volumes of the fluid value while the V is original fluid volume [48]

2.4.1.2.2 Isothermal Tangent Bulk Modulus

The tangent bulk modulus is expressed by the pressure to volume differential as shown in equation 2-28. It is generally defined as the product of fluid volume and the partial derivative of fluid pressure with respect to volume at constant temperature. The isothermal tangent bulk modulus is defined by the following expression [49]:

$$B_T = V\left(\frac{\partial P}{\partial V}\right) \qquad 2\text{-}28$$

B_T is the isothermal tangent bulk modulus, V_o is the initial volume value, ∂P is the change of the external pressure, ∂V is the change of the fluid volume

2.4.2 Analysis of Different Lubrication Zones in Cold Metal Rolling

Figure 2-5 shows a schematic illustration of the metal cold rolling process. The strip dimension is reduced in thickness from t_o to t_f by the radius R_o of the roll during the rolling process. As shown in Figure 2-15, the roll-bite is divided into three zones: inlet, work and outlet zone.

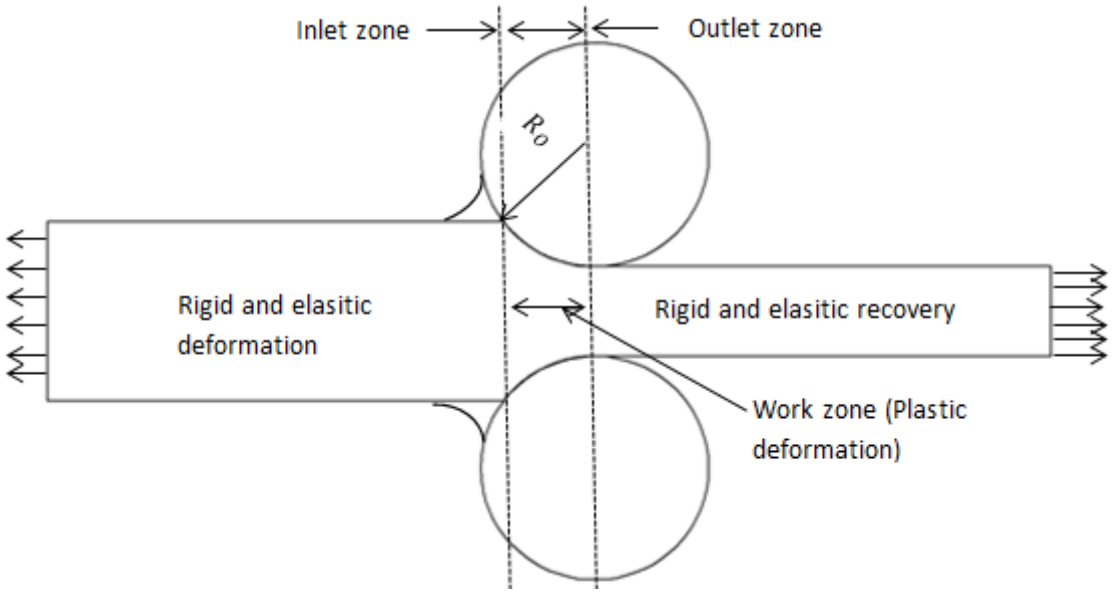

Figure 2-15: Schematic diagram of different rolling zones

2.4.2.1 Inlet Zone

The inlet zone length is usually short compared to the radius of the roll. As a result of this shortness, the roll shape of this zone is taken as a straight line within an angle α to the strip surface. In the zone, reduction of the asperities takes place by the differential pressure between the top asperity and the lubricant valley contact within the rolls and strip surfaces. As the rolls and strip contact area go through the roll-bite, the mean contact pressure within the two surfaces reaches the yield stress of the strip and leads to the plastic deformation of the material [50]. This plastic deformation occurs at the end point of the inlet zone and acts as the beginning of the work region.

The speed of the rolls is higher than the speed of the strip during the rolling process in this zone. Here, the strip is pulled into the roll gap with the aid of the friction force developing at the metal-to-roll interface during the rolling process. The thickness of the strip remains the same in this zone because the normal force acting on it has not gone beyond its yield stress [51].

2.4.2.2 Work Zone

The strip velocity increases from the inlet zone towards the neutral plane in the work zone during rolling. On this plane the velocity of the roll and the strip are equal [52] and the direction of friction forces between the strip and roll is opposite to one another. Ahead of this plane, towards the exit zone, the direction of friction force from the strip and roll is reversed. The velocity of the strip is higher than that of the rolls.

In this zone the mean contact pressure on the roll-bite is assumed to be equal or greater than the yield stress of the strip, which is why the strip is plastically deformed at this zone during the rolling process [53]. The lubricant dragged into the roll-bite during the rolling process is pressurized by the rolling pressure. The dragged lubricant dominates the roll-to-metal interface and reduces the frictional force arising from the roll-bite interface contact. Therefore, the oil thickness formed depends on the properties of the applied lubricant and other rolling parameters such as the applied rolling load and rolling speed. The lubricant viscosity is increased and separates the interface of the roll and strip during the rolling

process. This is due to the variation of the pressure developed and the dissipation of the heat generated from the oil at the asperity contact of the rolls and strip surfaces [54].

2.4.2.3 Outlet Zone

The outlet zone is the last zone along the roll-bite, shown in Figure 2-15. The lubricant thickness of this zone is slightly reduced compared to the inlet zone and its pressure drops to the ambient level. The strip becomes rigid immediately after the work zone due to the recovery of the plastic flow of rolled material. In this zone, the strip moves faster than the roll.

2.5 Numerical Modelling of Oil Film Formation in Cold Rolling

Figure 2-16 shows the roll-bite interface separated by the film thickness of the lubricant applied during the rolling process. Sutcliffe [55] explains that the inlet region cannot be treated independently of the work zone and the exit area. The oil film thickness determined in the inlet region can be assumed to be the same as at the work zone. Therefore, the elongation of the strip through the bite will tend to reduce the oil thickness in the entry region towards the work zone. The amount of lubricant at the roll-bite contact surface area (Figure 2-16) during the metal rolling has been predicted by various researchers [56-58]. Their predictions during the rolling operation were based on modelling approaches relating to the speed of the roll, the yield stress and initial thickness of the rolling material.

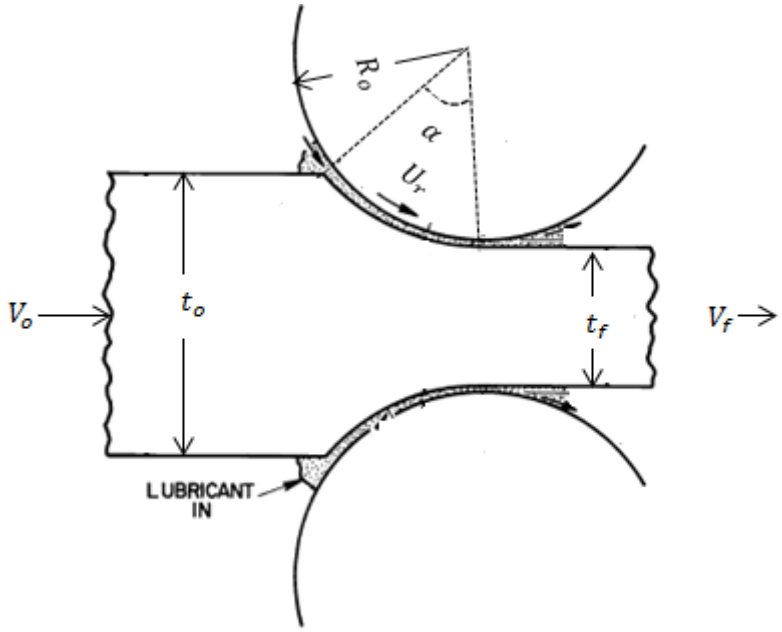

Figure 2-16: Schematic diagram of the roll bite separated by the oil film thickness [21]

Wilson and Walowit [59] applied Reynolds equation to predict the oil thickness at the roll-bite during metal rolling operation. This Reynolds equation is stated as follows:

$$h_o = \frac{3\eta_o\gamma(V_o+U_r)R'}{L[1-exp(-\gamma\sigma_y)]} \qquad 2\text{-}29$$

Where, η_o, is the dynamic viscosity of the used lubricant and γ is the pressure viscosity. The R' is the radius of the deflected roll, U_r is the roll surface velocity, V_o is the entry velocity of the strip and the$L$, is the projected contact length while σ_y is the average yield strength of the strip.

The oil viscosity pressure coefficient of friction at the roll-bite is given as:

$$\gamma = (0.6 + 0.965\log_{10}\eta_o) \times 10^{-8} \qquad 2\text{-}30$$

Therefore, if the thickness of the oil film is reduced, the asperities perforate through the lubricant. As the viscosity of the oil or the relative speed is increased, mixed lubrication is achieved, which leads to oil pockets and asperity contact. The oil film thickness is determined in the lubricating regime by comparing it with the asperity heights of the rolls and the rolled metal [60]. This ratio is defined as:

$$\Lambda = \frac{h_{min}}{\sqrt{R_{q1}^2 + R_{q2}^2}} \qquad 2\text{-}31$$

Where h_{min}, is the minimum film thickness obtained from the roll-bite, R_{q1} and R_{q2} are the surface roughness values of the strip and roll surfaces respectively. Then the proportions of film thickness for the corresponding lubrication regimes are roughly estimated at [28, 61]:

• Boundary lubrication, Λ< 1

• Mixed lubrication, 1 <Λ< 5

• Hydrodynamic lubrication, 5 <Λ< 100

2.6 Experimental Measurement of Oil Film Thickness in Metal Rolling

A series of film thickness measurement techniques have been developed by various scholars such as:

- The wiping off method;
- The oil drop on the surface of the strip;
- The valley interrogation method;
- The internal ultrasonic reflection measuring technique.

The aim of this section is to consider the experimental determination of oil film thickness measurement at the metal-to-roll interface with the above mentioned techniques and to compare them with the external ultrasonic layout that is the focus of this thesis.

2.6.1 Wiping Off Method

Whetzel and Rodman [62], explained the measurement of the oil film thickness by wiping off the adhered lubricant from the strip after the rolling process. The lubricant had been obtained by dipping it into the solvent after the rolling then allowing the adhered oil to dissolve into the solvent. The solvent was allowed to vaporize and the volume of remaining lubricant was measured.

Therefore, the oil film thickness at the inlet of the metal-to-roll interface denoted by h_o, was obtained from the weight and the density of the remaining oil and the oil-covered area. The inlet oil film thickness h_o, is expressed as:

$$volume = \frac{Mass}{Density}$$

While the, $Volume = Area \times h_o$

$$h_o = \frac{Volume}{Area} \qquad 2\text{-}32$$

The inlet oil film thickness (h_o) at the roll-bite interface was obtained with this technique. The thickness of 0.1 µm was obtained from the rolls and the strip in the entrance zone. The value was found to concur with the theoretical values obtained from the literature section of the paper.

2.6.2 Oil Drop on the Strip's Surface Technique

Katayama [63], developed the method introduced by Whetzel and Rodman [62] for further determination of oil film thickness on the roll-bite during the metal cold rolling. The experiment began by cleaning the rolls and strip surfaces with solvent, and small amount oil was dropped on the surface of the strip. The weight of the oil was obtained by subtracting the weight of the metal from the total weight of the strip and oil. The final strip weight reduction was measured by the chemical weight balance, instead of dissolving the adhered lubricant, by dropping the rolled strip in the solvent.

The area of the oil spot spread was traced and measured with a planimeter. This area was clearly visible and different from the unlubricated region. The oil film thickness at the inlet of the metal-to-roll interface denoted by h_o, was obtained from the weight and the density of the dropped oil and the oil-covered area. The oil film thickness was also determined by equation 2-32 shown in Section 2.6.1.

2.6.3 Valley Integration Method

Azushima [64] measured the oil film thickness at the roll-bite with the aid of the relationship between the strip and roll asperities being crushed after a rolling process. The roll surface was sandpapered with 400 emery paper and cleaned with benzene before the rolling process of the materials. The maximum roughness value of the roll and strip were measured, before and after the material was rolled. The sample profile of the rough surface of the roll and the strip is shown in Figure 2-17.

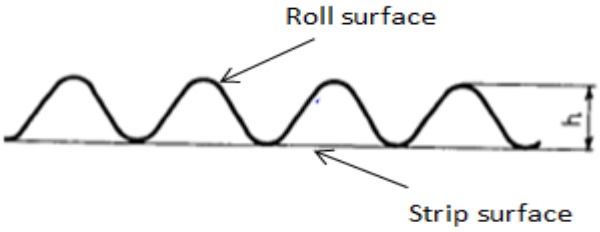

Figure 2-17: Schematic diagram of roll surface roughness sample

The roughness height at the surface of the roll was denoted as h while the surface of the strip is assumed to be flat before rolling, as shown Figure 2-17. The applied oil flowed across the roll surface and occupied the strip surface roughness space imprinted by the roll during the deformation process. The average thickness of this oil within the surface of the strip and roll after the rolling process was used to determine the oil film thickness at the metal–to-roll interface during the rolling process [64] and was expressed as follows:

$$h_o = \frac{1}{2}(R_{q1} + R_{q2}) \qquad 2\text{-}33$$

While the R_{q1} and R_{q2} are the roughness values of the roll and the strip and h_o is the film thickness at the inlet of the metal-to-roll interface respectively. The outlet film thickness was obtained at the roll-bite with the aid of the inlet oil film thickness value (h_o) in relation to the outlet strip and roll speeds respectively. Therefore, the oil film thickness of the outlet zone was denoted as h_1, and is expressed as follows:

$$h_1 = h_o \frac{U_o + U_r}{U_f + U_r} \qquad 2\text{-}34$$

The h_1 and h_o are film thicknesses at the work and inlet zones, U_o and U_f are the inlet and outlet strip speed while U_r denotes the roll speed. The mean value of 0.4 µm was obtained

at 4m/min rolling speed and increased to 4μm at 850m/min rolling speed. In accordance with Whetzel and Rodman [62], the results obtained are also in good agreement with the results from their literature review.

Sutcliffe [55], estimates the inlet film thickness at the roll-bite based on the first method described by Azushima [64]. The profile roughness value of the roll and strip were measured with the profilometer and converted to a digital value with the aid of a data logger. The inlet oil film thickness value (h_o) at the roll-bite was determined and used to estimate the outlet film thickness in relation to the outlet strip and roll speeds respectively. The percentage reduction of the strip was also considered and the relationship of these parameters is expressed as follows:

$$U_f = \frac{U_r t_f}{t_o} \qquad 2\text{-}35$$

Continuity of the mass flowrate of the fluid was considered; therefore the outlet film thickness h_1 at the roll-bite is expressed as follows:

$$h_1 U_r = \frac{h_o(U_f + U_r)}{2} \qquad 2\text{-}36$$

And

$$\frac{h_1}{h_o} = \frac{\left(1 + {}^{t_o}/_{t_f}\right)}{2} \qquad 2\text{-}37$$

U_f and U_r are the outlet strip and roll speed respectively while, h_1 and h_o are the outlet and inlet film thickness.

The results obtained by this technique were compared with those from the oil drop method is and are presented in Figure 2-18.

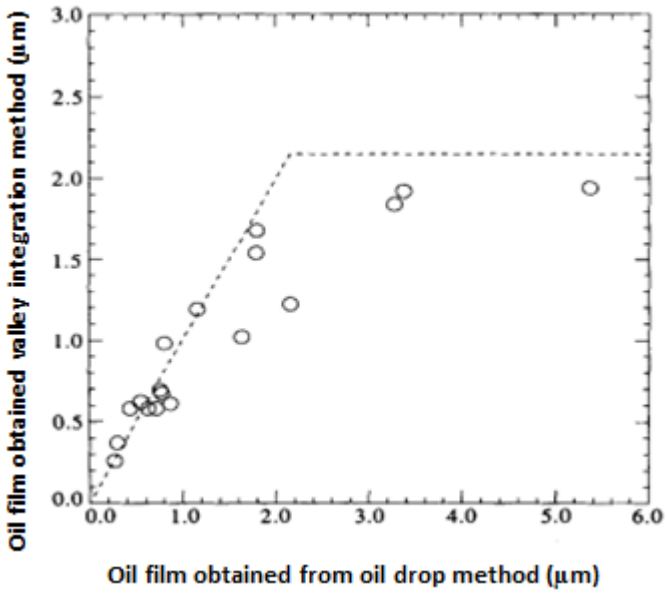

Figure 2-18: Oil film thickness obtained from different methods [64]

There is good agreement between the results obtained from both techniques. As shown (Fig. 2-18) they have the same trend.

Cuperus [57], explained the uses of a Rautaruuki meter for the measurement of oil film thickness at the strip surface. This is an infrared measuring device used to measure the oil film thickness during the metal rolling process. The outcome performance of the meter depends on the strip roughness and the lubricant properties. The strip surface was cleaned with the solvent, then the zero oil film thickness of 10 different points on the strip surface were captured and the average of the zero signals was recorded. Next, the oil was dropped onto various places on the surface of the strip. The measured oil film thickness was compared with the obtained from the oil dropping technique.

In addition, Cuperus also reviewed the measuring techniques listed above and improved the modes of applying lubricant into the roll-bite during the rolling process. A special piece of apparatus was designed to continuously drop the oil during the rolling process, instead of the manual oil drop method previously employed. These methods were undertaken separately to conduct experiments with the aid of two rolls. The rolls were prepared with the different values of surface roughness respectively. The results obtained from these techniques were prepared and are shown in Figures 2-19.

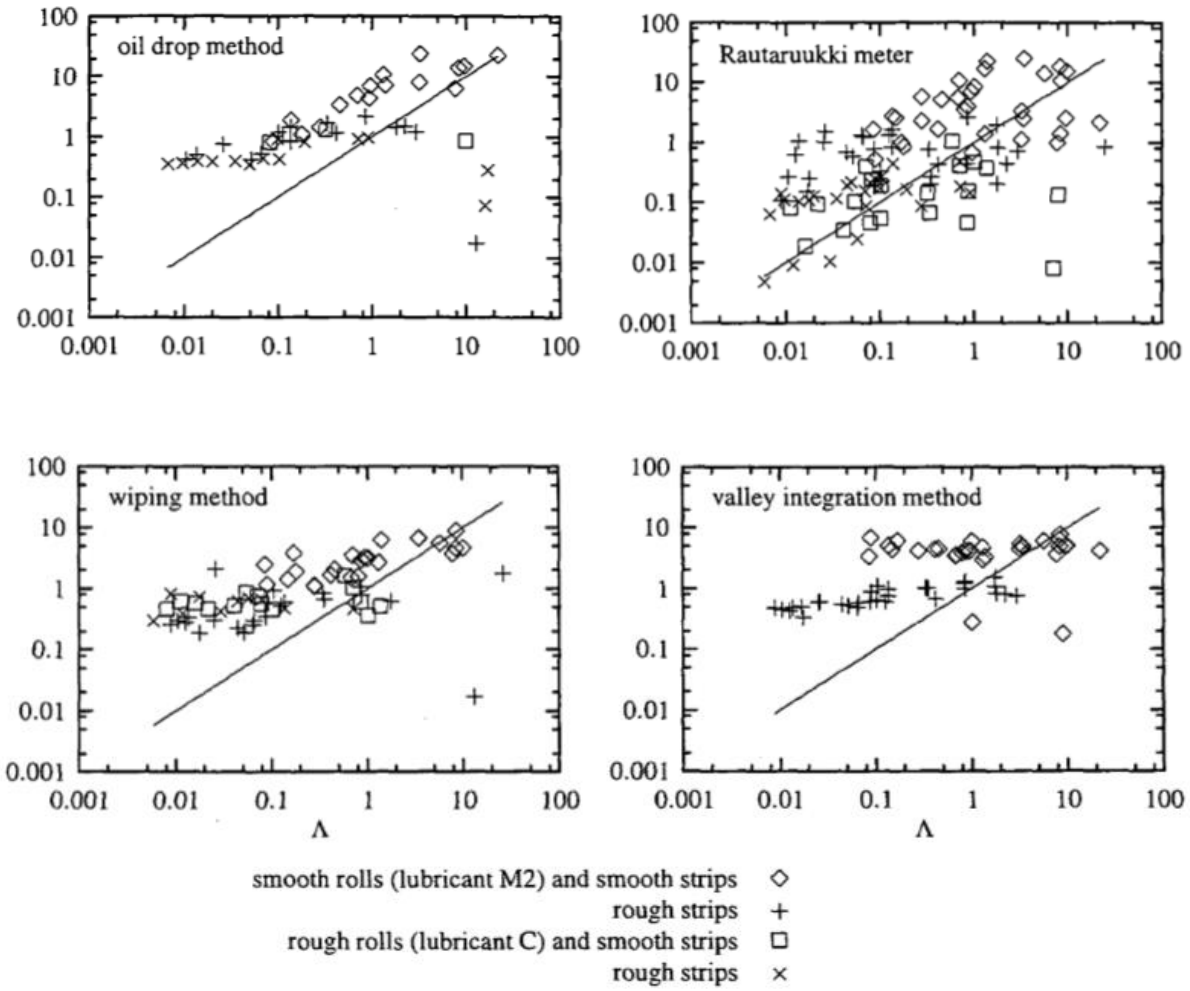

Figure 2-19: Oil film thickness results obtained from above mentioned techniques [57]

As shown in the figures above, the results obtained from these techniques are in good agreement since their results follow the same trend.

Azushima and Inagaki [65], employed the numerical method of the starvation model to calculate the inlet oil film thickness in cold sheet rolling. The method is based on the relationship between material surface brightness and thickness of the applied oil. The oil droplet-in-water emulsion was used as a lubricant during the experiment. The experiment was conducted with 0.4mm thickness, 30mm wide and 300mm length of the sheet metal and coil rolling. The emulsion was prepared in different beakers, one having 10% and another 20% of the polyoxyethylene alkyl ether in the same volume of water. The surfaces of the roll and the workpiece were cleaned with benzene before the experiments. The 15% of the sheet metal reduction was obtained by rolling at a 30 m/min rolling speed. The surface brightness of the material was measured at five different locations on the surface of

the rolled sheet, with a brightness meter, after the experiment. The inlet oil film thickness at the roll-bite was calculated with the aid of the oil and the surface brightness relationship and expressed as follows:

$$Gs = 335ln - {h_o}^2 6.65 \quad \text{2-38}$$

Gs is the surface brightness of the rolled sheet while the h_o is the inlet oil film thickness.

The values of the inlet oil film thickness of 0.097µm (10% emulsion) and 0.129 µm (20% emulsion) were obtained from the sheet metal and roll interface. The values of 0.270µm (10% emulsion) and 0.0.324µm (20% emulsion) were also obtained from the coil to roll interface respectively.

Azushima and Inagaki [40], reviewed and adjusted the 2009 technique with the application of the same materials and procedure. The modification of the technique was due to the inaccuracy of the calculation of inlet oil film thickness of the coil rolling during the rolling process. The oil film plate on the roll and a strip surface was considered to determine the inlet oil film thickness for the coil rolling. This technique was re-expressed as follows:

$$Gs = -6.65 - 335 \ln (h_o) \quad \text{2-39}$$

The values of inlet oil film thickness obtained were improved from 0.097µm to 0.192µm (10% emulsion) and from 0.129 µm to 0.301µm (20% emulsion) for the sheet metal. While the values of inlet oil film thickness for coil rolling improved from 0.270µm (10% emulsion) to 1.197µm and 0.0.324µm to 2.058µm (20% emulsion).

2.6.4 Internal Ultrasonic Reflection Measuring Technique

Dwyer-Joyce and Hunter [66] used ultrasonic reflection sensors internally installed in the roll, as shown in Figure 2-20, to measure the film thickness of the lubricant at the metal-to-roll interface during the cold metal rolling process.

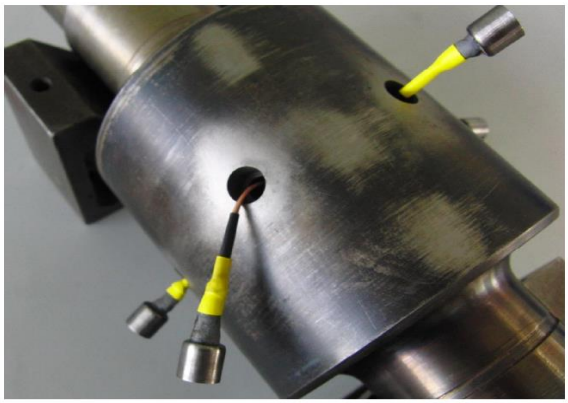

Figure 2-20: Roll with insert sensors [66]

The sensors were mounted in the radial holes drilled facing outwards from the roll so that the transmitted signal would be apparent to the roll-bite. This experiment was carried out with a pair of 108mm roll diameter of high rolling mills. The initial thickness of the metal strip was taken and lubricant was applied to both sides of the strip. Finally, it was manually fed into the rolling gap of the mill during the rolling process [66].

The electrical pulse was generated and sent from the pulser/receiver unit to the sensors to the metal-to-roll interface with the ultrasonic equipment. The reflected signals from the roll-bite surface were captured and stored for further analysis. The reflection coefficient of the reference and reflected signal captured from the roll-bite surface was calculated by dividing the reflected FFT by a reference FFT signal. The obtained reflection coefficient was used to calculate the oil film thickness at meta-to-roll interface with the of the spring model.

The summary of the oil film thickness measurement techniques reviewed, with research year and authors' names, is presented in Table 2-5. The disadvantages of these techniques are explained in Section 2.7.

Table 2-5: Oil film measurement techniques reviewed with the names of authors

Authors/Date	Method
Whetzel and Rodman (1956) [62]	Wiping off method
Katayama (1967) [63]	Oil drop on the surface of the strip
Azushima (1978) [64]	Valley Integration Method
Cuperus (1998) [57]	Rautaruuki meter
Azushima and Inagaki (2009) [65]	Numerical method of the starvation model
Azushima and Inagaki (2011) [40]	Numerical method of the starvation model
Dwyer-Joyce and Hunter [66]	Internal ultrasonic reflection measuring technique

2.7 Limitation of the Experimental Measurement Methods

The above reviewed experimental methods are straightforward and require little knowledge to conduct. They also appear to give reliable and promising experimental results. However, none of the experimental procedures were conducted with the application of the ultrasonic technique in any form. Moreover, most of the results obtained were from the inlet zone of the roll-bite, while the oil film thickness obtained at the work zone was based on the inlet film thickness. Furthermore, all of these methods based their lubrication on a small amount of oil volume, which means the techniques usually give rise to oil starvation at an inlet region of the roll-bite during the rolling process [40]. Therefore, these techniques are only meant for experimental purposes and cannot be implemented for large industrial projects.

In addition, the internal ultrasonic measuring technique employed by Dwyer-Joyce and Hunter [66] is more reliable and feasible for oil film thickness measurement than the above mentioned methods. The oil film thickness obtained crossed the roll-bite with this technique according to the report from the scholars. However, the internal ultrasonic technique installation is expensive and complex to build. It also requires significant roll modification.

Furthermore, the plug used to insert the sensor also caused some marks on the surface of the strip during the rolling process. This is acceptable for research, but unacceptable for production.

2.8 Conclusion

Various methods adopted by scholars to determine the value of the friction force have been reviewed. Furthermore, several experimental methods to measure oil film thickness during cold rolling have been discussed. The benefits and the contributions of the methods have been analysed, with limitations also discussed. The measurement of the oil film thickness using an internal ultrasonic technique was also examined.

It is important to develop a new measurement technique to measure the oil film thickness at the metal-to-roll interface, in order to overcome the limitations of the measurement techniques mentioned above. An external ultrasonic sensor layout that is the target of this research has not been applied to the measurement of oil film so far. Dwyer-Joyce and Hunter [66] made use of an internal ultrasonic arrangement and the limitations of this technique have been considered above. This new design will provide solutions to all these shortcomings of the internal ultrasonic and other approaches mentioned above. The method only requires a minor modification of the roll, and does not cause any marks on the surface of the strip during the rolling process. The technique is non-invasive and non-destructive. It is not complex, very cheaper and easier to install more than the internal ultrasonic measurement method.

Chapter 3

Ultrasonic Background

This chapter describes the fundamentals and principles of the interaction of ultrasonic waves with boundaries between different media in terms of the acoustic impedance. As explained in this chapter, the response of an ultrasonic wave at a boundary is determined by the acoustic impedance mismatch, the stiffness of the surfaces and the frequency of the sensor used. Determination of a film thickness at the interface of two materials by the ultrasonic spring model is also reviewed.

3.0 Introduction

Ultrasound is the propagation of waves in a frequency range of above 20 kHz , where the frequency is conventionally considered to be inaudible to human hearing. The ultrasound wave travels from one material to another due to the mechanical deformation of the medium. The energy transmitted is in an orderly movement as kinetic energy within the particles of the medium moves. The energy propagates due to electrostatic bonds of the particles that react like a spring. This stiffness of the bond permits the particles to rebound and re-collide with each other and causes the displacement of the adjacent particles. The disturbances and movement of the particles are transmitted to the next one step by step within the medium and the waves propagate continuously through the medium [67].

Ultrasonic techniques have been applied to measurement, monitoring and non-destructive mechanical testing in engineering and other fields such as medicine, construction and materials since the late 1990s. It is a non-intrusive and non-harmful method that always measures the ideal properties of the material interface [68]. Figure 3-1 shows the various types of ultrasound by the frequency range.

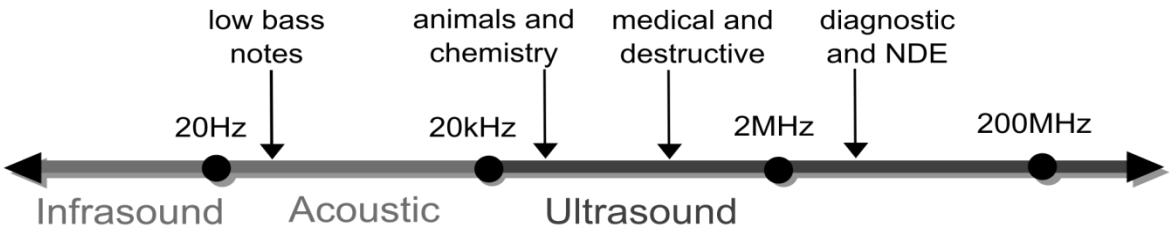

Figure 3-1: Acoustic sound ranges and frequency values

The first range, from 0 - 20Hz, is known as infra-sound. This is followed by the acoustic sounds in the frequency range of 20 Hz - 20 kHz. Finally, ultrasound is the last frequency ranging from 20 kHz to 200 MHz. Therefore, frequency is the number of the completed cycles of the sound of a wave per unit time and is measured in cycle per seconds (cps) or Hertz (Hz).

3.1 Generating Ultrasonic Wave

Ultrasonic waves are generated with the aid of the different components that combine to form an ultrasonic unit. The ultrasonic unit consists of transducers, a pulser and digitizer unit. The details of these components are fully discussed in Sections 3.1.1 and 3.1.2.

3.1.1 Ultrasonic Transducer

The transducer is a device that converts an electrical pulse generated from a pulser / receiver unit into a mechanical vibration. It also converts the returned mechanical vibration from the tested materials into electrical energy during the ultrasonic measuring process. Types of the transducer are shown in the tree diagram (Figure 3-2).

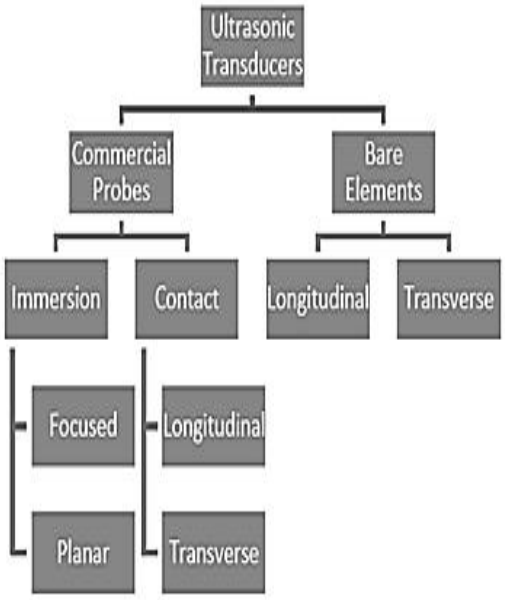

Figure 3-2: Tree diagram shows types of ultrasonic transducers

Figure 3-3 shows a schematic diagram of a commercial transducer [69]. The components of the sensor shown in Figure 3-3 are important to illustrate how the parts are arranged and interrelate.

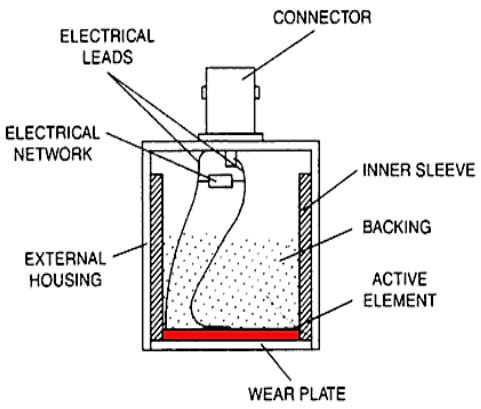

Figure 3-3: Standard/commercial transducer [70]

The transducer is one the essential components of the ultrasonic instrumentation system, which is incorporated with active elements. It converts the signals from the electrical to mechanical vibration and mechanical to electrical signals. The active component part of a transducer is made with different materials such as quartz (SiO_2) and barium titanate ($BaTiO_3$). Piezoelectric ceramic material is the most commonly used for the production of transducers because it can quickly be cut into different forms to generate various resolutions and sensitivity waves.

Barium titanate was the first piezo-ceramic produced in the late 1960s and was followed by lead zirconate titanate composite material that is now mostly used in ceramic transducers. The desired transducer frequency depends on the thickness of its active element; the thinner the active element the higher the frequency of the transducer [70].

The sensor performance is influenced by the nature of its material, the mechanical and electrical construction of the transducer and the applied load. The ultrasonic transducers are produced in different forms, which result in its properties such as frequency, bandwidth and its focusing ability.

Generally, the choice of the sensor is based on its sensitivity and resolution of the system. The sensitivity of the transducer is defined as the capacity to spot small discontinuities. The higher the frequency of the transducer, the higher the level of the sensitivity, but the lower the penetration depth [71]. There are many different sizes and shapes of transducers such as direct contact, immersion, dual element, delay line and angle beam transducers. They are grouped according to their applications. Images of the contact and immersion transducers explained above are shown in Figures 3-4 and 3-5 respectively.

Figure 3-4: Standard/commercial direct contact transducer

Figure 3-5: Standard/commercial immersion transducer

Images of the different sizes of the piezoelectric element described above as an active element (Fig. 3-3) of commercial transducer are shown in Figure 3-6.

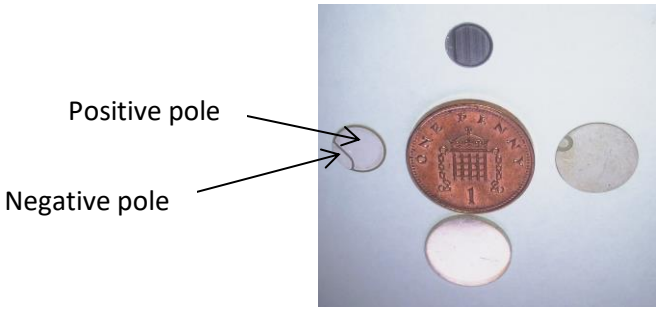

Figure 3-6: Typical piezoelectric element sizes

The piezoelectric element contains two different poles (positive and negative) to connect with the positive and negative poles of the cable during ultrasonic wave transmission. It has the same operating principle as the commercial transducer for the generating, sending and capturing of the reflected data during the ultrasonic signal transmission process. For this reason, it is generally used as an alternative to the commercial transducer. A piezoelectric element is very cheap compared with the commercial transducer and is easy to cut into different sizes and shapes.

3.2 Fundamentals of Sound Waves

3.2.1 Wave Propagation

The energy of wave propagation occurs through the transmission of kinetic energy from particle to particle of the host medium due to the electrostatic interaction between particle bonds (Figure 3-7). Elastic wave propagation is the process by which the wave transmits within the medium. This occurs due to the conversion of the electrical pulse into mechanical energy from the transducer.

Moreover, if the particles of the medium are compressed or in tension beyond the medium's elastic limit, the force is transmitted to the adjacent particles according to the stiffness of the bonds. This force causes the adjacent particles of the medium to move and set other particles to oscillate continuously.

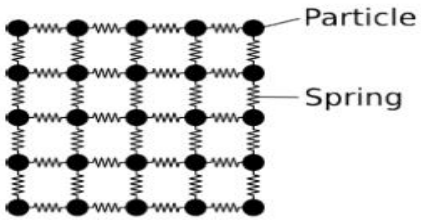

Figure 3-7: Schematic diagram of a model of an elastic body

Since the bonds between the particles are guided with the spring during the oscillations, as indicated in Figure 3-2 above, the rate of propagation of elastic wave transmission through the medium depends upon the material and the phase in which it exists. For the wave to be elastic, the initial and final locations of the particles must be identical following its passage. This is the situation for Non Destructive Test (NDT) applications [72].

3.2.2 Wave Mode

The propagation of sound waves can be in a longitudinal or shear in a bulk wave transmission, depending on the direction of the movement of the particles. These types of sound waves are fully discussed in Sections 3.2.2.1 and 3.2.2.2 respectively.

3.2.2.1 Longitudinal Wave

A longitudinal wave is one produced by the compression force of the host medium in which the particle vibration occurs in the same direction as the propagation wave. The compressed and stretched movement of the elastic bands within the particles are shown in Figure 3-8.

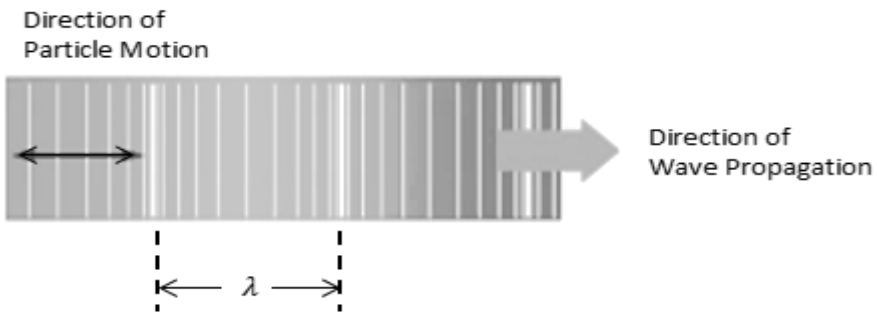

Figure 3-8: Schematic diagram of longitudinal wave

The longitudinal wave can also be generated in both liquid and solid media due to its ability to travel through the atomic structure during the compression and the refraction movement of the media.

3.2.2.2 Shear Wave

Ultrasonic shear waves are transverse waves in that their particle travel perpendicular or at right angles to the wave propagation direction as shown in Figure 3-9.

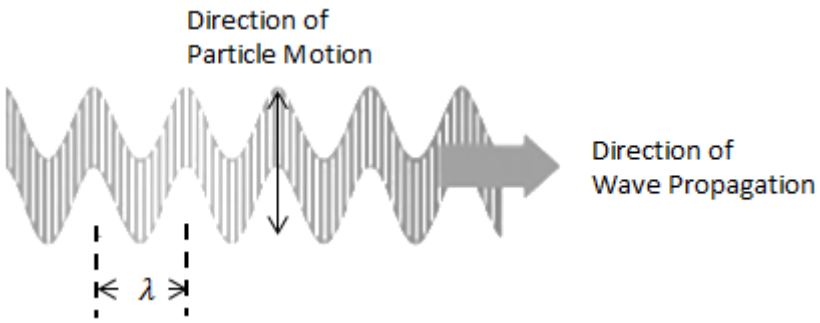

Figure 3-9: Schematic diagram of shear wave

Shear waves propagate efficiently through solid acoustic material. They are not propagated into liquid or gaseous materials. The shear waves are relatively weak compared with longitudinal ones. Shear waves are usually generated by the conversion of the longitudinal wave when it strikes the medium at an angle [72].

3.2.3 Ultrasound and Material Properties Relationship

The stiffness behaviour and damping properties of a given material can determine how a wave will propagate. The stiffness behaviour affects the wave speed of ultrasound, while the signal energy absorption and a reduction in amplitude of the waveform depend on the material particles' interactions and distance from the source. Therefore, material properties' effects in relation to ultrasound behaviours are outlined in the following subsection.

3.2.3.1 Speed of Sound

The rate of propagated sound waves depends on the properties of the material because the sound wave travels at a different speed in a material. Sound wave propagation depends on the density of a host material, being a primary function of the mass and volume occupied by the particles. It also depends on elastic forces within the particles of a medium that is

controlled by the amount of elastic constants such as, bulk modulus, shear modulus or the Young Modulus of the medium. The sound wave moves rapidly in the solid medium compared to a gaseous medium due to the compact ability of the material particles in solid form [73]. The propagation of sound waves in a material at a given time is defined as a product of frequency and wavelength. It is expressed as follows:

$$c = f\lambda \qquad 3\text{-}1$$

While c is the speed of sound, and it is measured in m/s^2, f is the frequency of the sound wave and it is measured in (Hz) and,λ, is the wavelength and it is measured as (m).

3.2.4 Fundamental Terminology of Ultrasonic Pulse

The terminology used to describe the ultrasound generated pulse is briefly described with the full details of the captured and processed signal description.

3.2.4.1 Frequency and Bandwidths

When the ultrasonic transducer is executed with an electric pulse, it becomes deformed and sets up a vibration that travels a number of cycles through the elastic medium, such as a liquid or a solid form. The decay of the transducer oscillation depends on its level of coupling and the damping ratio.

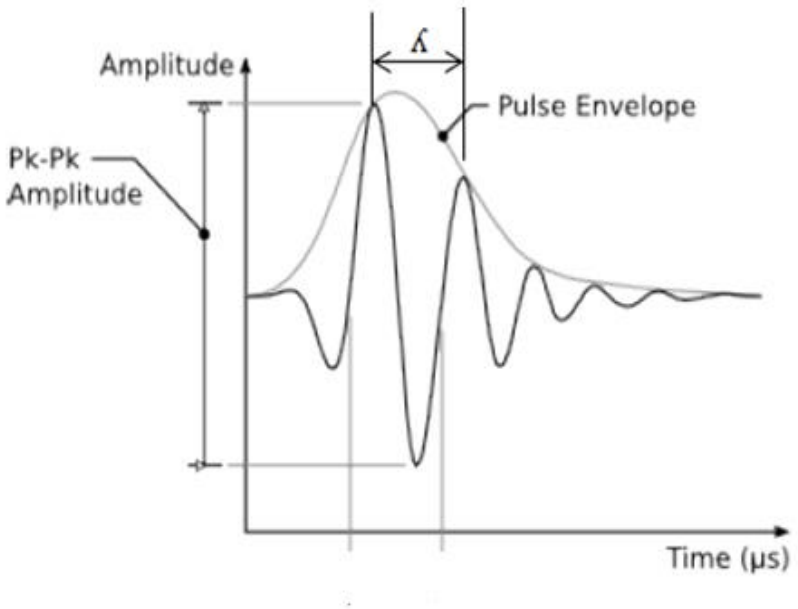

Figure 3-10: Schematic diagram of ultrasonic waveform in time domains [74]

Figure 3-10 shows the ultrasonic pulse waveform in the time domain. The peak-to-peak value of the signal indicates the strength of the computed signal. The transformation of the time domain of captured signal into the frequency domain provides the amplitude range, categorizing the frequencies of the transducer used, as shown in Figure 3-11.

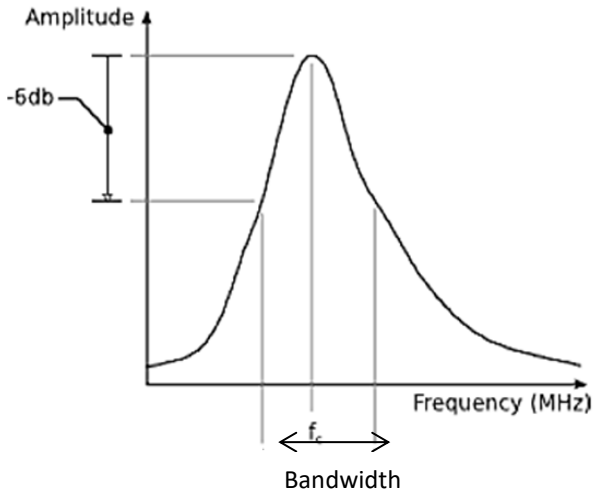

Figure 3-11: Schematic diagram of ultrasonic bandwidth in frequency domains [75]

Figure 3-11 shows the excitation of a transducer within the complete frequency a signal containing a range of frequencies is called a bandwidth. The bandwidth of the signal shows the range of useful frequencies and is typically set in terms of a proportion of the centre frequency.

3.2.5 Acoustic Impedance of Materials

Acoustic impedance is a material's ability to transmit ultrasound transmission from one material to another. The acoustic impedance property of the material is very useful in assessing ultrasound behaves at the interface of two different types of material. It is also reliable when estimating the acoustic transmission and the reflection at the interface of two different materials with various impedances [76]. Finally, it is a crucial consideration in the transducer design. The acoustic impedance of a material is a product of density of the particular host medium and wave speed that travel through it, and it is calculated as follows:

$$z = \rho c \qquad 3\text{-}2$$

The unit of Rayl (Pa.s/m^3) or $Kgm^{-2} \times 10^6$.

The transmission of signals across two materials boundaries depends on the nature of the bond of the materials interface and the acoustic impedance similarities of the materials. The difference in acoustic properties of the two materials is usually referred to as the impedance mismatch of the material.

3.2.6 Law of Reflection

Reflection is the diversion of an incidence ray direction when it hits the interface of the medium at an angle and is reflected at the same incidence angle, as indicated in Figure 3-7. Therefore, the Law of Reflection states that on a smooth surface, the angle at which an incidence wave hits the surface is equal to the angle at which it is reflected [77]. As illustrated (Figure 3-7) the incidence wave OP (v_1) strikes the interface of the specimen at an angle θ_1 at point **O**, and the reflected OQ (v_2) of the incidence ray at an angle θ_2. This is achieved with the aid of an imaginary line at point **O,** perpendicular to the interface of the specimen and is known as normal to the interface. The angle of incidence θ_1 is the same as the angle of reflection θ_2. Therefore, the Law of Reflection is stated as follows:

$$\theta_1 = \theta_2 \qquad 3\text{-}3$$

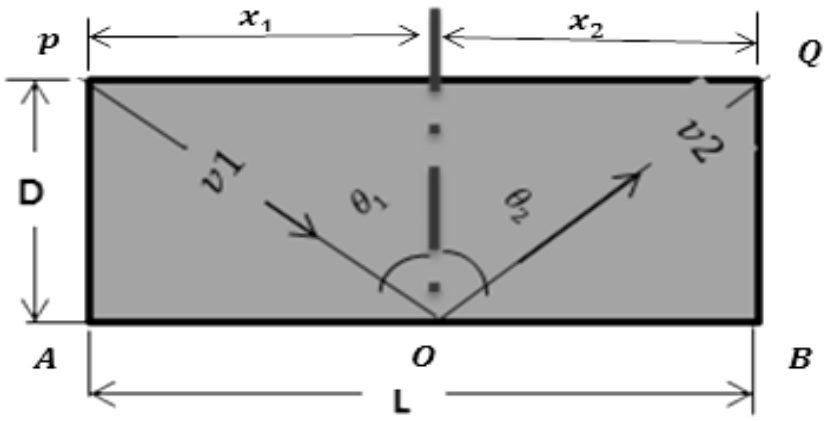

Figure 3-12: Diagram of the incidence and reflected rays

As shown in the figure above, the ultrasonic wave is reflected at the boundaries where there is a difference in acoustic impedances of the material involved. The reflection and transmission of the sent ultrasonic are calculated with the aid of the equation 3-3.

3.2.7 Attenuation

Attenuation is another property of sound waves. It is defined as the gradual reduction of sound wave energy as it travels through a material. The sound wave intensity diminishes in addition to the rate at which its amplitude peak reduces with distance as it travels through a material [78], as indicated in Figure 3-8. As shown in Figure 3-13, the amplitude and time-of-flight of the 1st reflection is 1500 mV and 7 µsec. This is followed by the 2nd reflection which has its amplitude and the time-of-flight value reduced to 1300 mV and 14 µsec and the final reflection (3rd) amplitude and time-of-flight is 1100 mV and 21 µsec on the same medium respectively. This transmission process, from the highest to the lowest value with increases in time-of-flight, is referred to as attenuation of the signal.

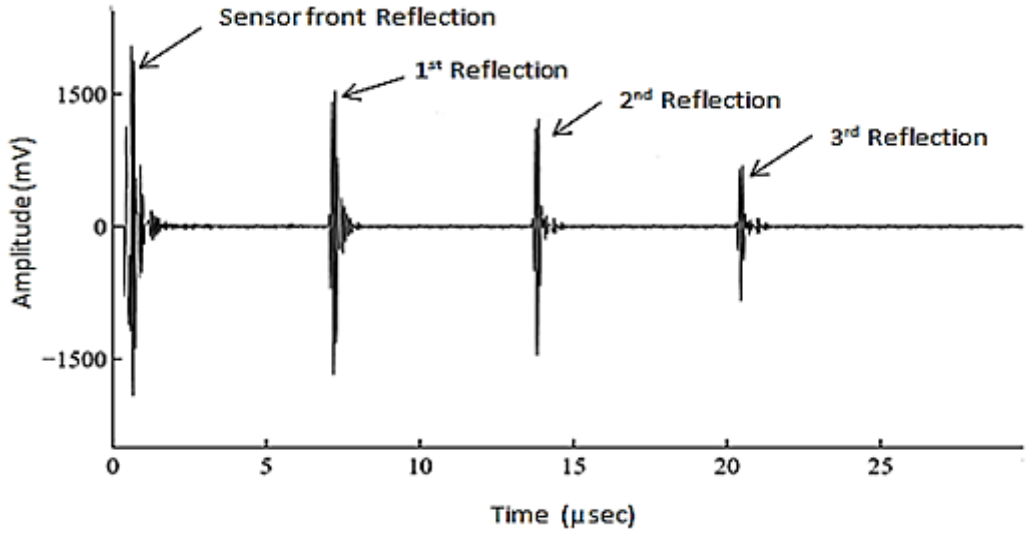

Figure 3-13: Ultrasonic wave attenuation within the medium

Attenuation is a function of the material properties. It produces an effect which weakens further the sound energy travelling through the medium. The attenuation of sound waves is useful in the determination of the actual distance a wave can be transmitted in a material before its energy is finally reduced. Ultrasonic Wave attenuation, therefore, is defined as the rate of ultrasound wave decay as it propagates through a medium, and is expressed as:

$$I = I_o e^{-\alpha x} \qquad [72]\ 3\text{-}4$$

α ($N_p m^{-1}$,) is the attenuation of the wave propagating at a distance, x (m) in a given material. I_o and I are the initial and final amplitudes of the wave pressure. The units of the

attenuation coefficient are in Nepers per meter and can be converted to decibels per meter by dividing by 0.1151 [77]. The causes of the wave energy reduction during the ultrasonic transmission are categorized as follows: scattering and absorption.

3.2.7.1 Absorption

Absorbed ultrasound is one of the effects responsible for the attenuation of the signal during its propagation through the material. It is the process by which the sound wave energy is converted to other forms of energy, thereby creating a reduction in strength as it travels through the material. Moreover, it usually turns into heat energy due to hysteretic losses in the metal bonding as a result of the particles vibrating at their positions. The rate of attenuation of the signal by absorption effect depends on the signal's frequency. The higher its frequency, the more the vibration of the material's particles, and the higher the absorption rate of the ultrasound energy.

3.2.7.2 Scattering

Scattering is the flection of sound waves in many different angles on the medium's surface due to its irregularity. Scattering is one of the factors which can cause the sound wave energy reduction. This is due to the loss of the energy concentration by reflections of the waves in many different directions. The change of direction of the sound wave occurs due to the presence of discontinuities in the material's body and its non-homogeneous nature. If the discontinuities of the medium are larger than the wavelength of the ultrasound transmitted wave, it will scatter more and reduce its penetrability energy.

3.2.8 Pulser /Receiver and Digitiser Unit

Ultrasonic waves were generated using a Film Measurement System (FMS) which consists of pulser and receiver unit as shown in Figure 3-14.

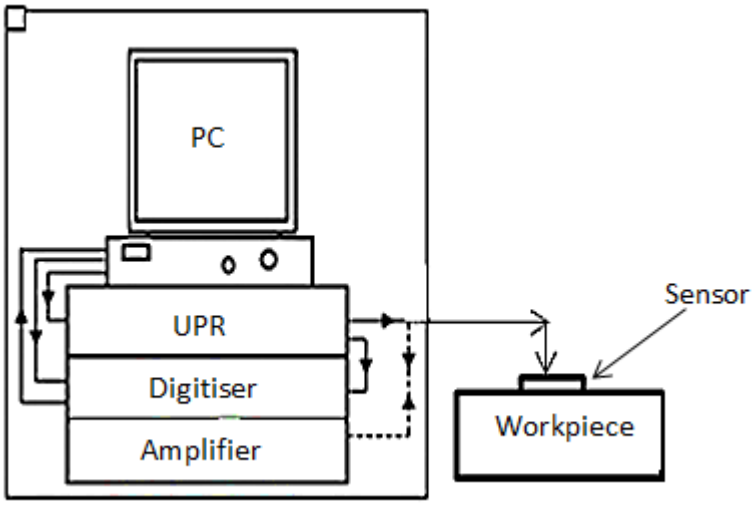

Figure 3-14: Schematic diagram of FMS ultrasonic equipment

This machine was built by Tribosonic/NDT Solutions Ltd purposely to generate, capture and process the reflection of the transmitted signal during the ultrasonic applications.

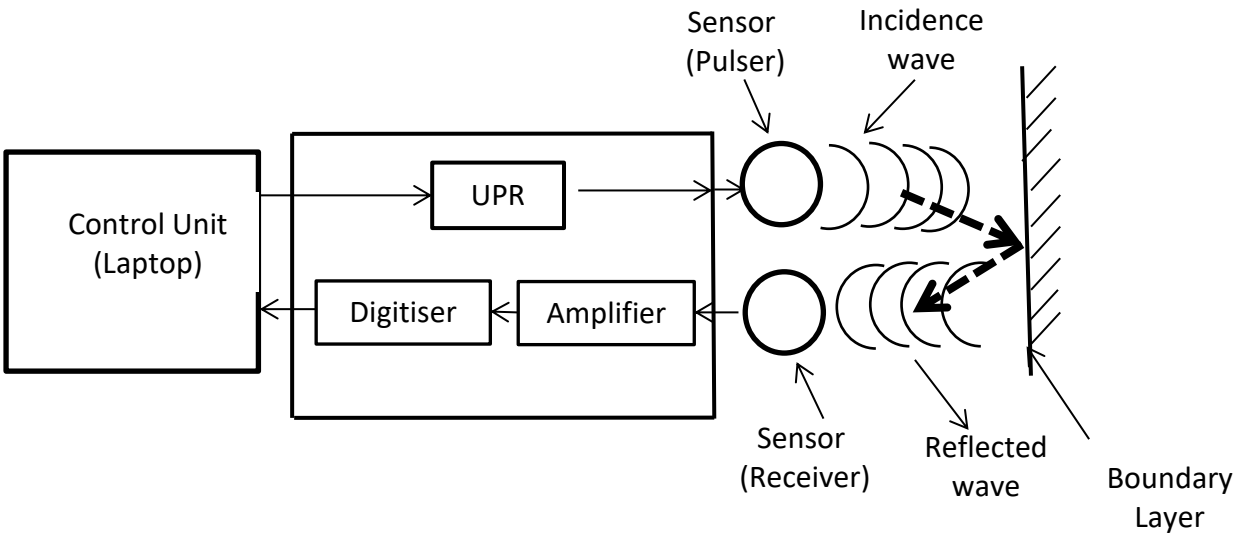

Figure 3-15: Line arrangement of ultrasonic pulsing and receiving apparatus

Figure 3-15 shows the typical line arrangement of the apparatus for the generation and processing of ultrasonic waves that are in oblique form. The configuration consists of a computer to display, control and monitor the wave properties. The apparatus contains an ultrasonic pulser/ receiver unit (UPR) which was used to generate a series of short duration voltage pulses to excite the piezoelectric transducer. The transducer is driven by the pulser/receiver unit, while both the pulser and digitiser are controlled by a PC.

The PC sends a controlled signal that triggers the pulser unit of the UPR to generate a high-frequency voltage pulse. The voltage pulse actuates the piezoelectric plate of the transducer, which converts the electrical excitations to ultrasonic signals, and these are consequently emitted through the medium to the targeted contact interface. The reflected ultrasonic signals from the interface strike the piezoelectric plate which then converts the motion of the ultrasound wave to a high-frequency voltage. The high-frequency voltage was then passed to the amplifier unit which amplifies the voltage signals before passing them to the receiver unit for onward transfer to the digitizer. The function of the digitizer is to convert the analog signals obtained from the receiver to digital form. The digitizer provides a wide range of bandwidths, sampling rates as well as dynamic range so that the signal frequency matches the broad spectrum of the ultrasonic measurement needs. For the present studies, the reflections were sampled at a resolution of 12 *bits* and at a rate of 100 million *samples/second*. The PC displays both the emitted and reflected signals.

3.2.9 Pulse Capturing Techniques

Reflected ultrasonic waves can be obtained either by pulse-echo or pitch-catch techniques, depending on the number and the position of the transducer used. In the pulse-echo method, a single sensor is used for both transmitting and receiving the ultrasonic signal, whereas in the pitch and catch, two transducers are used to send and receive the signal.

3.2.9.1 Pulse-echo technique

In the pulse-echo technique, the signal transmits through the specimen until it is reflected back at the interface of the sample to the same transducer as is illustrated in Figure 3-16.

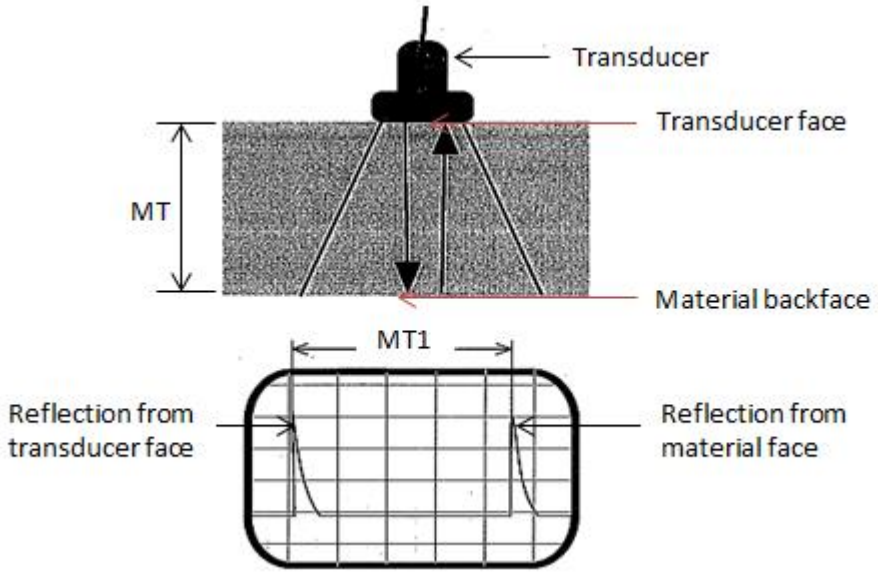

Figure 3-16: Schematic diagram of the pulse-echo signal transmitted layout

Figure 3-16 shows the signal transmitted from the sensor into the test material (MT). The two reflection signals appear as displayed in the ultrasonic graph shown above. The first reflected signal at the probe face is the initial pulse signal from the probe. The second reflected signal is from the material back face that is the echo of the transmitted signal from the back wall of the material. The distance (MT1) is the distance between the reflection from the sensor face and material back face, which represents the thickness of the used material.

3.2.9.2 Pitch-catch Technique

The pulser generates an electrical pulse electrifying a transducer and converting the electrical pulse input into mechanical energy, producing an ultrasonic wave. The wave transmits through the specimen until it is received on the other side of the material of the second transducer that acts as a receiver. Two sensors are also involved in the transmission of the signals in this technique while the mode of the sensor arrangement is based on Snell's Principle (Section 3.2.6). This principle states that the ratio of the angle of incidence and the reflection waves is equal to the ratio of the velocities of incidence and reflection of the waves that pass through the medium [79].

The transducers for the pitch and catch technique can be arranged in the opposite direction to each other, as shown in Figure 3-17. The incidence wave was transmitted perpendicular to the interface of the specimen and caught by a different second transducer acting as a receiver.

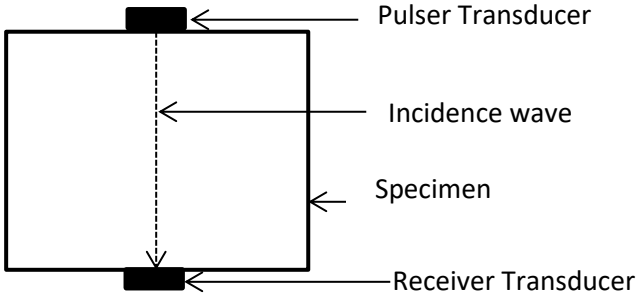

Figure 3-17: Pulse and catch technique with transducer in opposite arrangement

In- addition, the pitch-catch technique can be the mode of transmission of wave at an angle through the same material from one side to the other of the material, as shown in Figure 3-18.

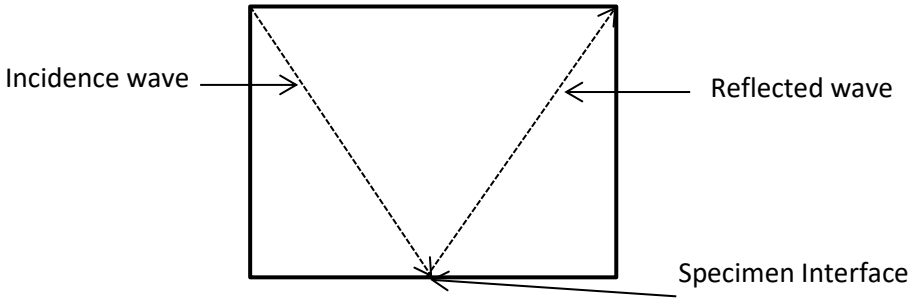

Figure 3-18: Pulse and catch technique with transducer arrangement edges

The configuration of the pitch and catch arrangements shown in Figures 3-17 and 3-18 depend on the area of application, but they both transmit and receive the wave reflection by using different sensors.

3.3 Reflection of Sound at an Interface

When an ultrasonic wave strikes an interface between two different materials that are entirely bonded together, part of its energy is propagated in the second medium, while the remaining energy is reflected back to the initial medium. The total amounts of the energy transmitted to the second material and quantities of the reflected back wave to the first

material depend on the acoustic impedance of the two materials. Furthermore, the involved media's interface is never perfectly smooth and thus always affects the transmission of the signal to the second media [80].

3.3.1 Perfect Interface

When an incidence ultrasonic wave is normal to the perfect boundary of the two materials, the proportion of the amplitude of the reflected wave pressure (A_1) to the amplitude of the incidence wave pressure (A_2) is known as the reflection coefficient and is expressed as:

$$R = {}^{A_1}/_{A_2} \qquad 3\text{-}5$$

However, the reflection of the wave depends on the properties of the materials and the boundary condition of the two materials. If the materials are different, as shown in Figure 3-18 (a), under the perfect interface, part of the incidence wave is transmitted and part of the wave reflected (Fig. 3-19 (a)).

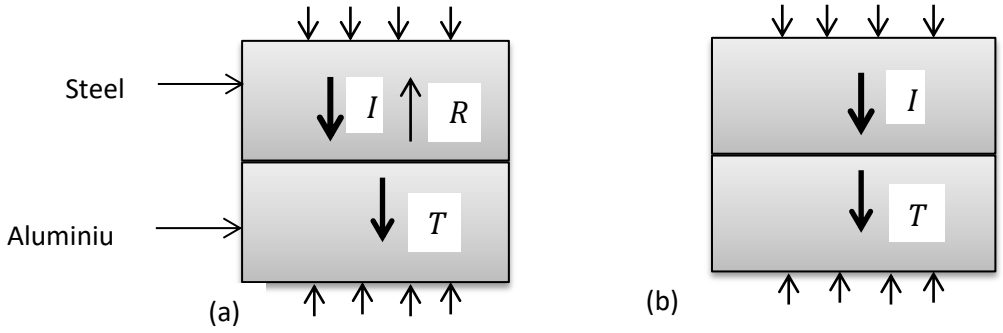

Figure 3-19: Tribology interface of perfect contact (a) similar media, (b) dissimilar media

The quantity of this reflected wave depends on the acoustic properties of the two materials, respectively. Therefore the reflection coefficient of the ultrasonic wave of the reflected signal is obtained by the following equation:

$$R = \frac{Z_2 - Z_1}{Z_2 + Z_1} \qquad 3\text{-}6$$

Additionally, if the wave is transmitted through the same materials at a perfect boundary, then the entire incidence wave is transmitted to the second material without any reflection,

as shown in Figure 3-19 (b). According to equation 3-6, the reflection coefficient of the reflected wave is zero.

3.3.2 Dry and Rough Surface Contact

When an ultrasonic incidence wave hits the rough and dry interface of two different solid materials, its reaction can be seen as in Figure 3-20 (a).

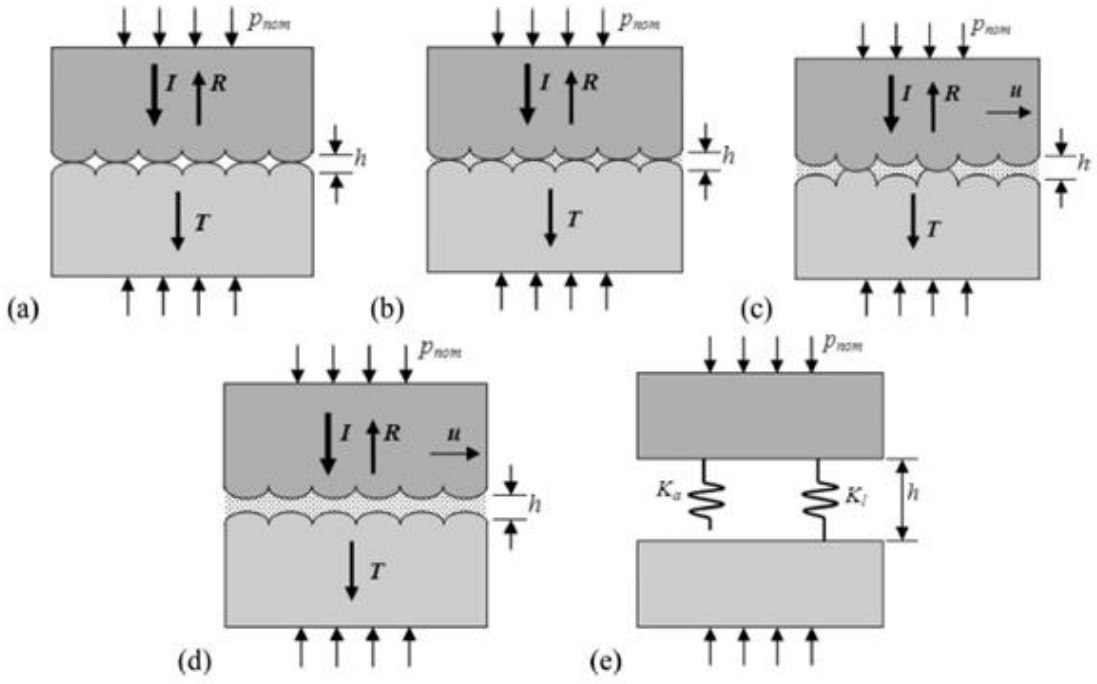

Figure 3-20: Tribology interface of (a) dry contact (b) wet contact (c) mixed lubrication interface (d) thick oil film contact (e) spring model representation [44]

As previously stated, the proportion of the amplitudes of the incidence and reflected wave, known as the reflection coefficient, depends on the stiffness of the interface of the two bodies involved. Kendall and Tabor [81] explained that, when the wavelength of the ultrasonic wave sent is larger than the size of the asperity contact, then the reflection of the wave from the interface of the used media is a function of the material interface stiffness. Therefore, the value of the reflection coefficient at the rough surface is obtained with the aid of the quasi-static spring model and expressed as follows:

$$R = \frac{Z_2 - Z_1 + i\omega(Z_1 Z_2 / K)}{Z_2 + Z_1 + i\omega(Z_1 Z_2 / K)} \qquad 3\text{-}7$$

[82][82][82][82][82][82][82][82]

While the reflection coefficient for the similar media is:

$$R = \frac{1}{\sqrt{1+\left({}^{2K}/_{\omega z\prime}\right)^2}} \quad 3\text{-}8$$

Because of the same acoustic properties of the materials ($z_1 = z_2 = z'$)

Where z_1, and z_2, refer to as the acoustic impedance of the material while ω is an angular frequency of the wave and is expressed as:

$$\omega = 2\pi f \quad 3\text{-}9$$

While K_a, is the stiffness of the dry contact and is expressed as:

$$K_a = {}^{-dp}/_{du} \quad 3\text{-}10$$

K_a is the stiffness of the rough contact area, and is expressed as the change in nominal contact pressure p, is required to cause the unit approach of the average lines of the medium surfaces. While *u*, is the mean separation lines of the two contacting surfaces. The stiffness of the contact area depend on the load applied; the higher the weight of the applied load, the greater the contact and stiffness in the area.

3.3.3 Oil Interface

If the lubricant is then introduced into the rough surface, as indicated in Figure 3-20 (b), an ultrasonic wave will also be reflected in the front face of the layer and some on the back face. For the thick lubricant layers', the reflected pulses will be separated, and it will be possible to distinguish the reflections in the time domain (Fig.3-20(d)). If the oil film thickness is slight, the reflected pulses closed together and behave as a single layer (Fig. 3-20(e)). The spring model approach used for the rough surface contact can also be applied to the measurement of the lubricant film's pressurised liquid stiffness K_l as a function of the bulk modulus (B) between the two infinite flat half spaces of the fluid and its thickness (*h*), as shown in the equation below:

$$K_l = {}^{\mathrm{B}}/_{\mathrm{h}} \quad 3\text{-}11$$

3.3.4 Mixed Lubrication Interface

The mixed lubrication interface consists of both liquid and solid contacts, as indicated in Figure 3-20 (c). As the asperity contact is crushed down by the materials, it leads to the

reduction of the oil film thickness and the solid contact becomes more significant as shown in Figure 3-20 (c). Therefore, the total stiffness K_t, at the interface is as a result of the asperity stiffness contact K_a, and the pressurized liquid stiffness K_l acting in a parallel form, as indicated in Figure 3-20 (e), is expressed as:

$$K_t = K_a + K_l \quad \text{3-12}$$

Due to the response of the sensors to the stiffness layers, the shear sensor has good responses to dry contact while the longitudinal sensor has effective responses to both wet and dry layers in the mixed interface respectively. Therefore, the reflection coefficient for the dry contact (asperities) will be obtained by the shear wave and reflection coefficients for the wet contact from the longitudinal wave as expressed in equation 3-6 above. The stiffness value for the dry (solid) contact K_a, obtained from equation 3-10, is expressed as follows:

$$K_a = \frac{\omega z}{2}\sqrt{\frac{1}{R1^2} - 1} \quad \text{3-13}$$

R_1 is the reflection coefficient of asperity contact obtained by shear sensor (if R_1 is equal to 1 it means no asperity contact, but if R_1, is less than 1 it means there is asperity contact). Additionally, the stiffness value for wet contact K_l, obtained from equation 3-11, is expressed as follows:

$$K_l = \frac{wz}{2}\sqrt{\frac{1}{R2^2} - 1} \quad \text{3-14}$$

$R2$ is the reflection coefficient of the wet contact obtained by longitudinal sensor.

The interface has both solid and liquid stiffness. Therefore, the normal stiffness denoted by K_σ is measured with a longitudinal wave while shear stiffness denoted by K_τ is also measured with shear wave. Both normal and shear stiffnesses are sum of their respective solid and liquid parts of the interface, expressed as:

$$K_\sigma = K_{\sigma a} + K_{\sigma l} \quad \text{3-15 (a)}$$

$$K_\tau = K_{\tau a} + K_{\tau l} \quad \text{3-15 (b)}$$

$K_{\sigma l}$ and $K_{\sigma a}$ are liquid and solid normal stiffness while $K_{\tau a}$ and $K_{\tau l}$ are solid and liquid tangential stiffness. Since liquid does not support shear load, the liquid tangential stiffness of $K_{\tau l}$ from the equation above will become zero (then K_τ is equal to $K_{\tau a}$) [32]. Then the longitudinal signal captured the total normal stiffness at the rolling bite interface. Therefore,

the lubricant stiffness is calculated by taking the dry stiffness value from the overall stiffness. This is done by the equivalent ratio of shear stiffness and average stiffness to the Poisson's ratio of the used material, and is expressed by the equation below:

$$\frac{K_{\tau a}}{K_{\sigma a}} = \frac{2(1-v)}{2(2-v)} \qquad 3\text{-}16$$

While the value of liquid normal stiffness $K_{\sigma l}$ is obtained from the equation 3-15 (a) above. Therefore, the oil film thickness was calculated by the liquid normal stiffness with the aid of the spring model, as expressed in the equation below:

$$K_{\sigma l} = \frac{B}{h} \qquad 3\text{-}17$$

while B is the bulk of the modulus of the applied oil and h is the thickness value of the applied lubricant at the interface of the roll and the metal during the mixed lubricant regime [44, 82-86].

3.4 Conclusion

The basic theory of ultrasound and its properties have been discussed in this chapter. This theory has been used to explain how ultrasonic waves are transmitted and reflected during their propagation through the medium. Additionally, generating ultrasonic wave components, the transducers, and pulser and digitizer unit, have been fully explained. Pulse capturing techniques have also been included in this section.

Finally, the reflection of sound waves from complete or perfect, rough, oil and mixed interfaces during the ultrasonic wave transmission have been fully analysed.

Chapter 4

Application of Ultrasonic Transmission Method to a Roll Model

This chapter describes two different configurations of separate experiments of normal and oblique incidence reflection, to study the metal-to-roll interface. A basic knowledge of ultrasonic approaches, illustrated in Chapter 3, has been used to design the sensor arrangement. The aim of these experiments was to determine the optimum ultrasonic sensor arrangement to study the metal-to-roll interface with minimal modification of the roll. Shear and longitudinal transducers were used to perform various tests in both configurations. The implementation of the chosen technique to study the roll surface conditions in Chapter 5 is based on the approach developed in this section.

4.0 Introduction

This non-destructive oil film thickness measurement technique has attempted to further develop the use of an external ultrasonic sensor to avoid all the challenges from the internal roll embedded sensor approach explained in Section 2.6.4. This chapter analyses two common conventional ultrasonic transmission modes with two different layouts of wave propagation. One mode consists of a metal block as a carrier of a longitudinal wave sensor for normal incidence pulse-echo design. The other consists of two longitudinal wave sensors externally mounted on the roll at an angle in a pitch-catch arrangement. The reflection of the sent signals for both layouts was captured and recorded for further processing. The pitch-catch transmission method was found suitable for this work due to the outcome of the experiments. The details of each test are explained in the remainder of this chapter.

4.1 Normal Incidence Sensor Carrier Approach

4.1.1 Basic Concept

The sensor carrier shown in Figure 4-1 was designed and manufactured from a 130mm by 65mm rectangular mild steel block.

Figure 4-1: Sensor carrier

The carrier was constructed with a 110mm internal diameter to accommodate the roll of 108mm diameter during the signal transmission process. The difference of 2mm radial was set-up between the roll and the sensor carrier to avoid direct contact during the rolling process. This radial clearance between the roll and the sensor's carrier was also made to accommodate the coupling gel for the proper transmission of the ultrasonic signal.

Figure 4-2 shows how the sensor carrier generated incidence signal hits the sensor carrier interface and is reflected back. This reflected wave is captured by the same sensor for further analysis.

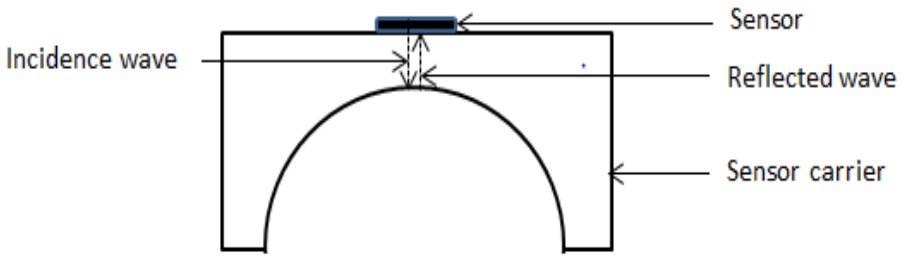

Figure 4-2: Sensor carrier with sensor

The coupling of the sensor carrier with a roll and the signal transmission process during the experimental work is shown in Figure 4-3. However, as illustrated in Figure 4-3 the meeting points of the sensor carrier and model roll were sub-grouped into two different interfaces. The first interface, at the top of the roll, is referred to as the sensor carrier-to-roll interface, and the second interface is at the bottom of the roll interface. Part of the generated signal is reflected from the first interface while the rest of the signal is transmitted through the roll. Almost all the signal transmitted through the model roll is reflected back at the second interface due to the discontinuity of the interface. However, this arrangement results in energy loss of sent signals at both interfaces before capturing back at the sensor mounted on carrier.

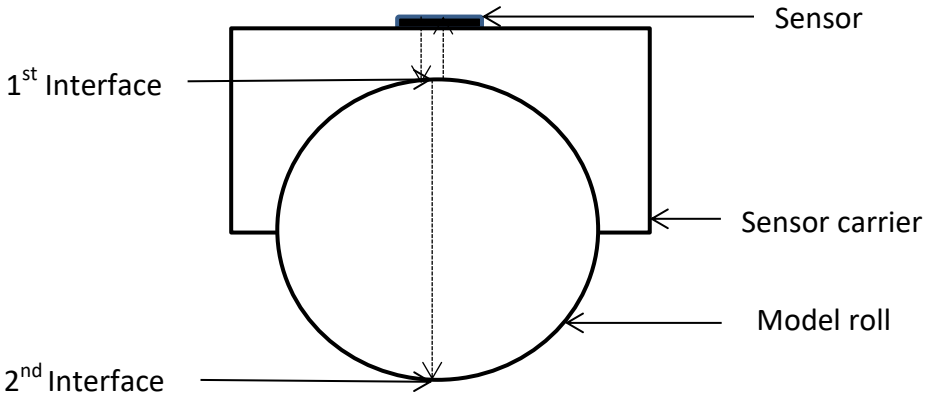

Figure 4-3: Sensor carrier coupled with a roll for signal processing

4.1.2 Experimental Method and Ultrasonic Apparatus

4.1.2.1 Transducer design

The piezoelectric elements were made from lead-zirconate-titanate due to its high sensitivity and excellent thermal stability of high operating temperatures. The longitudinal and shear piezoelectric elements, with a central frequency of 10MHz and 5MHz respectively, were used for the experiment for the provision of good penetration of signal into the metal-to-roll interface with clear and distinct reflected signals during the investigation. The piezoelectric element had a thickness of 0.2mm and a diameter of 7.0mm. The sensors were modified to form narrow strips of 2mm to improve the resolution, as shown in Figure 4.4.

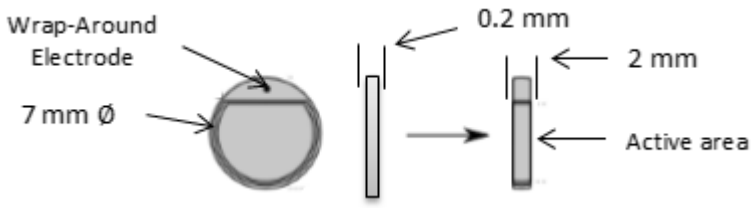

Figure 4-4: Inbuilt and modified piezoelectric element

The modification was done with the aid of two razor blades bonded together and separated by a suitable dimension for the space required within the two bonded edges. The cutting device was simultaneously used to remove the two 'wings' of the sensor, which left the central element strip.

The surface of the sensors was typically covered with gold or silver for the provision of a thin film layer for a more robust connection with the electrical wire during the soldering process. The transducers were bonded to the test specimen with M-Bond 610 onto the carrier surface, as shown in Figure 4-5. The carrier was put into the oven and heated to 100^0C adhesive curing temperature for 5 hours. The carrier with attached sensors was cured to remove the trapped air bubbles of the adhesive and also for the proper bonding of the sensor to the carrier surface. The material was allowed to cool in the oven to room temperature to avoid the re-contraction of the sensor.

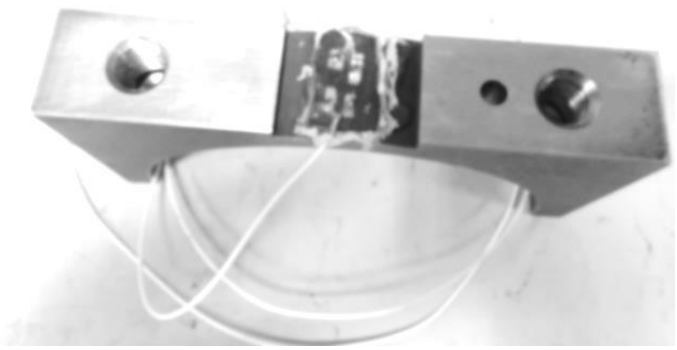

Figure 4-5: Instrumented sensor carrier

The cable was connected from the top of the element without disrupting the bond to the carrier surface (Fig. 4-5). The attached sensor layer was covered with epoxy to protect the sensor from rough handling during the investigation. The thinly cut elements were found to be more challenging to bond to the surface of a specimen and difficult to solder during the roll instrumentation.

4.1.2.2 Model Roll and Loading Frame

The metal-model roll used for the experiment was manufactured to 110 mm length by 110mm diameter with EN301 mild steel, as shown in Figure 4-6.

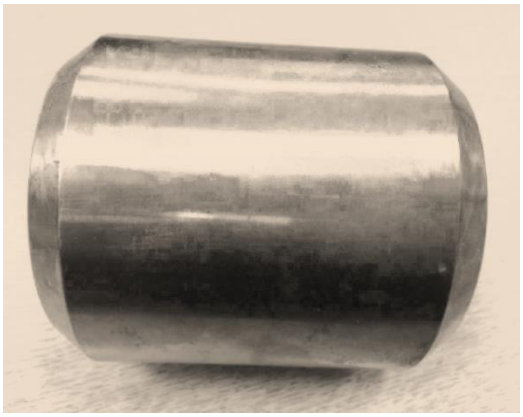

Figure 4-6: Model roll

Figure 4-7 shows the arrangement of the sensor carrier and the model roll before they were fixed into the hydraulic jack.

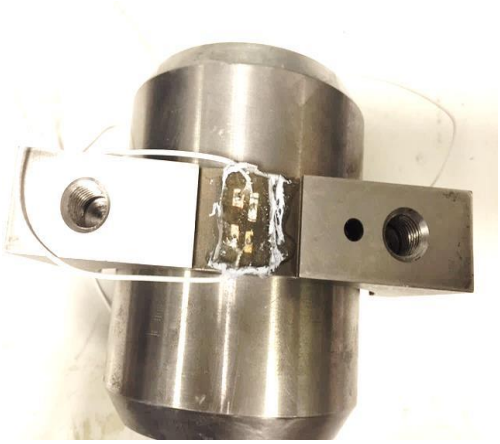

Figure 4-7: Model roll with sensor carrier

The experiments started by recording the reflected signal without any load on the carrier, as shown in Figure 4-8, as the reference signal. The model roll was inserted within the loading frame of the hydraulic jack shown in Figure 4-8**.**

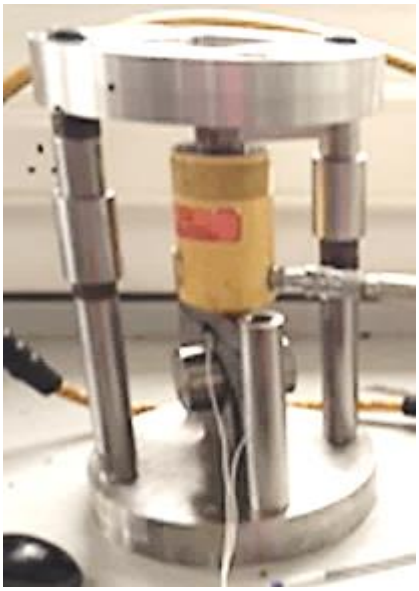

Figure 4-8: Model roll with loading frame

The jack was slightly raised against the model and loading structure to where line contact was established. The load was subsequently increased to 5kN, and the reflection of the

ultrasonic signal sent through the sensor at this weight was captured and recorded. This procedure was repeated as the pressures increased at 5kN intervals up to 20kN.

4.1.3 Data Acquisition and Processing

Figure 4.9 shows the schematic layout of the ultrasonic apparatus connected to the model roll with the sensor carrier. The apparatus consisted of a pulser-receiver unit, digitizer and a data acquisition unit. An industrial computer system contained all these components as PCI (peripheral component interconnect) cards, and was used to conduct this experiment.

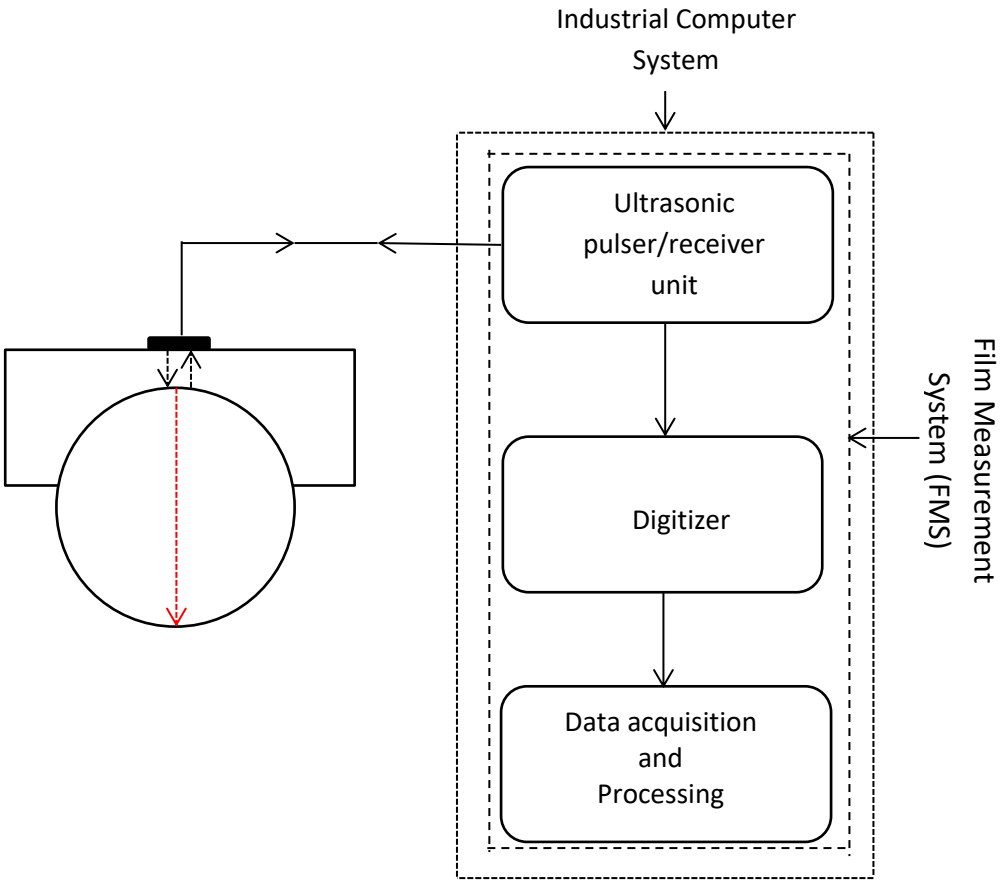

Figure 4-9: Schematic diagram of the ultrasonic apparatus

The industrial computer system used in this study was controlled with the aid of the ultrasonic pulsing hardware unit referred to as a Film Measurement System (FMS) from Tribosonics Ltd. This unit was used to generate, capture, display and record the ultrasonic signals during the transmission process. The ultrasonic pulse receiver unit is the main measurement unit. It generates and receives pulses from a medium through the transducer. The output signal of 25V with duration of 100ns was used. Then the ultrasonic pulse

propagated through the carrier was almost reflected at the discontinuing layer of the medium and received back by the same transducer. This signal processing and the display of the results were carried out using software written in the LabVIEW program installed on the PC. The ultrasonic reflected waves from the contact surface for each load were recorded and studied further.

4.1.4 Signal Processing

Figure 4-10 shows the arrangement of the ultrasonic equipment (FMS) used to generate wave and the employed hydraulic jack for the experiment.

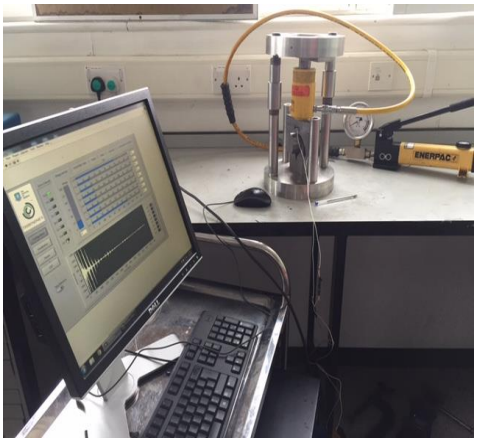

Figure 4-10: Ultrasonic apparatus with the loading frame

Part of the generated signals were transmitted through the roll and reflected back to the surface of the roll (2^{nd} interface) while part were reflected at the carrier surface (1^{st} interface) respectively (Fig.4-3). The signal processing was repeated for the number of loads applied during the experiment. The reflection of the transmitted signals was captured and stored with the aid of the ultrasonic apparatus (Fig. 4-10). The ultrasonic reflections obtained from the contact surface of the model for each applied load were converted to the time domain. This was done with the LabVIEW program installed on the personal computer.

4.2 Experimental Results

4.2.1 Longitudinal Waves

Figure 4-11a shows the transmitted signal process within the sensor and carrier surfaces when the carrier was not loaded against the roll while Figure 4-11b shows the transmitted signal when the carrier was loaded against the model roll. Part of the generated signal was

reflected at the carrier-to-roll surface while the remaining wave was transmitted through the roll and reflected at its back surface respectively.

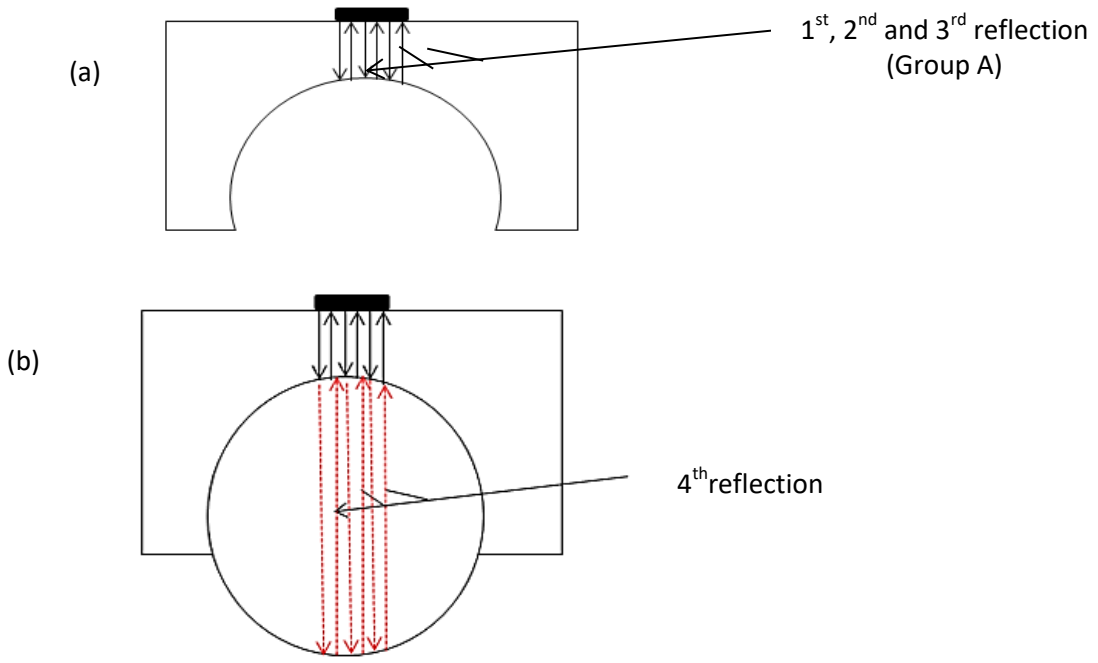

Figure 4-11: Transmitted signals within the sensor carrier and back surface of the roll mode

The waveform of the reflected waves formed from the sensor carrier and the back surface of the model roll during the signal transmission process is shown in Figure 4-12.

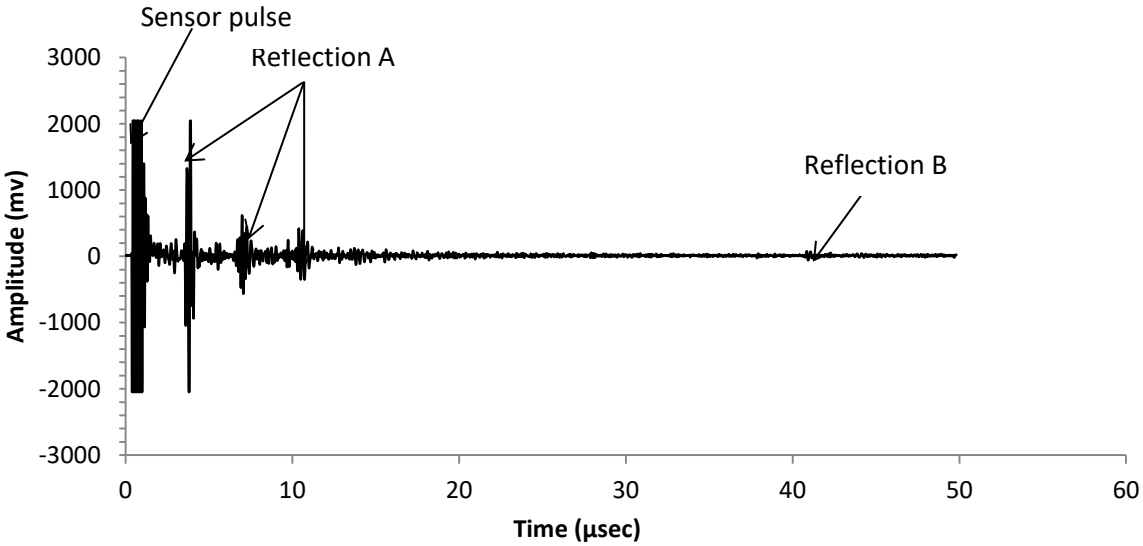

Figure 4-12: Reflected longitudinal wave graph from the back surface of the model roll

As shown in the Figure 4-11, the first waveforms of various reflections (group A) from the surface of the sensor carrier. The 1st reflection was from the surface of the carrier while the 2nd and 3rd waveforms were the re-bounced of the reflected signal from the same surface respectively. This was due to the discontinuity at the surface of the carrier. The interval between the two consecutive waveforms of the reflected signal is referred to as the ultrasonic Time-of-Flight (ToF). The ToF of the 1st reflection, which was the initial waveform at the surface of the sensor carrier, was 3.75 μsec. This value was read directly from the graph after the initial sensor pulse value and it compared with the actual thickness of the sensor carrier surface. The ToF of the 2nd and 3rd reflections were increased at an almost constant value of 3.75 μsec because the wave was re-bounced within the same thickness of the sensor carrier.

Reflection B was from the back surface of the model roll, indicated as a 4th reflection in Figure 4-11(b). The ToF of the reflected signal from the back surface of the model roll was located at 40.95 μsec from the graph. This value corresponded to the diameter of the model roll and the thickness of the sensor carried employed.

4.2.1.1 Effect of Loads on the Reflection Signal at the Back Surface Model Roll

This section focuses on discussion of the resolution and strength of the signal reflected from the back surface of the model roll. The effect of applied loads on the reflected signal obtained at the back surface of the model roll (Fig. 4-12) was separated and studied for this purpose. Figures 4-13 to 4-16, show the response of this wave reflection according to the values of load applied. The same range of 39 to 43 μsec was selected at the horizontal axis, while the effects of the loads were studied with the value of the amplitude in the vertical axis respectively. It was observed from these graphs that the values of amplitude increase as the loads applied increase.

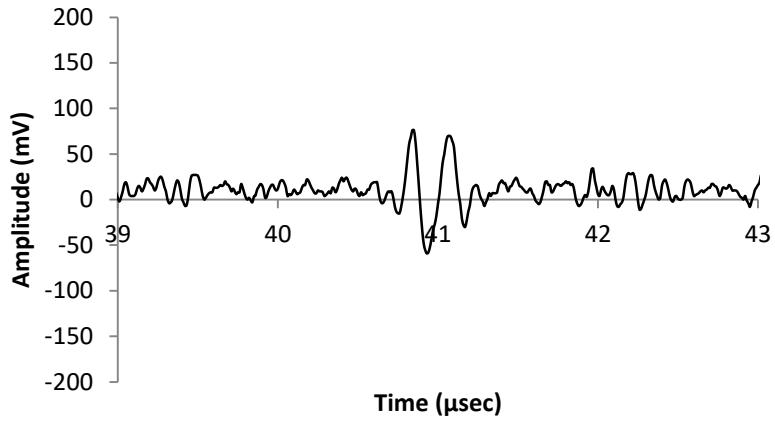

Figure 4-13: Reflected longitudinal wave graph at 5KN load

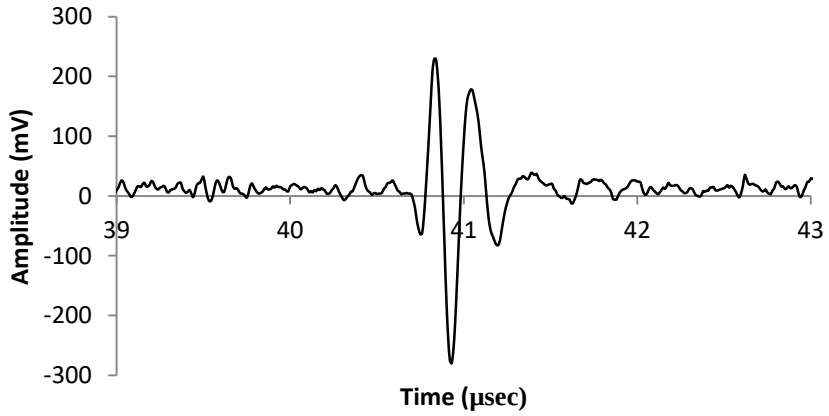

Figure 4-14: Reflected longitudinal wave graph at 10KN load

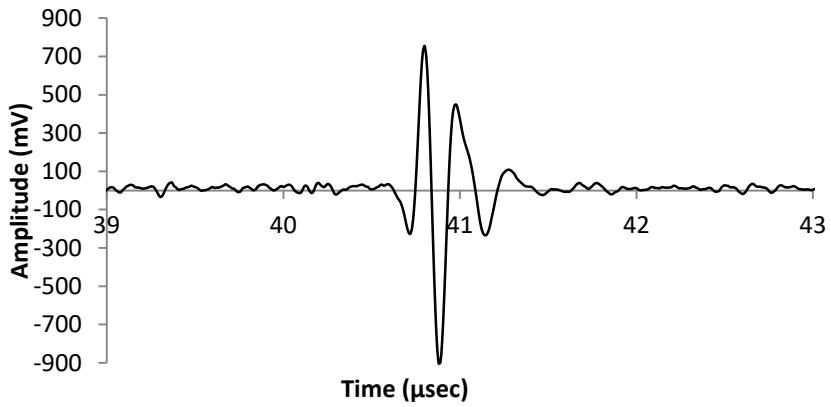

Figure 4-15: Reflected longitudinal wave graph at 15KN load

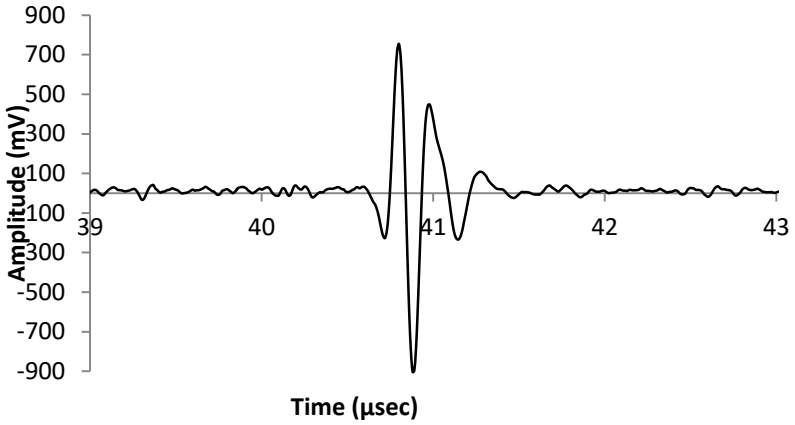

Figure 4-16: Reflected longitudinal wave graph at 20 KN load

The corresponding value of the wave reflected amplitude at the back surface of the 110 mm model roll diameters for the various applied are shown in Table 4-1.

Table 4-1: Reflected amplitude values from the model rolls diameter

Load (kN)	110mm thickness (Amplitude value) (mV)
5	76
10	208
15	720
20	755

The results clearly show that the applied rolling load has a significant effect on the energy of the wave reflection of the transmitted signal. The higher the rolling load, the higher the wave reflection from the back surface of the model. As shown (Figures 4-13 to 4-16), the amplitude value of the reflected wave was observed to increase as the applied load increased. This is due to greater closeness of the carrier-to-roll model surface contact (1st interface in Fig.4-3) that increased the energy of the transmitted signal through the model roll. The higher the applied load, the greater the closeness of the interface, then the higher the energy of the transmitted signal and the higher the amplitude of the reflected wave at the back of the roll. This means that high loads will be required before high strength signal energy can be transmitted through the roll.

4.2.2 Shear Waves

The same experiment was repeated with the application of shear waves and the 110mm diameter of model roll. Shear sensor was also tested with the same procedure employed for the longitudinal sensor. This was due to the important nature of the shear sensor to confirm the present of the solid contact at the metal-to-roll interface during the rolling process. The obtained wave reflection data was processed and is presented in Figure 4-17. None of the wave reflections were seen at the expected location on the back surface of the model roll after the analysis.

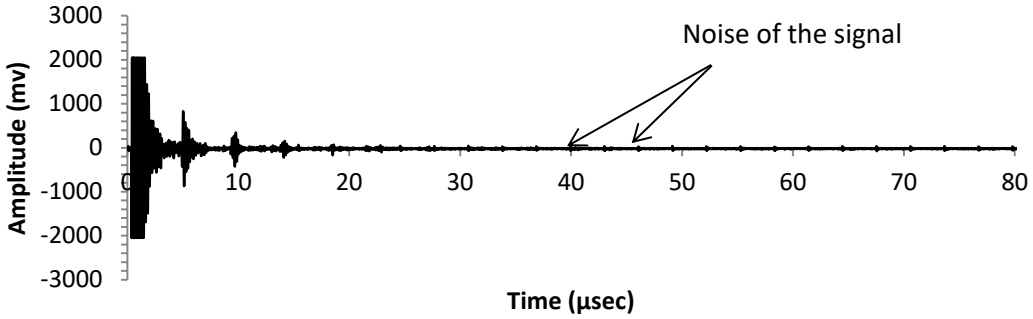

Figure 4-17: Reflection of the shear signal sent through the carrier at various loading

The noise ratio of the sent signal was observed instead of the wave reflection when the voltage of the ultrasonic equipment increased from 25V to 60V during the processing.

Additionally, the shear sensor negative responses was due to the reaction of the coupling gel used to couple the carrier with the model roll. Longitudinal waves were able to be transmitted from one medium to another with the presence of liquid while the shear wave attenuated very fast and diminished in the gel layer between the carrier and roll model. This is the reason why the shear wave did not reflect back on the surface of the model roll as shown (Fig. 4-17).

4.3 Oblique Reflection Approach

4.3.1 Basic Concept

Figure 4-18 shows the design of the pitch-catch ultrasonic transmission technique that was used to generate and transmit signals in the model roll with the transducers at the both sides.

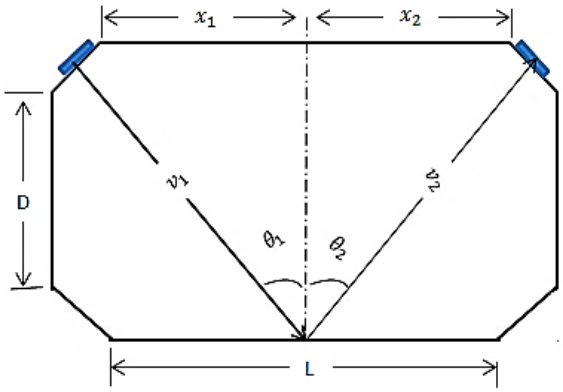

Figure 4-18: Schematic diagram of the oblique incidence and reflected rays

The ultrasonic wave hits the interface of the material at an inclined angle, and its reflection was captured at the other side of the roll, at the same angle of incidence. The incidence and reflected waves are denoted by v_1 and v_2 the angle of incidence and reflected are denoted by θ_1 and θ_2 respectively.

4.3.2 Experimental Procedure

Figure 4-19 shows the model roll after the material has been cut into the required angles at both sides. The model roll interface was prepared for mixed lubrication purposes; therefore a pair of longitudinal and shear transducers were attached to both side angles of the model roll.

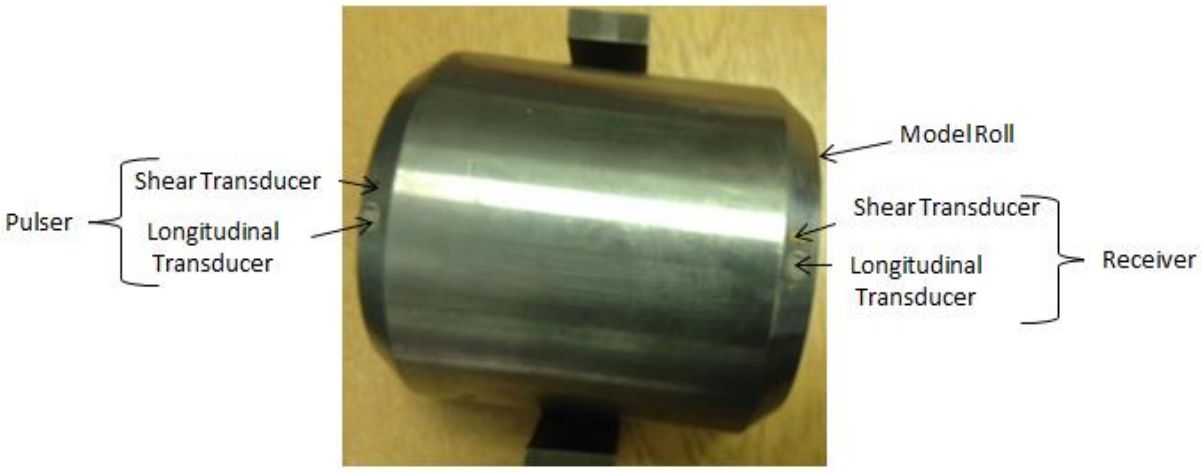

Figure 4-19: Model roll without sensor carrier

The experiment was conducted without applying any loads nor any carrier to the model roll during the process. The ultrasonic signal was generated and transmitted through the model

roll with the aid of the ultrasonic equipment. Refer to Sections 3.2.2 and 4.1.3 for details of the FMS and the software used.

4.3.2.1 Ultrasonic apparatus Data Acquisition process

The schematic diagram of the different combination of ultrasonic equipment units and model roll is shown in Figure 4-20. The layout consists of pulse-receiver transducers, a digitizer, an ultrasonic sensor and the model roll. The ultrasonic apparatus and model roll communicated through the pulser and receiver transducers during measurement. The data acquisition process used to obtain the ultrasonic wave reflection in Section 4.1.3 was also employed in this section. The only difference is that the oblique reflection technique was used in this section, which involved the application of the two separated transducers.

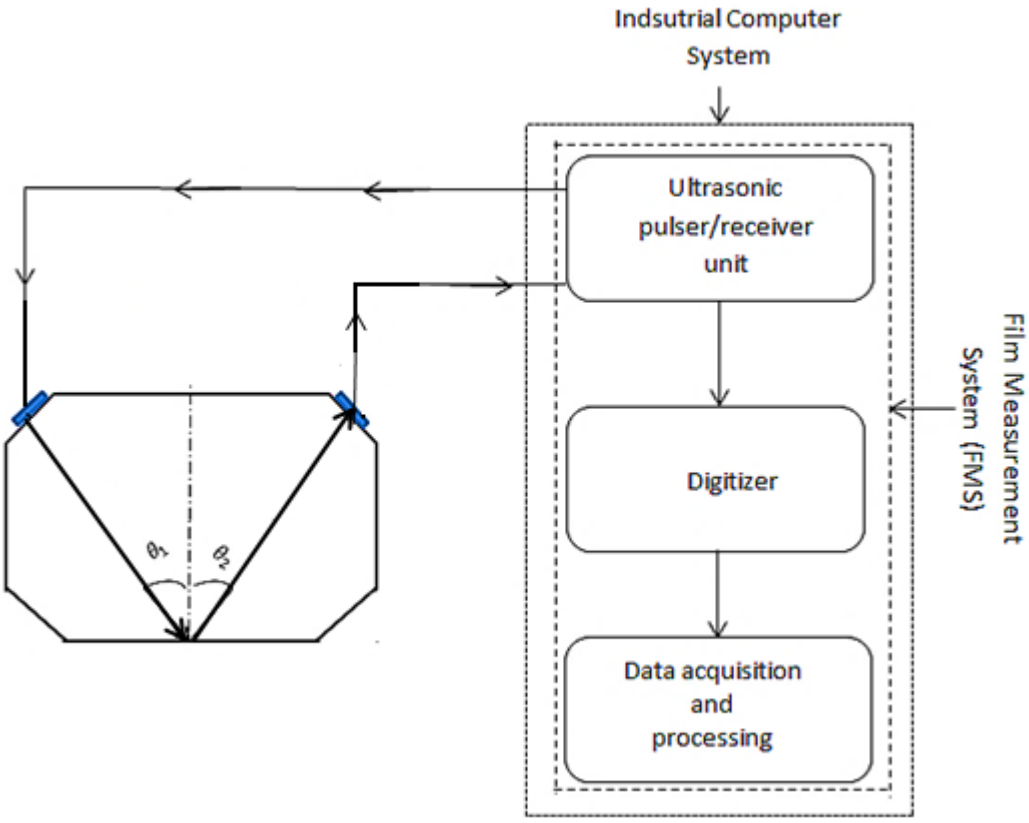

Figure 4-20: Ultrasonic apparatus with the model roll

The transmission methods of the generated and sent signals through the model during the investigation are illustrated in Figure 4-20. The incidence wave hits the back surface of the model roll and is reflected back at the same angle of incidence. This reflection was captured by the receiver transducer and processed using LabVIEW software installed on the PC. This

procedure was used to process both the longitudinal and shear wave employed during the experiment.

4.3.3 Experimental results

4.3.3.1 Ultrasonic Signal Transmission Process in the Model roll

Figure 4-21 shows the amplitude of the longitudinal wave reflection obtained from the back surface of the model roll. This procedure was done in the time domain using LabView on the PC. The Time-of-Flight (37.4µsec) of the wave reflection from the initial pulse at the surface of the sensor corresponded to the thickness of the used model roll. The higher value of the amplitude of the wave reflection of 1872 mV was obtained from the model roll without any load applied.

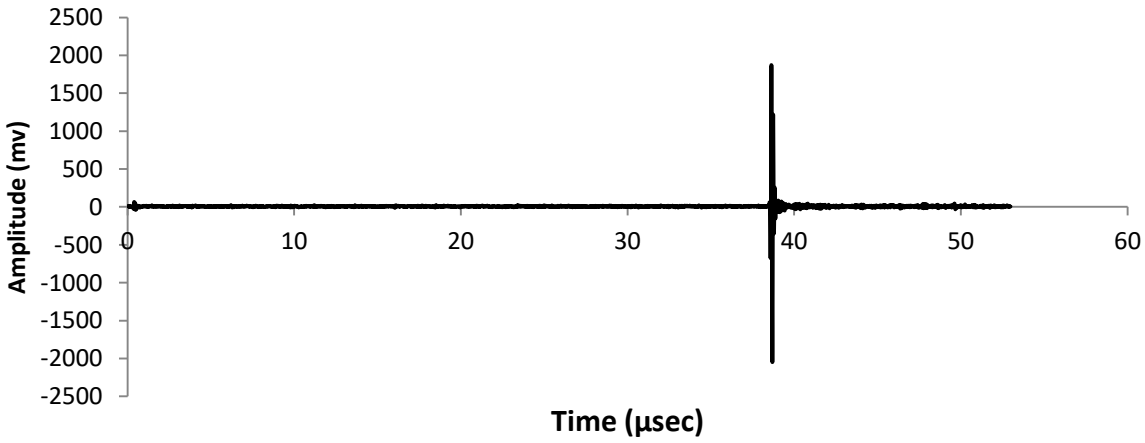

Figure 4-21: Reflection of the longitudinal wave sensor with pitch-catch method at unloaded state

The properties of the reflection obtained at the longitudinal wave sensor are shown in Table 4-2.

Table 4-2: Properties of the sent longitudinal wave

Load (kN)	Time-of-Flight (µsec)	Amplitude (mV)
0.0	37.4	1872

Given the discussion in Chapter 2, that the metal-to-roll interface generally undergoes mixed lubrication (solid and liquid contact) during the rolling process, the aim of this experiment was to study an ultrasonic signal energy transmitted through the model roll thickness and to study the wave reflection from its back surface. Therefore, shear and longitudinal sensors

were used to study the model roll interface respectively. The longitudinal wave was aimed to study whatever might happen in the roll liquid and solid contact interface while the shear wave was aimed to study whatever might happen in solid contact during the rolling experiment. Installation of the roll onto the pilot mill and using it to deform the strip was one of the objectives of this project.

Therefore, shear transducer was mounted and used to send signals and its reflection obtained was processed and presented in Figure 4-23. The Time-of-Flight of the reflection was obtained as 70.61 μsec. Larger Time-of-Flight was observed from the reflection of the shear wave (Fig. 4-22). This is due to the low speed of 3190 m/sec of the shear wave during its transmission process through the model roll. The Time-of-Flight of the wave corresponded to the thickness of the model roll. In addition, the 1797 mV amplitude value of the shear wave reflection from the back surface was also recorded.

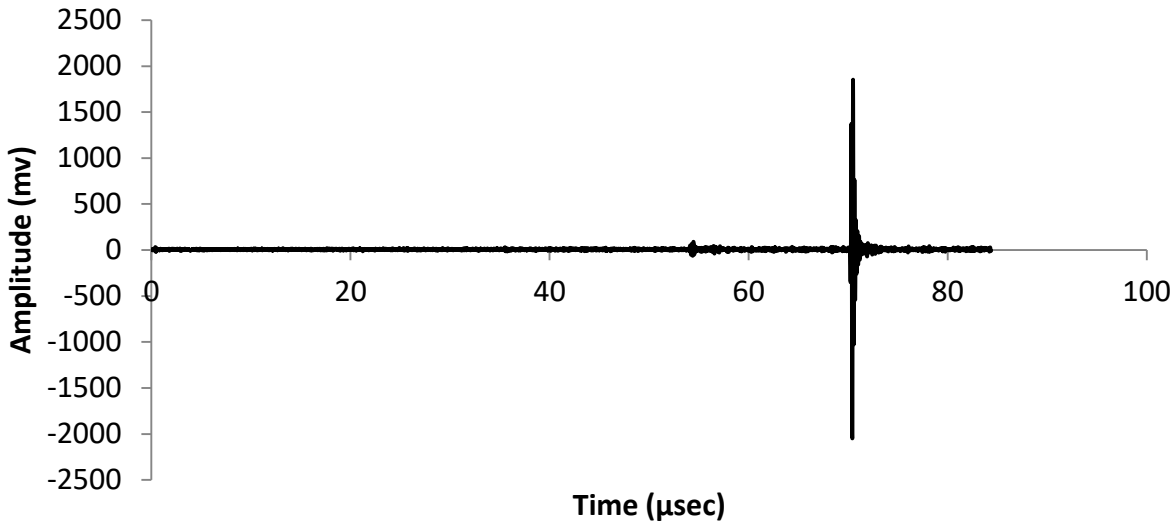

Figure 4-22: Reflection of the shear wave sensor with pitch-catch method at unloaded state

Table 4-3 shows the properties of the reflected shear wave obtained during the process.

Table 4-3: Properties of the sent shear wave

Load (kN)	Time-of-Flight (μsec)	Amplitude (mV)
0.0	70.61	1797

4.4 Discussion

The purpose of these experiments was to determine which of the two techniques described above provide the better external ultrasonic layout technique for understanding the model roll contact surface conditions. A high energy of the received ultrasonic reflection was observed with the oblique reflection technique at free load. This resulted in a very high signal-to-noise ratio achieved from both sensors applied through the layout configuration. The technique was able to capture a received signal from the back surface of the model roll with amplitude of 1872mV and 1797mV against a noise level for both longitudinal and shear wave sensors. Background noise was of order of 30mV for both signals (Figs 4-21 and 4-22). This gives a signal-to-noise ratio (SNR) for the reflection from the top surface in the range of 60.4:1 (longitudinal signal) and 59.9:1 for the shear sensor. The high signal-to-noise ratio is necessary in order to extract useful information to detect and locate size of the interface conditions during the metal rolling process.

Additionally, the sensors were able to transmit with high signal-to-noise level due to the direct attachment of the transducer to the model roll surface (Fig. 4-19) and that led to the lack of interface between the sensor and the model roll. This resulted in little or no energy loss during the transmission and that is the reason a large value of high signal-to-noise was also able to be achieved from longitudinal (Fig. 4-21) and shear (Fig. 4-22) sensors.

The ultrasonic reflections obtained from the back surface of the model roll with the second layout configuration (normal pulsing technique) increased when the applied loads were increased, which is related to the closeness of the carrier-to-roll interface during the experiment. This technique was performed below expectation due to a low signal level observed as the load applied to the model roll through the jack. The minimum reflected signal level received was increased as the applied load increased. Compared with the oblique reflection technique (free load), the amplitude value of 76mV with background noise of 33mV was recorded for the 5kN applied load (Fig. 4-13). This gives a signal-to-noise ratio range of 2:1. In ultrasonic testing, it is very important to put the level of the signal-to-noise ratio of the obtained reflected wave into consideration for better performance of the system. The higher the signal-to-noise ratio, the better the performance.

The disadvantage of the pulse-echo technique is that, a very long data capture time would be required on account of the delays due to the additional sensor carrier involved before installing onto the roll for signal transmission (Fig. 4-11).

In this layout, high quantity of signal-to-noise level of ultrasonic reflection observed at the carrier-to-model roll interface (Fig. 4-12) caused a reduction in the signal transmitted energy through the model roll. This was due to the discontinuity of the carrier surface to the model roll and absorption of the wave from the applied coolant gel to the carrier-to-model interface during the process.

In addition, it is not possible to view the shear wave reflected in the far side of the roll at the expected location (Fig. 4-17), due to the reason that signal received from shear sensor has low amplitude. The reduction in amplitude was partially caused by the losses of shear wave energy into the coupling gel applied to the carrier-to-model roll interface. The amplitude of the reflected signal from the back surface of the model roll was smaller than the amplitude of the noise. The signal-to-noise was less than 1:1, and the noise was totally masked the shear wave reflected signal. This was undesirable, because the reflected signal of the shear wave was not located at the expected point. The limitation of the pulse-echo technique in this configuration relates to the requirement for gel or liquid couplant as shear sensor cannot be used to obtain the required sufficient signal-to-noise ratio required.

4.5 Conclusion

This chapter has presented two experimental layouts to the model roll. The aim has been to ascertain the best external sensor layout arrangement for the ultrasonic transmission method to study the metal-to-roll interface conditions. This investigation was carried out with the sensor mounted on a sensor carrier and the transducer mounted on the model roll in a pitch-catch arrangement. However, when comparing data obtained from similar signal processing applied to both techniques, oblique reflection approach has been found to be significantly more sensitive in studying the metal-to-roll interface. The following conclusions can thus be drawn:

- This study has shown the ability to use the ultrasonic reflection to investigate and monitor the model roll interface conditions;
- The experimental findings in this study show that the oblique reflection arrangement was better than the normal pulsing layout. This result may be explained by the strong

signal-to-noise level of transmitting wave through the model roll that produced the highest amplitude wave reflection at the back surface of the model roll;

- The results show shear sensors cannot be used with the carrier configuration. This may be explained by the lack of interface between the shear sensor and the model roll that prevented the linkage of the signal during the transmission process. Due to this almost all the ultrasonic energy was reflected back from the back surface of the sensor carrier.

Chapter 5

Implementation of Ultrasonic Sensors on a Pilot Mill

This chapter describes the implementation of the pitch-catch technique on a pilot mill. The technique was used to measure the strip thicknesses statically on the mill and during rolling. The experimental results obtained from this technique were compared with independently measured values and the differences were studied.

5.0 Introduction

This chapter discusses the design and machining of a metal roll from a pilot mill to install an ultrasonic sensor; the instrumentation is also described. The ultrasonic approaches described in Chapter 4 have been used to study the application of Time-of-Flight of the reflected ultrasonic signal obtained from the roll back surface. The thickness of the strip was also determined using the Time-of-Flight of the reflected wave obtained from the front of metal roll and back surfaces of the metal rolled. This was done at both statically on the mill and during rolling. The value of the strip thickness obtained was compared with the measured value using a micrometre screw gauge.

5.1 Experimental Apparatus

5.1.1 The Pilot Mill

Figures 5-1 and 5-2 show the picture and the sketch of the pilot mill employed in this metal rolling experiment.

Figure 5-1: Pilot mill used for the work

This machine is a two roll mill type, with the upper and lower cylindrical rolls rotating in opposite directions. The average surface roughness of the roll was measured as Rq= 0.7µm with the aid of a Veeco Dektak 150 profilometer roughness measurement machine. The surface hardness of the metal roll was also determined as 750HV with the aid of the Vickers hardness machine. Figure 5-2a and 5-2b shows the front and side of the pilot mill respectively.

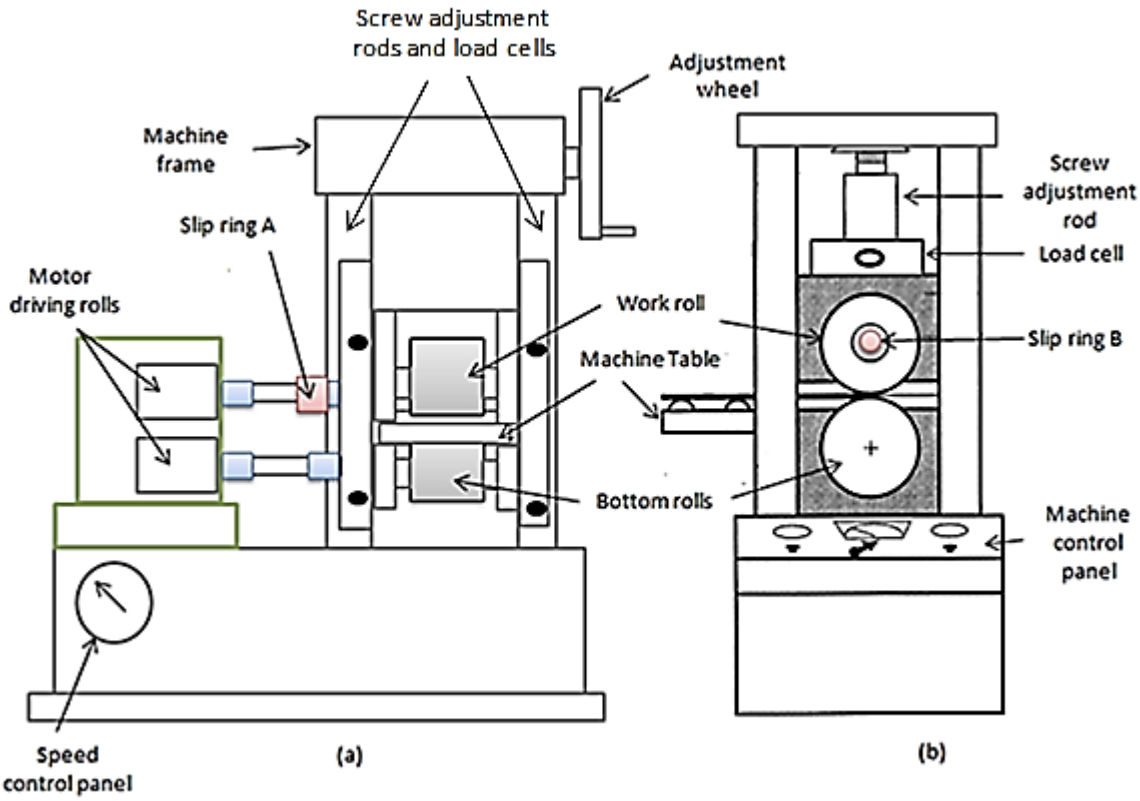

Figure 5-2: Sketch of (a) front (b) side view of the pilot mill employed

The mill consisted of two load cells mounted between the upper roll machine frames of the machine. One of the load cells is shown (Fig. 5-2b) while the remaining one is located on the other side of the machine. The machine contained screw adjustment rods on both stand sides of the machine frame to regulate the rolling force by screwing up and down. Roll spacing and adjustment was set manually using the adjustment wheel mechanism of the machine. Two slip rings were installed on both ends of the top link shaft of the machine roll. The speed of the machine was controlled via the control unit panel mounted on it to count the rate of passage of the gear teeth through the shaft linked with the upper roll. This rolling speed was monitored and measured with the machine speed panel, allowing the selection of various rolling speeds of the machine during the metal deformation process. The specification parameters of the pilot mill employed during the experiment are listed in Table 5-1.

Table 5-1: Specific values of the parameters employed in the experiment

PARAMETERS	VALUE
Roll diameter	110mm
Pilot mill load capacity	250kN
Rolling speeds	19 and 26 mm/sec
Maximum roll gap	5mm
Maximum strip width	50mm
Contact lengths	5, 7 and 9mm
Metal percentage deformation	10, 20 and 30%
Maximum tensile load of the material	50kN

The machine permits both dynamic and stationary operating conditions. Adding back and front tension during the rolling of the material was not possible due to the lack of tension devices on the machine.

5.1.2 Modification of the Roll

An EN 31 mild steel roll was modified, as shown in Figure 5-3. The roll modification dimensions were based on the outcomes of the dimensions obtained from the drawing method employed. This drawing method was based on the principle of Snell's Law, explained in Section 3.1.6. Figure 5-3 shows a photograph of the metal roll after the modification, including both machined sides of the roll into 19^{O} angles of incidence for mounting the sensors and for easy transmission of the signal.

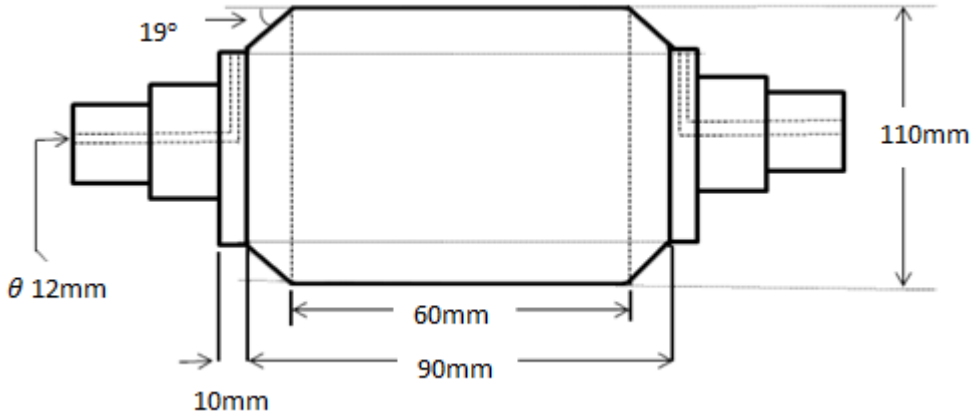

Figure 5-3: Sketch of the metal roll

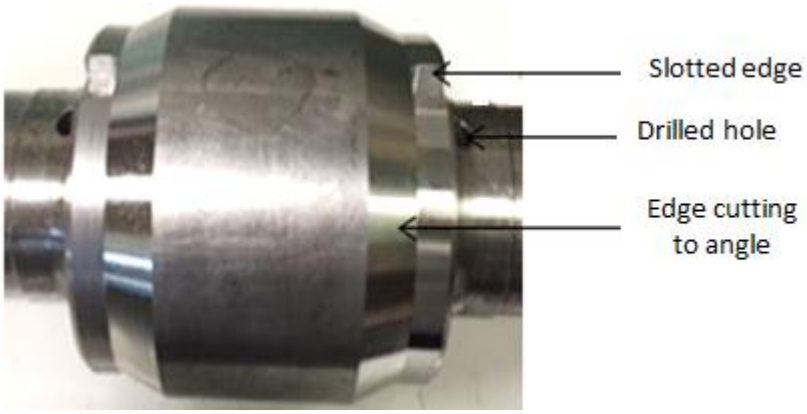

Figure 5-4: Roll photograph indicating the edge machined at an angle

The two extended parts of the roll were centre drilled, and the edge portion of the roll was slotted into a curved shape, as shown in Figure 5-4. This was to accommodate the cables during the roll instrumentation.

5.1.3 Transducer Layout

The design of the transducer used for the instrumentation has been described in Section 4.1.2.1. The sensors were arranged in line to each other and attached to the roll tapered edges as shown in Figure 5-5.

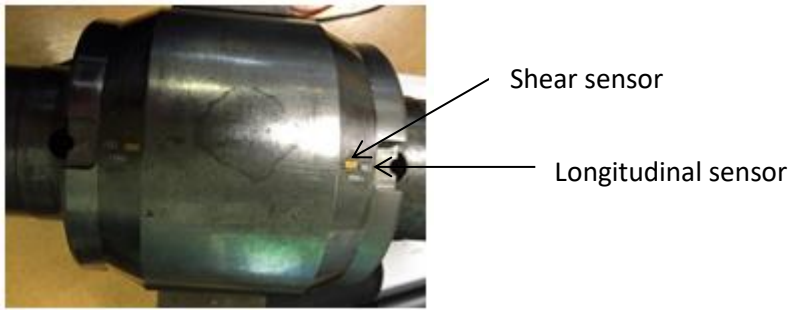

Figure 5-5: Arrangement of the sensors on the roll surface

The longitudinal and shear wave transducers were both bonded to the roll. The arrangements consisted of a pair of 10MHz and 5MHz longitudinal and shear sensors on both sides of the roll which serve as pulsers and receiver transducers.

As shown in Figure 5-5, the longitudinal and shear sensors were installed at the curved surface of the work roll at the required angle for the purpose of this research. The dimensions of these installed sensors are very important to make sure that the area of their excitation is smaller than the expected contact area of the measurement interface. The

resolution of the ultrasonic measurement is defined by the ultrasonic beam width. A smaller beam width results in higher resolution. For accurate measurement of the contact, the beam width needs to be smaller than the contact width. Due to the geometry of both the work roll and strip, a line contact is expected to form between the two, and thus contact length will be much larger than the width. Due to this, the beam width would be definitely smaller than the contact length for the entire applied load. In this research, 7mm x 2mm of the piezoelectric element sensors were used.

In order to estimate the beam width, the flat transducer equation 5-1 stated below was applied:

$$BD = 0.2568\ (D) * S_F \qquad \text{[87, 88] 5-1}$$

while BD is the beam diameter, D (7mm) element diameter and S_F is normalized focal length, which is the 1 for the flat transducer [87] . Therefore, the expected beam width of the reflected signal from metal-to-roll interface was calculated as 1.8mm, this value was obtained with the aid of equation 5-1.

Based on the comparison of beam diameter value obtained above, the expected interface line contact of 3.7mm obtained in equation 2-3 (at a minimum of 5% metal reduction), and high signal-to-noise of the applied technique (Section 4-4), it can be concluded that the ultrasonic element installed is capable of studying the metal-to-roll interface conditions during the metal rolling process without too much blurring of the obtained data.

5.1.4 Instrumentation Equipment

The complete sketch of the ultrasonic experimental layout with the external sensor arrangement is shown in Figure 5-6. As indicated, the cables soldered with the sensors on both sides of the roll were linked with the pulser/receiver unit through the slip rings.

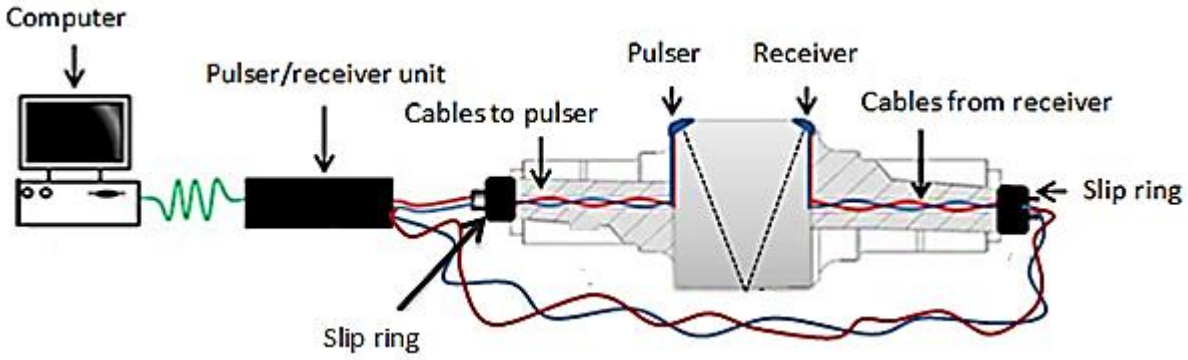

Figure 5-6: Schematic component diagram for the ultrasonic data acquisition system

These sensors were bonded to both sides of the roll, as shown in Figure 5-5. M-Bond 610 adhesive was used to attach the sensors to the roll surface before being clamped together for maximum pressure at the bonding interface. The clamped roll was placed inside an oven and was cured at approximately 140^{o}C for 5 hours. It was allowed to cool naturally in the oven to avoid uneven cooling of the sensor-to-roll interface. The connecting cable was soldered onto the sensors then coated with an epoxy for protection and to safeguard the cables during the rolling process.

As previously explained, the voltage generated from the pulser/receiver unit is transmitted to the transducer (pulser), which converts the electrical energy to mechanical energy and produces ultrasonic signals (sound waves with high frequency). The ultrasonic signal is generated by the transducer due to the vibration of the mechanical energy that is obtained during the conversion. The signals were transmitted through the metal roll, reflected back on the back surface of the roll and consequently captured by the receiver. The reflected signals were received and converted back to voltage by a transducer (receiver). The voltage was then transmitted back to the pulser/receiver unit before being passed to the digitizer, where the reflections were digitized and finally displayed on the computer. This whole process of generation and acquisition of signals was configured and controlled using a LabVIEW program.

5.1.5 Metal Strip Specimens and Rolling Lubricant

Steel grade EN24, with the chemical composition (from the manufacturer) shown in Table 5-2, was used as a specimen during the investigation. This steel was selected because of its low carbon content and therefore its relatively low tensile strength generating a rolling load below the maximum load capacity of the mill [89].

Table 5-2: Chemical composition of the specimen

Carbon	Silicon	Manganese	Chromium	Vanadium	Tungsten
0.9 – 1.05 %	0.15 – 0.35 %	1.0 – 1.25 %	0.05 - 0.7%	0.05 – 0.15 %	0.05 – 0.70%

The low carbon steel specimen was cut into a cross-sectional dimension of 5mm thickness, 50mm width, and length of 250mm. The average surface roughness of the strip specimen was measured with a Veeco Dektak 150 profilometer as 0.9µm. The strip surface hardness was determined as 270HV with Vickers hardness machine.

Gerolub 5525 lubricant was applied with a hand brush onto the strip surfaces before being fed into the roll gap during the rolling operation. This oil was chosen based on its high viscosity that allowed thick film formations at relatively high rolling loads and low rolling speeds. The properties of the oil and steel adopted for the experiment are shown in Table 5-3.

Table 5-3: Oil and steel properties used for the experimental work [28, 66]

Gerolub 5525 lubricant oil	
Density	810.2 (kg/m^3)
Dynamic viscosity @ 25^{o}C	65 (Pas)
Pressure viscosity coefficient	1.77 x10^{-8} (P^{-1}a)
Bulk modulus	1.5 (GPa)
Steel (Roll)	
Density	7800.0 (kg/m^3)
Longitudinal velocity	5900.0 (m/s)

5.2 Experiment on a Stationary Strip

5.2.1 Test Procedure

A series of percentage metal deformations were made with the application of various loads applied through the roll to the strip when stationary. The lubricant was applied to both sides of the strip using a hand brush, and it was manually fed into the rolling gap of the mill, as

shown in Figure 5-7. The strip was dragged into the roll gap due to the friction force that developed along the interface. The machine was stopped when the strip had been partially rolled. The roll was set in such a way that the signal sent was able to transmit onto the strip front and be reflected on the back surface of the strip. The initial and final thickness values of the strips were measured and recorded with the micrometre screw gauge before and after the process.

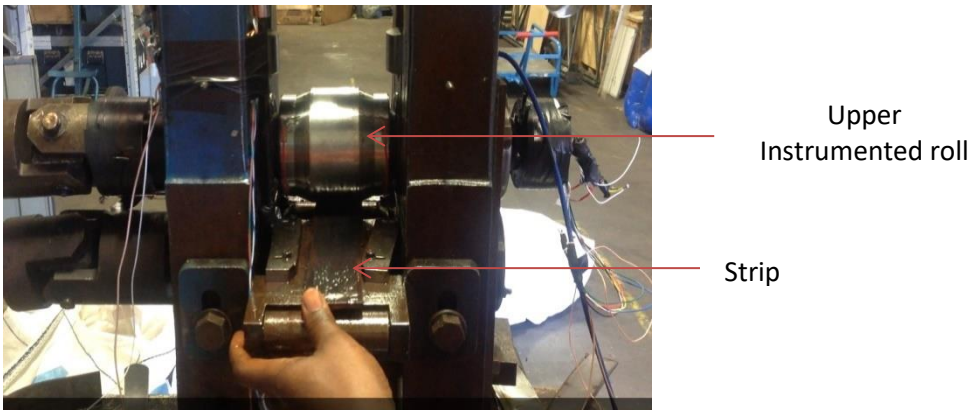

Figure 5-7: Manual feeding of the strip into the pilot rolling mill

The ultrasonic equipment (FMS) was set to pulse voltage of 25 volts, 1000Hz pulsing rate, and gain adjusted for each sensor before the commencement of the signal transmission process. The FMS digitiser runs at 100MHz sample frequency and has a vertical resolution of 12bits. The ultrasonic signal was sent to the interface. Therefore, a portion of the signal was reflected back at the interface of the two materials, while the remainder of the signal was transmitted through the strip and reflected from the strip back surface. The wave reflection was adjusted and amplified by the customized pulser and receiver digitizer card that had been built and installed on the FMS computer by the Tribosonics Company. The digitizer unit was controlled using the LabVIEW program during the data capture process. The adjusted reflected wave from the back surface of the strip, appeared in the time domain and was captured and stored for further use.

5.2.2 Signal Processing

The reflected signals at the surfaces of the strip at stationary were captured by the LabVIEW acquisition program on the PC. These reflected signals were processed in the Time domain. As stated, the Time-of-Flight of the wave reflection corresponded to the thickness of the transmitted medium, therefore the Time-of-Flight obtained was used to calculate the strip thickness rolled during the operation.

5.2.3 Reflection of Signal from the Strip Back Surface

The processed wave reflections of the generated signal sent through the roll to the strip interface are shown in Figure 5-8. The reflected signal amplitude values were plotted against the Time-of-Flight of the reflection signal obtained from the front and back surfaces of the strip respectively.

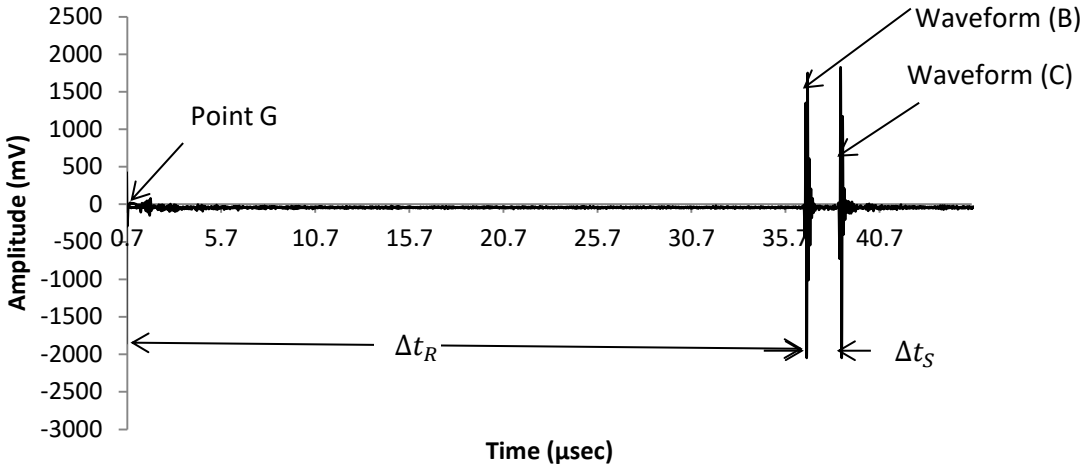

Figure 5-8: Reflection of the longitudinal wave from the strip surface

The path of the reflected signal obtained from front and back surfaces of the strip, shown in Figure 5-9, are illustrated in Figure 5-8. Waveform B was the reflected wave from the front surface of the strip (point B) while waveform C was the reflection of the wave transmitted from the back surface of the strip (point C) (Fig. 5-9).

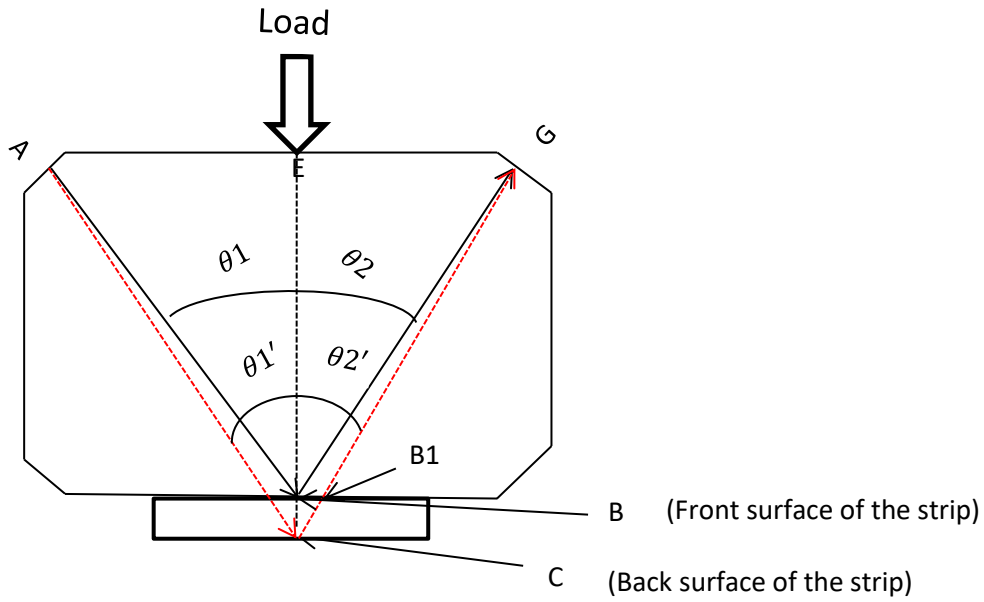

Figure 5-9: Sketch of roll and strip engagement

The Time-of-Flight of the reflected signal, that is, the distance between points B and G (Fig. 5-9) was denoted as Δt_R (Fig.5-8). While the Time-of-Flight of the wave reflection obtained from the back surface of the strip, that is the vertical distance between point B1 and C (Fig. 5-9) was also denoted as Δt_S (Fig.5-8).

5.2.4 Strip Thickness Calculation

Figure 5-10 shows the sketch of the signal transmission process from roll to strip and back to roll when the sensor was facing the contact interface.

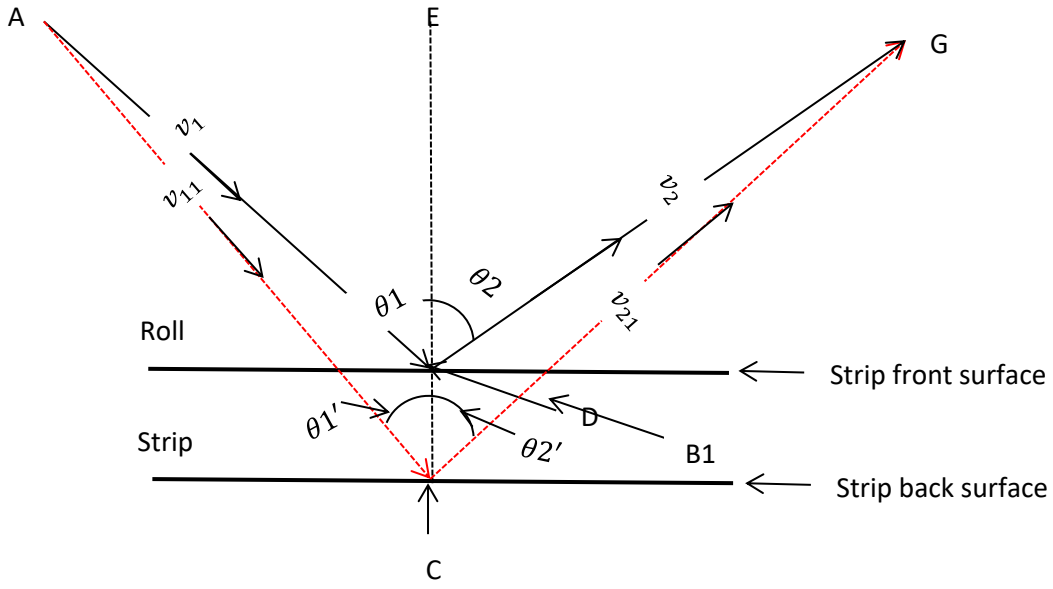

Figure 5-10: Sketch of signal transmission between rolls and strip interface

The diverged incidence beams (v_1 and v_{11}) from sensor A (pulser) hit the back surfaces of the roll and strip at angles $\theta 1$ and $\theta 1'$ respectively and the wave reflections denoted as v_2 and v_{21} are bounced from the back surfaces of the roll and strip at angles $\theta 2$ and $\theta 2'$ respectively which are then received by the sensor G (receiver). The transmission arrangements of the incidence and reflected beams illustrated in Figure 5-10 above show clearly the signals transmitted through the strip which has allowed for determination of the rolled strip thickness during the metal rolling process. Figure 5-11 is the triangle block extracted from the signal transmission sketch, shown in Figure 5-10, for the determination of the strip thickness employed. Line BC represents the actual strip thickness (t_f) value while line CB1 (Fig.5-11) is the path length of the wave reflection from the back surface of the strip.

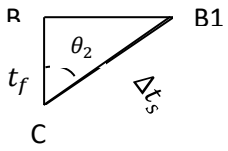

Figure 5-11: Trigometic ratio diagram to calculate the strip thickness

The thickness of the strip along */B1C/* was firstly calculated with the obtained Time-of-Flight of the wave reflection from its back surface with the ultrasonic equation expressed as follows:

$$/B1C/ = \frac{\Delta t_S \,.\, c}{2} \qquad 5\text{-}2$$

While c is the speed of the sound in the strip.

Then, the actual value thickness of the strip */BC/* was finally calculated by mathematical manipulation of the obtained value of /B1C/ with the trigonometric ratio principle expressed as follows:

$$\cos\theta_2 = \frac{/BC/}{/B1C/} \qquad 5\text{-}3$$

$\cos\theta_2$ is the angle of the incidence wave that has been proved to be equal to the angle of the reflected wave (Section 3.1.6). The angle of 19^o was employed as the incidence angle in this research. Therefore, /BC/ was the final value of the strip thickness obtained during the rolling process.

The properties of the wave reflection data obtained from the strip and roll surfaces, including the obtained strip thickness, were recorded in Table 5-4. The value of the strip thickness employed was also measured with a micrometre screw gauge before the experiment was conducted and recorded.

Table 5-4: Property values obtained from the reflected signal at static position

Time-of-Flight (µsec)	1.78
Speed of the sound in strip " c" (m/sec)	5900
Angle of reflection (Degree)	19
Length "/B1C/ "(mm)	5.25
Experimental thickness " /BC/"(mm)	4.86
Measured strip thickness (mm)	5.0

The strip values obtained from both measuring techniques were found to have slight differences of 0.14mm from each other (Table 5-4).

5.3 Experiment during Rolling

This section describes the detailed study to determine the strip thickness during the metal rolling process. The ultrasonic oblique reflection signal approach described in Chapter 4 was used for this operation.

5.3.1 Basic Concept

The measurement technique proven to be the optimum in Chapter 4 is applied to a rolling mill in this section. The sensor will rotate with the roll. When the sensors are over the strip (Fig. 5-12) ultrasonic signal will pass through the roll-strip contact and be reflected from the back of the strip.

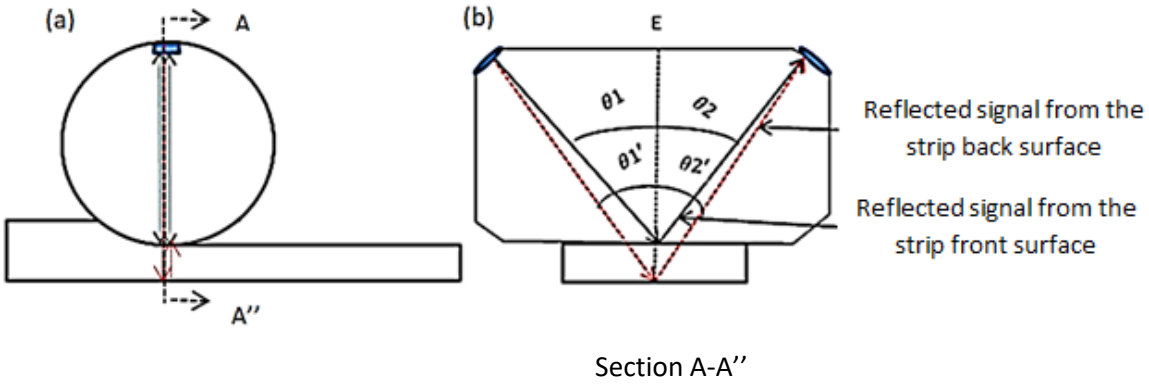

Figure 5-12: (a) Side and (b) front view when the sensor is over the roll-strip contact

Figure 5-13 shows the position of the sensors when rotating away from the strip-to-roll contact. The wave will be completely reflected from the roll-air interface.

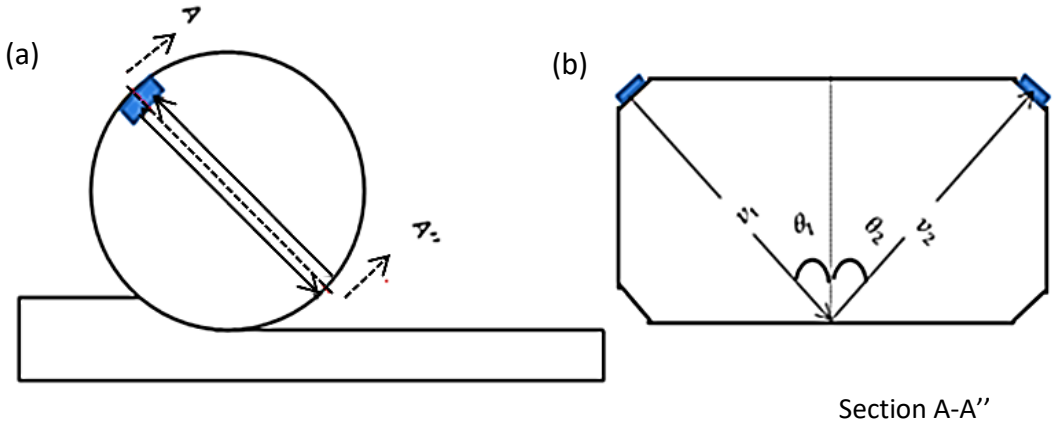

Figure 5-13: (a) Side and (b) front view when the sensor is away from the roll-strip contact

5.3.2 Signal Processing

During the dynamic operation of the rolling process, ultrasonic reflected signals are continuously captured from the surfaces of the strip as the roll rotates for a specific duration. Therefore, a large quantity of the reflected signal is generated, captured and digitized at this specified period, which is difficult to process in real-time. In order not to lose information during the process, the acquired data was streamed directly to the hard disk of the computer and stored in binary form for further processing. The stored reflected data along with reference data can then be processed using another in-house written LabVIEW program.

5.3.3 Experimental Procedure

The strip thicknesses were measured with a Vernier caliper both before and after each rolling operation. Trial and error was needed in adjusting the gap width screw, due to not having a roll gap measuring device. This was done to achieve the required strip thickness and desired percentage metal reduction during the rolling process. However, due to the low speed and high rolling load, the rolling metal experiences a deformation leading to mixed contact within the strip and roll surface. The ultrasonic equipment was set to the same value of pulse voltage and pulsing rate mentioned in Section 5.2.1. The captured window was delayed by 39.5 µsec from the initial pulse. Therefore the Time-of-Flight is the reflection time plus the delay. The equipment measurement scale was ranged from 0.0 to 5.4µsec before the commencement of the signal transmission process, and the equipment was runs at 100MHz sample frequency with vertical resolution of 12bits as mentioned earlier. The

generated signal was transmitted through the metal roll continuously to the strip during the rolling operation and the wave reflected at the strip back surface. This reflection was captured, analysed and the result obtained (Time-of-Flight) was used to calculate the strip thickness and the roll-bite contact length. The experimental details of the process are fully explained below.

5.3.4 Recorded Waveform

Figure 5-14 shows the waveforms of the wave reflection from the back surface of the roll when the sensor is away from the strip contact (Fig. 5-13).

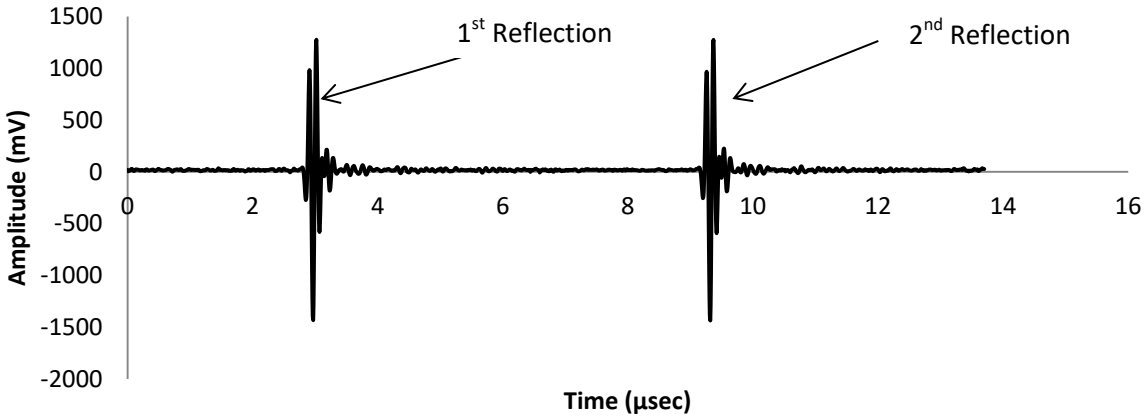

Figure 5-14: Reflected signal obtained when the sensor is out of strip-to-roll contact

The 1st reflection is the waveform of the reflected signal obtained from the back surface of the roll, while the 2nd reflection is the waveform of the bounced back echo of the 1st reflection. The positive amplitude of both waveforms are almost the same (1275 mV for the 1st reflection and 1273 mV for the 2nd) as almost all the reflected wave was bounced back.

Figure 5-15, also shows the waveforms of the reflected wave obtained when the sensing face was in contact with the strip surface (Fig. 5-12).

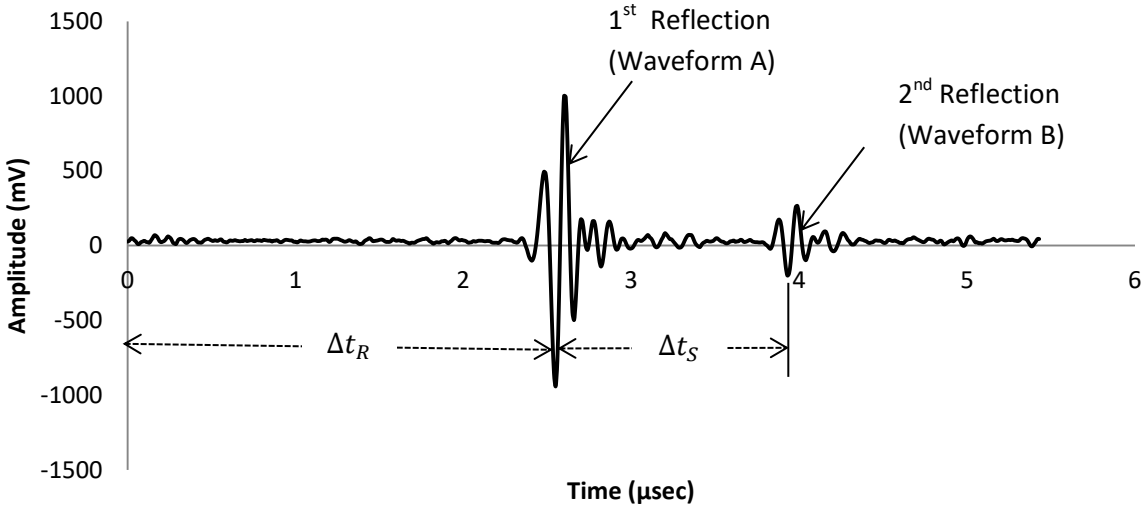

Figure 5-15: Reflected signal obtained when the sensor is in contact with strip-to-roll interface

The 1st waveform was the reflection of the reflected wave from the back surface of the roll, while the 2nd reflection was the waveform from the reflected signal back surface of the strip. The 2nd reflected waveform had the smallest value of amplitude (80mV) compared with the amplitude value of the 1st waveform (1028 mV).

The amplitude value of the 1st reflection, when the sensor was out of the roll-to-strip contact (Fig. 5-14), was a higher value of 1275 mV compared with the amplitude value of the 1st reflection 1028 mV when the sensor was in contact with the roll-to-strip interface. The reduction in the amplitude value of the 1st waveform reflection (Figure 5-15) was due to part of the waves having been transmitted while part were reflected back from the back surface of the roll. The Time-of-Flight of the reflected signal obtained from both metal roll and rolled strip back surface were donate as Δt_R and Δt_S respectively.

As shown in Figure 5-15, the rolled strip thickness was able to be determined due to the better reflected signal received from front and back surfaces of the strip during the rolling process. The peak to peak amplitude of both front (left-hand side) and back (right-hand side) pulses shown in Figure 5-16, was plotted against the pulse number for both front and back surfaces from Figure 5-15.

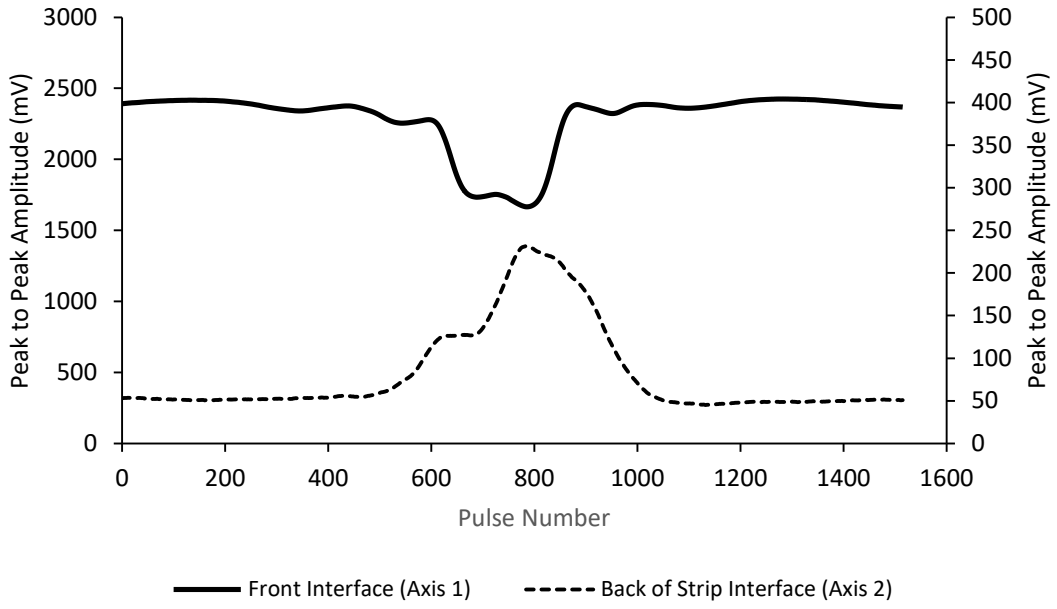

Figure 5-16: Amplitudes of the wave reflection received front and back surfaces of the rolled strip

As can be seen from Figure 5-16, the amplitude of the reflected signal from the front surface of the strip was of acceptable magnitude while the amplitude of the reflected signal from the back surface of the strip is moderate. This shows signal amplitude for both reflections is sufficient to calculate an accurate measurement of strip thickness during the rolling process.

The raw reflected data obtained during the rolling operation contained both reference and reflected wave data obtained during the metal rolling operation. The process of separating the reflected signal from the metal-to-roll interface from the obtained data is shown in Figure 5-17 (a-c).

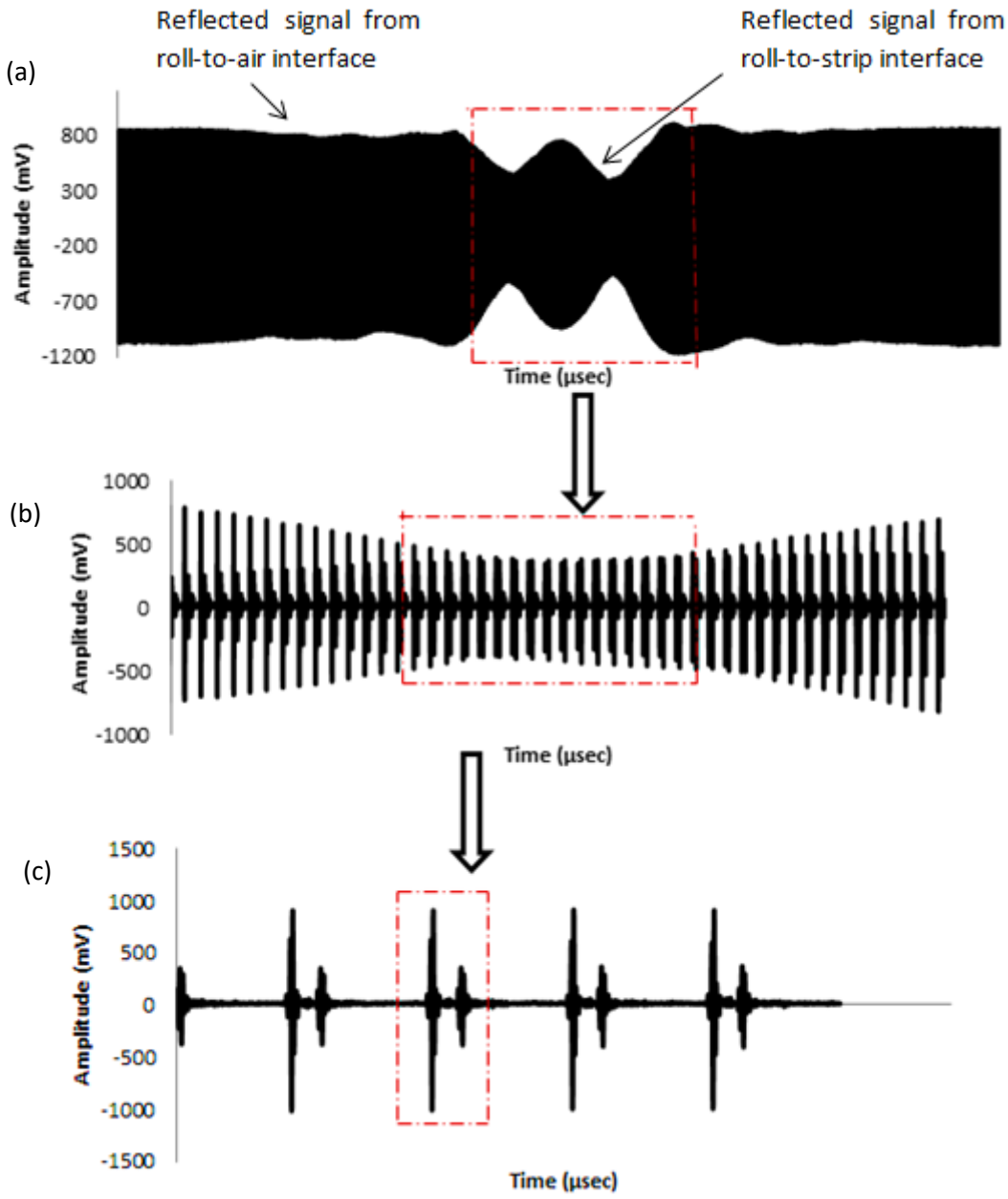

Figure 5-17: Sample of ultrasonic data extracted for the determination of strip thickness; (a) stream of processed reflected data for one complete strip rolling; (b) sub-section of data when a sensor approaches the strip position; (c) single extracted reflected data from the front and back surfaces of the strip.

Figure 5-17 (a) shows the raw data obtained from the metal and roll surfaces during the rolling process. These series of reflections are from both metal-to-air and metal-to-roll contact interfaces during a full metal rolling operation with the normal rolling load of 70kN. These reflections were captured, processed and stored for further use.

Figure 5-17 (b) shows another sub-set of a series of the reflected data obtained from the first processed data (Figure 5-17 (a)). This is a series of the generated reflected signal from the sensor to the roll the moment the strip is within the sensor's view during the

deformation process (Figure 5-12 (a)). The dotted lines in Figure 5-17 (a) show the sensor reflection signal from the roll-to-strip interface when the sensor surface focuses on the compression of the strip and roll contact. The effect of the strip deformation by the rolling passage obviously cleared on the amplitude of the reflected signals (Figure 5-17 (b)). Therefore, when the sensors move away from the strip, then the amplitude of the reflected ultrasound wave from the metal-to-air interface (Figure 5-13) was restored back to the original value. The reduction in the value of the amplitude varied slightly as the attached sensors' focus moves towards and away from the strip during the rolling process.

Furthermore, Figure 5-17 (c) shows the actual required reflected data indicating the changes in Time-of-Flight of the reflection between the strip front and back surfaces, which was used to calculate the strip thickness.

5.3.4.1 The Nature of the Time-of-Flight Variation along the Roll-Bite

Smooth curves for processed Time-of-Flight variation of the reflected signal as shown in Figure 5-18 are expected along the metal-to-roll interface whenever the sensor surface is in contact with the strip during the rolling process as discussed in Carretta et al. [90].

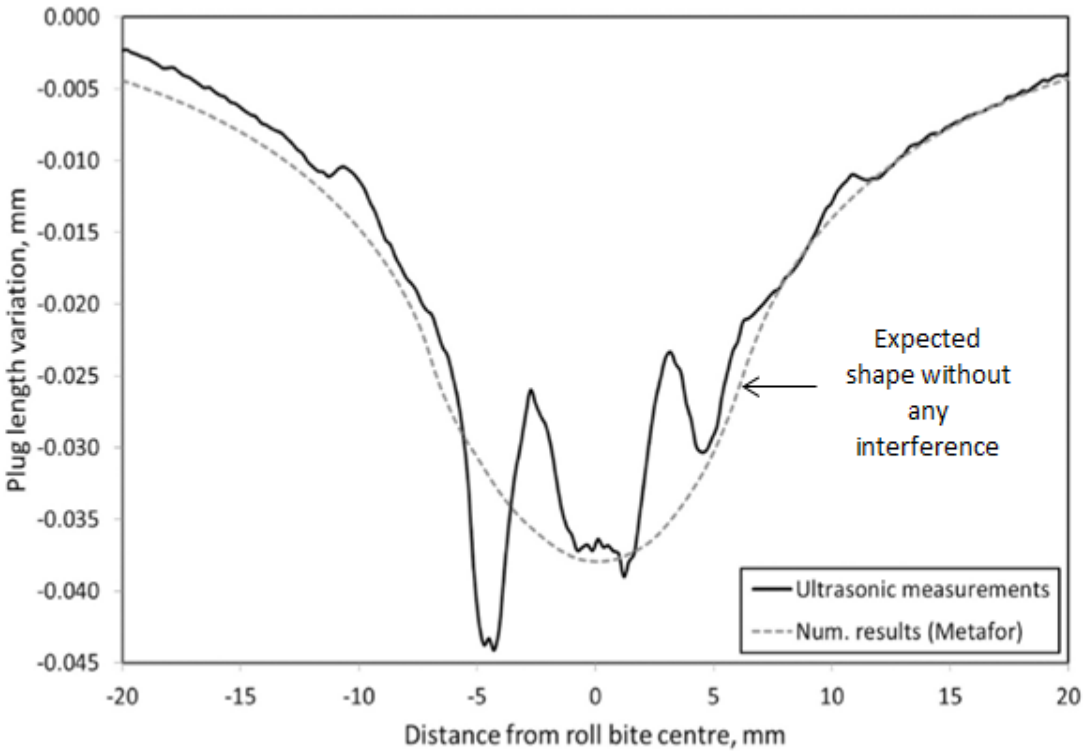

Figure 5-18:Experimental and stimulation, various Time-of-Flight along the roll-bite [90]

Figure 5-18 shows that the experimental data varies from the expected shape. The reflected signal at the contact interface of the rolling process is complex and the causes for the variation are not well understood in the literature. Carretta et al. [90], explained that the fringe pattern observed in Figure 5-18 can sometimes be observed instead of the smooth curve graph. As discussed in the paper, this was due to the interference of the transmitted signal as the signals hit the contact interface at slightly different times and the bounce back. The same effect was also reported during the measurement of rolling bearing contact by Howard [91].

The shape of Time-of-Flight variation observed along the metal-to-roll interface in this research is in double-dip pattern (Fig. 5-17) which was different from the Time-of-Flight variation observed by Carretta et al. [90] and Howard [91]. This difference may be due to the distance of the sensor to the contact interface, the number of the sensor involved and the signal pulsing technique. The main point however is that the smooth curve graph shown in Figure 5-18 was not achieved and the reason for this effect remains an open question.

The data shown in Figure 5-19 is a sample of the processed data obtained from the metal-to-roll interface which includes both reference and reflected signals captured in terms of Time-of-Flight along the roll-bite during the rolling process. The set of the data was processed with the aid of an FFT LabView program so as to separate the reference from the reflected signal in the frequency domain.

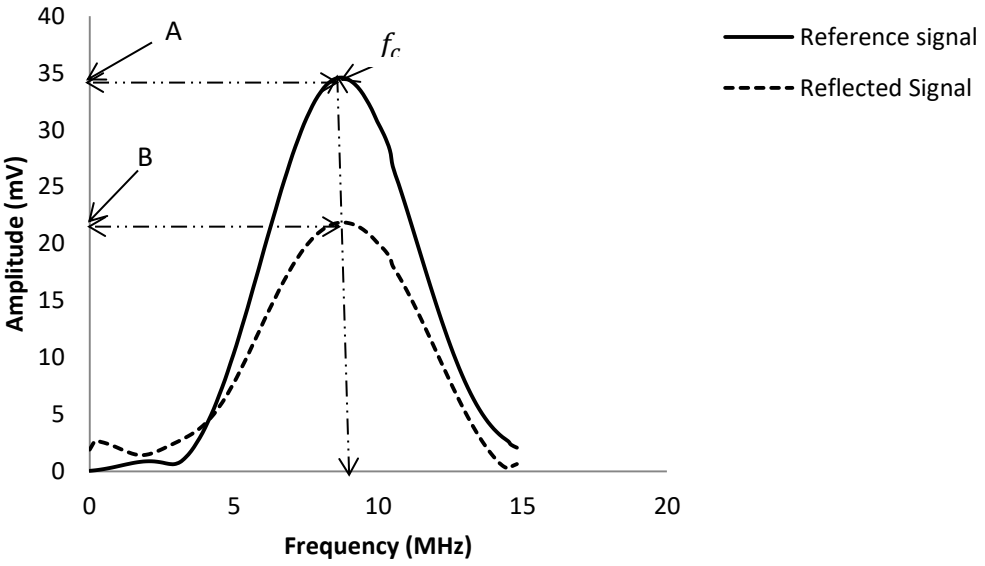

Figure 5-19: Wave amplitude against frequency

As shown in the Figure 5-19, point A is the reference peak amplitude value (34.0mV), point B is the reflected peak amplitude value (21.8mV), while f_c is the centre frequency (8.9MHz). The reflection coefficient obtained from the diagram is 0.64 using equation 3-5.

Figure 5-20 shows the reflected signal captured and processed using the LabVIEW program at various positions across the roll-bite during the metal rolling process. The figure shows the double-dip pattern described earlier.

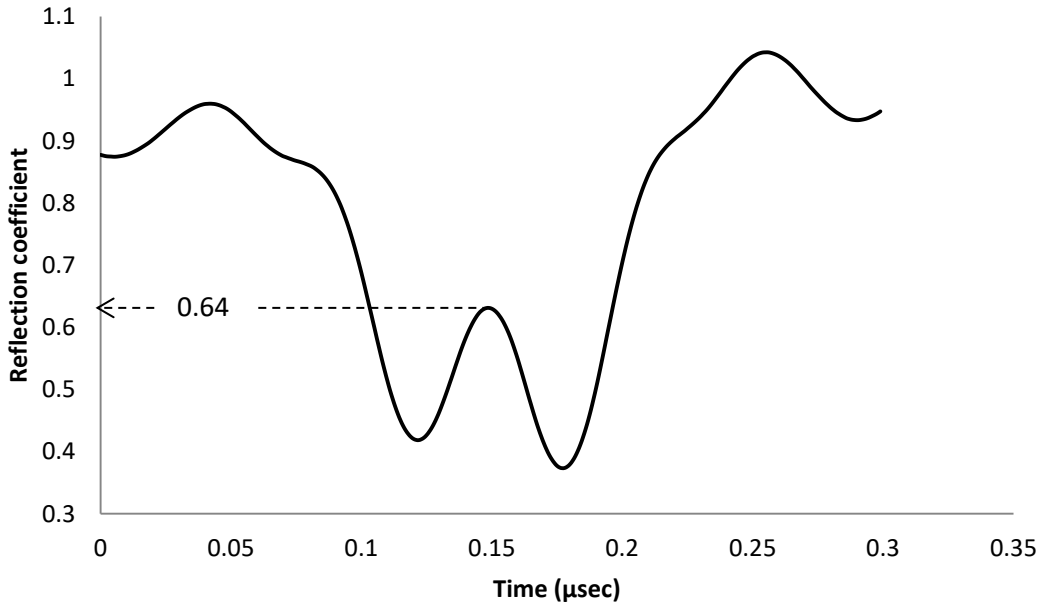

Figure 5-20: Reflection coefficient against Time-of-Flight

The reflection coefficient at the centre of the roll-bite was selected as this occurs between the dips at a point of no-interference. In Figure 5-20, a reflection coefficient of 0.64 was obtained at a peak amplitude value for the centre of the roll-bite, which was the same with the reflection coefficient value obtained from the frequency domain shown in Figure 5-19. Therefore, the entire reflection coefficient values utilised in this research was obtained by the technique explained and shown in Figure 5-20.

5.3.5 Effect of Loads on the Wave Reflection from the Back Surface of the Strip

Figure 5-21 shows the processed reflected signal obtained from the strip surfaces at each applied load. Waveforms A and B, shown in Figure 5-15, are the wave reflections from the front and back surfaces of the strip. The quality of the reflected waveform mainly depends on the strip thickness and the applied load. The strip thickness is determined with the

mathematical manipulation of the Time-of-Flight (Δt) between waveform signals A and B and the speed of the sound of the strip.

The Time-of-Flight (horizontal distance from the left edge of the graph) between the two waveforms (Figure 5-21) and depends on the rolling gap (vertical distance between the two adjacent rolls). The roll gap is usually controlled by the load applied through the screw stands of the milling machine. Moreover, the greater the applied load the less the roll gap distance and the smaller the strip thickness. Therefore, the Time-of-Flight of the reflected signal from the back surface of the strip reduces.

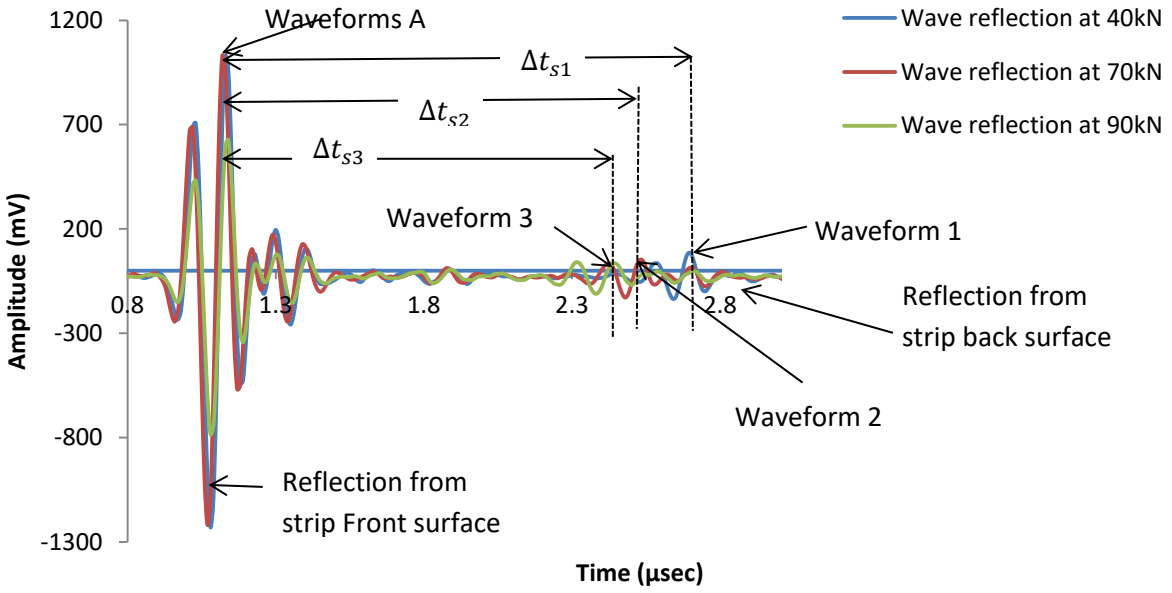

Figure 5-21: Wave reflection of the transmitted signal through the roll

Figure 5-21 shows the effects of applied loads on the reflected signal from the back surface of the strip. These waveforms were arranged on the same axis for ease of studying the effect of loads on the wave reflection from the back surface of the strip.

Furthermore, as the strip loaded during the rolling process, the wave path length of the reflected wave reduces. Also, the speed of the ultrasound in the stressed material increases, which leads to a reduction in ToF from waveform 1 to waveform 3. Hence, the energy of the wave reflected reduces due to wave transmission and dispersion at the metal-to-roll interface. This leads to the reduction in reflected wave amplitude value and the wave path length as is shown in Figure 5-21.

Figure 5-22 shows the waveforms of the wave reflection obtained from the back surface of the strip during the rolling process under the various loads applied. This figure has been separated from Figure 5-21 for improved visibility of the effect of the loads on the amplitude values of the reflections and the location of the Time-of Flight for each reflection.

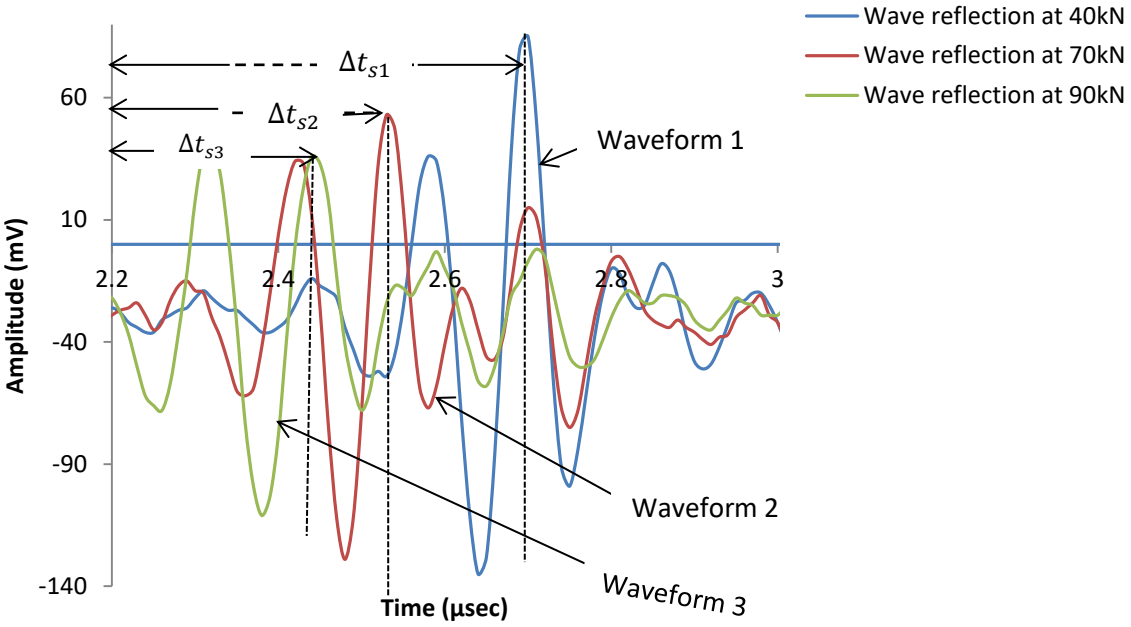

Figure 5-22: Effects of the applied loads on the reflected signal from back surface of the strip

The decrease in the amplitude value of the reflected signal (Fig. 5-22) was due to losses of the ultrasonic energy during the signal transmission through the lubricant and strip thicknesses. Therefore, as the load increases, the strip thickness decreases and loss of the reflected signal energy increases as more signal is transmitted. In addition, the Time-of-Flight of the reflected waves from the back surface (waveforms 1, 2, and 3) under the different loads applied, decreased as the applied load increased. As explained above, the position of all these waveforms (Time-of-Flight) corresponded to the strip thickness at the adjacent side of the roll gap during the operation. It is clearly shown that the higher the applied load the shorter the Time-of-Flight of the reflected signal transmitted through the strip.

Table 5-5 shows the Time-of-Flight of the reflection values measured between maximum peak from front and back surface waveforms shown in Figure 5-12 under the various rolling loads applied. The Time-of-Flight obtained from the distance between these two waveforms

was used to determine the strip thickness during the rolling operation. This is due to the fact that they are the most visible and formed in the same side of the graph.

Table 5-5: Values of the waves reflected parameters obtained from the back surface of the strip

Load (KN)	Percentage reduction (%)	Waveform of the rolled strip	Different of Time-of-Flight "Δt_s" (µsec)	Amplitude Value (mV)
40	8.4	1	1.58	85
70	14.4	2	1.45	53
90	24.0	3	1.34	36

Consequently, this measurement technique was utilised in order to obtain the Time-of-Flight value between the two waveforms which was then used to calculate the rolled strip thickness during the metal rolling operation that explained in Section 5.3.6 below.

5.3.6 Calculation of Strip Thickness

Figure 5-23 shows the illustration of wave reflections (Fig. 5-22) from the back surface of the strip during the rolling process under the various applied loads when the sensors are in contact with the roll and strip interfaces. The wave reflected Time-of-Flight graphs (Figs. 5-21 and 22) represent the reflections from different back surfaces of the strip in accordance with their thickness during the rolling process. From Figure 5-23 below, the 1st interface represented the strip front surface (1st thickness) during the first loading (40 kN), while the 2nd and 3rd interfaces represented the strip front surfaces during the second (70 kN) and third (90 kN) loading respectively.

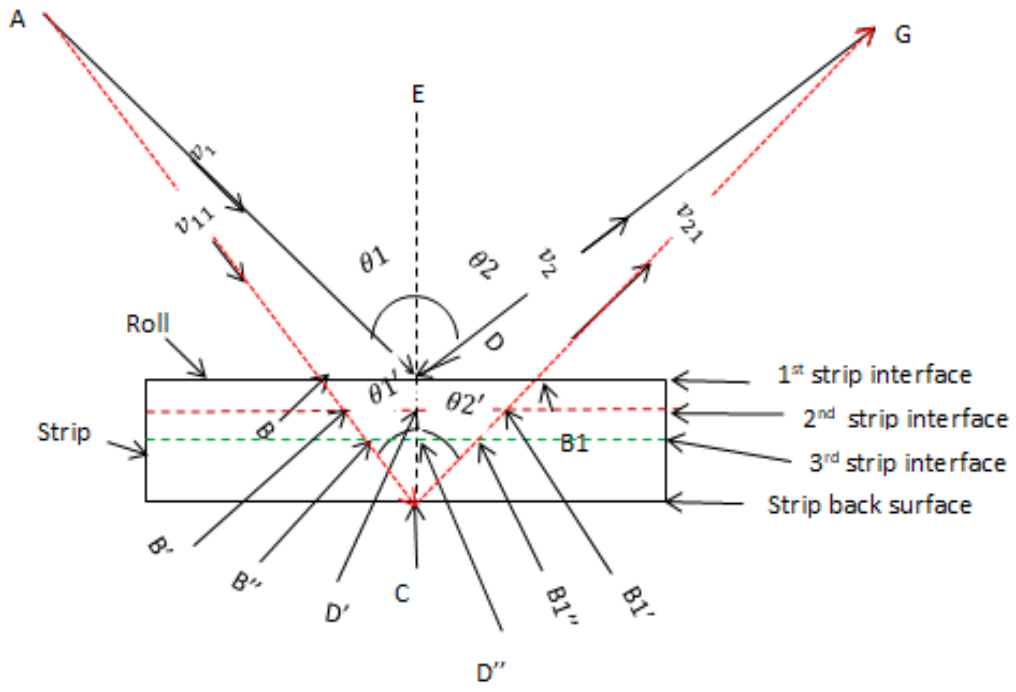

Figure 5-23: Sketch of signal transmission between rolls and strip interface under various applied loads

v_1 and v_{11} are diverged incidences wave sent by sensor A (pulser) that hit the strip at front and back surfaces at angles while v_2, and v_{21} are the reflection of the incidence waves from both front and back surfaces of the strip received by the sensor G (receiver) respectively. These parameters were assumed to denote the reflection of the waves from the surfaces of the media under the various loads applied. Therefore, B and B1 represented the wave incidence and reflected points for the first applied loading at the 1st interface, B' and B1' for the second loading at 2nd interface while B'' and B1'' for the 3rd loading at the third interface respectively. Points D, D', D'' and C were located at neutral planes.

In addition, Figures 5-24 (a-c) are the triangle blocks extracted from the signal transmission sketch, shown in Figure 5-23, to determine the thickness of the rolled strip under the various deformation loads applied. The lines DC (Fig. 5-24 (a)), D'C (Fig. 5-24 (b)) and D''C (Fig. 5-24 (c)) represented the actual strip thickness (t_f) value under the 40kN, 70kN and 90kN. While lines CB1 (Fig. 5-24 (a)), CB1' (Fig. 5-24 (b)) and CB1'' (Fig. 5-24 (c)), denoted the Time-of-Flight of the wave reflection from the back surface of the rolled strip under the various values of loads mentioned above.

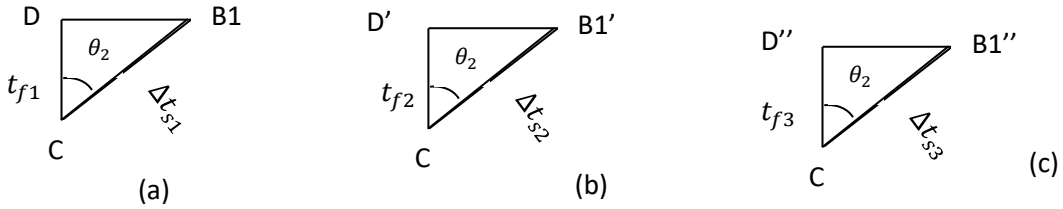

Figure 5-24: Trigometic ratio diagram to calculate the strip thickness under the various load applied

The properties of the wave reflection data obtained from the strip and roll surfaces, under the various loads applied, are shown in Table 5-5. These properties were used with the properties of the transducers employed to determine the value of the rolled strip thickness under the various applied loads.

The thickness of the strip along the path length of the signal transmission (lines CB1, CB1' and CB1'' in Fig. 5-23) was firstly calculated with the obtained Time-of-Flight of the wave reflection from its back surface for the applied loads with equation 5-1.

Then, the actual value thickness of the strip was finally obtained by mathematical manipulation of the obtained value of the first of the strip thickness with the trigonometric ratio principle expressed in equation 5-3.

An angle of 19^{o} was employed as the incidence angle in this research. The final value of the strip thickness obtained during the rolling process was calculated with the individual applied load and is presented in Figure 5-25. The value of the rolled strip thicknesses obtained were plotted against the Time-of-Flight and applied loads. Figure 5-25 shows the decrease in the strip thickness value with increases of applied loads. It also shows the related decreased Time-of-Flight of the reflected wave from the back of the strip.

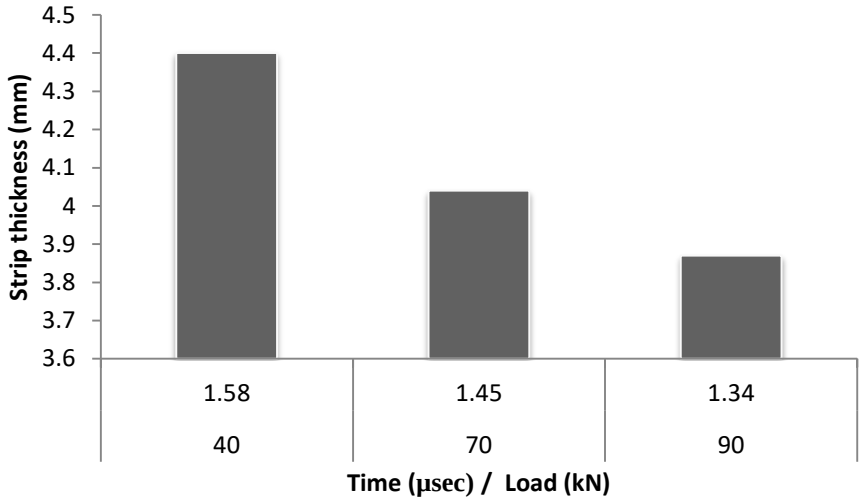

Figure 5-25: Strip thickness values obtained by the ultrasonic measurement technique

Figure 5-26 shows the relationship between the ultrasonic measured rolled strip thickness and the applied loads. The strip thicknesses obtained by ultrasonic measuring techniques were slightly different from those measured values achieved with a Vernier calliper. The difference between strip thicknesses obtained from the ultrasonic oblique reflection and the other obtained by the Vernier calliper measuring device after the process is shown in Figure 5-26.

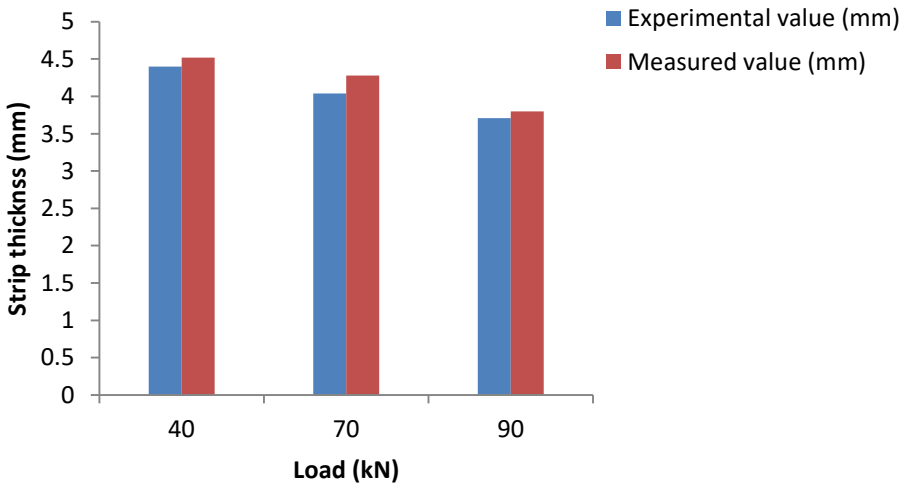

Figure 5-26: Strip thickness values obtained the by ultrasonic and manual measurement techniques

Furthermore, the small differences in strip thickness measured value (Figure 5-26) between the ultrasound and the manual (Vernier calliper) measurement methods, may have been due to either human error or device error. An imperfectly smooth surface may also cause a problem on the strip. This method is also suitable to determine the strip thickness during the

rolling process once the ultrasonic reflection Time-of-Flight of the transmitted signal is known.

5.3.7 Determination of the Strip Thickness using th Strip-To-Roll Interface Profile

Figure 5-27 shows the front page of the software written in NI LabVIEW used for the analysis of the reflected data obtained from the roll-to-strip interface profile during the rolling process.

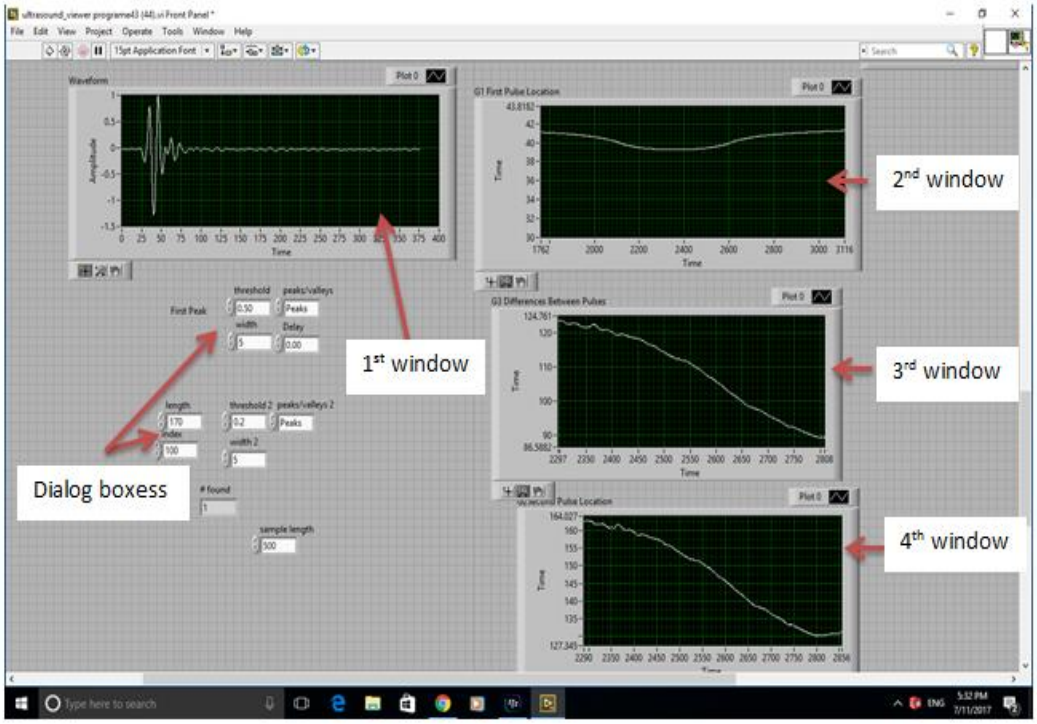

Figure 5-27: Front page of the software used to extract the wave reflected data

The page consists of four different windows and some dialog boxes. The 1st window shows the raw data from which the Time-of-Flight between the waves reflected from the strip-to-roll interface and the back surface of the strip during the rolling process.

Figure 5-28 shows the waveform of the roll-to-strip interface and strip back surface reflections imported from the 1st window.

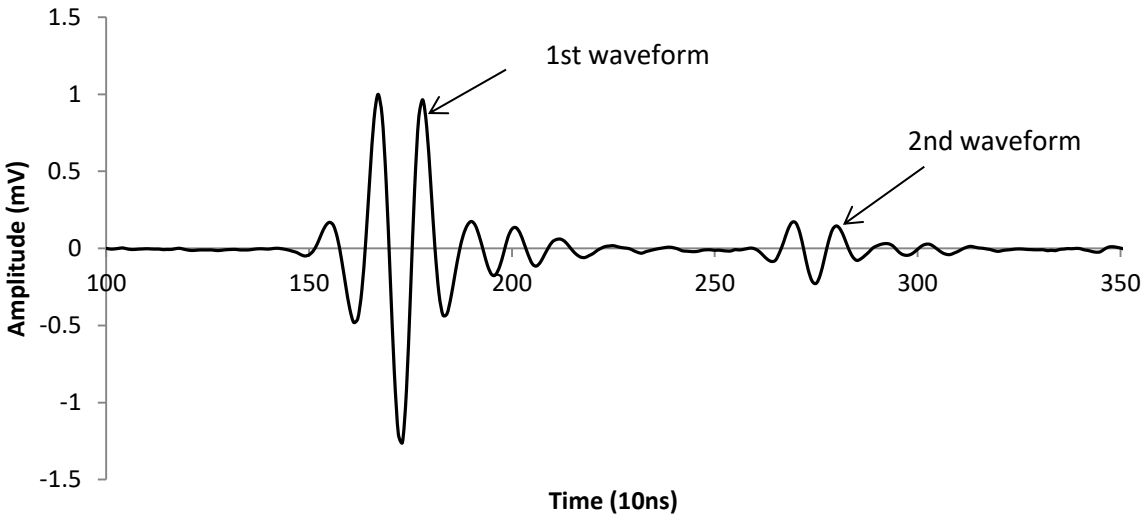

Figure 5-28: Wave reflection obtained between the rolled strip and roll

As shown from Figure 5-28, 1st waveform is the wave reflection obtained from the strip-to-roll interface while 2nd waveform is the reflection obtained from the back surface of the strip.

The strip profile reflection data program from the 3th window is plotted in terms of Time-of-Flight against pulsing number as shown in Figure 5-29.

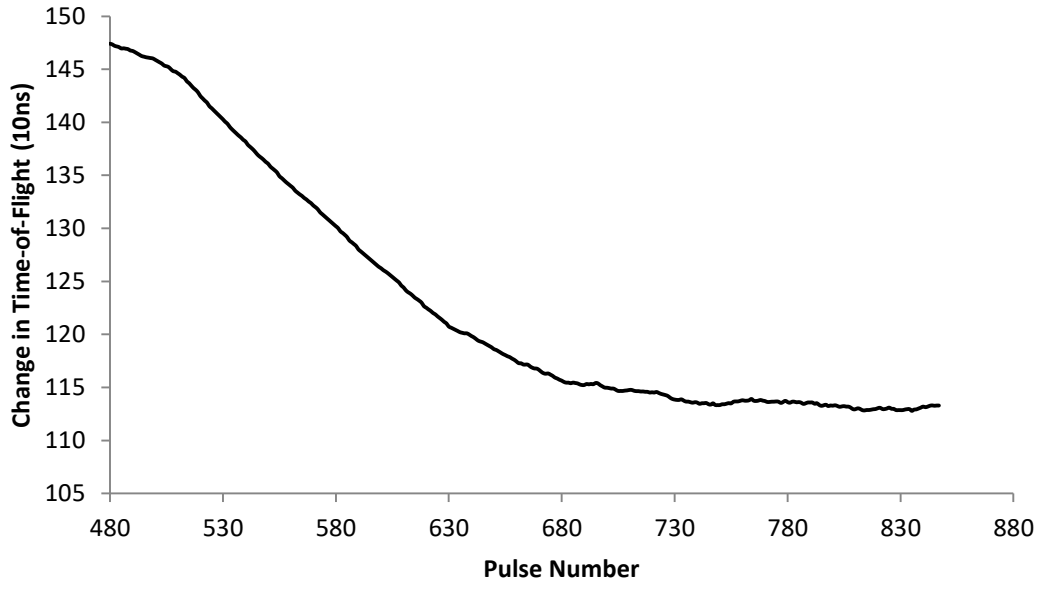

Figure 5-29: Time-of-Flight difference and pulse number between the rolled strip and roll

The strip thickness was determined with the aid of the extracted data shown in the figure above. This was done by mathematical manipulation of the obtained change of Time-of-Flight data into strip thickness with the aid of equations 5-2 and 5-3. The distance across the roll-bite is obtained by dividing the pulse number by the pulse rate (1000/sec) and multiplying by the roll speed (26mm/sec) and is presented in Figure 5-30 below.

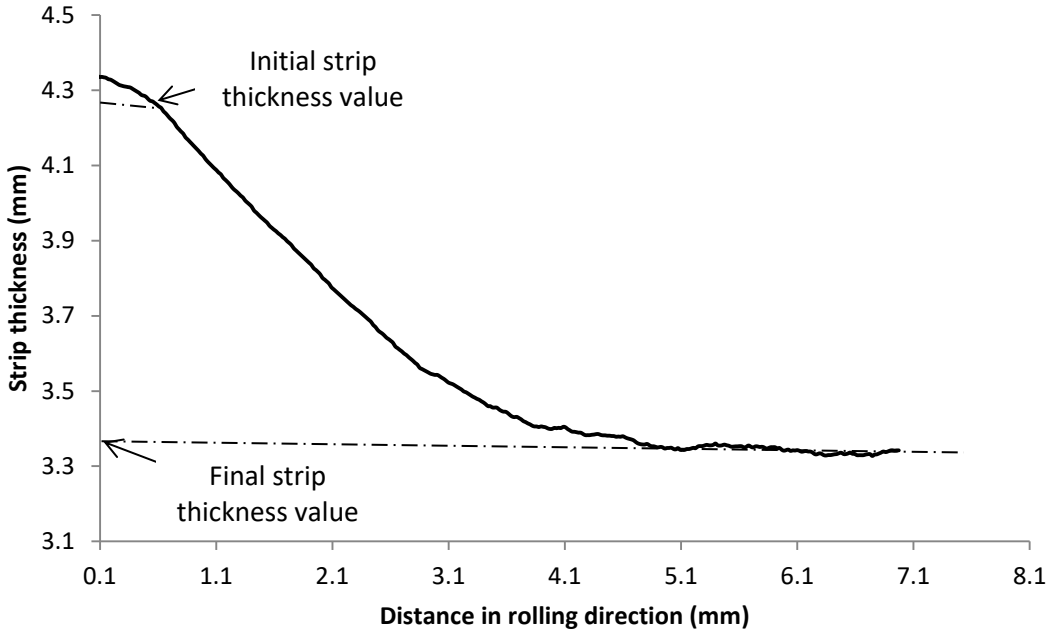

Figure 5-30: Experimental determination of strip thickness

The initial strip thickness was located on the graph at a point where the curve line started while the final strip thickness was sited where the graph curve line remain constant. The determination of the strip thickness explained in this section show the full picture of the strip thickness from the initial to final thicknesses. This is useful for extracting further details on the rolled strip such as, change-in-strip thickness and percentage metal thickness deformation, which is not possible by the method employed in Section 5.3.6.

Finally, the dimensions of the strip thicknesses were measured with a micrometre before and after metal rolling and compared with the experimental value in Table 5-6.

Table 5-6: Strip thicknesses obtained from different measurement techniques

Parameters	Ultrasonic measured values (mm)	Vernier calliper measured values (mm)
Initial strip thickness	4.28	4.50
Final strip thickness	3.40	3.78

The experimental values obtained had a difference of 0.22mm from the initial and 0.38mm from the measured values. This may have been a speed of sound value, caliper accuracy and elastic and plastic deformation of the strip during the rolling process.

5.3.8 Determination of the Roll-Bite Length

As explained in chapter 2, the roll-bite is simply the distance between the entry and exit zone of the of the metal-to-strip interface. Therefore, Figure 5-29 shown in Section 5.3.7 was reproduced as Figure 2-31 due to the reason that it was already used to calculate the distance across roll-bite contact length. This was used as information to determine the roll-bite experimentally. Rolling time can be converted to contact length via the rolling speed as no roll skidding was observed during the metal roll process, possibly due to the low rolling speed, the small percentage value of the metal reduction and the moderate thickness (5mm) value of the strip applied during the operation.

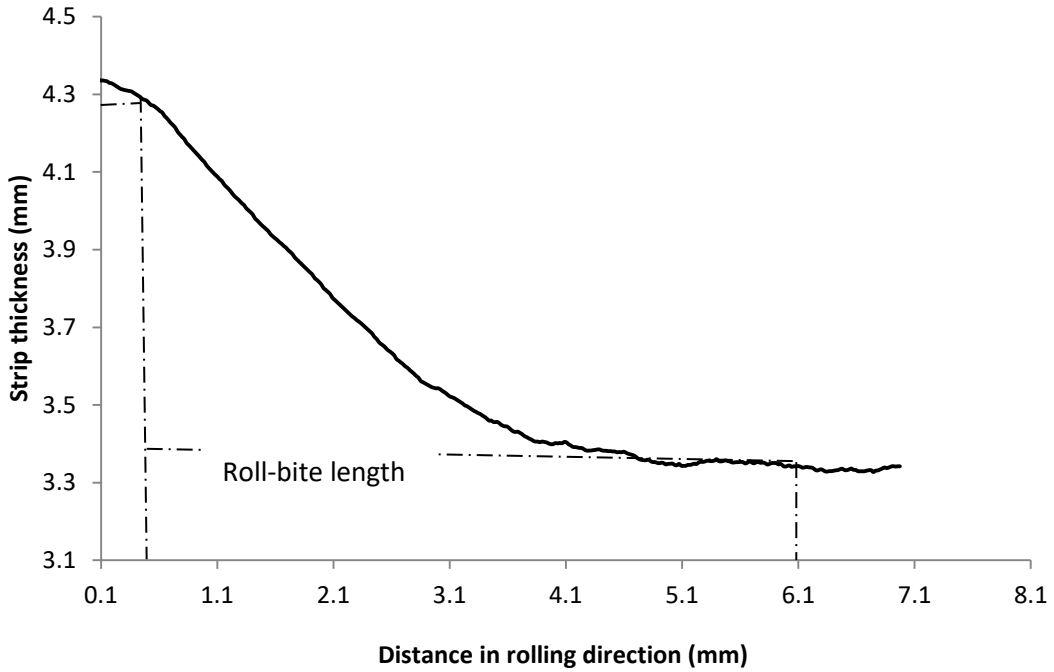

Figure 5-31: Roll-bite length between the strip-to-roll interface

The roll-bite length was sited along the curve line of the graph for the reasons stated in Section 5.3.7. The value of 5.59mm was obtained as the roll-bite length from the distance between the initial (0.51mm) and final (6.1mm) points sited along the curve line in the graph (Figure 5-32). The theoretical approach for the roll-bite length was discussed in Section 2.2.; this principle was used to calculate the roll-bite length theoretically with equation 2.3., and

the measured strip data stated in Table 5-6. In Section 5.3.7., a value of 6.29mm was obtained and these two results were compared with the aid of Figure 5-32.

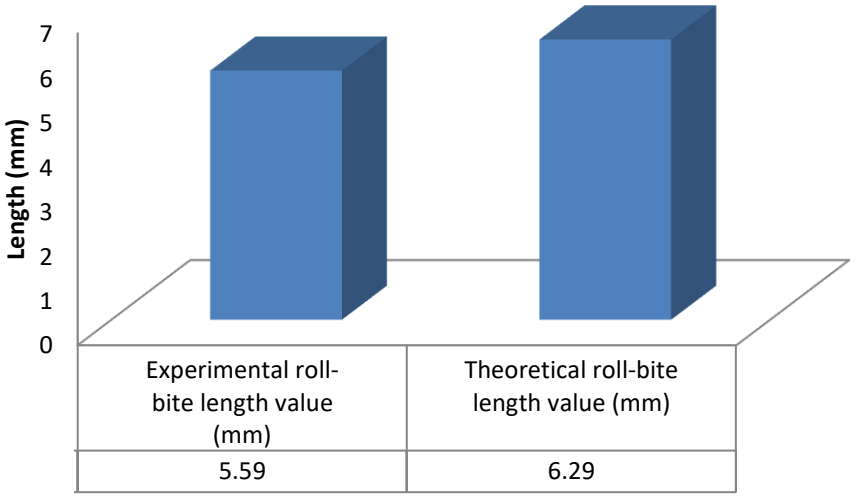

Figure 5-32: Comparison of roll-bite length values

Although, they are differ by 0.7mm, the causes of the difference may be due to assumptions made during the formulation of the theoretical background of the approach. It had been assumed that the roll should be perfectly curved, which is not possible during the rolling process.

After the expected ultrasonic sensor beam size at the metal-to-roll interface was estimated in Section 5.1.3, it was discovered that the line contact of metal-to-roll interface is large enough to accommodate the transmitted ultrasonic signal with minor blurring that may be developed the process without significant effect on the obtained data. Due to the fact that the small diameter of the sensor produces the small size of the beam width that interacts with the interface during the experiment, this minimized the error that may occur during the measurement. The smaller the diameter of the sensor the more the sensitivity and the lesser measurement error obtained. The experimental contact length obtained is 5.59mm compared to the 1.79mm ultrasonic beams width estimated. Therefore, little or no error is expected due to the fact that the ultrasonic beam width point will always be at the centre of the interface for every rolling operation.

5.4 Comparison with the Literature

Carretta et al in [92] applied the same ultrasonic technique (pulse-echo) with internal sensors fitted in the work roll to determine the rolled strip thickness and roll-bite length during the metal rolling process. They explained that the experiment was performed using an industrial rolling mill with 387mm roll diameter, 22.5m/min (375mm/s) roll speed and 2.8mm thickness, 100mm width and 490m length of IF steel. In-addition, it was reported that the investigation was conducted for 30% metal reduction as well as application of ultrasonic shear signal of 3252m/s propagation speed in the rolling material. Figure 5-33 shows the wave reflections obtained from the front (roll interface) and back surfaces of the strip during the rolling process. The time difference between the rolled strip front and back surfaces waveform is equivalent to the rolled strip thickness.

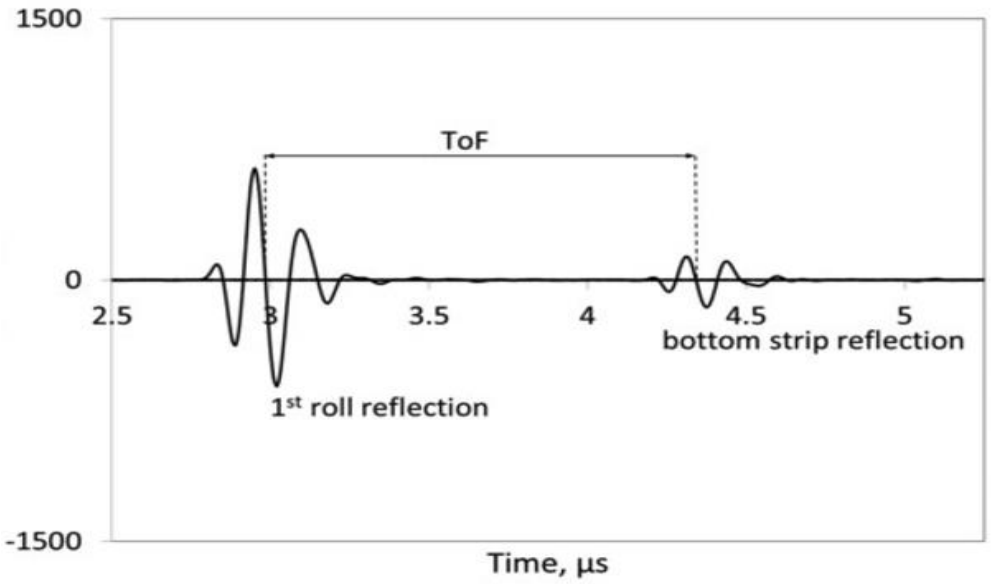

Figure 5-33: Wave reflection obtained between the rolled strip and roll surface [92]

As can be seen from the figure above, the value of 2.11mm (1.3µsec) rolled strip thickness is obtained using the time-of-reflection method. This compares well to the expected exit strip thickness of 2.14mm, with a 1.42% error.

As demonstrated in this chapter, an oblique reflection technique was employed to measure the rolled strip thickness and roll-bite length during the metal rolling process in this research. The experiment was conducted using pilot rolling mill at 26mm/s roll speed with 14.4% (0.72mm) metal reduction for 5mm thickness of mild steel. The details of the rolling material as well as pilot mill used are shown in Table 5-1.

Despite the difference in the sensor configurations, percentage metal reduction and roll speed, the wave reflections obtained in this research when the sensor surfaces are in contact with the metal-to-roll interface show similar trend with those obtained in Carretta et al. [92] (Figs. 5-15 and 5-33).

The comparison of the strip thickness results of the proposed approach in this research with those of the theoretical calculations has been discussed extensively in Section 5.3.6. As can be seen from Section 5.3.6 (that shows oblique and caliper values for the various applied rolling load/percentage metal reductions), the technique employed in this research is accurate with only minor difference of 0.24 (6%) between the rolled strip thickness value and the rolled strip thickness value obtained with the caliper (for 70kN rolling load/14.4% metal reduction). The error in both this work and reported in literature [92] are both low, 6% and 1.42% respectively. These errors are by a number of factors. Firstly, a tabulated value for the speed of sound (5900m/s) was used in this research, this may differ slightly from the actual speed of sound in the applied strip. Secondly, in this work a longitudinal sensor was used. This has a shorter Time-of-Flight than the shear waves used by Carretta et al. [92], due to the higher speed of sound. Therefore, any error in the ToF measured will have larger error on the thickness measurement.

As already mentioned, Carretta et al. [92] applied modelling and experimental procedure to measure the roll-bite length during the metal rolling with the rolling parameter conditions stated above. The obtained experimental data and simulation value were used to plot the strip thickness against the roll-bite length as shown in Figure 5-34.

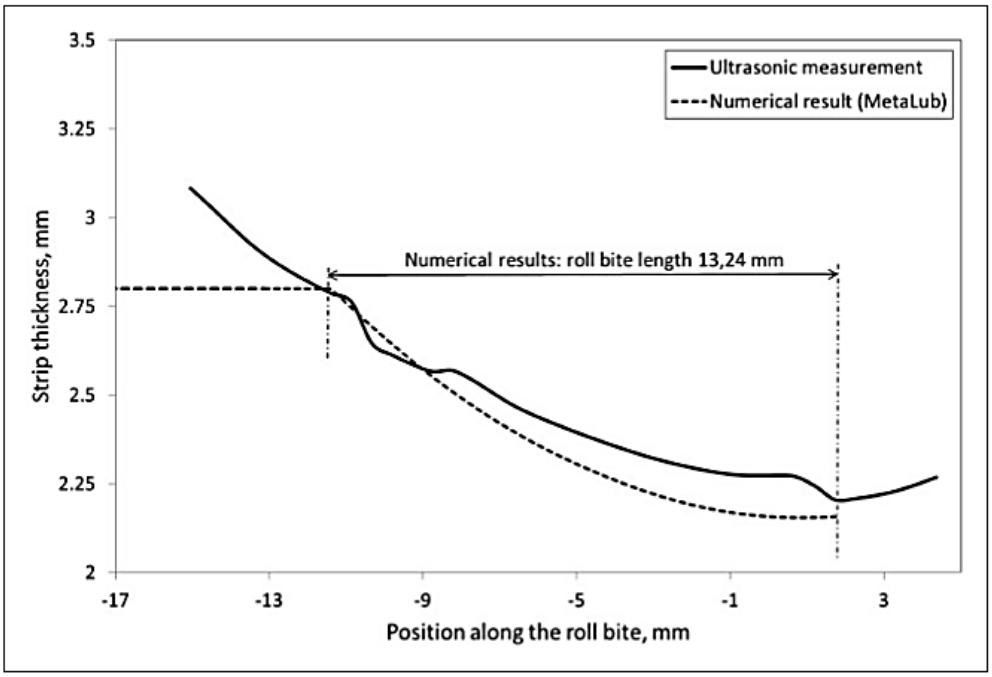

Figure 5-34: Strip thickness against the roll-bite length [90]

As can be seen in the figure above, the obtained results (Figure 5-34), shows a similar trend with the strip thickness against roll-bite length obtained in this research (Fig. 5-31), despite the difference of the rolling parameters condition involved. The results obtained from this proposed approach have been extensively discussed and compared with the theoretical calculations value of roll-bite length obtained in Section 5.3.8.

The contact length measured by Carretta et al. [92] was 13.24mm, whereas the theoretical value for these rolling conditions is 11.146mm. This gives an error of 15.8%. A relatively minor difference of 0.7mm (12% error) was observed between this research value and the theoretical value. The reason for the variation of the theoretical value and the value of this research has been discussed in Section 5.3.8. Similar magnitude of errors is seen in both works with the results in this work showing less error. There may be some error selecting the entry and exit points of the roll-bite. Additionally, the theoretical values assume a perfect condition. This is not practically possible.

Detailed comparative studies were carried out between the obtained data from Carretta et al. [92] as well as those of theoretical and direct measurements via the measuring device on strip thickness and roll-bite length values. Similar trends were observed in these comparative studies. In particular, it is shown that the two techniques (external and internal ultrasonic sensor layout methods) correspond to one another which implies the reliability of

the measurement system. The external ultrasonic technique employed by this research looks more accurate, due to the minor percentage variation of a roll-bite length and strip thickness obtained compared with the roll-bite length obtained by theoretical approach. Although, it is difficult to compare the accuracy of the values obtained in [92] with the values obtained by this research; due to the difference of the rolling parameter conditions applied by both approaches.

This external sensor layout configuration used in this research has been applied to study the roll gaps conditions and this arrangement does not result in markings on the rolled product surface under large contact pressure when compared with the existing techniques. As such, the experimental methodology is suitable for real-time measurements in the roll-bite of an industrial mill.

5.5 Conclusion

This chapter has described the design and construction procedure for the development of a new external ultrasonic experimental technique for studying metal-to-roll interface conditions. These arrangements have been implemented on the pilot rolling mill and tested using two experiments (stationary and dynamic) conditions. The following conclusions are drawn:

- The instrumented roll was successfully installed and implemented onto the pilot roll mill,
- The strip thicknesses at both stationary and at rolling conditions were able to be determined using the reflected wave obtained from the strip back surface,
- The effect of the loads on the ultrasonic wave reflection from the back surface of the strip and strip thickness was successfully viewed and studied,
- The length of the roll-bite value was experimentally determined and compared with the calculated values,
- Strip thickness profile across roll-bite was observed.

Chapter 6

Modelling of Normal and Oblique Reflection at an interface

This chapter describes and compares the obtained sound wave reflection coefficient at an interface between two media with pulse-echo and pitch-catch ultrasonic measurement techniques by modelling and experimental processes. Modelling of the incidence angle at 0^{o} and 19^{o} was carried out with matrix techniques for multi-layered inspection theory. The experimental part of the study was carried out on a pilot metal rolling mill, with an instrumented upper roll, equipped with piezoelectric elements at 0^{o} to the roll surface for pulse-echo and 19^{o} for pitch-catch measurement techniques.

6.0 Introduction

The aim of this section is to create a model of the oblique reflection process and compare with the experimental reflection of an ultrasonic signal transmitted to the interface of thin fluid contact at different incidence angles. The use of ultrasonic oblique reflection methods for measurement is quite challenging due to its layout arrangement.

Some researchers [93-98] have used normal and oblique ultrasonic pulsing techniques, and compared the reflection coefficient obtained from the two. They have mostly concluded that minor differences are observed in their reflection coefficient values, up to 22.5^0 of incidence angles. The reflection coefficient obtained between the model and experiment approach shows that the oblique reflection ultrasonic technique may play an important role in the determination of the roll interface conditions during the metal rolling process.

6.1 Relationship for Oblique Reflection and Transmission

The oblique transmission and reflection of longitudinal and shear incidence waves at a solid-to-solid interface is shown schematically in Figure 6-1.

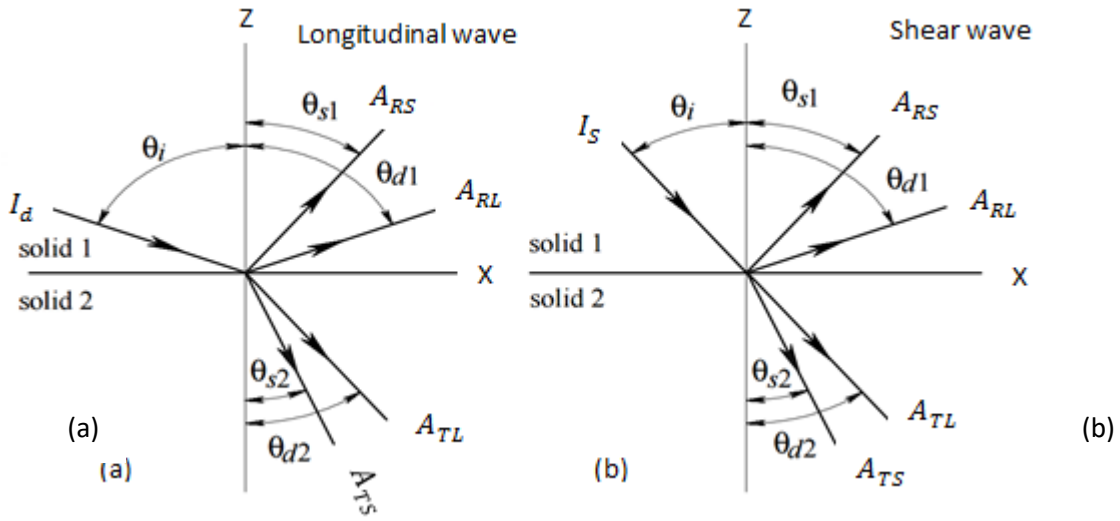

Figure 6-1: Longitudinal and shear wave interaction with a solid-to-solid interface

Where; I_d is a longitudinal incidence wave and θ_i is the angle of incidence. As shown in the figures above, A_{RL}, A_{RS}, A_{TL}, and A_{TS} are the reflected longitudinal, reflected shear, transmitted longitudinal and shear transmitted waves respectively, while θ_{s1} and θ_{d1}, θ_{d2} and θ_{s2} are angles of reflection and transmission of each wave. When a longitudinal wave hits the perfectly bonded interface of the two materials, at any angle θ_i (either longitudinal

or shear) some portion of the wave is reflected at the same angle with reflected angle θ_{d1} for the longitudinal wave (Figure 6-1 (a)) and θ_{s1} for the shear wave (Figure 6-1 (b)). The remainder of the wave that is transmitted into the second material and divided into two parts; longitudinal with an angle of θ_{d2} and shear with an angle of θ_{s2}. This kind of wave mode conversion takes place for both longitudinal and shear waves when crossing from one boundary to another. The angles of reflection and refraction of the transmitted waves depend on the acoustic properties of the materials, the angle of incidence and the nature of the interface (either liquid or gas).

The angles of reflection and refraction of the transmitted signals can easily be determined by Snell's Law, once the incidence angle and speed of sound in the material are known [98]. The relationship between the incidence and reflected angles at the materials interface shown Figure 6-1 and the speed of sound traveling in them during the process are expressed as follows:

$$\frac{\sin\theta_i}{C_{Id}} = \frac{\sin\theta_{dI}}{C_{RL}} = \frac{\sin\theta_{sI}}{C_{RS}} = \frac{\sin\theta_{d2}}{C_{TL}} = \frac{\sin\theta_{s2}}{C_{TS}} \qquad 6\text{-}1$$

In acoustic analysis, the speed of sound c and the wave-number k relationship is expressed as follows:

$$c = \frac{\omega}{k} \qquad 6\text{-}2$$

Substituting equation 6-2 into equation 6-1, gives:

$$k_{Id}\sin\theta_i = k_{RL}\sin\theta_{dI} = k_{RS}\sin\theta_{sI} = k_{TL}\sin\theta_{d2} = k_{TS}\sin\theta_{s2} \qquad 6\text{-}3$$

Reflection and transmission of oblique incidences can now be considered, once Snell's Law is understood [99].

6.1.1 Effects of Media Properties on the Mode of Wave Reflection and Transmission

Figures 6-2 (a-d) show the reflection of the incident wave as it hits different types of interface. Figure 6-2 (a) shows the reflection of the longitudinal signal from a fluid to a vacuum interface. The entire incidence signal is reflected at the same angle ($\theta_i = \theta_r$). The reason is that sound waves correspond to a mechanical energy that only transmits through

the media. This phenomenon occurs for both shear and longitudinal waves because neither can transmit through a vacuum.

However, the shear signal is attenuated faster in a fluid medium than a longitudinal signal. This is the reason why the generation of the shear signal conversion on the opposite side is not possible in a liquid medium, unlike in a solid to vacuum interface, as shown in Figure 6-2 (c). In Figure 6-2 (b), which is the fluid-to-fluid interface, the angle of reflection and the transmission of the longitudinal wave are obtained based on Snell's Law. The reflected and transmitted modes of longitudinal wave (I_d) are shown in different media in Figure 6-2a and 6-2b, which is not possible for the shear wave (I_s). This is due to the fact that both gases and liquids are not capable of transmitting the shear wave. Therefore, the shear wave can only penetrate through the solid material during the signal transmission process [77]. The reflection of the longitudinal and shear waves occurred as shown in Figure 6-2 (c and d) respectively; because they are slowly attenuated in solid media. The transmission and mode of the shear and longitudinal signals conversion with the media are shown in Figure 6-1 (a and b).

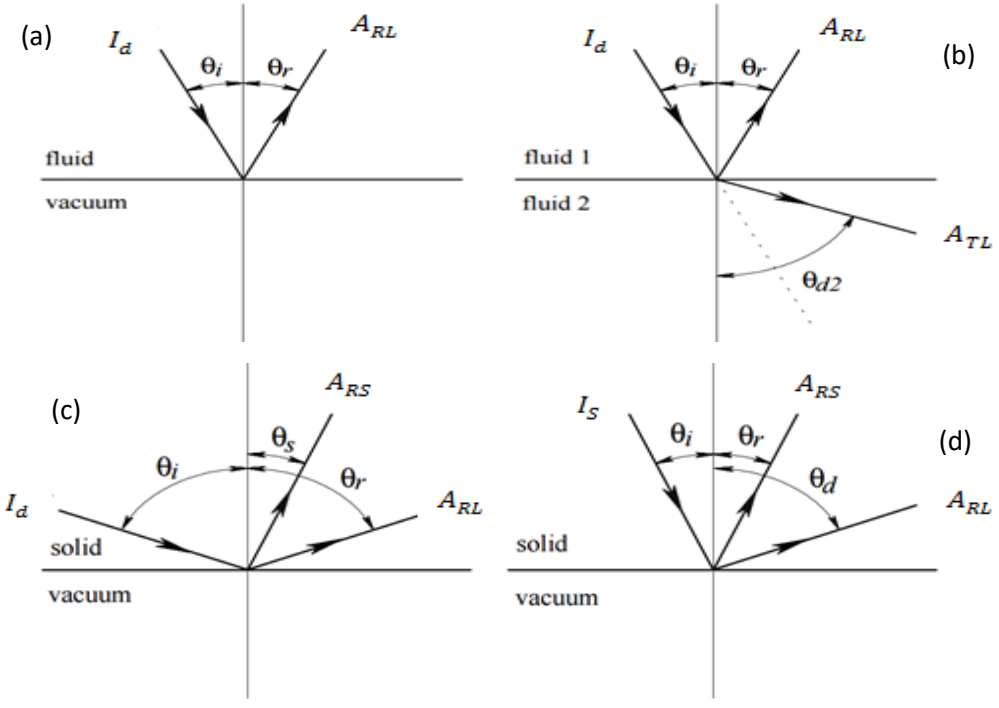

Figure 6-2 (a – d): Interaction waves with different interfaces [77]

6.2 Propagation of Oblique Incidence Wave through an Embedded Layer

The characteristics of the reflection and transmission of an oblique longitudinal incidence wave within a thin layer of fluid are shown in Figure 6-3. The layer is considered as a microscopic interface with effective properties dependent on the interface structure [9]. The angles of reflection and transmission indicated are derived from equation 6-1. Their relationship is shown in equation 6-3 in Section 6.1, above.

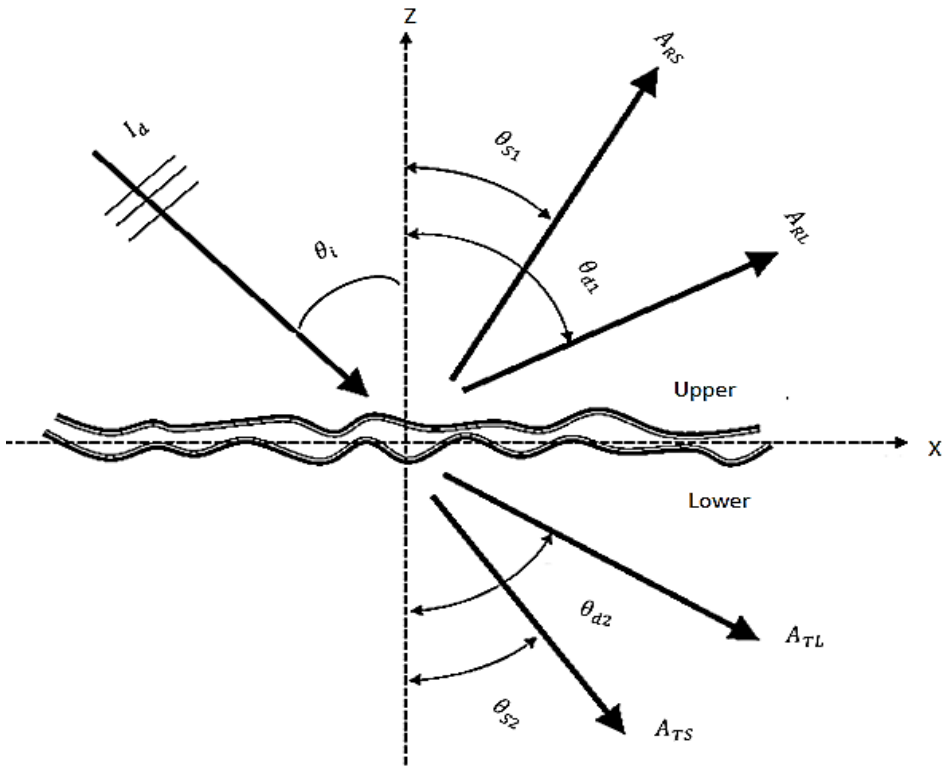

Figure 6-3: Transmission of an incidence longitudinal wave through the embedded layer [98]

The wave reflections and interactions within the interfaces of the embedded liquid layer of the solid-to-solid contact (semi-infinite media), shown in Figure 6-3, are presented in Figure 6-4. In this figure, the interface between the two solid media considered as a single layer. The particle velocities (or displacements) and stresses on the upper and lower interfaces between the layer can be related to each other with the aid of a transfer matrix expressed as follows:

$$\begin{Bmatrix} \sigma_{zz} \\ \sigma_{zx} \\ w \\ u \end{Bmatrix}_t = [M] \begin{Bmatrix} \sigma_{zz} \\ \sigma_{zx} \\ w \\ u \end{Bmatrix}_b \qquad \text{[95, 96] 6-4}$$

[M] is 4 X 4 matrix. The subscripts b and t denote the bottom and top layers, while σ_{zz} and σ_{zx} are the normal and tangential stresses. Also, w and u are the vertical and horizontal displacements. While the elements of the matrix M depends on the layer property. Equation 6-4 can be regarded as the boundary condition, which relates the stress and particle displacement between the top and the bottom layered interfaces.

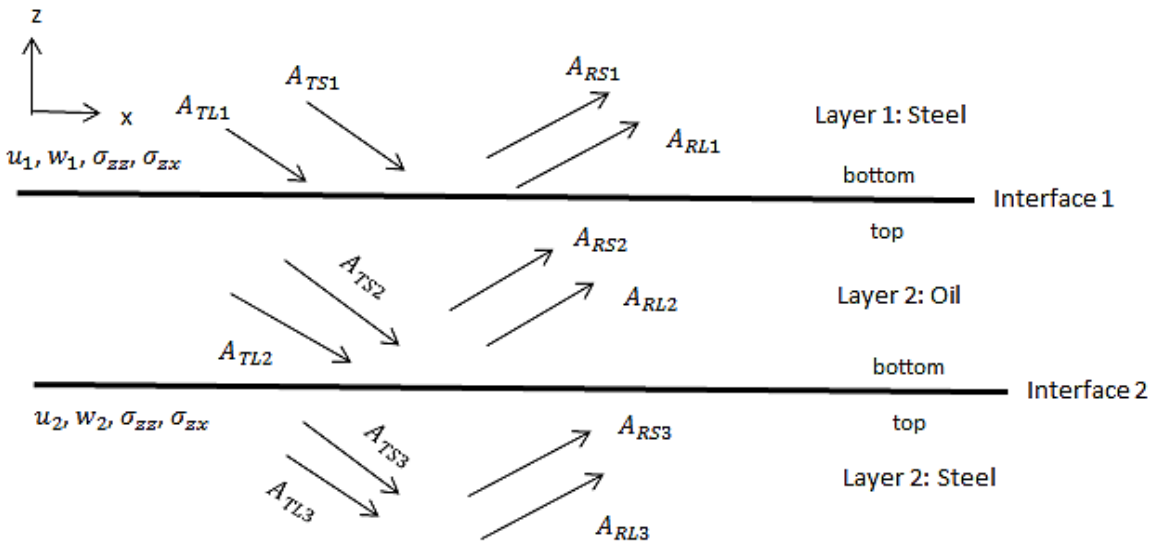

Figure 6-4: Interaction and the signal mode conversion within the embedded layer

Once the longitudinal wave strikes interface 1 (bottom of layer 1) at an angle, the transmitted and reflected waves produce a unique stress and displacement on both sides of the layer [100]. The amplitudes of the reflected and transmitted waves may be found by using the matrix Equation 6-4. The deflections of the longitudinal and shear wave are given by Pilarski [94]:

1. For the horizontal displacement,

$$u_L{}^+ = A_L{}^+ \sin\theta_{d2} e^{(ik^L \cos\theta_{d2} Z)} \quad \text{6-5}$$

$$u_T{}^+ = -A_T{}^+ \cos\theta_{s2} e^{(ik^S \cos\theta_{s2} Z)} \quad \text{6-6}$$

$$u_L{}^- = A_L{}^- \sin\theta_{d1} e^{(-ik^L \cos\theta_{d1} Z)} \quad \text{6-7}$$

$$u_T{}^- = A_T{}^- \cos\theta_{s1} e^{(-ik^S \cos\theta_{s1} Z)} \quad \text{6-8}$$

2. For the vertical displacement,

$$w_L{}^+ = A_L{}^+ \cos\theta_{d2} e^{(ik^L \cos\theta_{d2} Z)} \quad \text{6-9}$$

$$w_T{}^+ = A_T{}^+ \sin\theta_{s2} e^{(ik^S \cos\theta_{s2} Z)} \quad \text{6-10}$$

$$w_L{}^- = -A_L{}^- \cos\theta_{d1} e^{(-ik^L \cos\theta_{s1} Z)} \quad \text{6-11}$$

$$w_T{}^- = A_T{}^- \sin\theta_{s1} e^{(-ik^S \cos\theta_{d1} Z)} \quad \text{6-12}$$

The u and w in the x and z axes are presented the displacement vectors of the longitudinal and shear waves in the upper and lower parts of the layer boundaries. The value of v was set to zero, because the structure is assumed to be in two dimensions and the y coordinate axis is implicit and is omitted in the mathematical expression. The superscripts (+) and (-) indicate the up and down movements of the wave at the layer interface respectively. While z is distance in the direction of wave propagation and A_L and A_T are the amplitudes of the displacement waves. In addition, k^L and k^S are longitudinal and shear wave numbers and expressed as follows:

$$k^L = \frac{\omega}{C_L} \text{ and } k^S = \frac{\omega}{C_S} \quad \text{6-13}$$

while C_L and c_S are the velocities of longitudinal and shear waves in the infinite isotropic medium. Normal and tangential stresses can be determined at any point within the isotropic and homogeneous boundary layers with the stress and strain relations:

$$\sigma_{ij} = \Lambda_{ij}\varepsilon_{kk} + 2\mu\varepsilon_{ij} \quad \text{6-14}$$

The relationships between the Lame constants $(\Lambda + \mu)$, density and velocities of longitudinal and shear waves shown in equations 6-15 and 6-16 below can used to calculate the stresses and displacement components in both x and z axes respectively. The relationships are expressed as follows:

$$\sigma_{xx} = \Lambda\frac{\partial u_z}{\partial z} + (\Lambda + 2\mu)\frac{\partial u_x}{\partial x} \quad 6\text{-}15$$

and

$$\sigma_{zx} = \mu(\frac{\partial u_x}{\partial z} + \frac{\partial u_z}{\partial x}) \quad 6\text{-}16$$

while

$$\mu = \rho {c_S}^2 \quad 6\text{-}17$$

and

$$\Lambda + 2\mu = \rho {c_L}^2 \quad 6\text{-}18$$

The normal and tangential stresses and displacements at the material boundaries can be determined by the relationships 6-5 to 6-18. These serve as the foundation for the analyses in subsequent sections.

As previously explained, the oblique longitudinal or shear wave reflection coefficient at an interface can be obtained with a transfer matrix approach [95, 96]. This can be done by relating the stresses and displacement components at the top face with those at the bottom. The bottom layer is denoted as k-th while the top layer is denoted as k+1. For the boundary conditions, the continuity of the normal and tangential stresses and displacements between the top and bottom faces are satisfied and expressed by the following matrix equation:

$$\left[M_{k,b}\right]\begin{Bmatrix}A_{RL,k}\\A_{RS,k}\\A_{TL,k}\\A_{TS,k}\end{Bmatrix}=\begin{Bmatrix}\sigma_{zz}\\\sigma_{zx}\\w\\u\end{Bmatrix}_{b} \quad \text{6-19}$$

$$\left[M_{k+1,t}\right]\begin{Bmatrix}A_{RL,k+1}\\A_{RS,k+1}\\A_{TL,k+1}\\A_{TS,k+1}\end{Bmatrix}=\begin{Bmatrix}\sigma_{zz}\\\sigma_{zx}\\w\\u\end{Bmatrix}_{t} \quad \text{6-20}$$

$$\left[M_{k,b}\right]\begin{Bmatrix}A_{RL,k}\\A_{RS,k}\\A_{TL,k}\\A_{TS,k}\end{Bmatrix}=\begin{Bmatrix}\sigma_{zz}\\\sigma_{zx}\\w\\u\end{Bmatrix}_{b}=\begin{Bmatrix}A_{RL,k+1}\\A_{RS,k+1}\\A_{TL,k+1}\\A_{TS,k+1}\end{Bmatrix}=\begin{Bmatrix}\sigma_{zz}\\\sigma_{zx}\\w\\u\end{Bmatrix}_{t} \quad \text{6-21}$$

For the solid-oil-solid system, equation 6-21 is chosen according to the generalised multi-layered system. Therefore, the relationship of interface 1 and interface 2 in Figure 6-4 is expressed as follows:

$$\left[M_{1,b}\right]\begin{Bmatrix}A_{RL,1}\\A_{RS,1}\\A_{TL,1}\\A_{TS,1}\end{Bmatrix}=\left[M_{2,t}\right]\begin{Bmatrix}A_{RL,2}\\A_{RS,2}\\A_{TL,2}\\A_{TS,2}\end{Bmatrix} \quad \text{6-22}$$

$$\left[M_{2,b}\right]\begin{Bmatrix}A_{RL,2}\\A_{RS,2}\\A_{TL,2}\\A_{TS,2}\end{Bmatrix}=\left[M_{3,t}\right]\begin{Bmatrix}A_{RL,3}\\A_{RS,3}\\A_{TL,3}\\A_{TS,3}\end{Bmatrix} \quad \text{6-23}$$

The problem is solved by assembling equations 6-19 and 6-20 and presented as follows:

$$\begin{bmatrix} [M_{1,b}] & -[M_{2,t}] & [0] \\ [0] & [M_{2,t}] & [M_{3,t}] \end{bmatrix} \begin{Bmatrix} A_{RL1} \\ A_{RS1} \\ A_{TL1} \\ A_{TS1} \\ A_{RL2} \\ A_{RS2} \\ A_{TL2} \\ A_{TS2} \\ A_{RL3} \\ A_{RS3} \\ A_{TL3} \\ A_{TS3} \end{Bmatrix} = \{0\} \quad \text{6-24}$$

In summary, four waves, longitudinal transmission, longitudinal reflection, shear transmission and shear reflection are considered in each medium (Figure 6-4). The boundary displacements and stresses of each layer are expressed in the form of matrix equations. These boundary conditions are satisfied by equating two sets of matrix equations involving displacements and stresses. The final equation to obtain the reflection coefficient is expressed as follows:

$$[M_b]\{X\} = [M_t]\{Y\} \quad \text{6-25}$$

$$\{X\} = [M_b]^{-1}[M_t]\{Y\} \quad \text{6-26}$$

In Equation 6-26, M_i generally explained the relationship between the amplitudes and the normal and shear stresses and displacement at any location on the media. As explained by Liaptsis [97], the amplitude of the incident longitudinal and shear waves in layer 3 will be equal to zero because the input wave was from layer 1.

Once the material properties and the incidence angle are known, the reflection coefficient is easily solved by the matrix equations shown in 6-27 and 6-28. Since the amplitude value of the incident wave is 1, the elements in the vector $\{X\}$ are the reflection coefficients to be found.

$$[M_b] = \begin{bmatrix} i\omega\rho_1\alpha_1\psi_1/g_{l1} & 2i\omega\rho_1 s{\beta_1}^2\xi_1/g_{s1} & -i\omega\rho_2\alpha_2\psi_2/g_{l2} & 2i\omega\rho_2 s{\beta_2}^2\xi_2/g_{s2} \\ -2i\omega\rho_1 s{\beta_1}^2\gamma_1/g_{l1} & i\omega\rho_1{\beta_1}^2\psi_1/g_{s1} & -2i\omega\rho_2 s{\beta_2}^2\gamma_2/g_{l2} & -i\omega\rho_2{\beta_2}^2\psi_2/g_{s2} \\ \alpha_1 s/g_{l1} & -\xi_1/g_{s1} & -\alpha_2 s g_{l2} & -\xi_2 g_{s2} \\ -\gamma_1/g_{l1} & -\beta_1 s/g_{s1} & -\gamma_2 g_{l2} & \beta_2 s g_{s2} \end{bmatrix} \quad 6\text{-}27$$

$$[M_t] = \begin{bmatrix} i\omega\rho_2\alpha_2\psi_2/g_{l2} & 2i\omega\rho_2 s{\beta_2}^2\xi_2/g_{s2} & -i\omega\rho_1\alpha_1\psi_1/g_{l1} & 2i\omega\rho_1 s{\beta_1}^2\xi_1/g_{s1} \\ -2i\omega\rho_2 s{\beta_2}^2\gamma_2/g_{l2} & i\omega\rho_2{\beta_2}^2\psi_2/g_{s2} & -2i\omega\rho_1 s{\beta_1}^2\gamma_1/g_{l1} & -i\omega\rho_1{\beta_1}^2\psi_1/g_{s1} \\ \alpha_2 s/g_{l2} & -\xi_2/g_{s2} & -\alpha_1 s g_{l1} & -\xi_1 g_{s1} \\ -\gamma_2/g_{l2} & -\beta_2 s/g_{s2} & -\gamma_1 g_{l1} & \beta_1 s g_{s1} \end{bmatrix} \quad 6\text{-}28$$

Vector $\{Y\} = \begin{Bmatrix} 0 \\ 0 \\ 1 \\ 0 \end{Bmatrix}$ for longitudinal incident wave.

While the matrix symbol parameters defined as follows:

$$s = \frac{\sin\theta_{IL}}{\alpha} = \frac{\sin\theta_{IS}}{\beta} \quad 6\text{-}29$$

$$\gamma = \sqrt{1 - \alpha^2 S^2} \quad 6\text{-}30$$

$$\xi = \sqrt{1 - \beta^2 S^2} \quad 6\text{-}31$$

$$\psi = 1 - 2\beta^2 S^2 \quad 6\text{-}32$$

$$g_l = exp\left(\frac{i\omega\gamma y}{\alpha}\right) \quad 6\text{-}33$$

$$g_s = exp\left(\frac{i\omega\xi y}{\beta}\right) \quad 6\text{-}34$$

Matrices $[M_b]$ and $[M_t]$ are employed in equations 6-27 and 6-28 to determine the reflection coefficient matrices $\{X\}$ as shown in Appendix 1.

6.3 Modelling of a Steel-Oil-Steel Interface

Computer simulations of the reflection coefficient of the incident wave were conducted at two different load levels from an interface of two media with the various ultrasonic sensor layout arrangements described in Chapter 4. This was done to study the effect of the incident angles in ultrasound wave propagation at the interface of two similar media.

The interface between two solids with a thin liquid layer at the middle is very complicated. For instance, the formation of a thin interface layer when two solids are bonded together either with a thin layer of another material, e.g., glue or oil, depending on the properties of

this layer. The boundary between the two solids may behave as slip, perfect, or neither. Its state has a significant effect on the wave reflection and mechanical behaviour of the interface [101].

Rokhlin and Wang [102], classified a solid-oil-solid interface into two classes, namely rigid and slip interfaces. These classes depend on the interface thickness layer, hence slip in solid-oil-solid can be achieved if the interface layer is a thin ideal liquid. One can assume that a liquid will behave in the interface as an ideal if the thickness of the layer is significantly large enough to separate the interface.

However, if the lubricant layer is very thin then this will not be sufficient to separate the media interface. Therefore the interface consists of isolated asperity contacts surrounded by the gaps filled with liquid and is referred to as mixed contact interface.

In this work, modelling developed by Pialucha [9] has been considered as the best software to investigate the effect of sound wave reflection from solid-oil-solid contact interface at the 0^{o} and 19^{o} angles of incidence the process. This is due to the relevance of the software application to the present research.

6.3.1 Modelling Parameters

The properties of oil and steel adopted for the modelling are shown in Table 5-3 in Section 5.1.5. Together with the experimental values of embedded oil film thickness $2.32\mu m$ and $1.27\mu m$ obtained under the rolling loads of 60kN and 90kN with the 26mm/sec roll speed. Frequencies of 0 to 10 MHz were used because the modelling will be validated with the transducer of the same frequency. This modelling was carried out with the solid-oil-solid interface of the same acoustic impedance properties.

6.3.2 Modelling Procedure

As stated above, the mathematical analysis of the modelling was conducted in the MATLAB R2010b version scripts written by Li [99] with the Pialucha [9] method. The method was used by Pialucha to evaluate the ultrasonic oblique reflection coefficient incidence for non-destructive characterization of the adherent / adhesive interface of bonded joints. The ultrasonic sensor was mounted at an inclined angle, operating in a pitch-catch orientation. The experimental value of the reflection coefficient obtained was found to be within 5 % of the predicted value [9].

This script was modified into the 19° angle of incidence and the properties of the tested materials were changed to suit this study. This modified script is shown in Appendix A (Angle Frequency vs Coeff.m). The simulations were run for longitudinal waves between the incidence angles of 0° and 19°. The reflection coefficients of the signals obtained from the modelling were stored for further studies.

6.3.3 Modelling Results

Figure 6-5 shows the variation of the longitudinal reflection coefficient obtained from a steel-oil-steel interface with different angle of incidence during the modelling process.

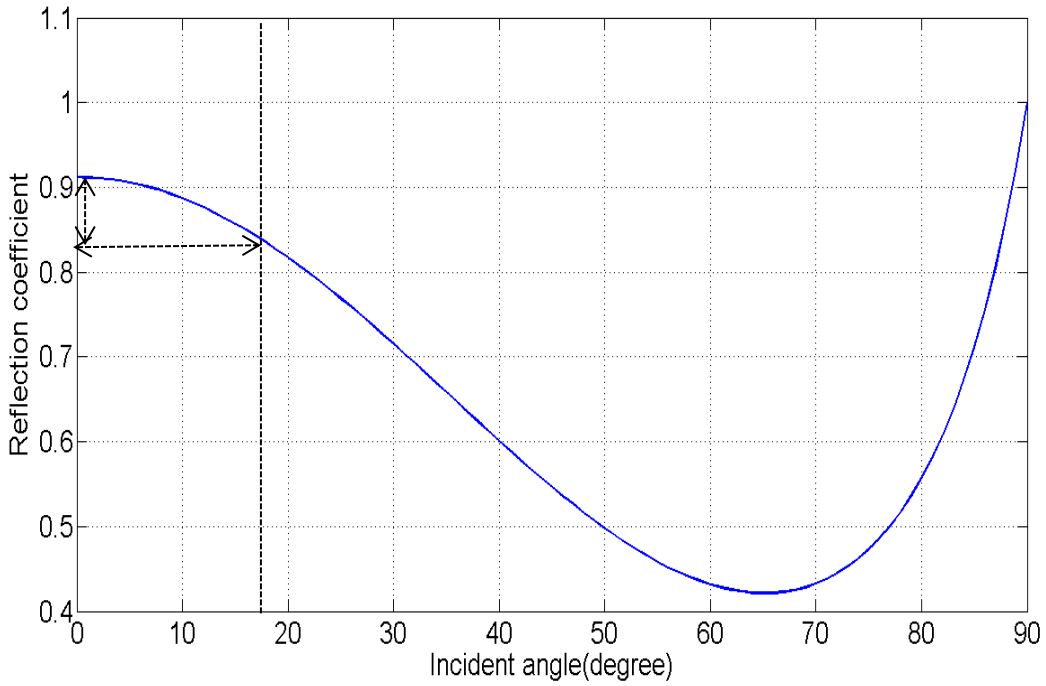

Figure 6-5: Reflection coefficient from steel-oil-steel interface under the various angles of incidences

As can be seen from the figures above, it is noted that the angle of incidence wave has little significant effect on reflection coefficient to much extent as the maximum variations occur at normal incidence of about 9% up to 19° of an incidence angle. As previously discussed, this as also been proved and authenticated by another researcher (Section 6.0).

Figures 6-6 and 6-7 show the reflection coefficient at 0° and 19° angle of incidences under the variable values of the oil film thicknesses as a function of frequency. This was done to investigate the effect of the incidence angle on the reflection coefficient at the interface for the specific angles illustrated in Figure 6-5 above. The blue dotted line (Figs. 6-6 and 6-7) indicates the reflection coefficient from the pulse-echo ultrasonic technique (0° angle of

incidence) while the black line indicates the reflection coefficient from the pitch-catch (19^o angle of incidence) under the value of 2.32μm and 1.27μm film thickness embedded layers. The maximum values 0.9 and 0.82 of the reflection coefficient were observed from a 0^o angle of incidence followed by the value, 0.81 and 0.73 for the reflection coefficient from the 19^o angle of incidence from both figures respectively. Small changes of 0.08 reflection coefficient value were seen as the angle of incidence increased from 0^o to 19^o from the results obtained from both embedded layers respectively.

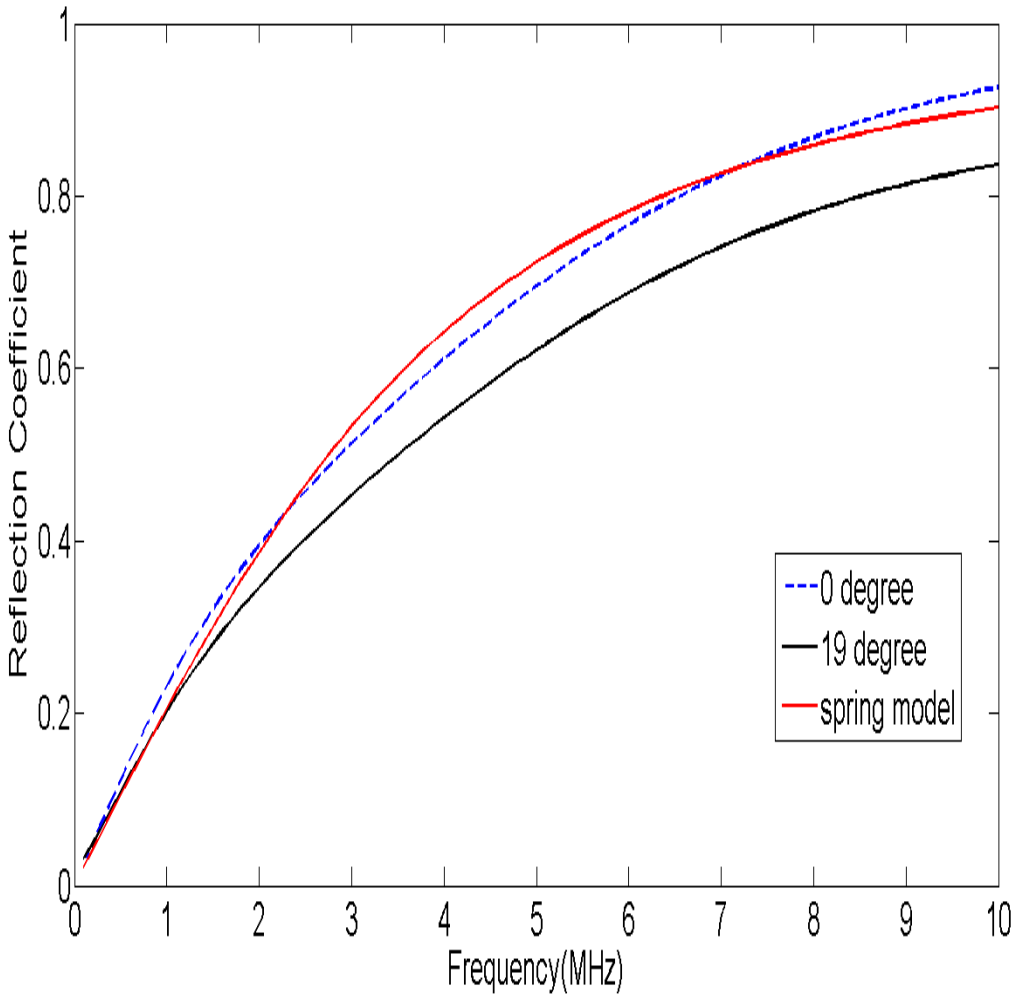

Figure 6-6: Reflection coefficients obtained from modelling under 2.32μm oil film thickness

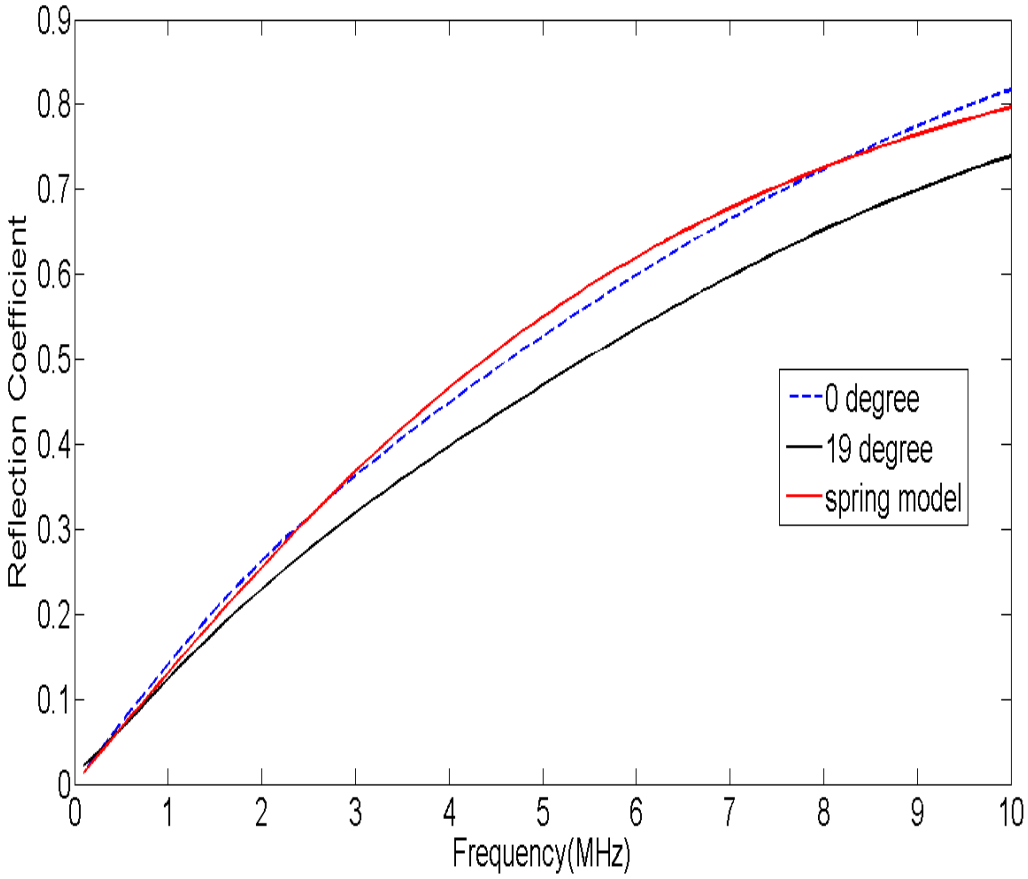

Figure 6-7: Reflection coefficients obtained from modelling under 1.27µm oil film thickness

Additionally, the oil film thicknesses (interface layers) applied during the modelling was used to determine the surface stiffness with the aid of bulk modulus property as expressed in equation 3-11. The stiffness values obtained were used in the spring model equation 3-8 to determine the reflection coefficient values for the frequency range 0 to 10MHz. These reflection coefficient values obtained were plotted against the frequency for the differing values of the layer (oil film thicknesses) applied for the modelling (Figs. 6-6 and 6-7). This was done to check if the modelling was conducted in the spring model regime.

As shown in Figures 6-6 and 6-7, the graphs obtained with the aid of the spring model equation are indicated by the red lines. This shows that the modelling was conducted within the spring model regime. This was due to the fact that the graphs obtained from modelling in normal pulsing technique and the graph obtained using the spring model were almost the same with approximately equal reflection coefficient values at frequency of 10MHz which was the sensor frequency.

Furthermore, Figure 6-8, was used to illustrate the relationship between the changes in reflection coefficient with angle of incidence wave in respect to the oil film thicknesses.

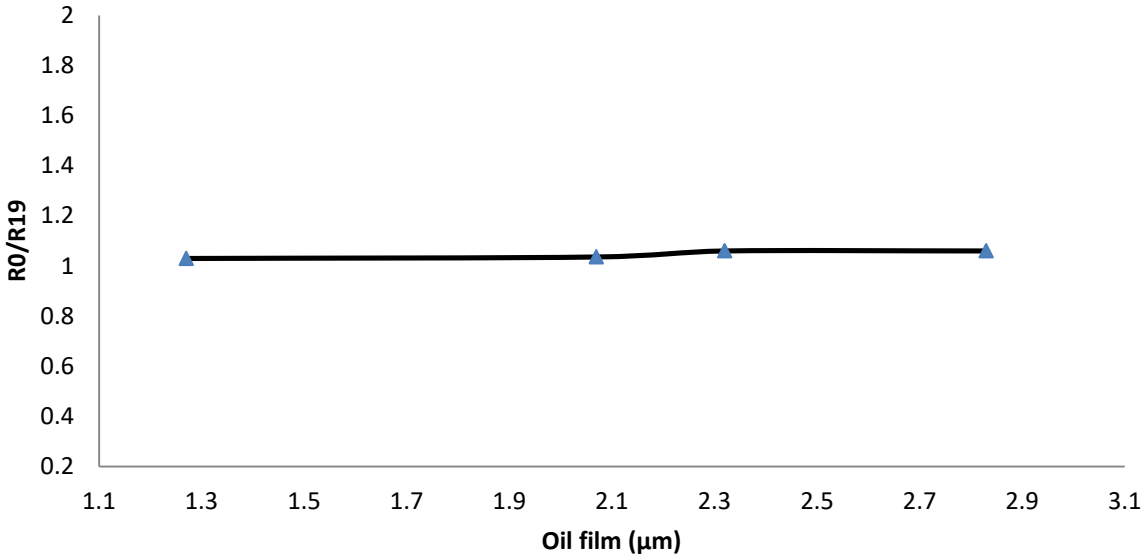

Figure 6-8: Change in reflection coefficient with angles against the oil film thicknesses

The normal stiffness value of the applied longitudinal sensor with the pulse-echo technique (0 degree) was calculated. This was done by the mathematical manipulation of the experimental oil film thickness obtained from the pitch-catch technique with the bulk modulus value of the applied lubricant as shown in equation 3-11. The obtained normal stiffness value was employed to determine the pulse-echo technique reflection coefficient values using spring model equation 3-8. The ratios of the reflection coefficient of both techniques were calculated against the oil film thickness obtained during the process. This graph was plotted with the ratio of the reflection coefficient obtained at 10MHz for 0 degree (pulse-echo) and 19 degree (pitch-catch) of angle of incidence with respect to the value of the obtained oil film thickness (interface layers). As can be seen from the graph, oil film thickness has only a minor effect on ratio of the reflection coefficient value to changes to the angles of incidence. This is shown by the slight changes of horizontal line drawn for the ratio of the reflection coefficients obtained at angles 0 and 19 degrees for the two values of the oil film thickness layer applied. The constant ratio of $R0/R19$ regardless of the film thickness means that no adjustment needs to be made for different film thickness. This makes practical implementation easier.

6.3.4 Comparison of Model Results with the Literature

The longitudinal reflection coefficient values obtained at the experimental and simulation of paraffinic oil and polyphenol ether at various wave incidence angles by Xiangwei [99] are shown in Figure 6-9 and 6-10 respectively. These results show the same trend with the longitudinal reflection coefficient values obtained from both modelling and experimental processes applied in the chapter.

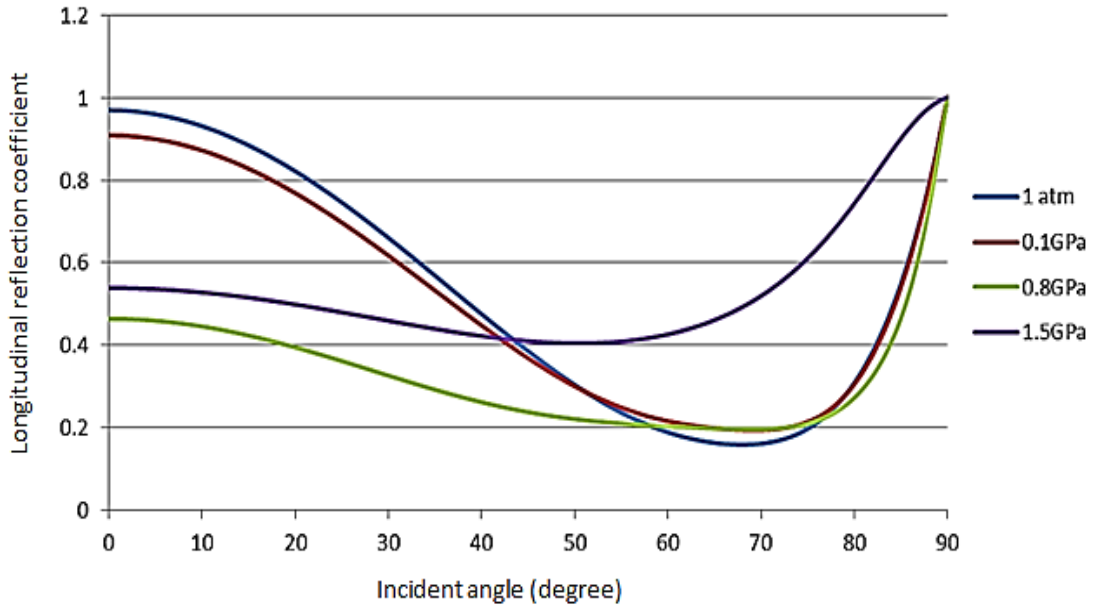

Figure 6-9: Reflection coefficient obtained at various angles of incidence under experiment [97]

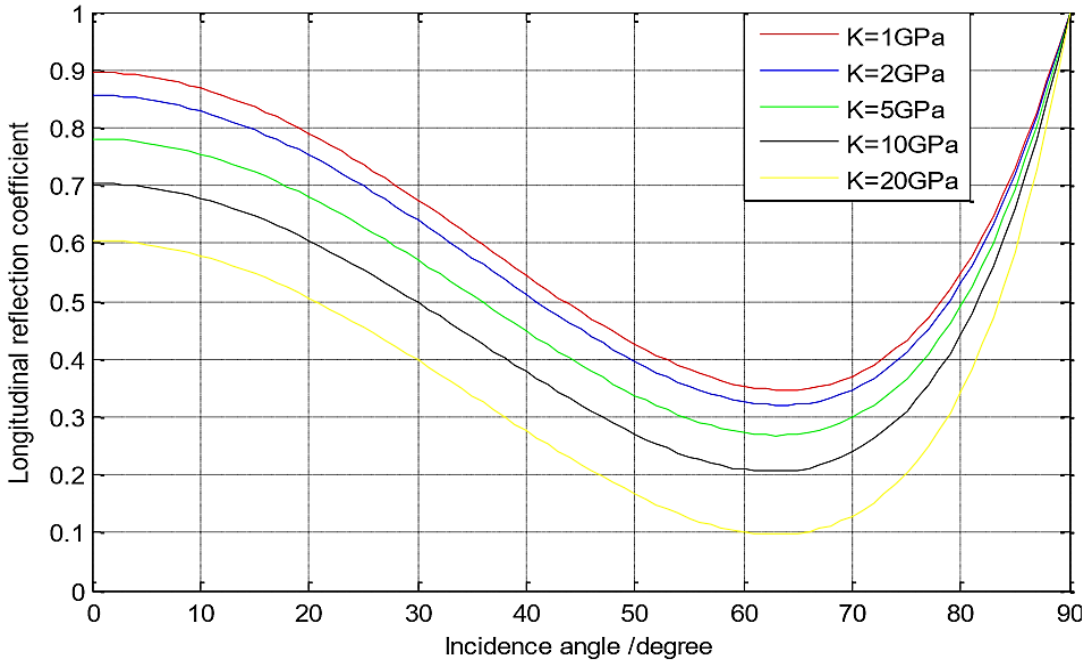

Figure 6-10:: Reflection coefficient obtained at various angles of incidence under stimulation [99]

As can be seen from the figures above, the reflection coefficient were observed to have little effect on incidence angles up to 19°, likewise in the obtained model results shown in Figure 6-5 respectively. The largest effect of incidence angle was observed from 25° upward on the reflection coefficient as indicated from the model results and from the literature results.

Liaptsis [97] also observed a decrease in the longitudinal wave reflection coefficients values for a steel-to-steel contact with a small quantity of oil at their interface and increases of the incidence wave angles at a surface difference stiffness ratio value, as shown in Figure 6-11. This shows the same trend as the longitudinal reflection coefficient value obtained from the modelling process of the reflection coefficient against angles of incidence shown in Figures 6-5.

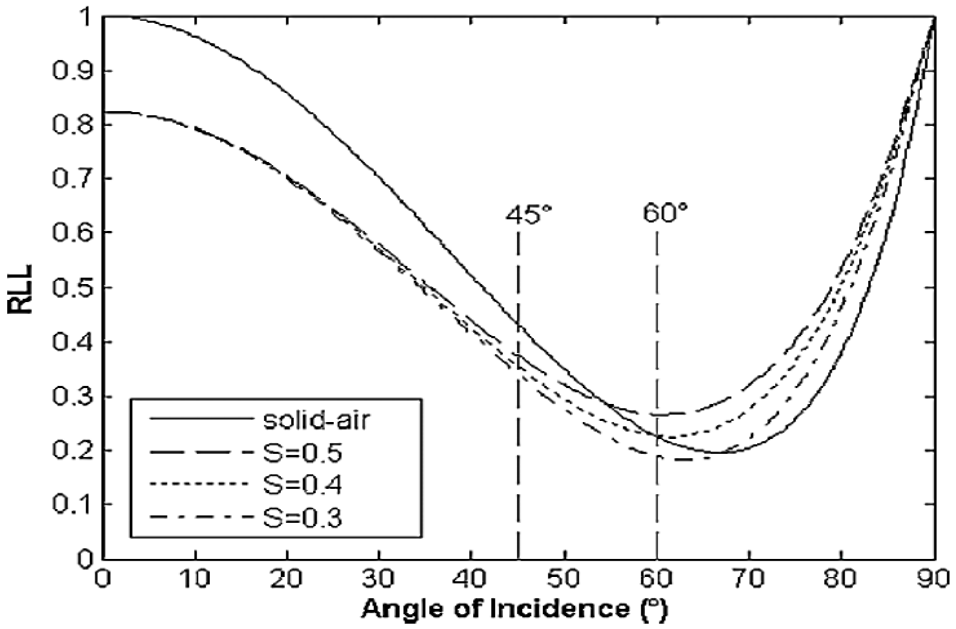

Figure 6-11: Longitudinal reflection coefficient against the angle of the incidence wave [97]

The change in the reflection coefficient value of the wave is due to the increase in the path length that the signal travels during the transmission process. The higher the angle of the incident wave the larger the path length and the lower the reflection coefficient value of the wave obtained.

Furthermore, Chen et al. [103] also proved from their findings that the reflection coefficient of the longitudinal wave decreased with increasing frequency value when the wave incidence angle was more than the 30°. Pilarski [94] explained that the sensitivity of the interface weakness detection achieved by introduction of the oblique incidence technique without the necessity of high frequency. Nam et al. [98] concluded that the longitudinal

reflection coefficients obtained at a 22.5° angle of incidence are similar to those obtained at a normal incidence longitudinal wave. They stated that the characteristics of the reflection coefficient at this oblique incidence angle 22.5° are mainly influenced by the normal interface stiffness.

6.4 Experimental Validation

6.4.1 Experimental Set-up

The roll was instrumented with 10 MHz and 5 MHz central frequencies of longitudinal and shears sensors for resonance transmission of the signal. As shown in Figure 6-12, the sketched layout arrangement consists of mounting sensors centrally and at both edges of the roll.

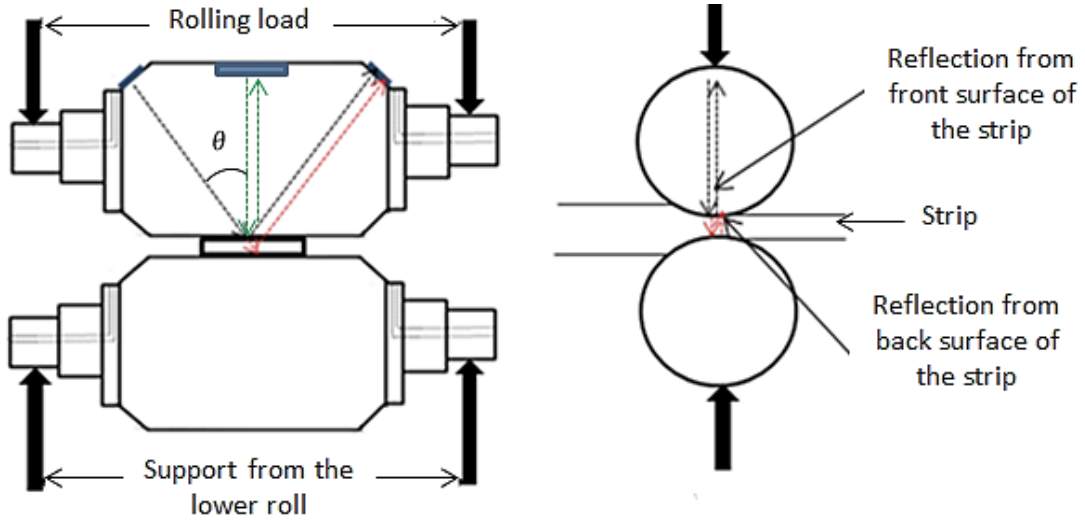

Figure 6-12: Rolls and the sensor layout arrangement

Four sensors (two longitudinal and two shear) were mounted on both sides of the upper roll. The first pair of sensors on the right side of the roll is longitudinal and shear sensors, which act as pulsers to generate signals during the transmission process. This was followed by another pair of sensors (longitudinal and shear) on the left side of the roll, acting as receivers for the reflected signal from the metal-to-roll interface (thin layer) during the operation. The sensors were mounted in accordance with the transmission angles of incidence θ. The remaining two sensors (shear and longitudinal) were arranged on the top surface of the roll for the normal ultrasonic transmission technique (pulse–echo) as shown in Fig. 6-12.

6.4.2 Test Procedure

This experiment was conducted using a 5 mm thick, 25 mm wide and 250 mm length of strip. The strip was manually loaded between the rolls of the pilot rolling machine (Fig. 5-8) after the lubricant was applied to the surface of the strip. This experiment was conducted during the metal rolling process under the rolling loads of 70kN and 90kN for each operation respectively. Ultrasonic signals were sent through the roll to the metal-roll-interface during the rolling process. The ultrasonic reflected signals were continuously captured from the surfaces of the strip as the roll rotates for a specific duration. A large quantity of the reflected signal was captured and digitized. The acquired data was streamed directly to the hard disk of the computer and stored in binary form for further processing. This was done to prevent loss of information during the process.

6.4.3 Signal Processing

The reflected and reference data that was stored together during the rolling process was processed using a LabVIEW acquisition program on the PC as shown Figure 6-13.

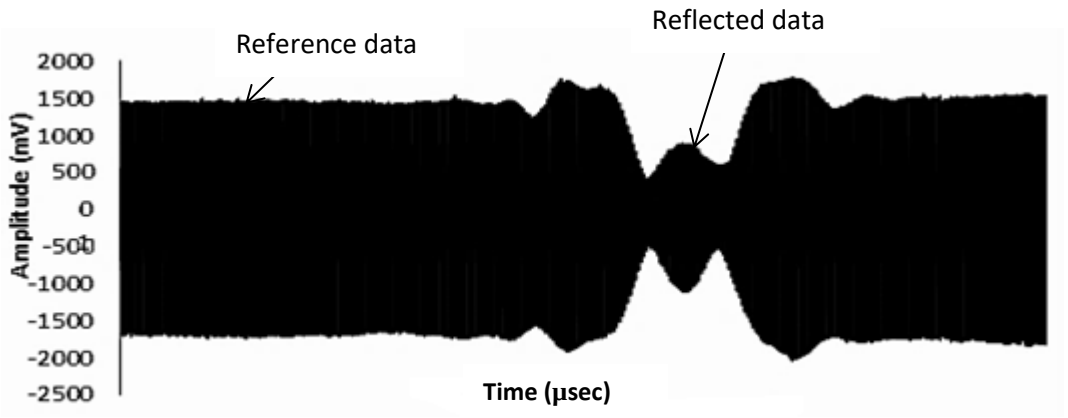

Figure 6-13: Entire ultrasonic reflected data extracted during the metal rolling operation

The above data (Figure 6-13) was also processed further with the aid of LabVIEW on a PC to separate the reference (reflected signal from metal-to-air interface) and reflected wave (reflected signal from metal-to-roll interface) from the raw data. The two reflected values were in terms of the amplitude value and frequency domain. Reflection coefficient of the longitudinal wave sent from the metal-to-roll interface was obtained by dividing the reflected peak amplitude value with the reference peak amplitude value respectively. This reflection coefficient value was used further to calculate the stiffness value at the metal-to-roll interface during the rolling process.

The various reflection coefficients obtained along the roll-bite with Time-of-Flight are shown in Figure 6-14. The centre value of this figure was used as the reflection coefficient of the reflected signal obtained from the metal-roll interface.

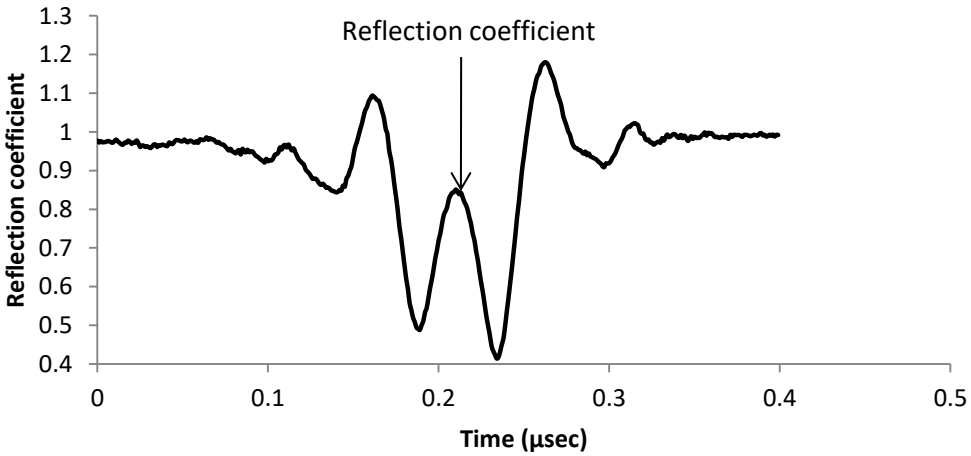

Figure 6-14: Longitudinal signal transmission at strip-to-roll interface during the rolling process

The obtained reflected signal was processed in the frequency domain in terms of the reference and reflected amplitude values. As previously explained this is done in the easy calculation of the reflection coefficient of the transmitted signal using the reflected and reference amplitude value ratio. The data obtained under the applied rolling loads from both techniques are presented in terms of the frequency domain in Figures 6-15 and 6-16 respectively. These (Figure 6-15 and 6-16) show decreases in the amplitude of the reflected signal as the applied load increases for both applied approaches.

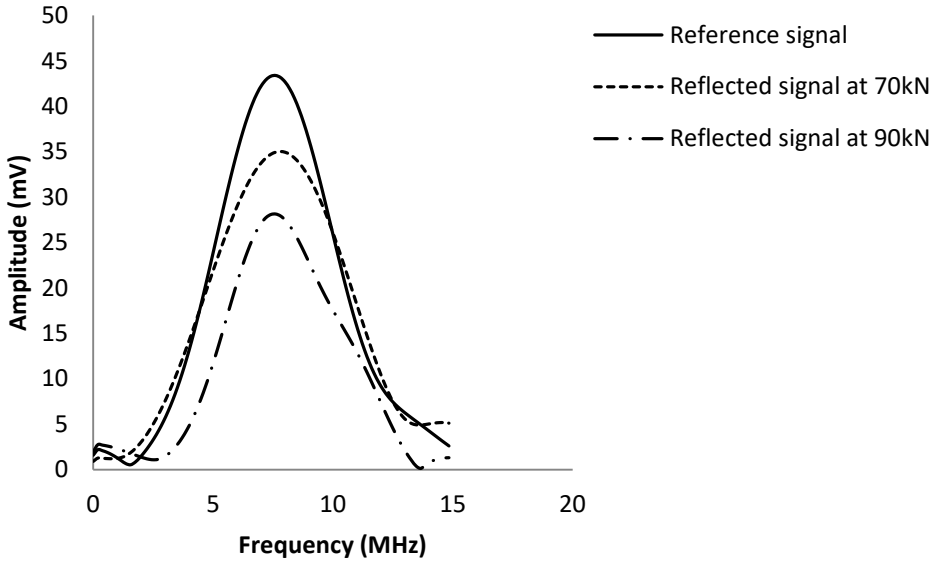

Figure 6-15: Wave amplitude spectrum of the pulse-echo values as load is increased

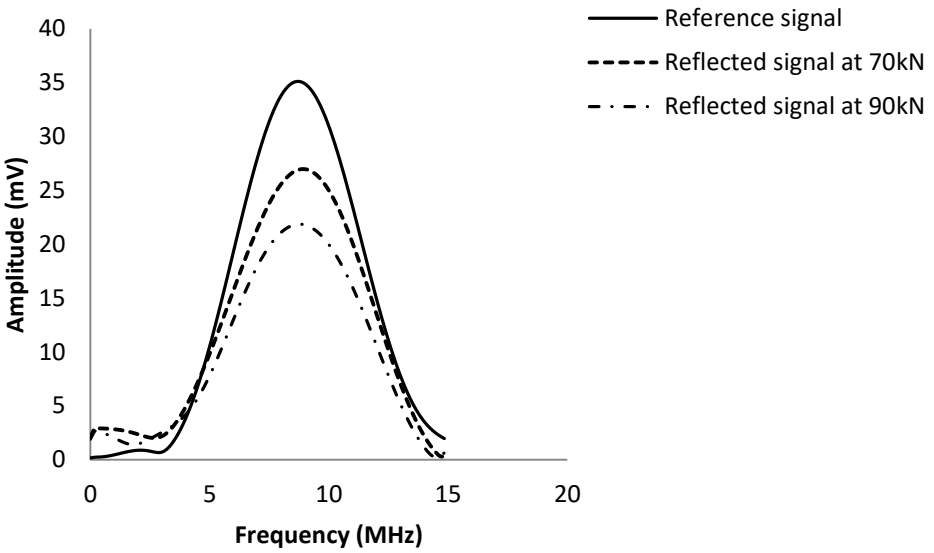

Figure 6-16: Wave amplitude spectrum of the pitch-catch values as load is increased

Figure 6-17 and 6-18 show reflection coefficients against frequency results from pulse-echo and pitch-catch ultrasonic transmission techniques obtained during the metal rolling process. Results are shown for frequencies lying within the bandwidth of each reference spectrum, as shown in Figures 6-15 and 6-16.

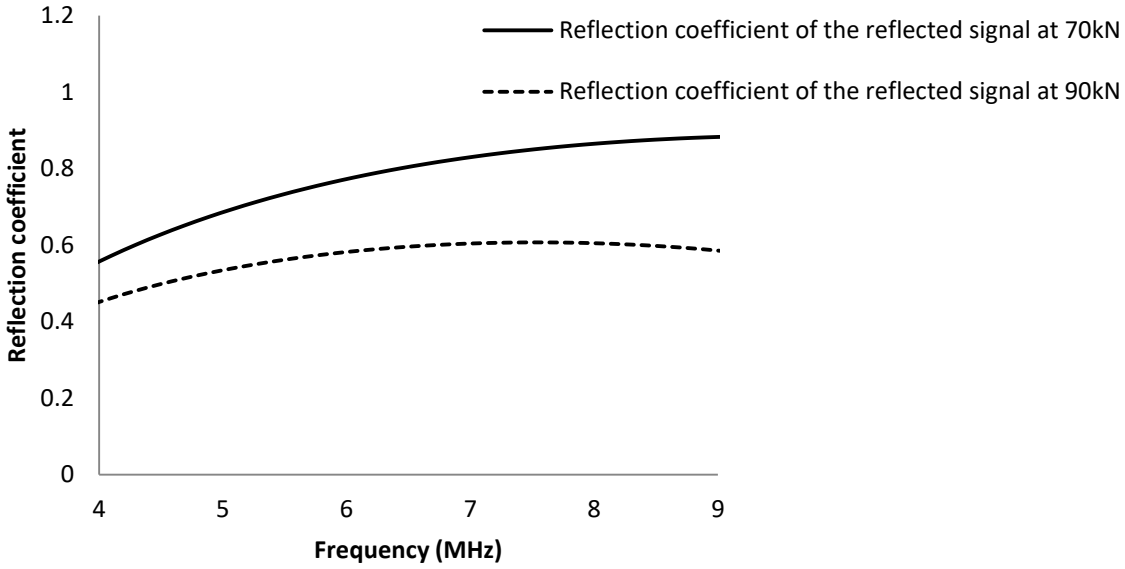

Figure 6-17: Longitudinal reflection coefficient against the frequencies with pulse-echo technique

As shown in Figure 6-17, the experimental reflection coefficients across the bandwidth of the sensor through the pulse-echo technique were observed to be frequency dependent.

The reflection coefficient from the metal-to-roll interface was found to increase as the frequency increases for both applied rolling loads. This implies a good agreement with the spring model prediction indicated with a red line in Figures 6-6 and 6-7.

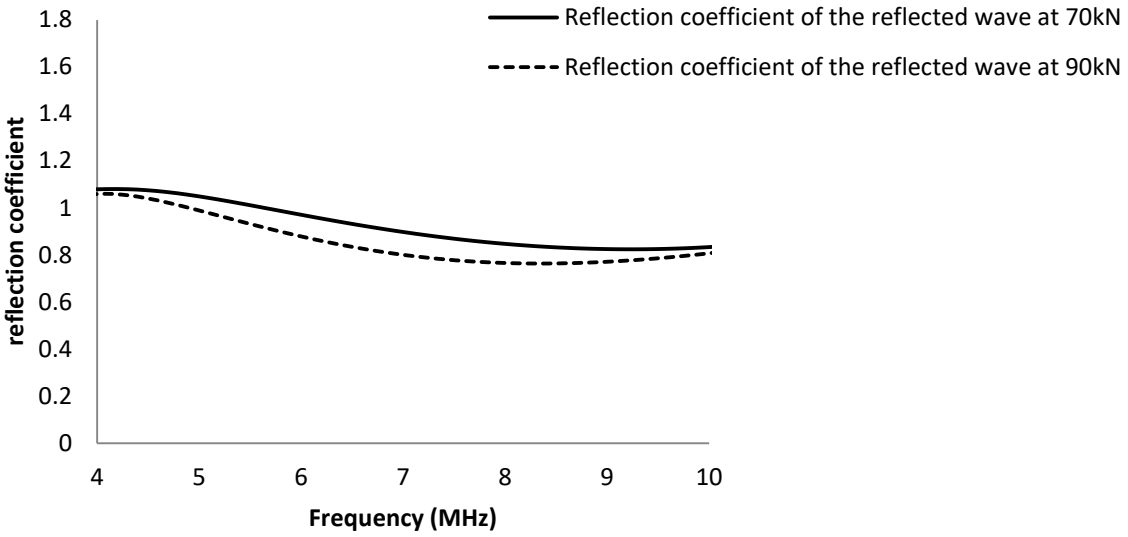

Figure 6-18: Longitudinal reflection coefficient against the frequencies with pitch-catch technique

Figure 6-18, shows the variation of the experimental longitudinal reflection coefficient with frequency for 70kN and 90kN applied rolling loads. The reflection coefficient appears to decrease over the bandwidth of the sensor (4–10MHz), which is poor agreement with the spring model predictions as shown in Figures 6-6 and 6-7. The reason for this disagreement is not clear, but the disagreement is consistent and was seen across all results. Liaptsis [97], explained that this poor agreement was due to the increase of the angle orientation of the sensor that leads to the divergent beam in the steel that can result in reflection from more than the centre region of the interface contact.

6.4.4 Experimental Results

The experimental reflection coefficient values obtained from Section 6.4.1., were utilised for calculating the interface stiffness values obtained from both techniques (pitch-catch and pulse-echo). These stiffness values were used to determine the oil film thicknesses formed. The obtained oil film thickness values were then utilised to model thickness layers between the two surfaces to obtain the model reflection coefficient values.

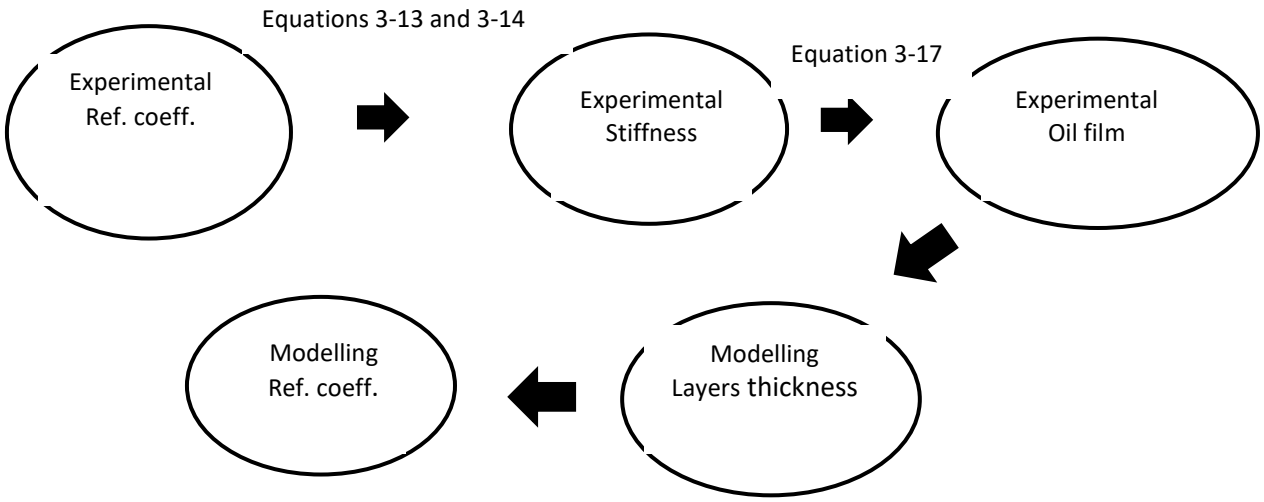

Figure 6-19: Flow chart of shown the step of obtaining the modelling reflection coefficient

Figure 6-19, illustrates the process of obtaining modelled reflection coefficient from the experimental reflection coefficient. The obtained reflection coefficients from the two techniques under the modelling and experimental procedure are shown in Figure 6-20.

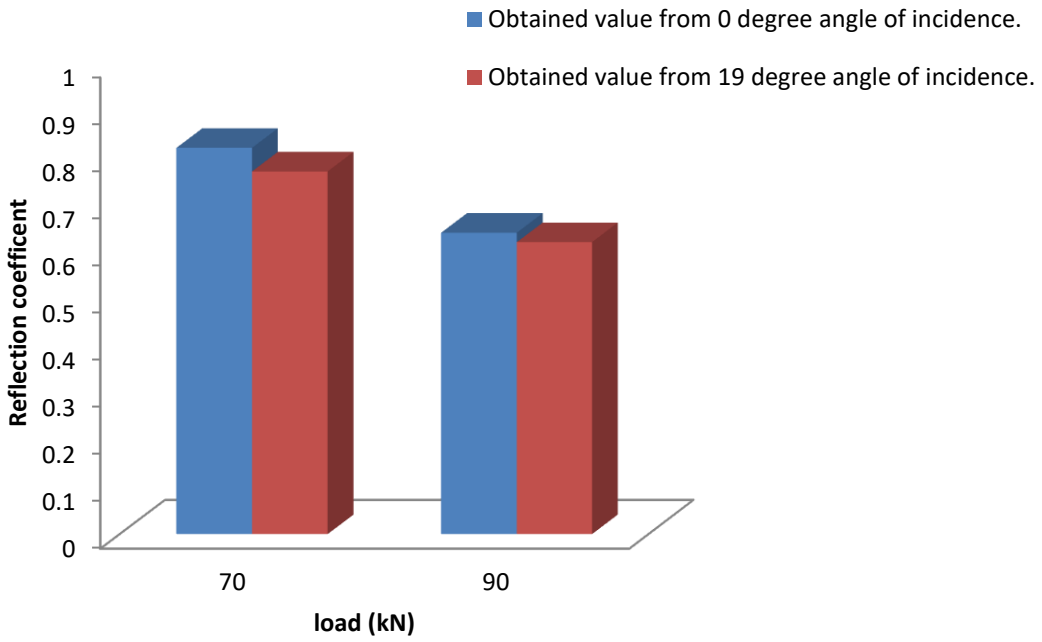

Figure 6-20: Reflection coefficient obtained from both applied measurement techniques

The reflection coefficients from both techniques were found to decrease as the applied load increases. The reason for this has been already mentioned above.

The normal stiffness's of this interface was calculated using the equation 3-13 in Section 3.3.4, with the aid of the reflection coefficient values obtained above. The obtained stiffness from these techniques under the applied rolling load is shown in Figure 6-21.

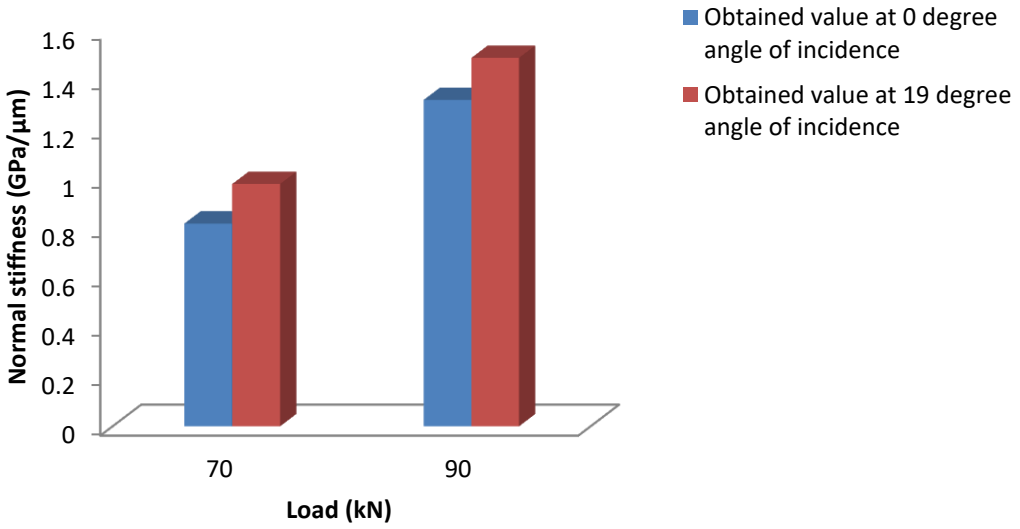

Figure 6-21: Stiffness obtained from both applied measurement techniques

The reflection coefficient and the normal stiffness values obtained during the experiments conducted under the applied rolling loads that were presented in Figures 6-20 and 6-21 are summarized and shown in Table 6-1 below.

Table 6-1: Experimental reflection and stiffness value obtained

Load case	Reflection coefficient value obtained		Stiffness values obtained	
(kN)	0^o incidence angle	19^o incidence angle	0^o incidence angle (GPa/µm)	19^o incidence angle (GPa/µm)
70	0.82	0.77	0.82	0.98
90	0.64	0.62	1.32	1.49

Figures 6-22 and 6-23 show the reflection coefficient values obtained by equation 3-5 against frequency as the stiffness of the interface at the different angles of incidence used under the two applied load during the metal rolling process.

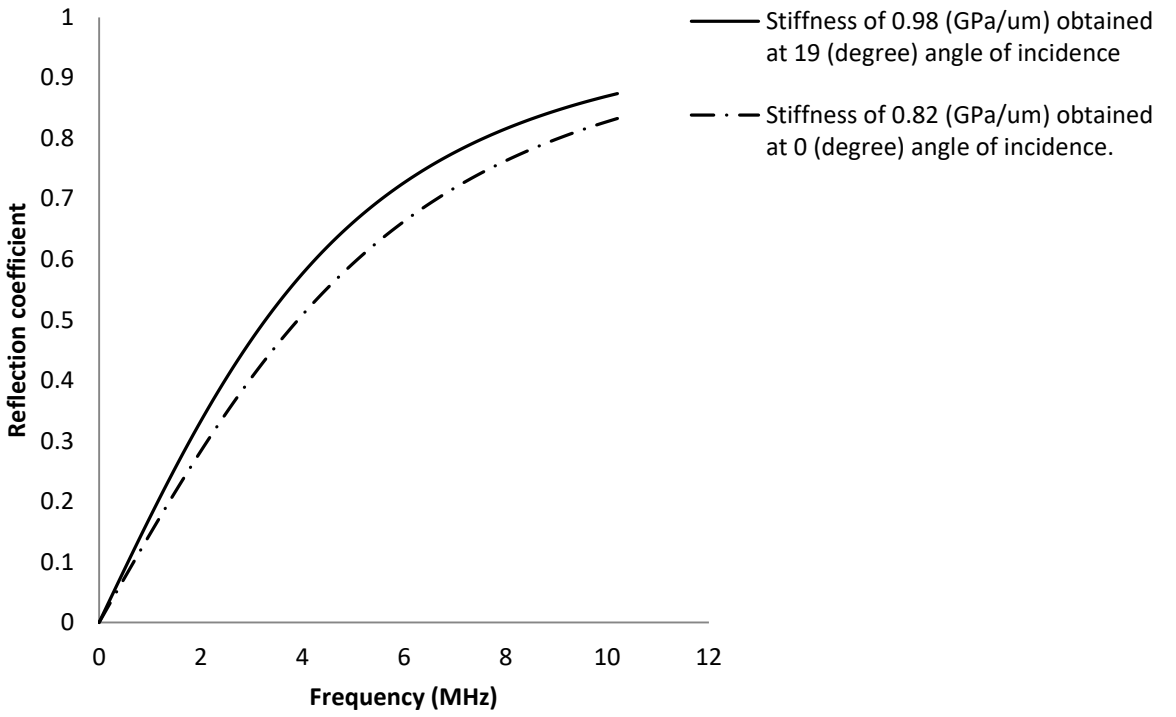

Figure 6-22: Reflection coefficient against frequency with stiffness values under the 70kN rolling load

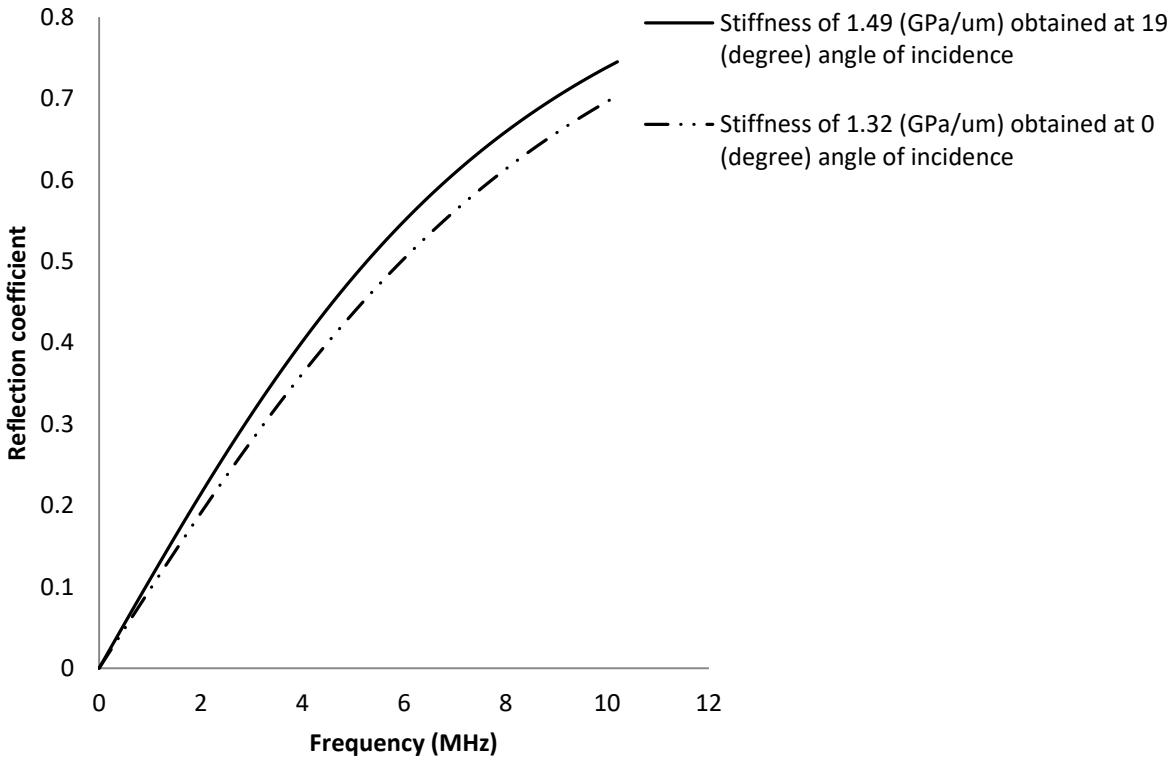

Figure 6-23: Reflection coefficient against the frequency with stiffness values under the 90kN rolling load

As can be seen from the figures above, the longitudinal reflection coefficient for steel-oil-steel interface at 19 and 0 degree angle of incidence was plotted as a function of frequency

for various stiffness values. The higher stiffness values are recorded from the 19° angle of incidence for both figures, followed by the stiffness value obtained by the 0° angle of incidence. It can be seen that the angle of incidence showed some degree of effect on the experimental stiffness value obtained from steel-oil-steel interface. This is due to the double effect expressed on reflection coefficient value from the spring model used to calculate the stiffness from the oblique approached. The spring model is generally authenticated for the normal pulsing technique, but it was used to calculate the stiffness from the data obtained by the pitch-catch technique. This was due to the small variation observed from the reflection coefficient of a sound wave between the 0° and 19° angles of incidence. Additionally, this variation has been proved to be insignificant by some authors as stated earlier in Section 6.0. Some authors proved that oblique reflection ultrasonic transmission techniques are the best way to study the sensitivity interface of the two materials with low frequency and the appropriate angle of incidence sound wave [93, 94, 101]. Therefore, the difference in the stiffness observed between the two configurations under the applied rolling loads is still negligible and proved to be within the expected range of error.

6.4.5 Comparison of Experimental Results with Model Results

Figures 6-24 and 6-25 show the comparison between the reflection coefficient of the incident wave obtained from the experiments and the modelling for both the pulse-echo and pitch-catch measurement techniques with 2.32µm and 1.27µm oil film thickness embedded layer. This was calculated ultrasonically using oblique reflection technique.

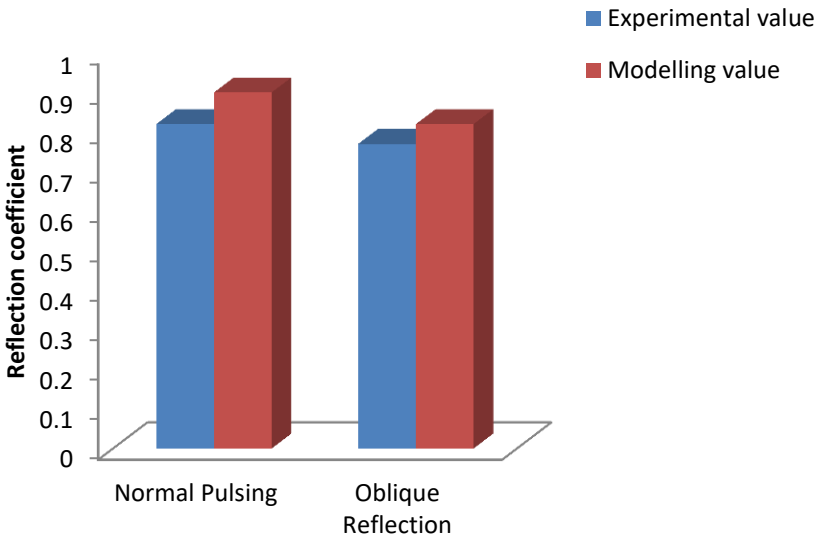

Figure 6-24: Reflection coefficient values obtained from modelling under 2.32μm oil film thickness

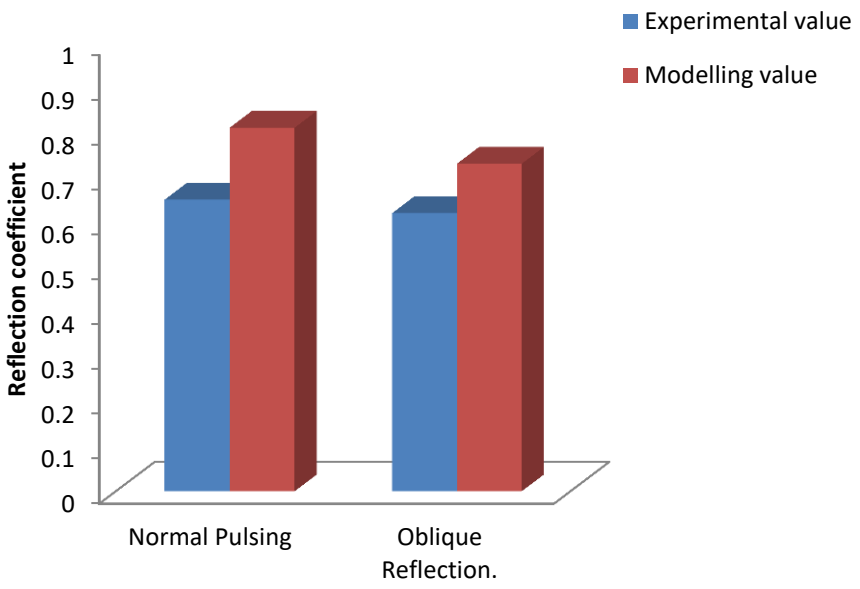

Figure 6-25: Reflection coefficient values obtained from modelling under 1.27μm oil film thickness

Table 6-2, shows the obtained reflection coefficient value from the various angles of the incidence applied from both experimental and modelling under the difference value of the embedded layers (oil film thickness).

Table 6-2: Reflection coefficient obtained during both applied process techniques

	Reflection coefficient obtained			
	Experimental results		Modelling results	
Oil film thickness (µm)	0^o angle of incidence	19^o angle of incidence	0^o angle of incidence	19^o angle of incidence
2.32	0.82	0.77	0.9	0.82
1.27	0.64	0.62	0.81	0.73

As can be seen, the highest values of the reflection coefficients were obtained from the modelling process and decrease as the oil film thickness (embedded layer) decreases. However, the difference of the reflection coefficients between the two measurement techniques employed is negligible due to their small value. Additionally, the reflection coefficient obtained from the processes is of the same trend, that they decreased by the decreased value of the embedded layer of the interface. Due to more contact of the asperities of both surfaces that developed at the metal-to-roll interface through the reduction of the embedded layer (oil film thickness) that promotes more signal transmission and reduces the reflected wave amplitude value during the rolling process. Once the

reflected amplitude value reduced compared with the reference amplitude value, then the reflection coefficient value obtained will reduce.

6.4.5.1 Determination of Percentage Error from Obtained Values

The percentage error of the reflection coefficient values from both processes under the different measurement technique applied were determined by relating the reflection coefficient and the angle of incidence waves values with the expression shown below:

$$\%E = \frac{R\theta_o - R\theta_i}{R\theta_o} \qquad 6\text{-}35$$

Where:

$R\theta_o$ Is the reflection coefficient value obtained at normal pulsing (0^o) measurement technique and $R\theta_i$ is the reflection coefficient obtained at oblique pulsing (19^o) measurement technique.

The percentage error of the reflection coefficients were obtained from normal pulsing and oblique reflection measurement techniques for both modelling and experimental processes (Figures 6-24 and 6-25) with the aid of equation 6-35. Therefore, the percentage error of the reflection coefficients obtained under the differentiating value of 2.32µm and 1.27µm the applied embedded thickness layers are shown in Table 6-3 below.

Table 6-3: Reflection coefficient percentage error obtained from both employed techniques

Difference in reflection coefficient obtained from both configurations		
Embedded layer thickness (µm)	Experimental values %	Modelling values %
2.32	6.4	8.8
1.27	3.1	9.8

As can be seen from the above table, the percentage errors obtained from the reflection coefficient at experimental values were very small compared with the error recorded from the modelling. Various values for the reflection coefficient were obtained from both ultrasonic techniques under the different approaches above mentioned. The best result of reflection coefficient was achieved at both ultrasonic techniques from the experimental procedure due to the lower value of the percentage error obtained under the two different values of embedded layers employed. This shows the reliability of the oblique reflection measurement techniques for the studies of the metal-to-roll interface as proposed.

Therefore, the effect of angle of incidence wave on ultrasonic reflection coefficient in this research is negligible.

6.5 Conclusion

The model of Pialucha [9] was used and simulations were conducted for the solid-oil-solid case to study the effect of the incidence angle on the longitudinal wave reflection coefficient. Experimental tests were carried out to validate the results of the model using pulse-echo and pitch-catch measurement techniques under two different embedded thickness layers. This leads to the notion that the expression for reflected coefficient obtained is correct. This also illustrates the validity of the use of the ultrasound normal pulsing technique at this recommended angle of incident. The following can thus be concluded:

- This study has shown the ability to use the ultrasonic reflection to study the effect of the angle of incidence wave on the reflection coefficient of the obtained reflected wave;
- The reflection coefficient value obtained from normal and oblique ultrasonic transmission methods are slightly different from each other under the same experimental conditions;
- Higher percentage errors were recorded from the reflection coefficient obtained at modelling process;
- The stiffness value obtained from both normal and oblique ultrasonic transmission techniques is a little different of 16% (at 70kN) and 7% (at 90kN) from each other;
- This study has shown that the modelling was running in the spring model regime;
- This study has proven that the reflection coefficient obtained from the interface layers is only minimally affected by the incident angle.

Chapter 7

Measurement of oil film thickness during the rolling process

This chapter presents the results obtained from the application of the external ultrasonic sensor technique for the measurement of metal and roll lubrication condition interface during cold rolling. This method was used to measure the formation of oil film thickness under various rolling loads and speeds. The investigations were achieved using the reflection coefficient at the roll-bite interface during the rolling operation. The effects of the parameters mentioned above on the formation of oil film thicknesses are fully discussed in the remainder of this chapter.

7.0 Introduction

A plethora of techniques exist for calculating the oil film thickness in cold metal rolling operations. Some are based on the prediction of the oil film obtained at the roll-bite inlet zone to calculate the oil film formation at metal-to-roll contact (section 2.6). Only a handful of methods exist to measure oil film thickness in the working zone during metal rolling. The ultrasonic method developed by Dwyer-Joyce and Hunter [66] which involves applying internal insert sensors to measure oil film thickness across the roll-bite can pose great difficulties, as explained in Section 2.7. The focus of this study was to measure the oil film across the roll-bite without any assumption of other zones with the aid of the oblique reflection ultrasonic technique. In this section, the oil film thickness was determined by oblique reflection technique (pitch-catch) and included the investigation of the rolling parameters on the oil film thickness sections (Sections 7.4.2 and 7.4.3). Normal pulsing technique (pulse-echo) was also applied in Section 7.4.1.4 to determine the oil film thickness. This was done to validate the results obtained with oblique technique 7.4.1.3.

7.1 Basic Concept

7.1.1 Determination of Reflection Coefficient

Experimentally, the oil film reflection coefficient was obtained by dividing the peak amplitude values of the wave reflections from the oil layer at the metal-to-roll interface (Figure 5-14) and the metal-to-air interface (Figure 5-13). This is because the entire transmitted signal from the metal-to-air interface is small, due to the low value of the acoustic impedance of the air. Hence, the reflection coefficient of the ultrasonic signal was determined with the aid of Equation 3-11. The value of the obtained reflection coefficient was applied to properties of the oil and the strip to determine the oil film thickness at the roll–bite surfaces with the aid of the stated spring model (Equation 3-16).

7.2 Experimental Approach

The test device implemented in this section was similar to the one described in Section 5.1.1. This process is also briefly discussed with the details of the experimental procedure used and the materials employed in Section 7.3.2.

7.2.1 Rolling Mill

The oil film measurement was conducted with the aid of the rolling mill that was already discussed in section 5.2.1. The roll speeds of the machine were limited to 19 and 26 mm/sec due to the short length of the strip (250 mm) and for safe operation of the mill. The two upper parts of the roll were fixed with two load-cells to measure force development at the roll-bite surface during the rolling operation. These two load-cells were located between the mill screw and top part of roll bearing host as shown in Figure 7-1.

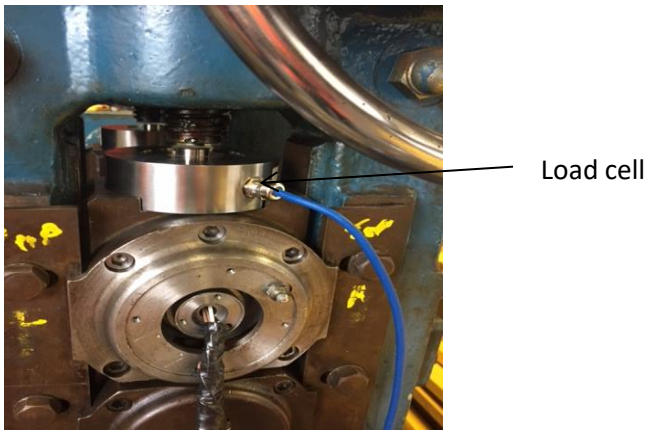

Figure 7-1: Load cell location (Scale: 1:15)

There was no provision to give both entry and exit tension on the strip to enhance the operation during the rolling process. The vertical position of the mill can be adjusted to the required rolling gap through the adjuster screw wheel of the machine that is shown in Figure 5-2. This was to ensure the correct rolling gap during the rolling operation.

7.2.2 Material and Lubricant

The rolls and strip (mild steel) material employed in the research study have been fully described in sections 5.1.2 and 5.1.5. Two sets of different dimensions of the strip were used for the experiment. The first set had a 5mm thickness, 50mm width, and 250mm length. The second set had a 4mm thickness, 40mm wide and 250mm long. Both materials were low carbon steel with the same chemical composition. Gerolub 5525 lubricant was used during the experimental process and its properties are shown in Table 5-3, Section 5.1.5.

Generally, the thickness of the applied lubricant obtained at the metal-to-roll interface depends on the oil stiffness and its bulk modulus property. The bulk modulus of the oil value depends on pressure and temperature of the metal-to-roll interface respectively. Therefore, the applied lubricant will draw in and fill the pockets between the asperity contacts during

the rolling process. It is assumed that the lubricant can freely flow between the valleys due to the random distribution of the surface which means that the oil is under ambient atmospheric pressure [90].

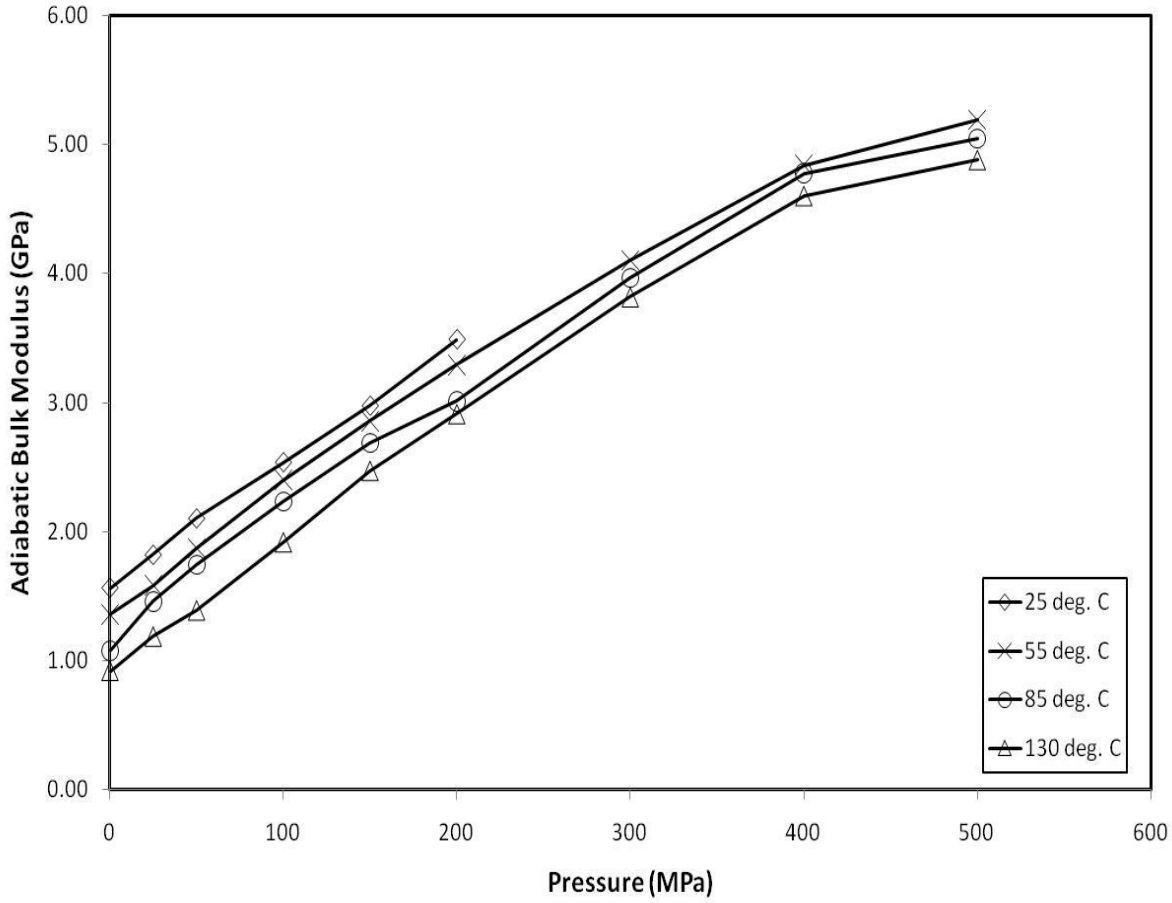

Figure 7-2: Bulk Modulus for Gerolub 5525 at various temperatures and pressures [66]

The Bulk modulus value of the oil used in this research was calibrated against pressure and temperature by Dwyer-Joyce and Hunter [66] as shown in Figure 7-2. This was used to estimate the thickness of the lubricant at the roll-bite during cold metal rolling.

7.2.3 Procedure

The strips were manually fed into the mill roll gap at a roll speed of 26mm/Sec, before being dragged by the rolls during the rolling process, after the application of the Gerolub 5525 lubricant oils under 40kN rolling load. This was done due to the high load experienced by the strip at the beginning of the rolling operation**.** The value of the applied rolling loads was monitored and measured with the load cells positioned within the machine frame shown in Figure 7-1. The instrumentation settings applied in Section 5.3.3., were also followed for the

two sensors used. The ultrasonic signals were sent using both pitch-catch and pulse-echo techniques at the same time. The reflections obtained from the strip-to-roll interface during the experiment were captured and processed with the aid of LabView. The processed data were used to calculate the oil film formed at the strip-to-roll interface during the experiment.

The experiment was repeated for different rolling loads of 40kN, 70kN and 90kN and also for two different speed values, 19 mm/sec and 26mm/sec separately. The reflections of the signal sent during the process were captured, processed and used to study the effect of rolling loads and roll speeds on the oil film thickness formation. The parameter values and material properties used during this experimental process are listed in Table 7-1.

Table 7-1: Properties values used during the experiment

Parameters	Values
Roll radius	55mm
Strip dimensions	5mmx 50mm x250mm
Initial strip thickness	5.0mm
Final strip thickness	4.52mm
Metal reduction	0.48mm
Rolling load	40kN
Roll speed	19.0mm/sec
Strip speed	18.4mm/sec
Steel yield stress	250MPa
Quadratic roughness of the strip	0.9µm
Quadratic roughness of the roll	0.7µm

7.3 Signal Processing

As previously explained in section 5.3.2, the receiver sensor picked up several reflections from the metal-to-air (reference signal) and metal-to-roll (reflected signal) interfaces during

the rolling process respectively. The raw data obtained during the rolling process (both reference and reflected signal) were saved on a single file and processed further with the aid of the LabView program into time-of-flight domain. This was done to identify the reference

signal from reflected signals as shown in Figure 7-3 (a). This data (Figure 7-3 (a)) was processed further to separate the reference signal from the reflected signal and presented in terms of Time-of-Flight as shown in Figure 7-3 (b). The data obtained in Figure 7-3 (b) was processed into the frequency domain and shows the reference and reflected signals amplitude values (Figure 7-3 (c). Finally, the reflection coefficient of the reflected signal was obtained by dividing the amplitude value of the reflected signal with the amplitude value reference signal with equation 3-11. In addition the various reflection coefficients of the reflected signal along the roll-bite were obtained in terms of Time-of-Flight from the raw data as shown in Figure 7-3 (a) with the aid of the LabView program. This process can also be used to obtain the reflection coefficient for the applying sensor during the rolling process. The liquid and solid stiffness value of the strip and roll surfaces were calculated with the longitudinal wave reflection coefficient obtained. The solid stiffness of the surfaces was calculated by the reflection coefficient obtained from the shear wave sensor. The liquid stiffness was obtained by subtracting the solid stiffness obtained from the total (solid and liquid) stiffness's determined by the longitudinal sensor. The oil film was finally determined by dividing the bulk modulus of the oil with the liquid stiffness obtained. This process is fully discussed in Section 7.4.

7.4 Results

7.4.1 Reflection Coefficient, Stiffness and Film Thickness

Figure 7-3 (a) shows the processed ultrasonic data (reference and reflected) obtained from the strip and roll surfaces during the metal rolling process. The signal process procedure of this reflected data obtained during this experiment has already been explained in section 7.3 above.

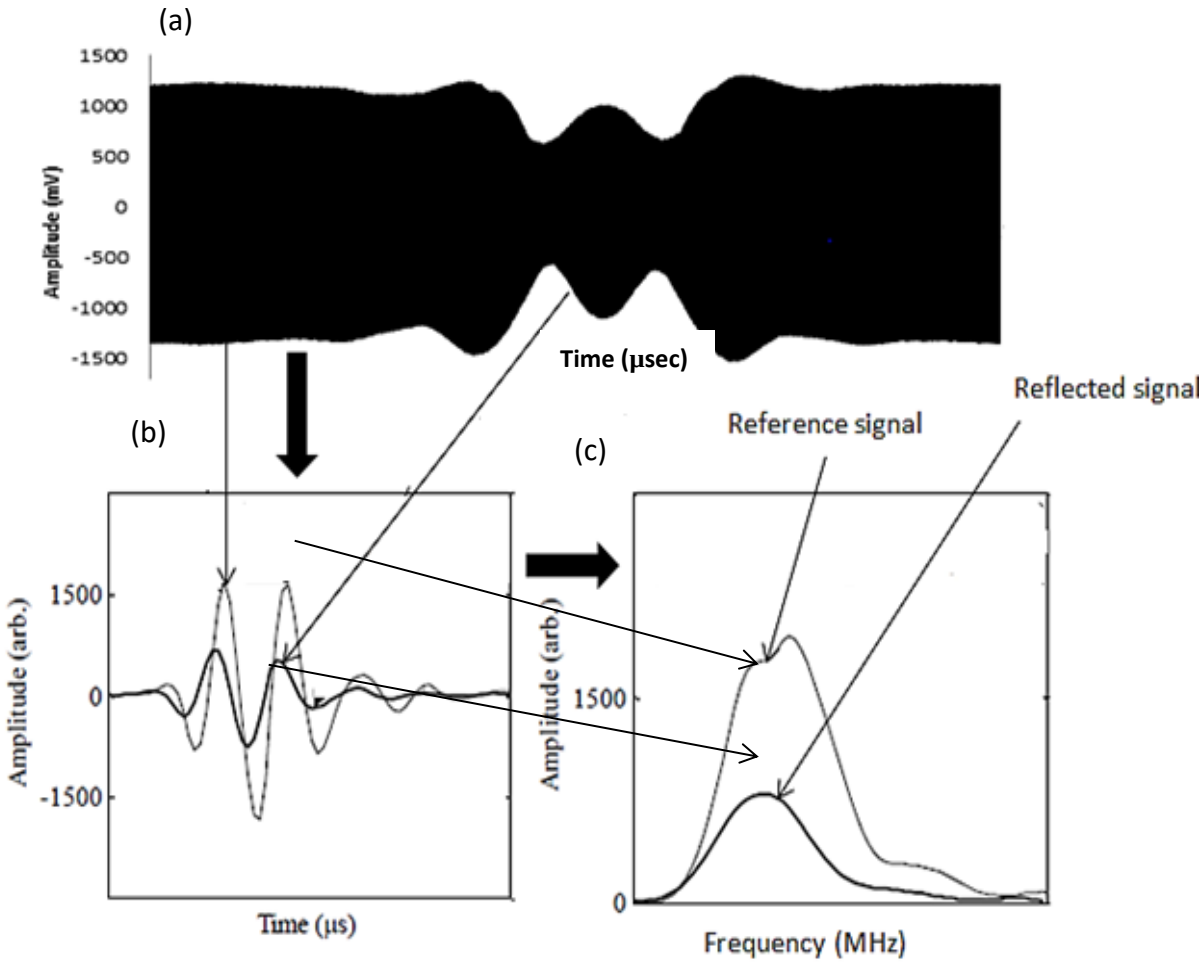

Figure 7-3: Processed reflected signal obtained from metal-to-roll interface during the rolling operation

The reflection coefficient of the transmitted signal is calculated by dividing the value of the reflected signal with reference signal values (Equation 3-11).

Figures 7-4 and 7-5 show the amplitude of the reference and reflected longitudinal and shear signals obtained from the strip and roll surface at roll speed of 19mm/Sec with Gerolub 5525 lubricant oils under 40kN rolling load. The graph was obtained from the reflected data captured after the rolling process and processed with the aid of the Labview program installed on the PC.

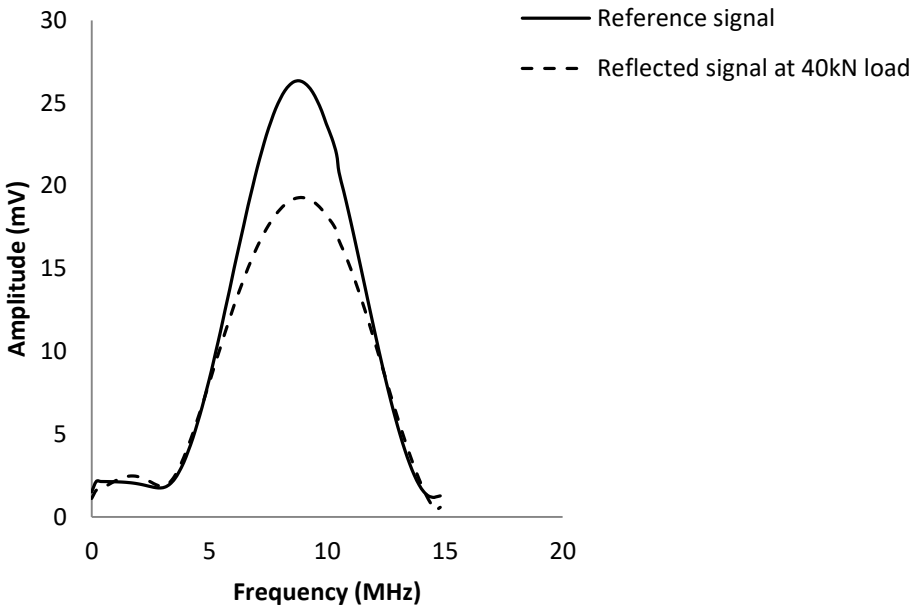

Figure 7-4: The reflected amplitude value against Frequency of the longitudinal wave sensor

The reference signal is of maximum amplitude when the sensor is out of contact with the strip. This amplitude value of the signal dropped immediately when the strip engaged with the sensing face under the rolling load during the cold metal rolling process (Figure 7-4). This is due to the deformation of the asperity contact of the strip and roll surfaces [104], where some of the energy is transmitted through the metal-to-roll interface during the rolling process.

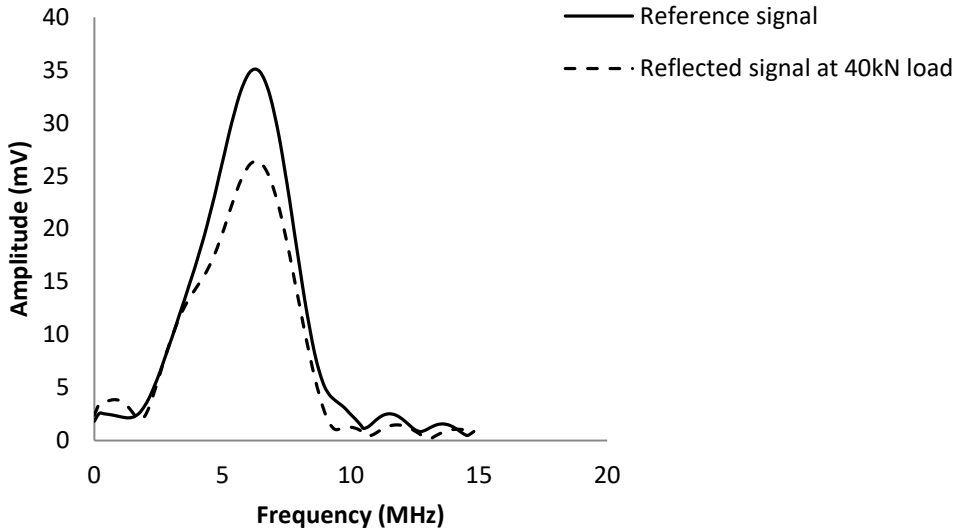

Figure 7-5: The reflected amplitude value against Frequency of the shear sensor

Figures 7-6 and 7-7 show reflection coefficient against frequency results obtained from pitch-catch ultrasonic transmission techniques using longitudinal and shear sensors during the metal rolling process at the centre of the roll-bite. Results are shown for frequencies lying within the bandwidth of each reference spectrum of Figures 7-4 and 7-5.

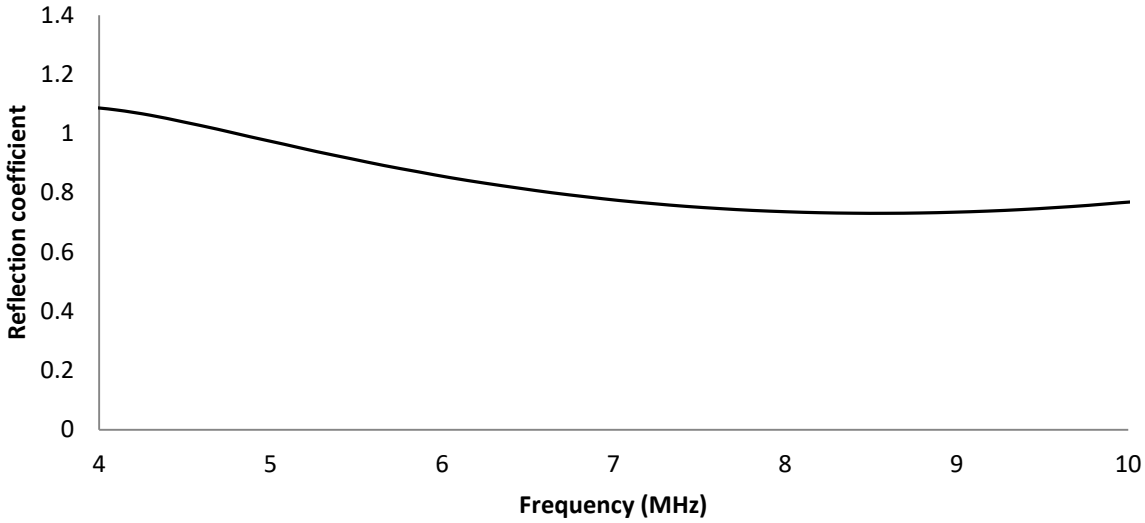

Figure 7-6: Longitudinal wave reflection coefficient against the frequency

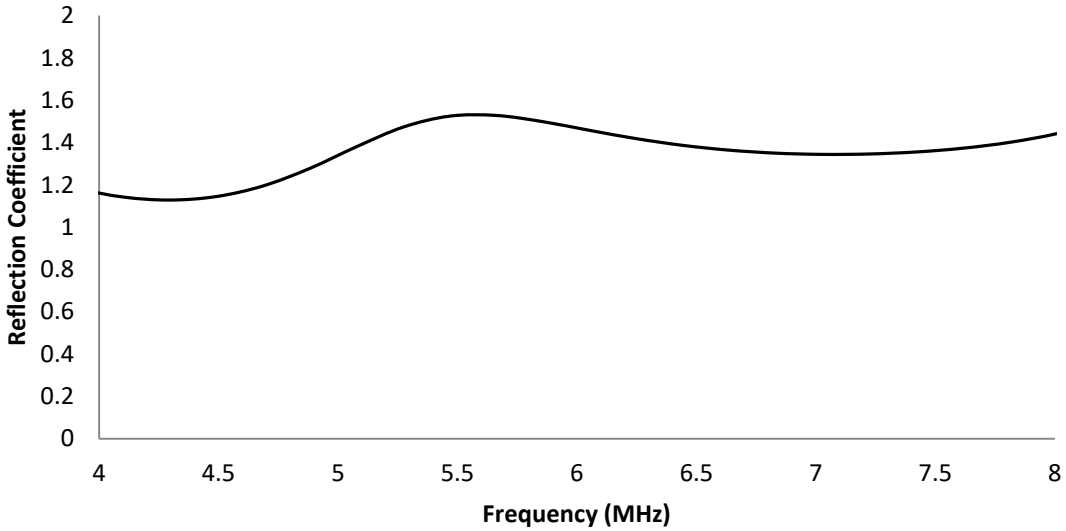

Figure 7-7: Shear wave reflection coefficient against the frequency

As can be seen from the figure above, there is a poor agreement between experimental coefficient reflections across the bandwidth of both sensors used, compared with the spring model predictions shown in Figures 6-6 and 6-7. A possible reason given by Liaptsis [97] has

been previously discussed in Section 6.4.3., although this trend is noticed across all results, and the reason for this poor agreement requires further analysis.

7.4.1.1 Determination of Reflection Coefficient

As explained in Section 3.3.3, the reflection coefficient was the proportion ratio of the peak amplitude value of the reflected wave to the peak amplitude value of the reference wave at 8.9MHz and 6.2MHz centre frequency for longitudinal and shear sensor waves respectively. The reflection coefficient of the signal was obtained by dividing the FFT of the measurement signal (reflected from the metal-to-roll interface) by the FFT of the reference signal (reflected from the metal-to-air interface). The values of 0.73 and 0.74 were obtained as the reflection coefficient for the Longitudinal and shear wave sensors respectively.

Usually, the longitudinal wave reference data should be captured from metal-to-air interface condition so that sensor surface is not in contact with oil; but this is always difficult during the experimental processing. Therefore, the reflection coefficient of roll-to-air and roll-to-oil was calculated in an ideal situation with the aid of equation 3-4 in section 3.3.1 to compensate for the losses of the longitudinal wave energy before the signal transmission process. The 0.9998 and 0.936 reflection coefficient values were obtained for metal-to-air and metal-to-oil interfaces respectively; giving a proportional value of 1.068. This value was acquired by dividing the obtained metal-to-air reflection coefficient value by the reflection coefficient of the metal-to-oil value. In this project, longitudinal reference number was multiplied by this value (1.068) before using it to calculate the reflection coefficient of the obtained wave reflected data. This only applies to the longitudinal wave reflection because oil does not have a significant effect on the shear wave during the transmission process.

Figures 7-8 shows the variable values of the longitudinal wave reflection coefficients obtained along the roll-bite during the metal rolling process. The longitudinal wave reflection coefficient obtained from the Figure 7-8 should be close to 1.0 at inlet zone, when the roll is not engaged with the strip, but it was less than one due to the reason given above. As the sensor surface on the roll and strip come into contacts, the contact reflection coefficient reduces. The reason for this reduction in the reflection coefficient is the increase in the metal-to-roll interface contact area during the rolling process. As the contact area increases, transmission of waves through the interface increases resulting in lower reflection coefficient value. Hence, the longitudinal reflection coefficient value of 0.72 was obtained as

shown in Figure 7-8 (from the maximum amplitude value of the frequency of the ultrasonic sensor applied Figure 7-4).

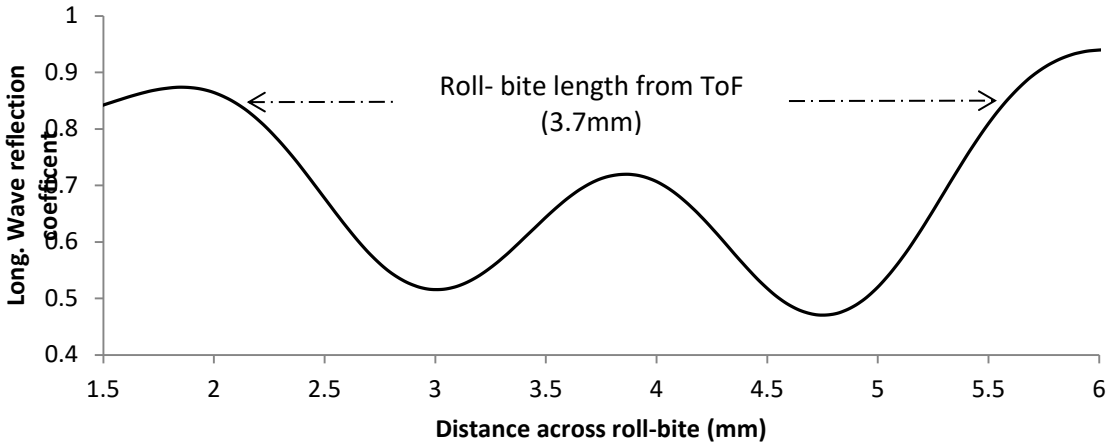

Figure 7-8: Variation of the longitudinal reflection coefficient signal sensor along the roll bite

The horizontal distance between the entry and exist points (experimental roll-bite length) was determined using the change of Time-of-Flight with the pulse number of the varying positions of the longitudinal reflected signal along the roll-bite (Fig. 7-8) during the metal rolling process. The obtained data was processed using the LabView program as explained in Section 5.3.8. The distance value of 3.7mm obtained as entry to exit was demonstrated as shown in the figure above. The expected theoretical value of the roll-bite length (5mm) was obtained with the same procedure discussed in Section 5.3.8. The experimental and theoretical values of the roll-bite length obtained are presented in Figure 7-9.

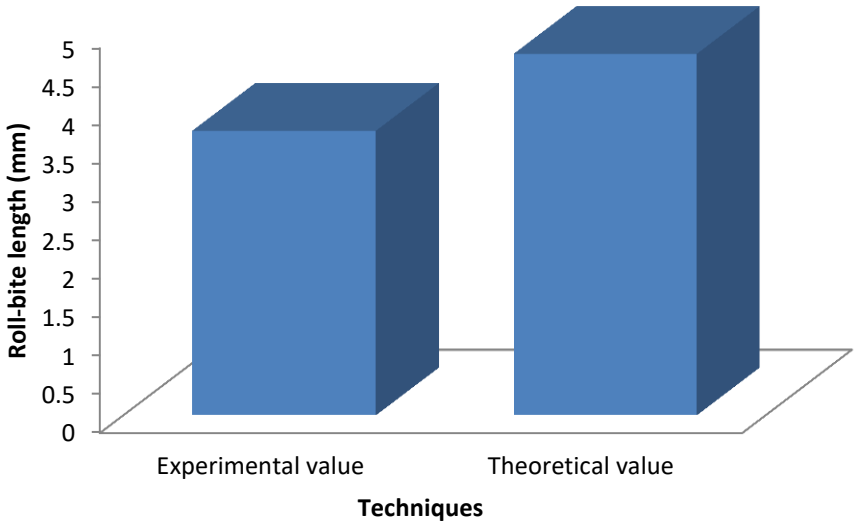

Figure 7-9: Roll-bite value obtained from mentioning techniques

As can be seen in Figure 7-9, some differences can be noticed between the theoretical and experimental roll-bite length values, and the reasons for these differences have been discussed in section 5.3.8.

Figure 7-10 shows the variable value of the shear wave reflection obtained along the roll-bite during the metal roll process. The value of the reflection coefficient obtained at the inlet zone was approximately 1.0 when there is no contact between the sensor and strip and due to the reason that liquid does not have any effect on shear sensor transmission. As strip and sensor contacts the reflection coefficient reduces to 0.74 at the maximum amplitude of the applied sensor frequency (Figure 7-10).

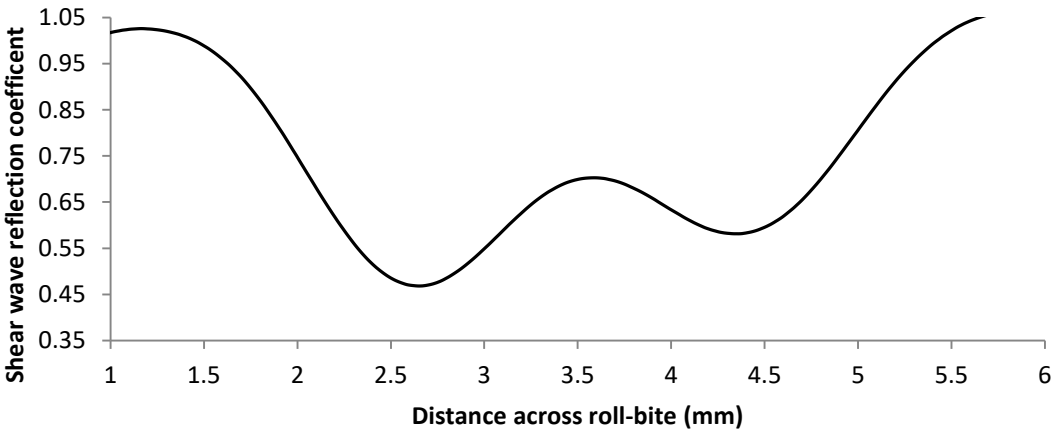

Figure 7-10: Variation of the shear reflection coefficient signal sensor along the roll bite

7.4.1.2 Determination of Stiffness

The reflection coefficient values obtained from the above section were employed with Equations 3-12 and 3-13 (for both wave sensors) and acoustic properties of the roll and strip to calculate the stiffness experienced at metal-to-roll interfaces. The normal and tangential stiffness's obtained from the longitudinal and shear waves were calculated and presented in Figure 7-11 and 7-12 respectively.

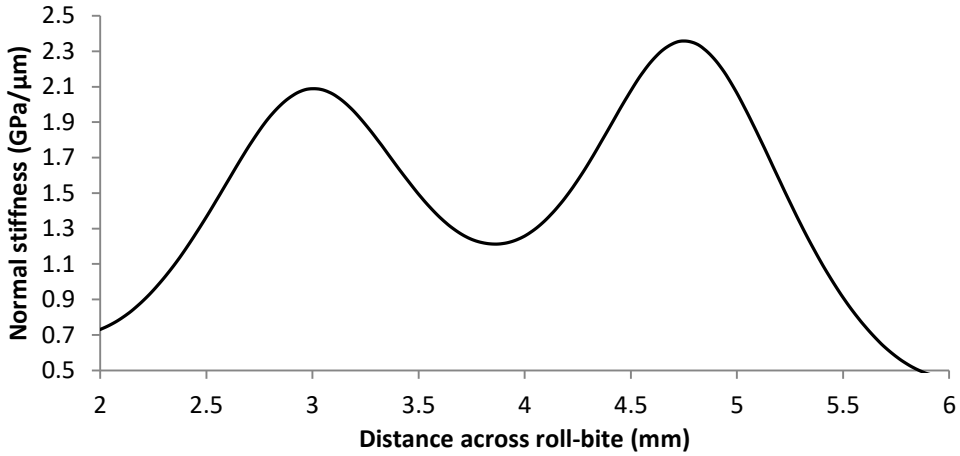

Figure 7-11: Normal stiffness obtained along the roll-bite during the rolling process

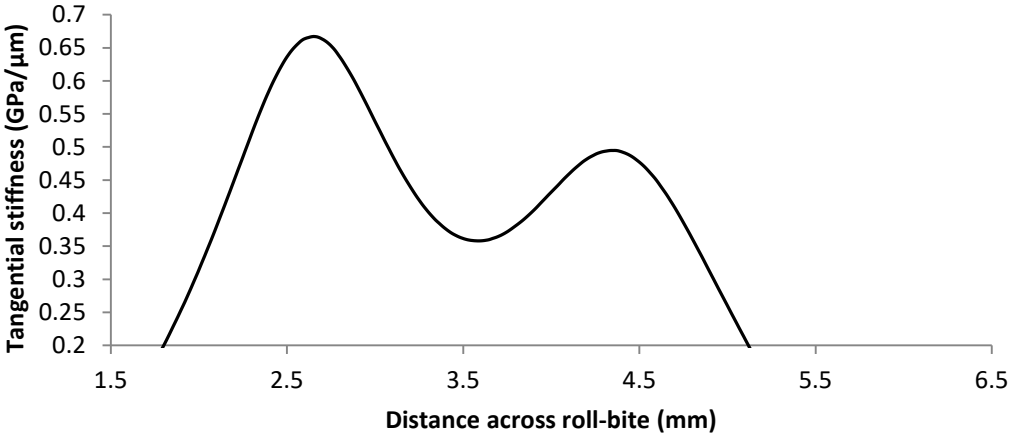

Figure 7-12: Tangential stiffness obtained along the roll-bite during the rolling process

The normal stiffness of 1.21GPa/µm and 0.36GPa/µm for the tangential stiffness values were selected at the centre frequency, the same to the frequency where the reflection coefficient used for the calculation was obtained.

7.4.1.3 Determination of Oil Film Thickness

As previously explained in section 3.3.4, the oil film thickness value was calculated using the normal and tangential stiffness obtained from the reflected data of the transmitted signal after the rolling process. The longitudinal normal stiffness contained stiffness's from both liquid and solid contacts while the shear stiffness contained only stiffness from solid contact and this was expressed in equations 3-14 (a and b) in Section 3.3.4 [66]. Since liquid does not support shear force, then Liquid shear stiffness in equation 3-14 (b) was equivalent to zero and the shear stiffness obtained by the shear sensor was equivalent to solid shear stiffness contact. Therefore the normal stiffness at liquid contact was obtained by equating the ratio shear stiffness at solid contact and normal stiffness at the solid contact to the Poisson's ratio

of the used material with the aid of equation 3-15. The oil film thickness at strip-to-roll interface was obtained with the aid of normal stiffness at liquid contact; the oil film thickness and Bulk modulus of the oil are expressed in equation 3-16. The oil film thickness obtained is presented in Figure 7-13.

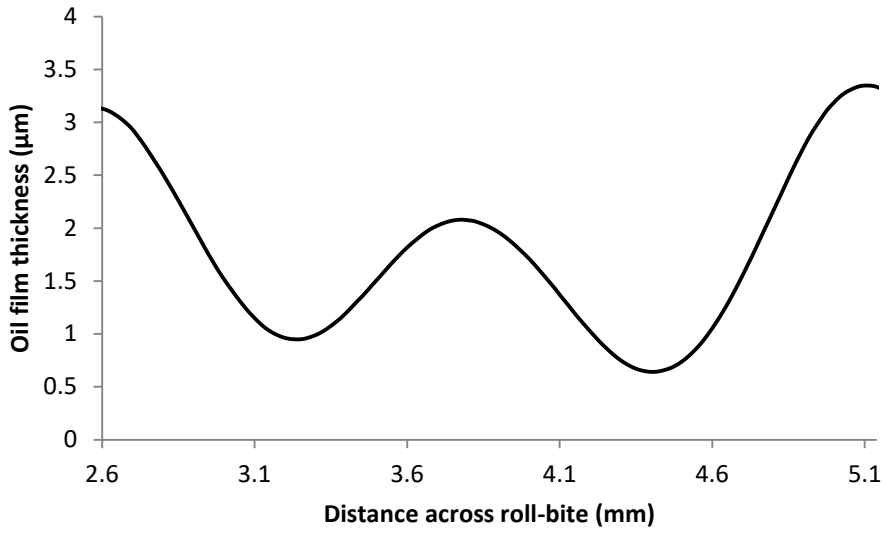

Figure 7-13: Oil film thickness obtained at the roll-bite during the rolling operation

7.4.1.4 Determination of Oil Film Thickness with Pulse-Echo Technique

Figures 7-14 and 7-15 show the longitudinal and shear reflection coefficients obtained from the pulse-echo measurement technique.

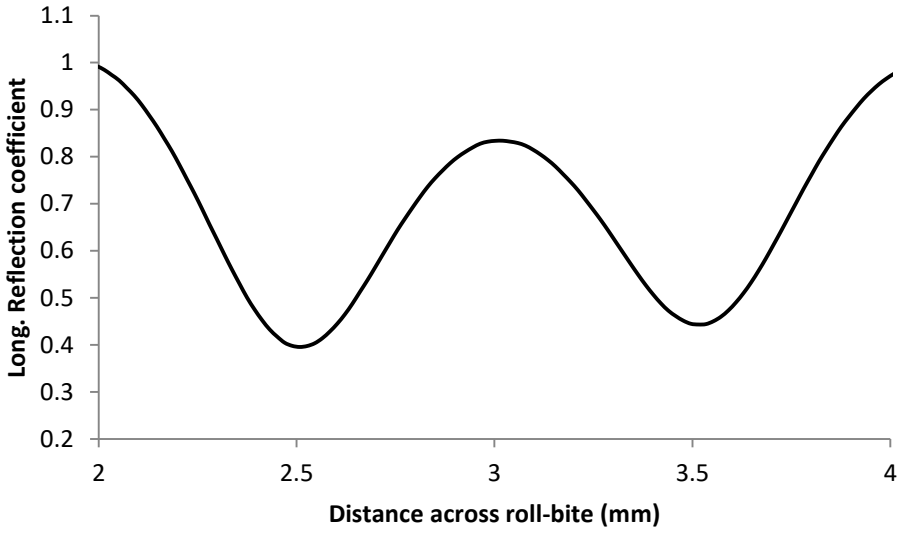

Figure 7-14: Longitudinal reflection coefficient obtained from the pulse-echo measurement technique

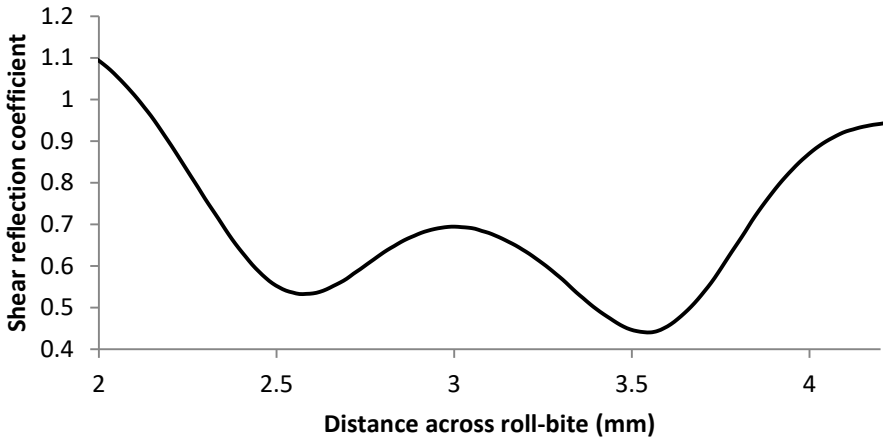

Figure 7-15: Shear reflection coefficient obtained from the pulse-echo measurement technique

These values were obtained with the same approach used to determine the longitudinal and shear reflection coefficient from the data obtained using the pitch-catch technique in Section 7.4.1.1. The reflection coefficients obtained from this technique are of higher value than the reflection coefficients obtained from the pitch-catch technique.

Figures 7-16 and 7-17 show the normal and tangential stiffness obtained from the longitudinal and shear wave reflection data under the pulse-echo approach during the metal rolling process.

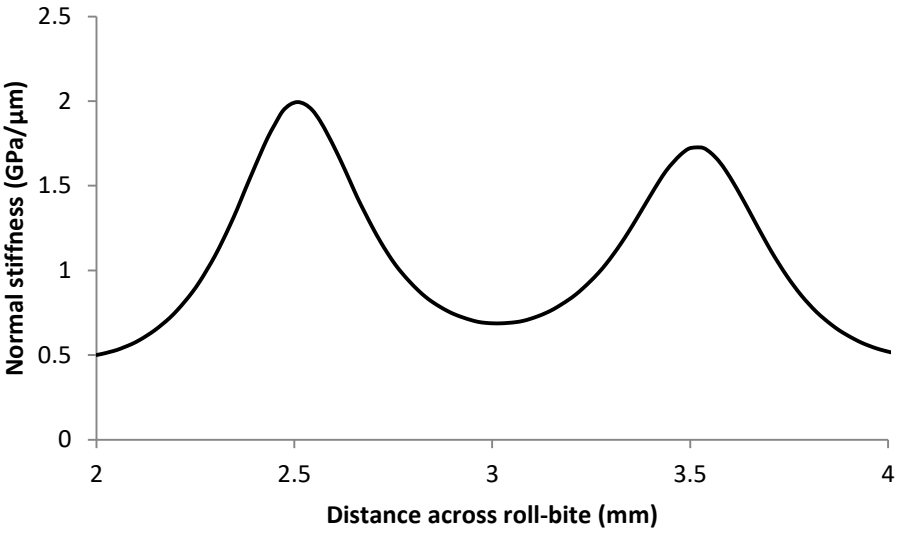

Figure 7-16: Normal stiffness value obtained from the pulse-echo measurement technique

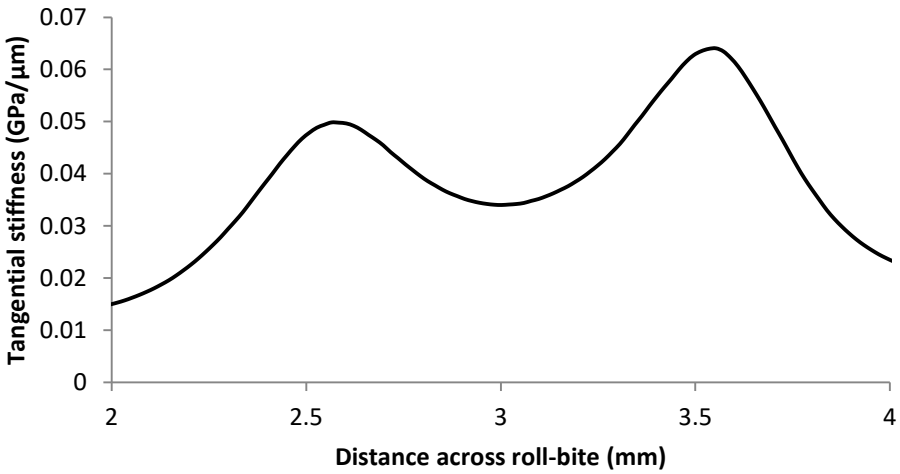

Figure 7-17: Tangential stiffness value obtained from the pulse-echo measurement technique

Both stiffness values were calculated from the reflections obtained from the sensor using the same approach applied to the data obtained using the pitch-catch technique in Section 7.4.1.2. The normal and tangential stiffness obtained from the pulse-echo technique are of lower values compared with both the stiffness values obtained from pitch-catch technique due to the higher value of the reflection coefficient obtained from the pulse-echo measurement above.

Figure 7-18 shows the various oil film thicknesses obtained across the roll-bite using the pulse-echo technique. These values were obtained with the same mathematical manipulation used to obtain the oil film from the pitch-catch measurement technique in Section 7.4.1.3.

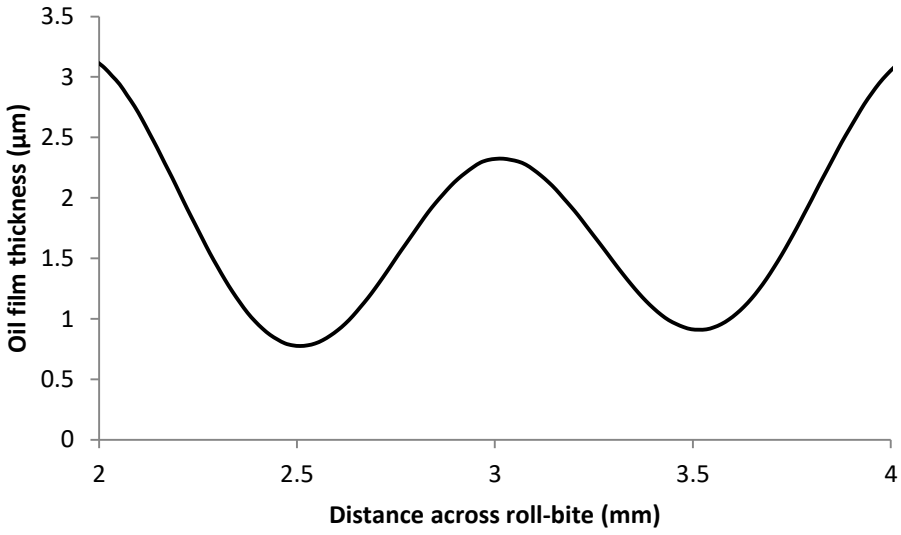

Figure 7-18: Oil film thickness value obtained from the pulse-echo measurement technique

Figure 7-19 shows the various oil film thicknesses obtained along roll-bite length contact from both pitch-catch and pulse-echo measurement techniques under the same metal rolling conditions.

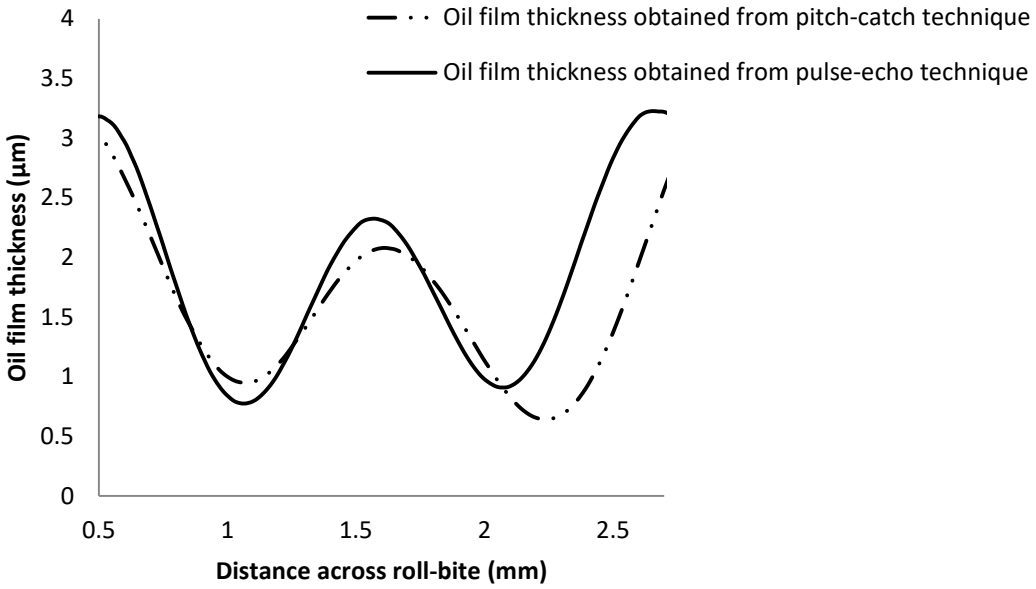

Figure 7-19: Oil film thickness obtained from both measurement techniques

As can be seen from the figure above, the value of the oil film thickness observed t the centre of the roll-bite using the pulse-echo technique (2.32µm) is a slightly higher than the oil film thickness obtained from the pitch-catch (2.07µm) measurement technique. A 7.7% higher value for oil film thickness was reported using the pulse-echo technique compared to the pitch-catch technique.

The theoretical oil film thickness at the metal-to-roll interface was calculated using equation 2-29 in Section 2-5 with material property's itemized in Tables 5-3 and 7-1 and contact length from equation 2-3. The theoretical oil film thickness obtained was assumed to be constant across the roll-bite. The experimental and the theoretical values of oil film thickness obtained are presented in Figure 7-20.

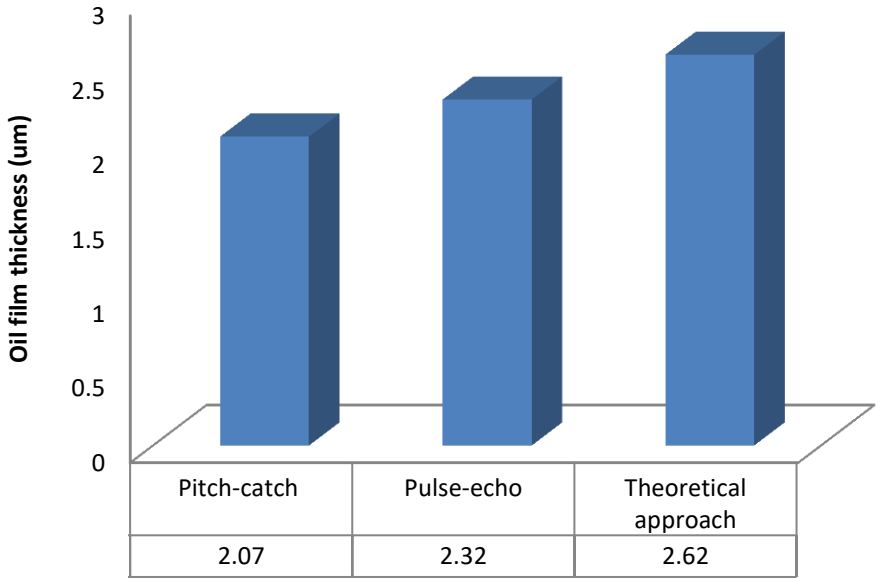

Figure 7-20: Experimental and theoretical oil film thickness obtained during the metal rolling process

As shown in Figure 7-20, there is a marginal difference between the two experimental oil film thicknesses obtained and the theoretical result. This may be because the equation was derived to calculate the oil film thickness at inlet section while the experimental results show the oil film thickness at the work zone. For this reason it is expected that the theoretical approach will report a higher value for film thickness, and this is what is observed.

Finally, the Lambda ratio of the lubrication system was calculated using equation 2-31 in Section 2-5 and Lambda ratio 1.8 was obtained from the oil film thickness obtained under the pitch-catch measurement technique. The value was calculated using the experimental oil film thickness obtained and roughness values of the strip and roll measured before the experiment (0.87µm). The lubrication system was classified as mixed lubrication regime since the oil film thickness value was greater than the roughness value of the surfaces.

7.4.2 Effect of Applied Rolling Loads on Oil Film Thickness Formation

Figures 7-21 and 7-22 show the reflected data obtained from longitudinal and shear wave sensors from the different applied loads. Increasing the applied load reduces the amplitude of the reflected signals. The reason for this reduction in the amplitude value of the reflected wave was the increase in the metal-to-roll contact area that increases with the increase of the rolling load. Hence, the rate of the signal transmitted through the interface increased;

therefore, the low value in the amplitude wave reflection was recorded. Additionally, reduction in reflected wave amplitude during the metal rolling was due to the increment in rolling load that increased the contact area of metal-to-roll interface. Hence, as the loads on the rolled metal increase, the metal-to-roll contact interface increases and more waves are transmitted to the strip. Due to this, a reduction in the amplitude value of the reflected waves was recorded. Figures 7-21 (for longitudinal) and Figure 7-22 (for shear) shows the reduction in wave reflected amplitude values against the frequency of the applied sensors in terms of the rolling loads applied.

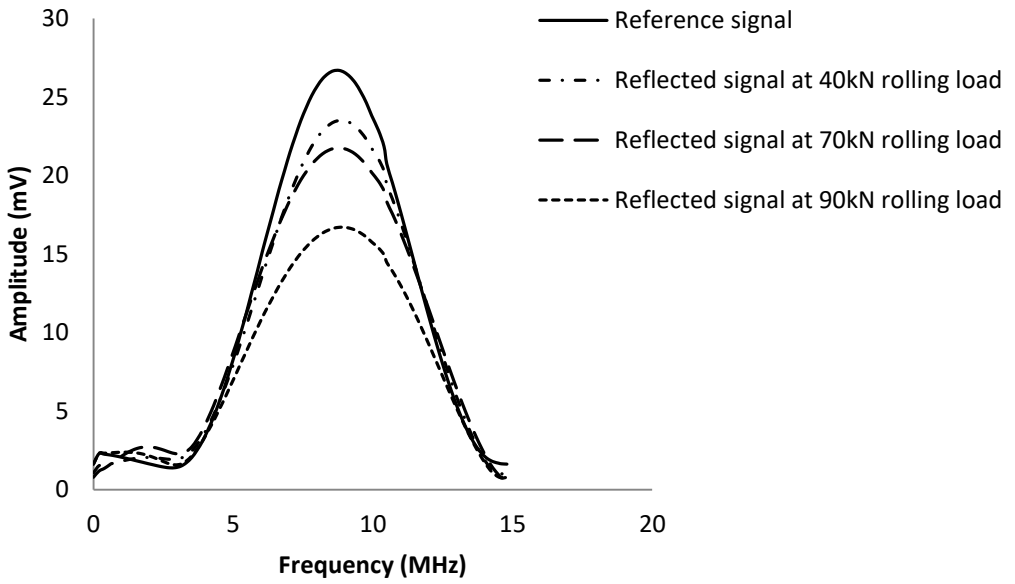

Figure 7-21: Amplitude of longitudinal sensor reflected wave at various loadings

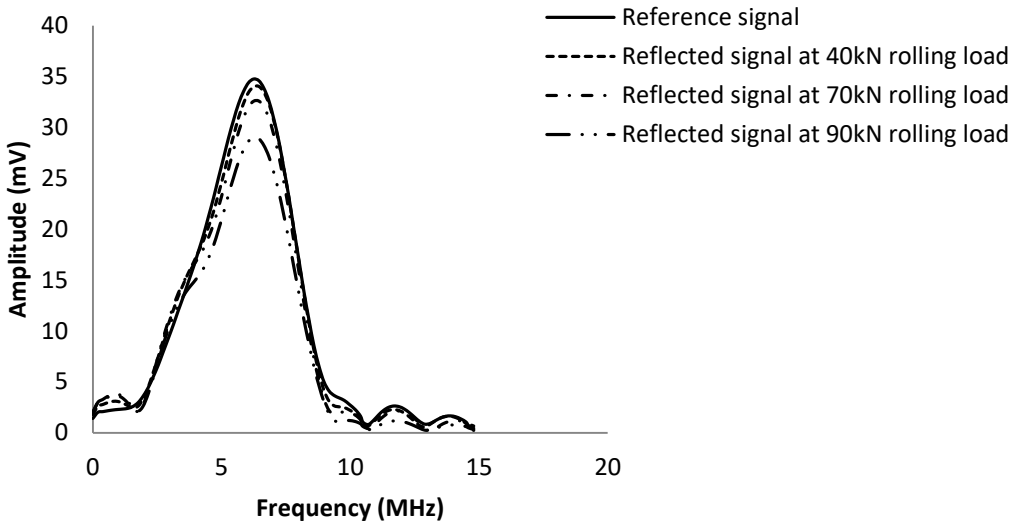

Figure 7-22: Amplitude of shear sensor reflected wave at various loadings

Therefore, the greater the applied load, the more the contact of the interface length and greater reduction in the amplitude value of the reflected waves. The reflection coefficient of the reflected data obtained at each load applied during the experiment was calculated as explained in Section 7.4.1.1, above.

Figures 7-23 and 7-24 show the various reflection coefficients obtained from metal-to-roll interface during the metal rolling operation with longitudinal and shear wave sensors. It is noted that the reflection coefficient amplitude has some fringes when the roller entered or departed from the sensor active measurement zone. The amplitude of the reflection coefficient reduced to a minimum level at metal-to-roll contact interface. That is, when the rolled strip is underneath the sensor, at the distance of 3.7mm to 6.9mm, for the rolling loads applied. The Longitudinal and shear wave reflection coefficient values obtained were reduced from 0.87 to 0.54 and 0.93 to 0.72 as the applied rolling loads increased from 40kN to 90 kN respectively.

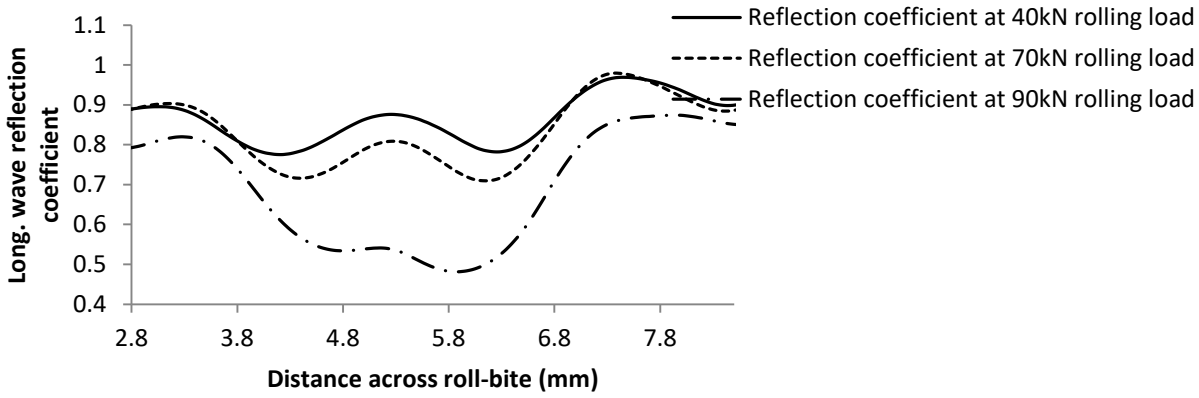

Figure 7-23: Reflection coefficient of the longitudinal wave sensor along the roll-bite during

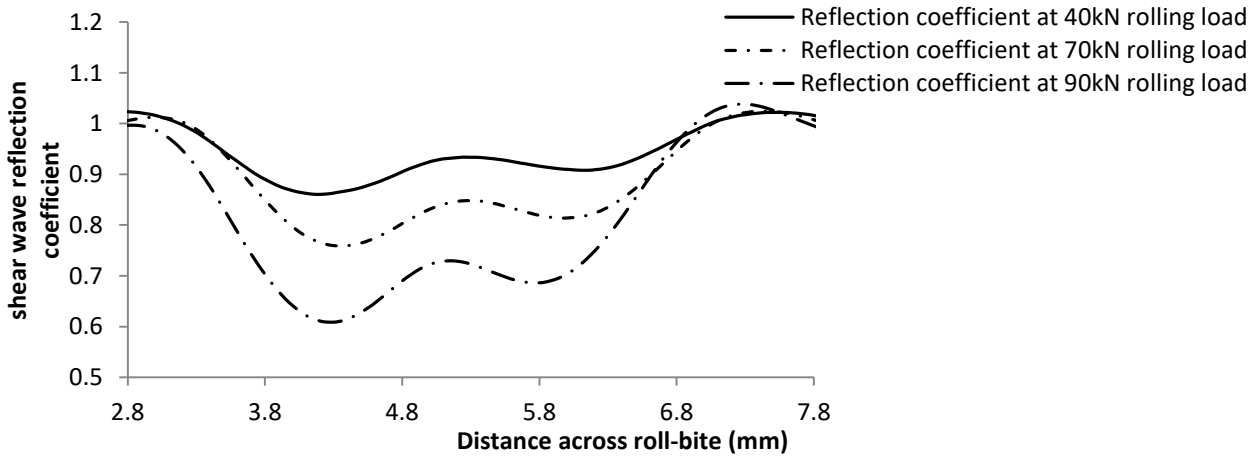

Figure 7-24: Reflection coefficient of the shear wave sensor along the roll-bite during

The overlapping signals can be seen to contain some shoulders during application of the rolling loads at 3.3mm (right hand side) and 7.2mm (left hand side) along the roll-bite length in Figures 7-23 and 7-24 respectively. Additionally, the obtained reflected signals change at the shoulder as can be seen in the graphs with respect to the loads. The reason for the reaction of the signals to load increment at these points is not well understood. However, the center values of the graph are the main focus of this is research and these centre values conform adequately to changes in the applied rolling loads.

The reflection coefficients from the applied sensors against the loads during the cold metal rolling are processed by the same method explained in Section 7.4.1.1, and obtained results are shown in Figures 7-25 and 7-26.

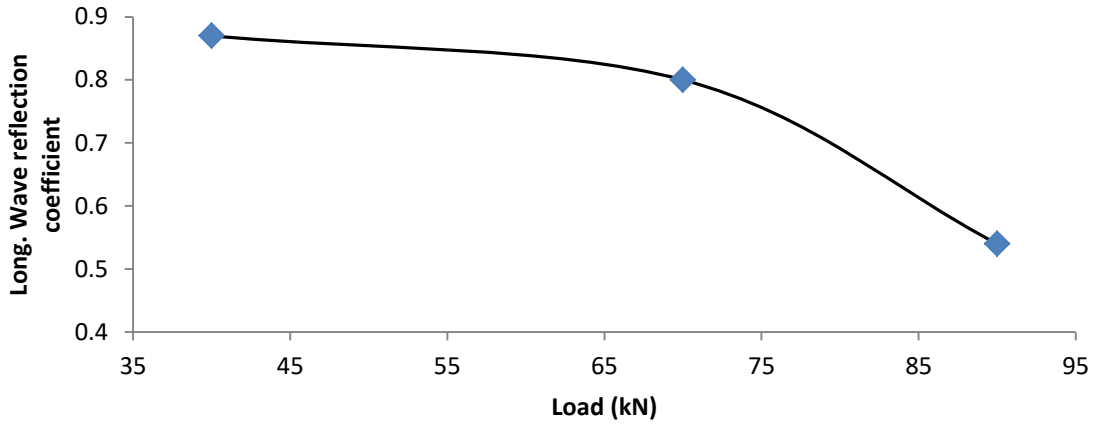

Figure 7-25: The reflection coefficient of longitudinal wave sensor against deformation loads

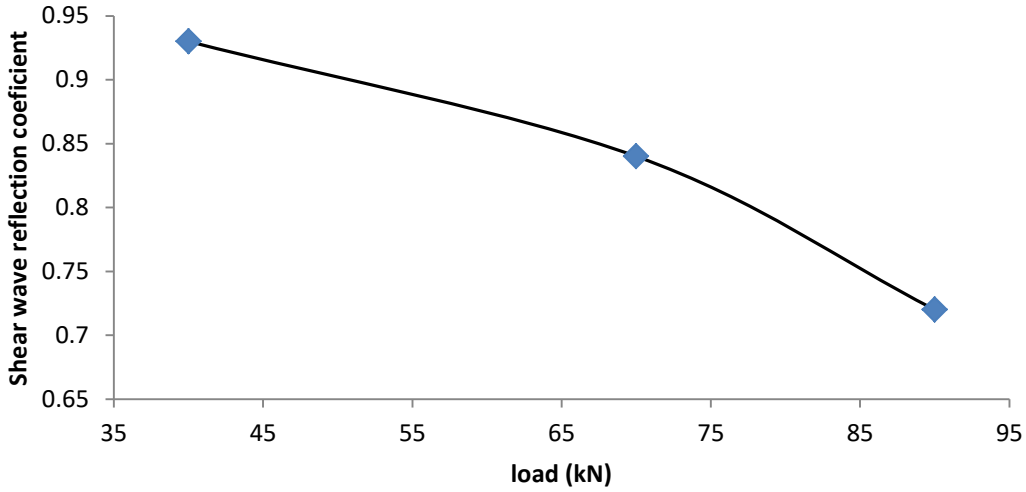

Figure 7-26: The reflection coefficient of shear wave sensor against deformation loads

As explained in the previous section, the more the rolling load increase, the more the plastic and elastic deformation at strip-to-roll interface increases. Hence the greater transmission of signals from the roll to strip and the less reflected signal obtained during the rolling process. It can also be observed that there is a decrease in the values at the tail end due to the high rolling load applied, which leads to low reflection coefficient value (Figure 7-25). This gradual tailing-off is due to the large signals transmitted to the strip during the rolling operation.

Furthermore, the experimental values of the longitudinal and shear stiffness at the metal-to-roll interface were calculated with the same approach employed in Section 7.4.1.2, and the obtained results are presented in Figures 7-27 and 7-28 respectively.

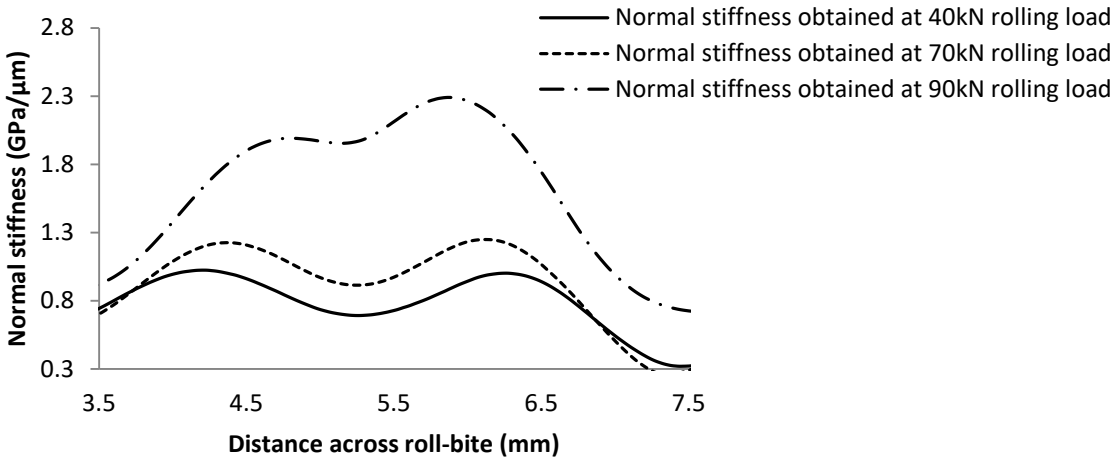

Figure 7-27: Normal stiffness obtained from the longitudinal wave sensor at the roll – bite

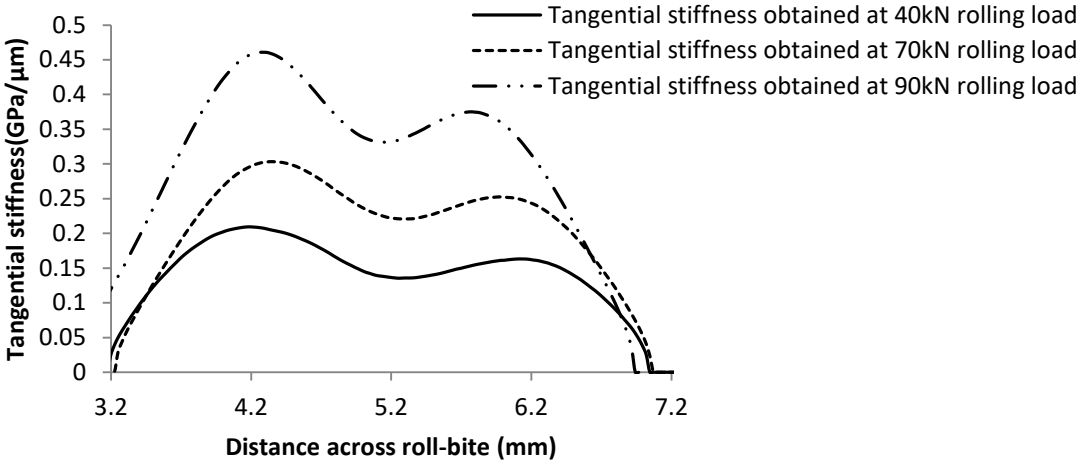

Figure 7-28: Tangential stiffness obtained from shear wave sensor at the roll - bite

Figures 7-29 and 7-30, show the values of the normal and tangential stiffness plotted against the loads applied respectively.

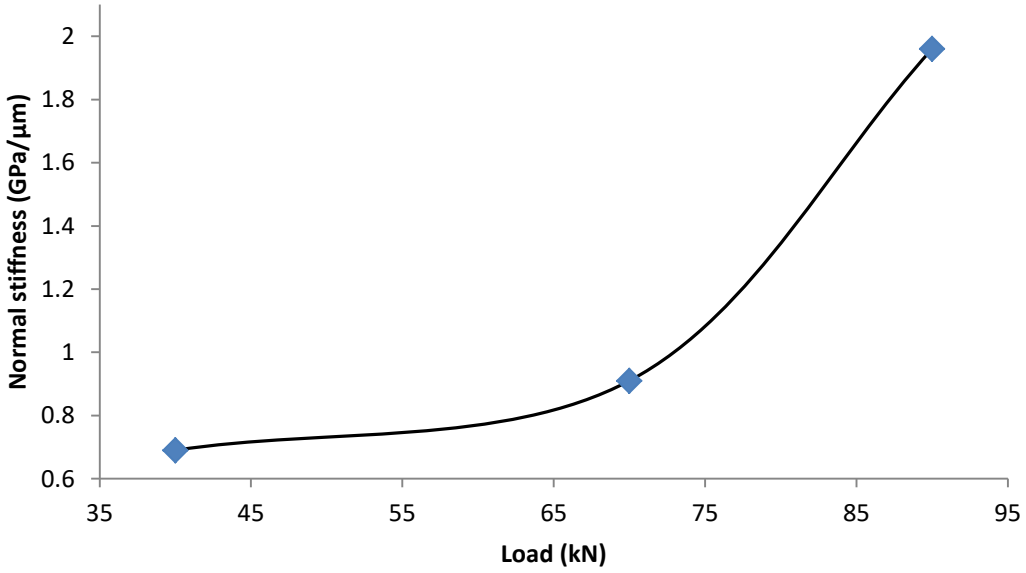

Figure 7-29: Normal stiffness and applied deformation load relationship

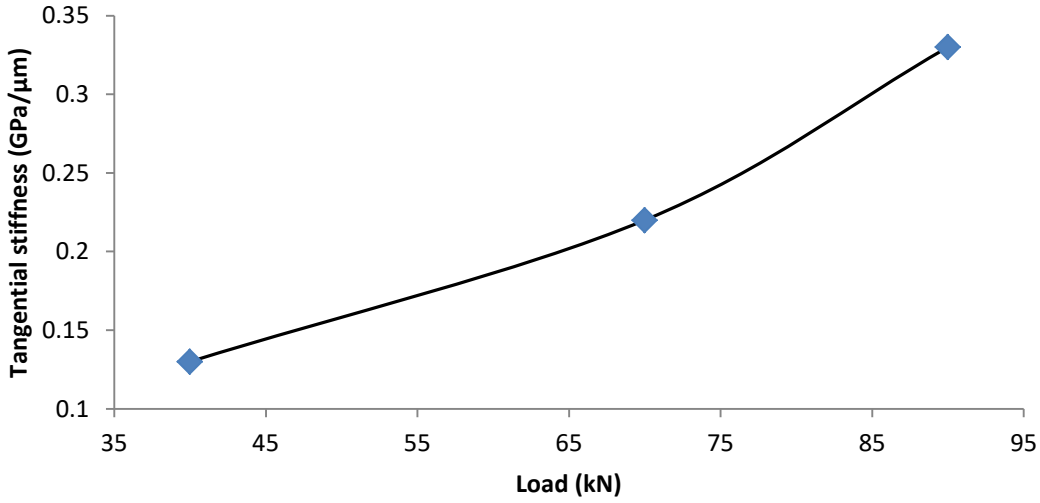

Figure 7-30: Tangential stiffness and applied deformation load relationship

The normal and tangential stiffness's were found to be in an approximately linear relationship with the applied loads during the rolling process. That is, the stiffness value

increases as the applied rolling load increases due to increased closeness of the gap in the contact interface area of the metal-to-roll during the increment of the applied load.

The normal and tangential stiffness value obtained were used with the method employed in Section 7.4.1.3, to determine the oil film thickness formed at the metal-to-roll interface under the various loads applied and presented in Figure 7-31.

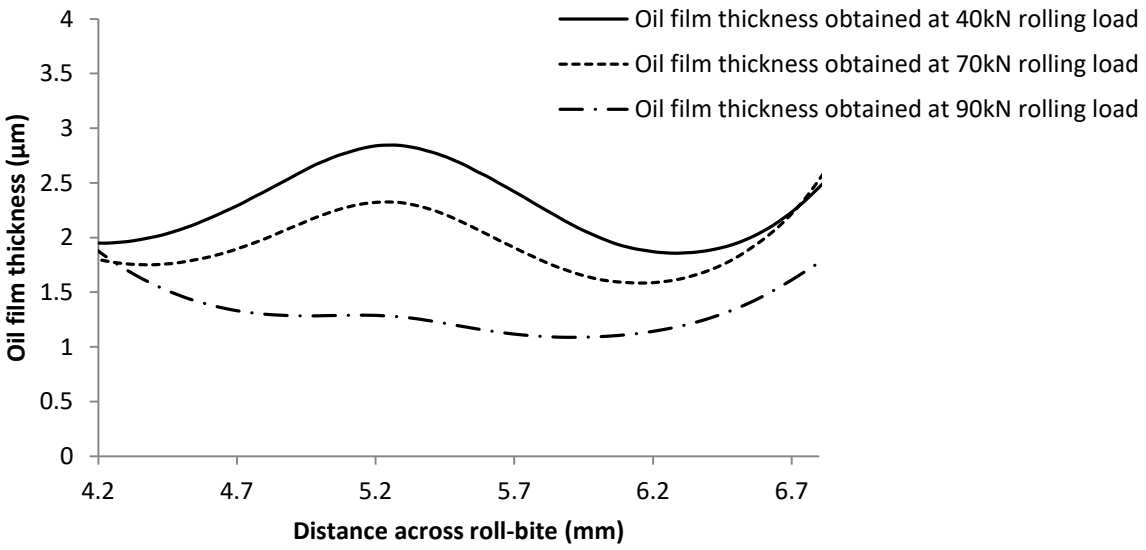

Figure 7-31: Oil film thickness formed at the roll - bite during the rolling process.

The oil film values obtained were plotted against the loads applied during the rolling process and is shown in Figure 7-32.

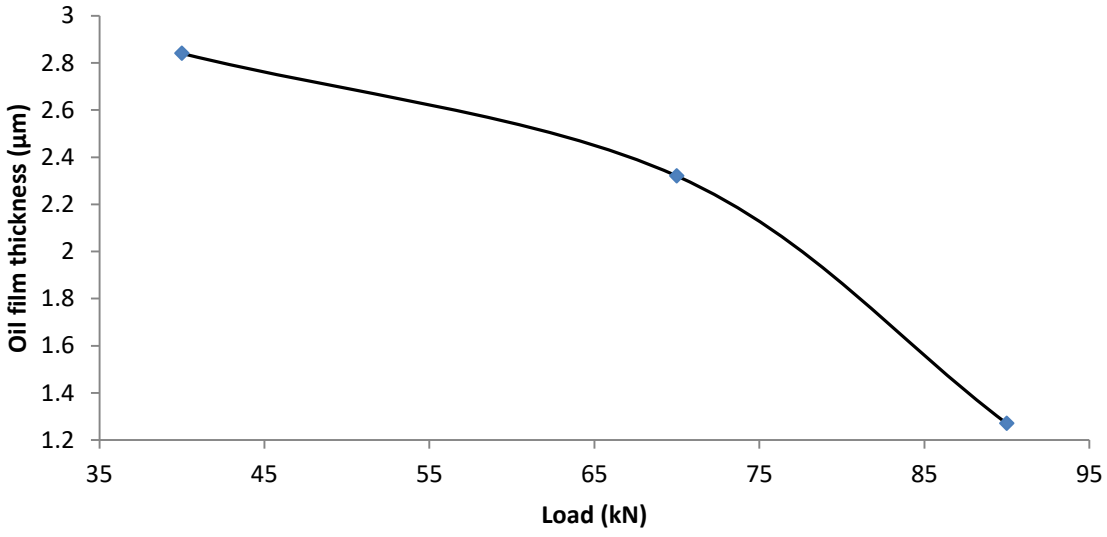

Figure 7-32: Oil film against the loads applied

It is clearly shown in Figure 7-32 that as the applied rolling loads increase, oil film thickness at the strip-to-roll interface gradually decreases. This is because the increase in the applied loads causes an increase in the contact at the metal-to-roll interface. In addition, this leads to the reduction in the volume of the oil that is drawn into the roll surface and causes a decrease in the thickness of the oil at the strip-to-roll interface during the process.

Furthermore, the oil thickness was theoretically calculated as explained before in Section 7.4.1.3, with the values of 0.48mm, 0.72mm and 1.2mm metal reduction observed under the rolling loads applied. The difference between the theoretical and experimental oil thickness obtained are presented in Figure 7-33.

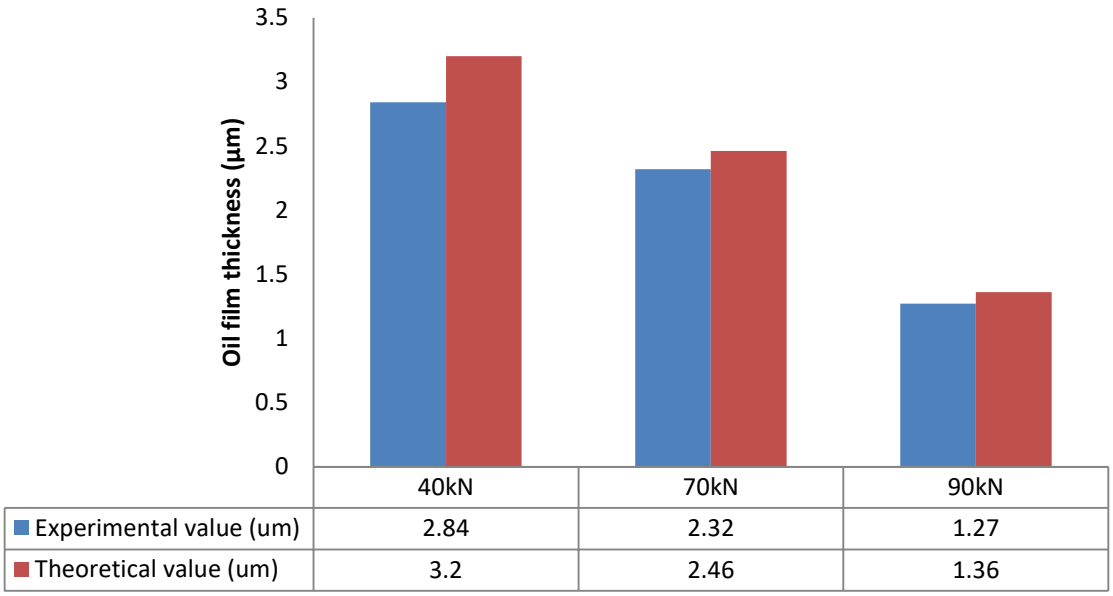

	40kN	70kN	90kN
Experimental value (um)	2.84	2.32	1.27
Theoretical value (um)	3.2	2.46	1.36

Figure 7-33: Theoretical and experimental oil film thicknesses obtained under the various rolling loads

As shown in Figure 7-33, there is little variation between the theoretical and the experimental value of the oil film thickness presented. This may be due to the effect of the lubricating oil properties which can be varied from the ideal properties used for the prediction formulae. Additionally, the oil film thickness values obtained from the theoretical approach are the oil film at the inlet zone while experimental values are from the work zone respectively. However, both values obtained from the two methods are reasonably close within ranges of accuracy. There ranges are, 12.6% for 40kN, 6.0% for 70kN and 7.0% for 90kN.

Finally, lambda ratio of the lubrication system was calculated as explained Section 7.4.1.3, last paragraph and presented in Table 7-2.

Table 7-2: Lambda ratio value obtained during the experiment

Loads (kN)	Lambda ratio	Lubrication regime
40	2.47	Mixed
70	2.02	Mixed
90	1.10	Mixed

As can be seen, the various loads applied for the different metal reduction processes during the rolling operation are operating within the mixed lubrication regime.

7.4.1 The Investigation of Roll Speed on the Oil Film Thickness Formation

The effect of roll speeds was investigated on the formation of oil film thickness under various rolling loads with the aid of the ultrasonic reflection measuring technique in this section. The experiments were conducted using two different values of roll speeds (19 and 26 mm/sec) under the 40kN and 70kN rolling loads respectively. The captured data from the reflected waves were used to calculate the thickness of the oil film at roll-bite during the rolling process.

7.4.1.1 The 19mm/sec and 26mm/sec Roll Speeds at 40kN Rolling Load

The reflected wave data received from the metal-to-roll interface during the application of the same rolling load (40kN) to 19mm/sec and 26mm/sec roll speeds were analyzed and presented in Figures 7-28 and 7-29 respectively. As explained in Section 7.4.2, pressure on the metal-to-roll interface increases with increasing rolling load while it decreases with increasing rolling speed. This can be seen clearly from the increasing of the wave reflected amplitude obtained at various speeds under the same rolling load (Figures 7-34 and 7-35). These Figures show the increasing of the amplitude value of the reflected wave with the increasing of applied roll speed and this was due to the increases of the lubrication resistance during the rolling process. This increase of the roll speed also caused the increasing frictional resistance within the layer of oil and separated the strip-to-roll interface during the rolling process [105]. Additionally, an increase in roller speed also increases the volume of oil drawn into the contact surface and reduces the contact length of the two surfaces. Therefore, the higher the rolls speed, the higher the amplitude value of the

reflected wave. This was experienced from the two applied sensors under the same applied rolling loads.

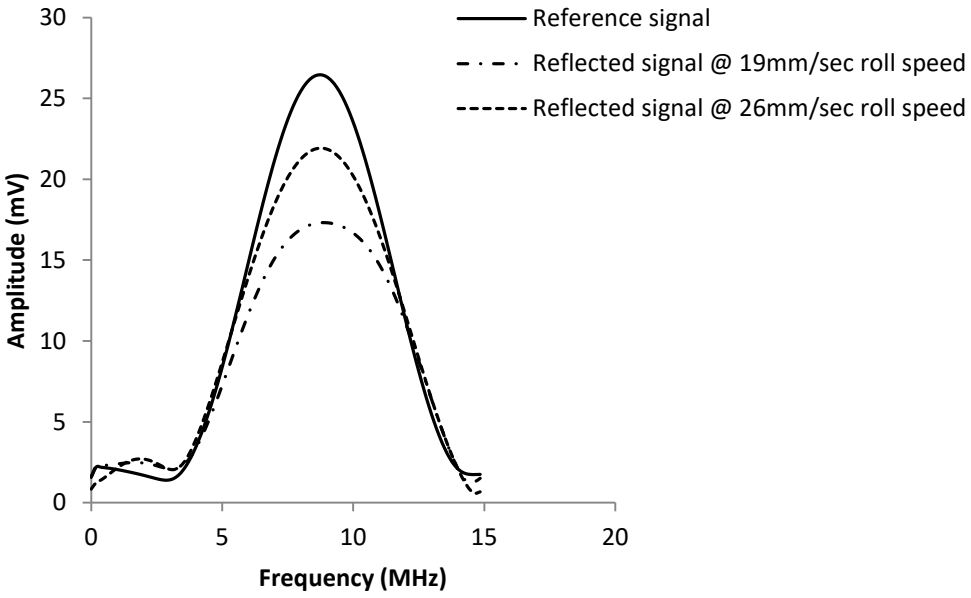

Figure 7-34: Amplitude of longitudinal reflected wave at 40kN applied rolling load

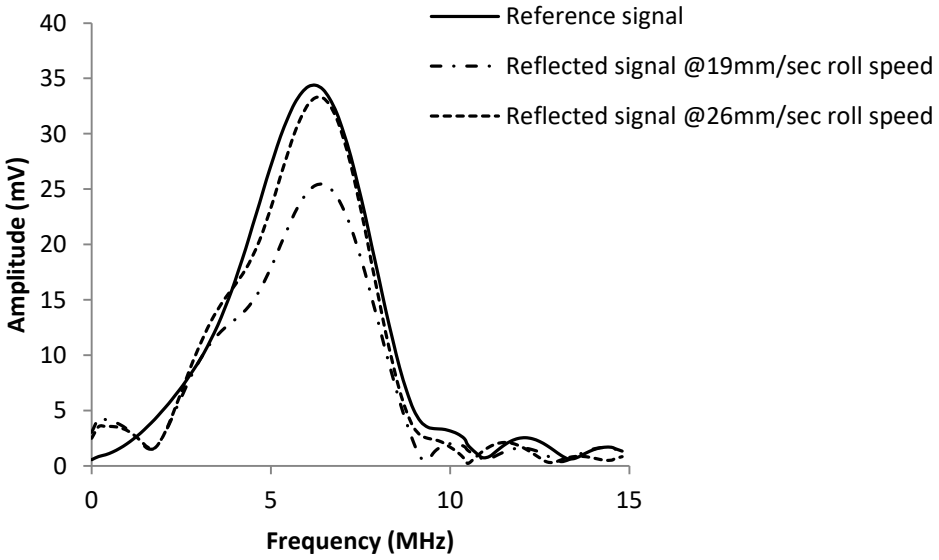

Figure 7-35: Amplitude of shear reflected wave at 40kN applied rolling load

As previously explained and calculated in Section 7.4.1.1, the reflection coefficients of the reflected signal was obtained by dividing the amplitude of the reflected signal by the

amplitude of the reference signal. The reflection coefficient obtained from the reflected data captured by these roll speeds was compared with the aid of the Figures 7-36 and 7-37

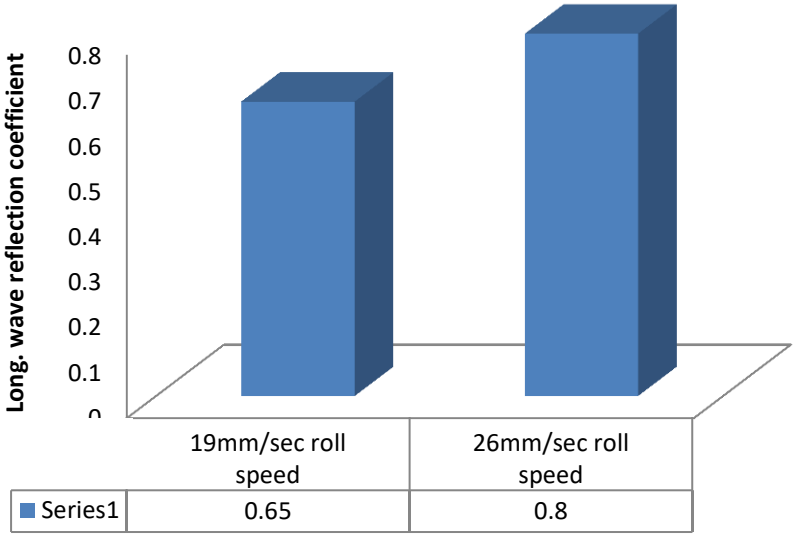

Figure 7-36: Reflection coefficient of the reflected wave at 40kN applied rolling load

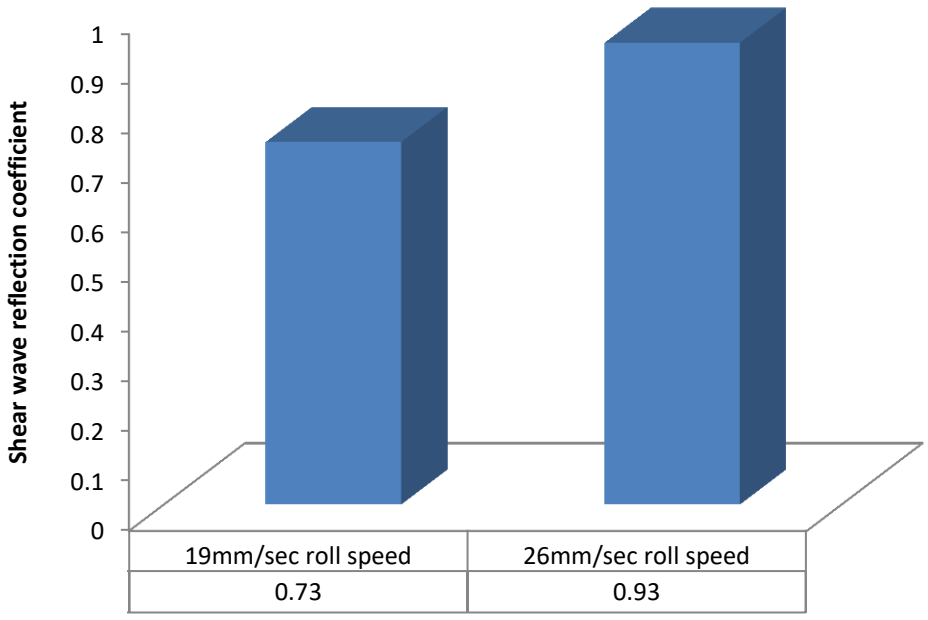

Figure 7-37: Reflection coefficient of the reflected wave at 40kN applied rolling load

As can be seen from these Figures, as the roll speeds increased the longitudinal and shear reflection coefficient values of the reflected waves obtained increased under the same rolling load. The reason for this is explained in more detail below.

Furthermore, the various longitudinal reflection coefficient values obtained along the roll-bite are shown in Figure7-38 while the shear reflection coefficient obtained is also shown in Figure 7-39 respectively. The higher the roll speed the more lubricant is penetrated into the interface, then the lesser the contact length due to the separation of the interface by the penetrated oil. Additionally, the reduction in the surface asperity contact was experienced and less wave transmission occurred and the high reflection coefficient value was recorded. As shown in Figure 7-38, the longitudinal reflection value at 19mm/sec is 0.67, while it increased to 0.83 at 26mm/sec roll speed. Also, Figure 7-38 shows the increases of shear reflection coefficient from 0.64 at 19mm/sec to 0.85 at 26mm/sec roll speed. In addition, the increase of the roll speed has a significant effect on the roll-bite contact length as shown in the figures. This was due to more volume of the lubricant flowing into the metal-to-roll interface and causing the separation of the interface thereby creating more film thickness along the roll-bite. The higher the separation of the contact surface, the lesser the roll-bite length obtained.

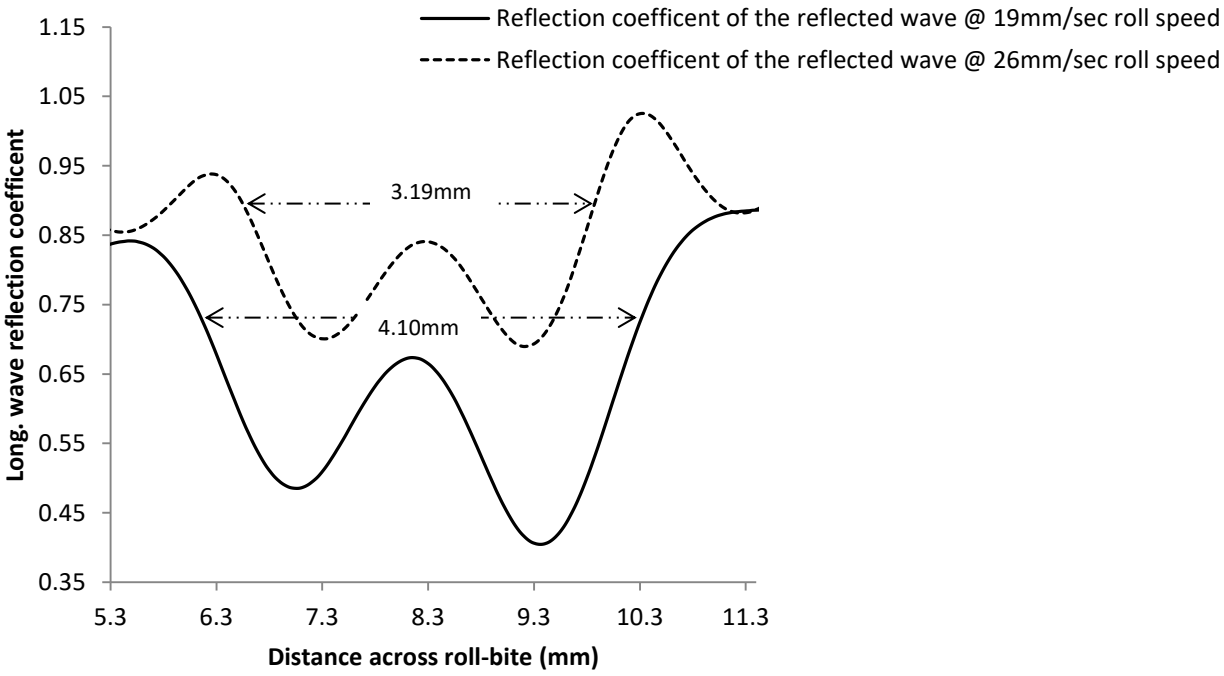

Figure 7-38: Reflection coefficient of the reflected wave along the roll-bite at 40kN rolling load

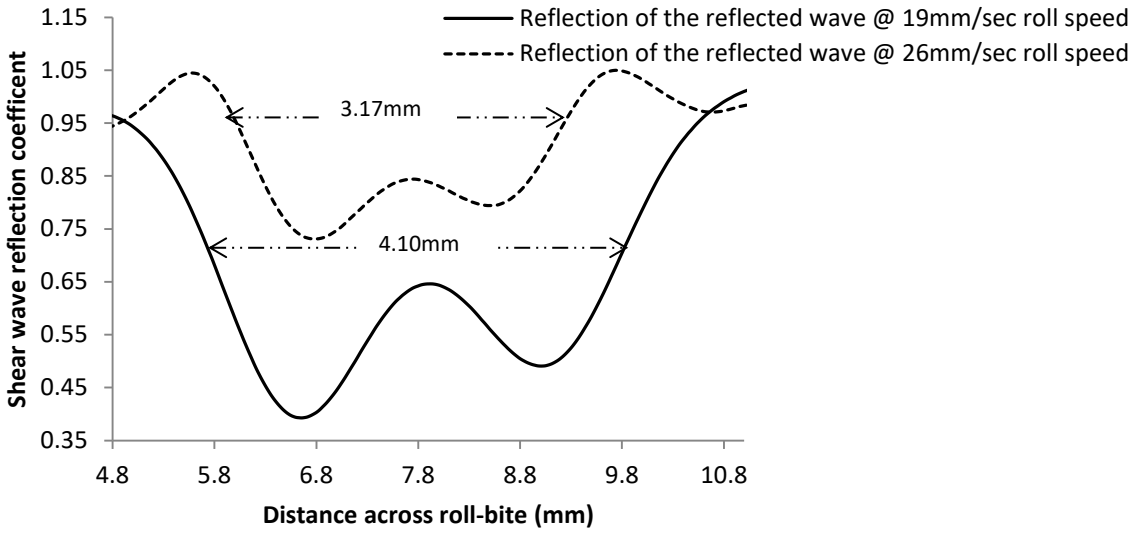

Figure 7-39: Reflection coefficient of the reflected wave along the roll-bite at 40kN rolling load

As shown in Figures 7-38 and 7-39, the length of the roll–bite was located in the middle of these figures as previously explained in Section 7.4.1.1. The length of the roll-bite obtained at 19mm/sec was larger than the length of the roll-bite achieved at the 26mm/Sec under the same rolling load. This was due to the reason explained above.

In addition, the normal and tangential stiffness values of the strip-to-roll interface were calculated with the same approach explained in Section 7.4.1.2. This was done for the reflected data obtained for both the 19mm/sec and 26mm/sec roll speeds under the same applied rolling load of 40kN and the obtained results are presented in Figures 7-40 and 7-41.

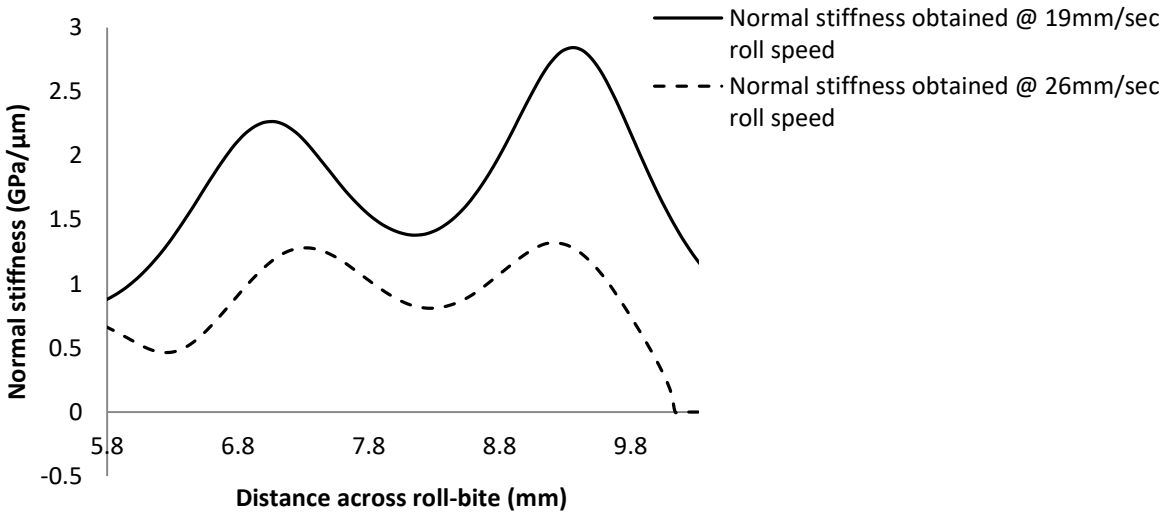

Figure 7-40: Normal stiffness of the reflected wave along the roll-bite at 40kN applied rolling load

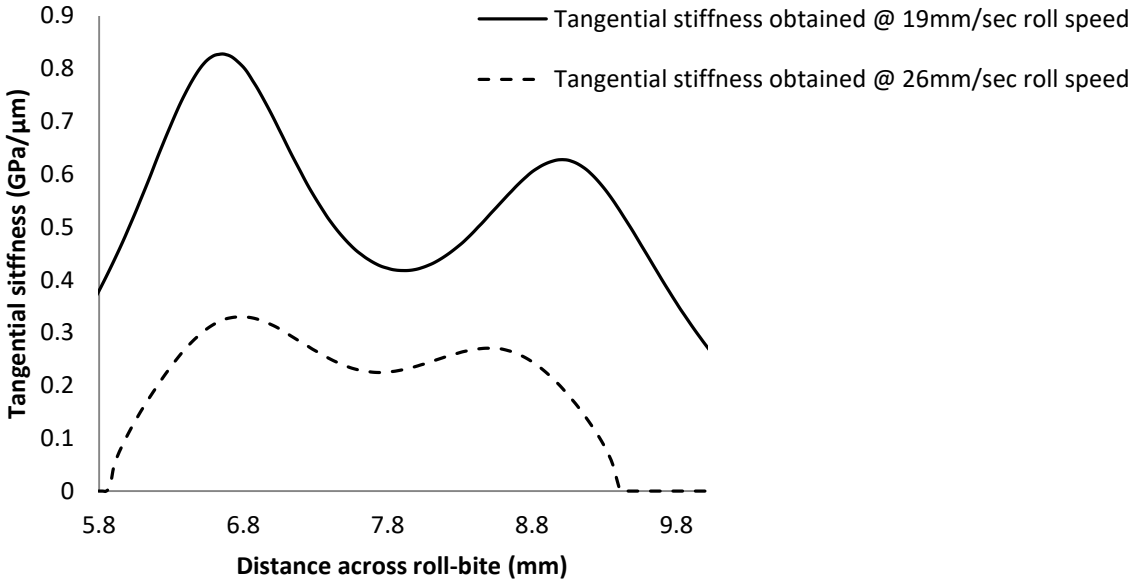

Figure 7-41: Tangential stiffness of the reflected wave along the roll-bite at 40kN applied rolling load

The values of both stiffness's obtained at the applied sensors under the same rolling load are reduced as the roll speed increased, due to the reason already explained above.

Finally, the oil film thickness formed at metal-to-roll interface was calculated with the same methods explained in Section 7.4.1.3, under various roll speeds and presented in Figure 7-42.

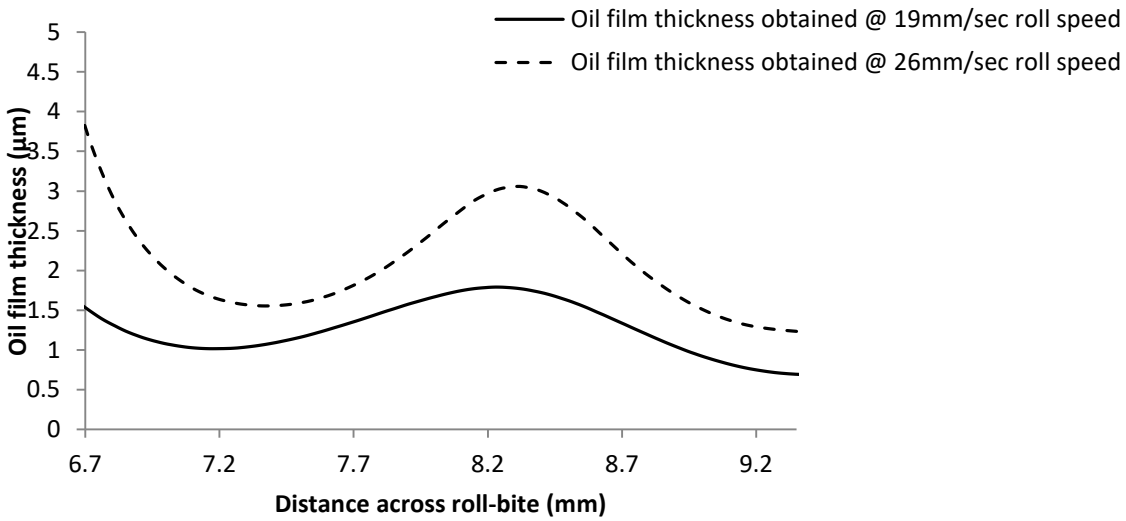

Figure 7-42: Oil film thickness obtained at roll-bite during the rolling process

The difference of the oil film thickness obtained from the roll speed applied during the metal rolling process is obvious as shown in the figure above due to the reason explained earlier. The higher the roll speed, the higher the oil film thickness obtained.

Finally, the theoretical oil film thickness was calculated with the same approach used in Section 7.4.1.3, and the obtained results were compared with the experimental value and are presented in Figure 7-43.

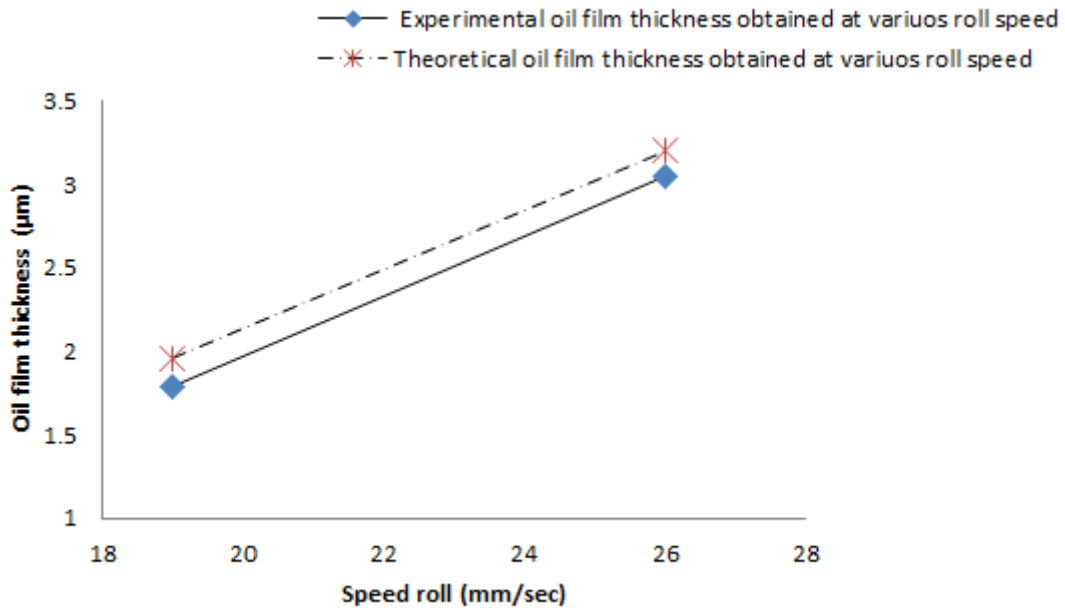

Figure 7-43: Theoretical and experimental oil film thickness obtained at 40kN rolling load

As can be seen from Figure 7-43, the oil film thickness obtained from both the theoretical and experimental values is of the same trend. That is, the value of oil thickness increases with the increase of the roll speed. Although, the theoretical oil thickness value obtained at lower speed was higher than the experimental value, due to the reason mentioned earlier in Section 7.4.1.3, but they both followed the same incremental trend of the subsequent increase in roll speed.

7.4.1.2 The 19mm/sec and 26 mm/Sec Roll Speed at 70kN Rolling Load

As explained in Section 7.4.3, the effect of 19mm/sec and 26mm/sec roll speeds on film thickness under the same 40 kN rolling load were studied. The results obtained from these conditions were analysed and presented in the above section. These loads were increased to

70kN under the 19mm/Sec and 26mm/sec roll speeds and their effect on the oil film thickness was studied in this section.

The behavioural trend of the increased amplitude was observed with 70kN applied rolling load, as compared to 40kN rolling load in Section 7.4.3.1. However, some level of marginal difference in their values occurred. In the 70kN rolling load the amplitude value of the reflected signal increases from 19mV to 23mV (Figures 7-44) and 26mV to 32mV (Figure 7-45) for longitudinal and shear wave sensors from the 19mm/sec to 26mm/sec roll speeds, while the amplitude value of the reflected signal increases from 17mV to 21mV and 25mv to 31mV for both longitudinal and shear wave sensors under same mentioned roll speeds of 40kN applied rolling load.

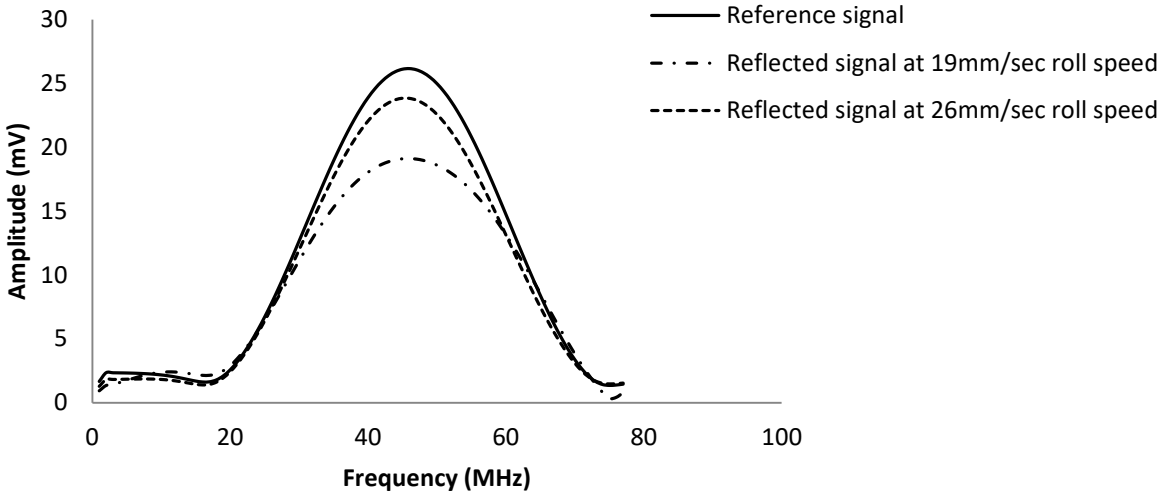

Figure 7-44: Amplitude of longitudinal reflected wave at 70kN applied rolling load

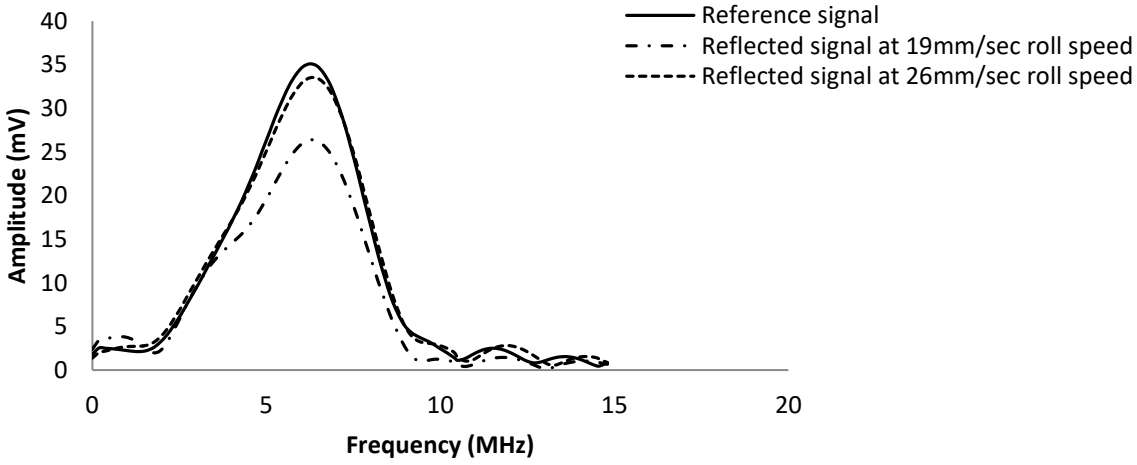

Figure 7-45: Amplitude of shear reflected wave at 70kN applied rolling load

The reflection coefficient of the wave reflected during the rolling processes was calculated for both applied sensors by the same method applied in section 7.4.1.1. The obtained values of the reflection coefficient from both sensor waves employed at the various roll speeds under the same rolling load were presented in Figures 7-46 and 7-47.

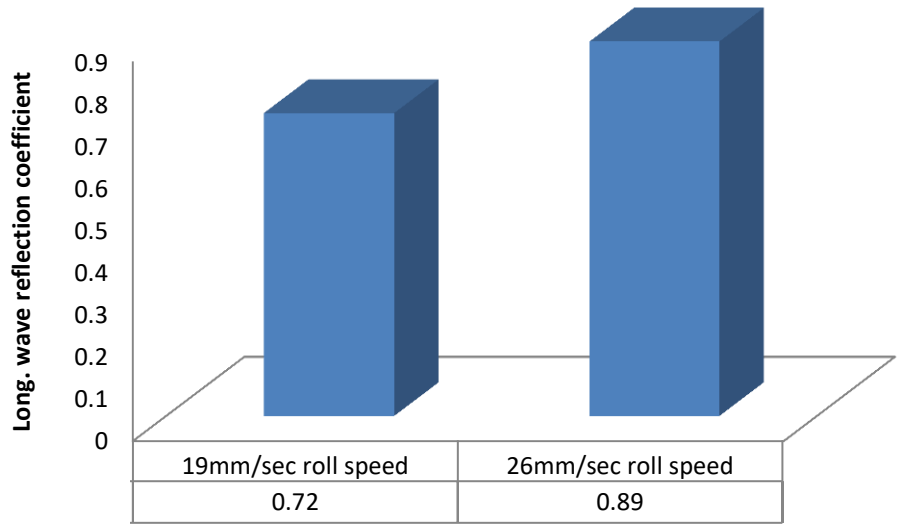

Figure 7-46: Reflection coefficients among the various roll speeds at 70kN rolling load

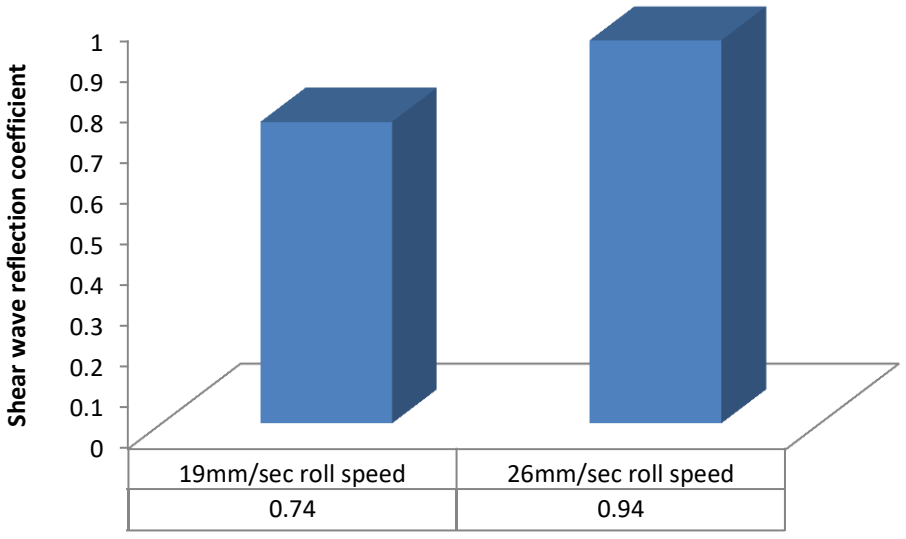

Figure 7-47: Reflection coefficients among the various roll speeds at 70kN rolling load

As indicated in the above figures, the values of the reflection coefficients of the waves were found to increase as the roll speed increased under the same rolling load.

Additionally, the various reflection coefficient value along the roll-bite were extracted with the aid of the LabVIEW program in terms of Time-of-Flight in the roll-to-metal interface for both roll speeds and the same rolling load applied. The obtained Time-of-Flight was used with the roll speed employed to determine the roll-bite length with the aid of the ToF ultrasonic formulae for both sensor waves employed and presented in Figures 7-48 and 7-49.

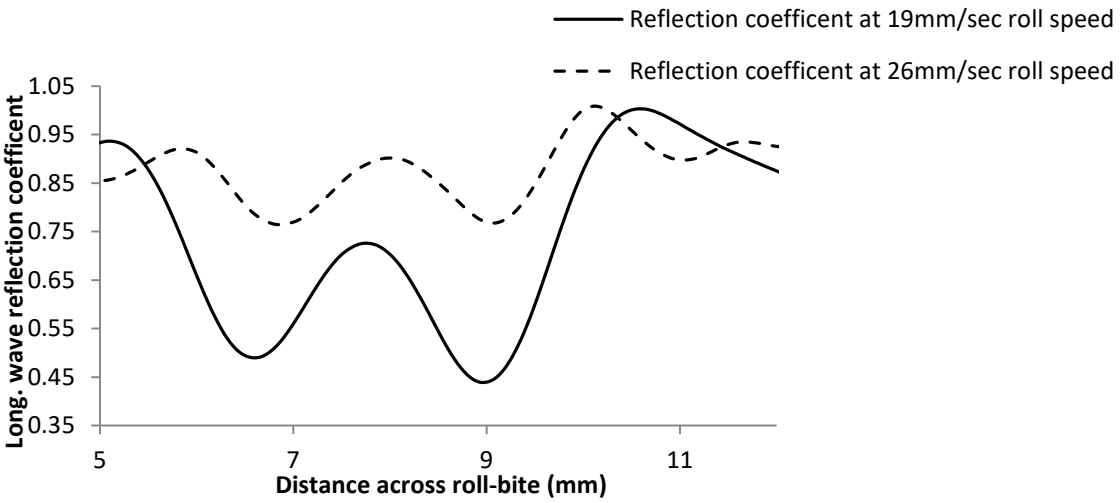

Figure 7-48: Reflection coefficients obtained along roll-bite at various roll speeds at 70kN load

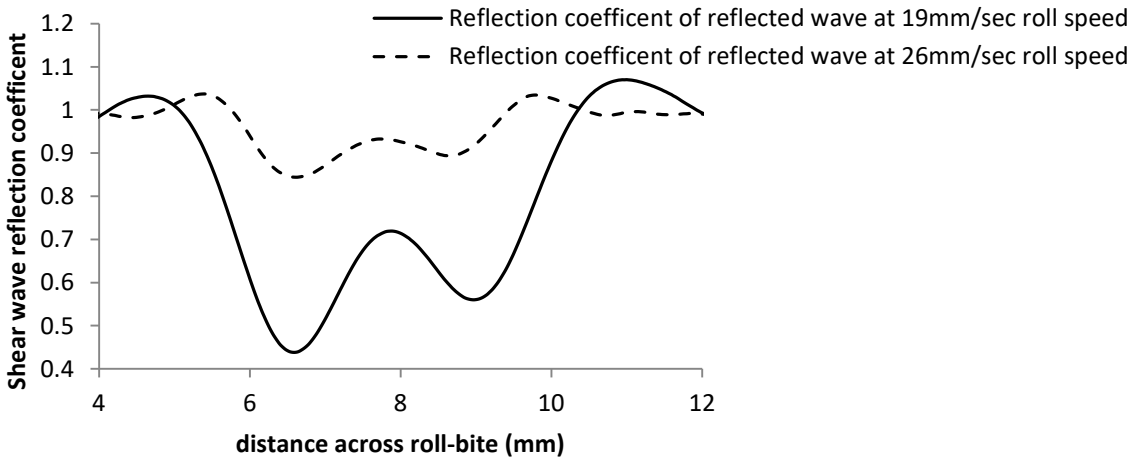

Figure 7-49: Reflection coefficients obtained along roll-bite at various roll speeds at 70kN load

As illustrated in the figures above, the higher the roll speed, the lesser the contact roll-bite length.

Furthermore, the values of the reflection coefficient obtained from the applied sensors were utilized with the other parameters explained in Section 7.4.1.2 to calculate the normal and tangential stiffness, and are in Figures 7-50 and 7-51.

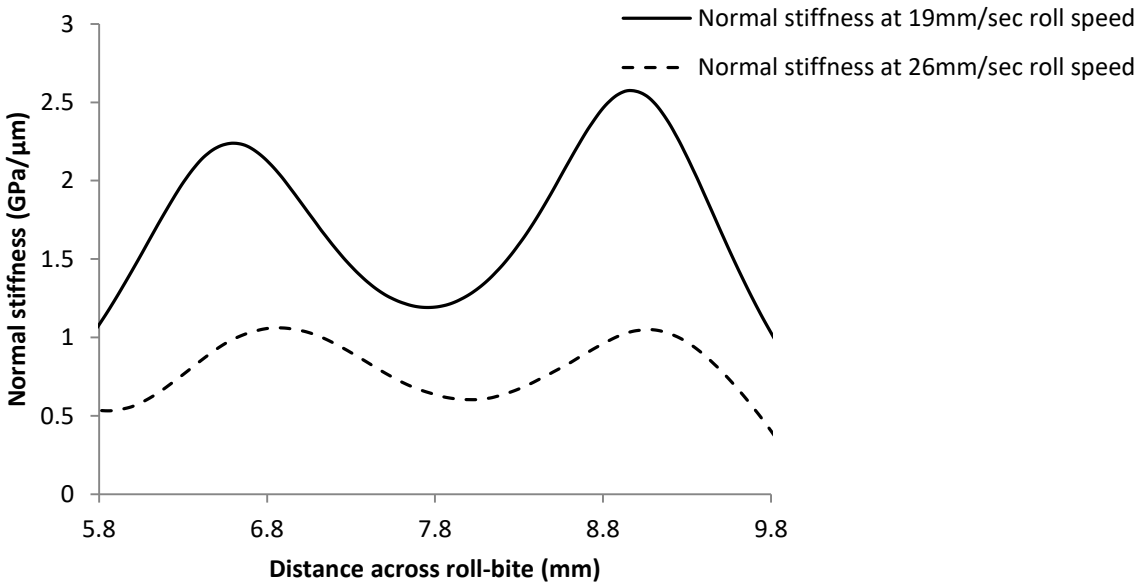

Figure 7-50: Stiffness obtained at the roll-bite, under the various roll speeds at 70kN load

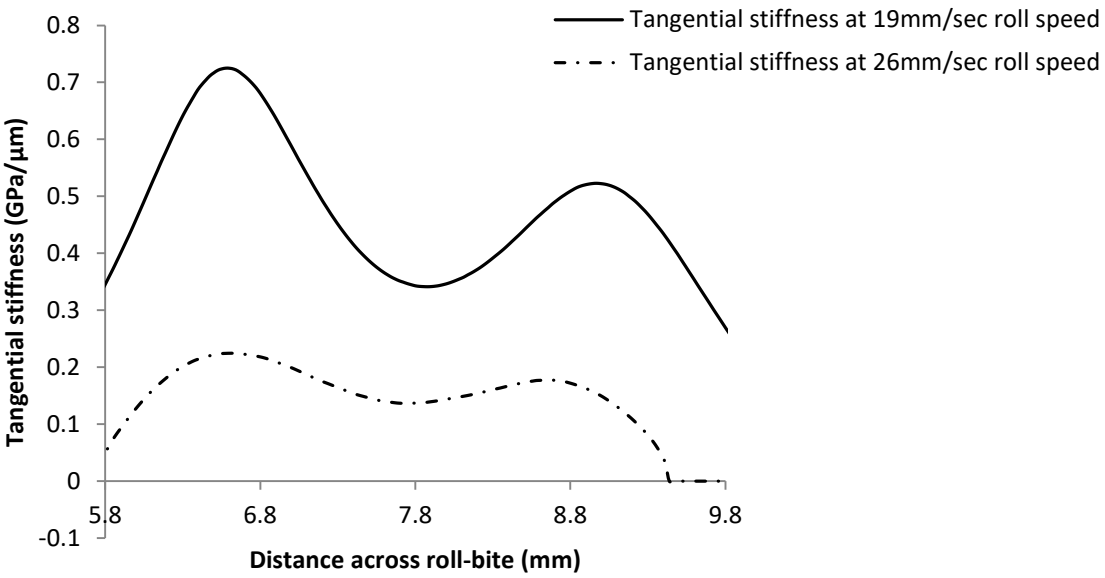

Figure 7-51: Stiffness obtained at the roll - bite, under the various roll speeds at 70kN load

As shown in the figures above, the values of both normal and tangential stiffness are reduced as the applied roll speed increased under the same 70kN of the rolling load.

The film that was obtained under the same applied rolling load with various roll speeds were calculated with the same procedure applied in Section 7.4.1.3. The oil film thickness values obtained from these various roll speeds are presented in Figure 7-52.

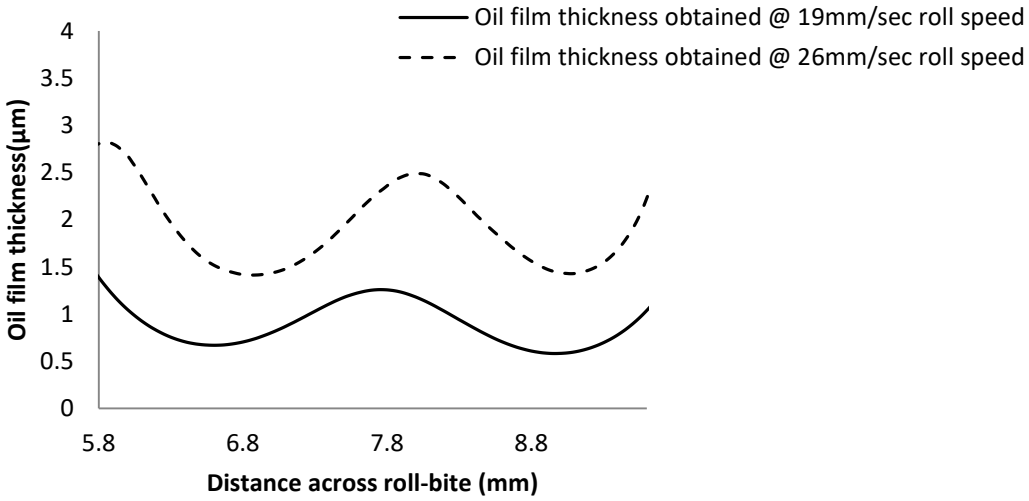

Figure 7-52: Oil film thickness at roll-bite during the various roll speeds at 70kN rolling load

The theoretical oil film thickness computation employed in Section 7.4.1.3 was used in this section and the theoretical results obtained were compared with the experimental values and presented in Figure 7-53.

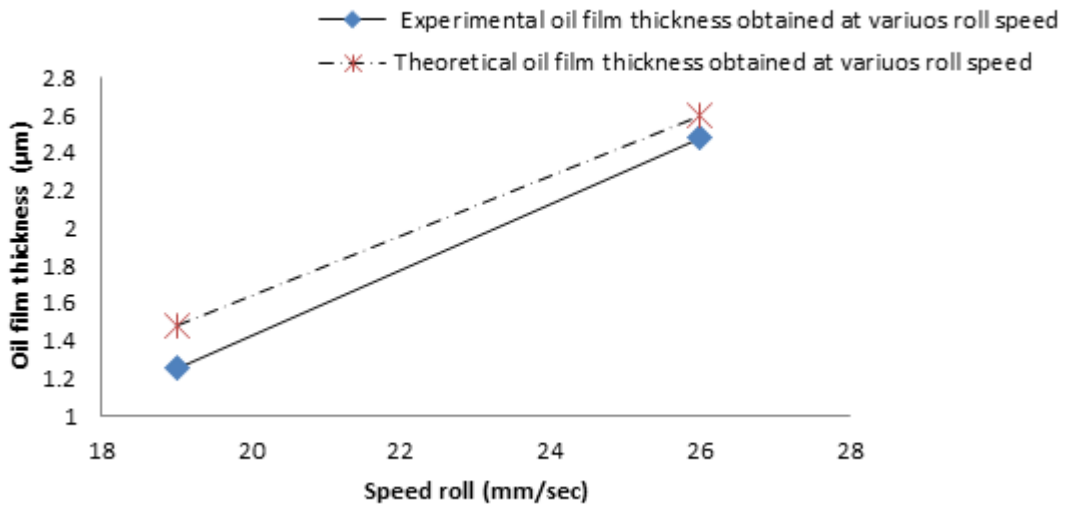

Figure 7-53: Experimental and theoretical oil film thickness obtained at various roll speeds under 70kN load

As it can be seen in the figure above, the experimental and the theoretical oil film thickness values have the same response to the increment of the roll speed under the same rolling load applied. The theoretical oil film thicknesses obtained were found at the higher values of the graph due to the reason explained in Section 7.4.1.3.

Finally, Figure 7-54, shows the combination of the obtained results from 19mm/sec and 26mm/sec under the rolling loads of 40kN and 70kN for the comparison of the acquired oil film thickness values.

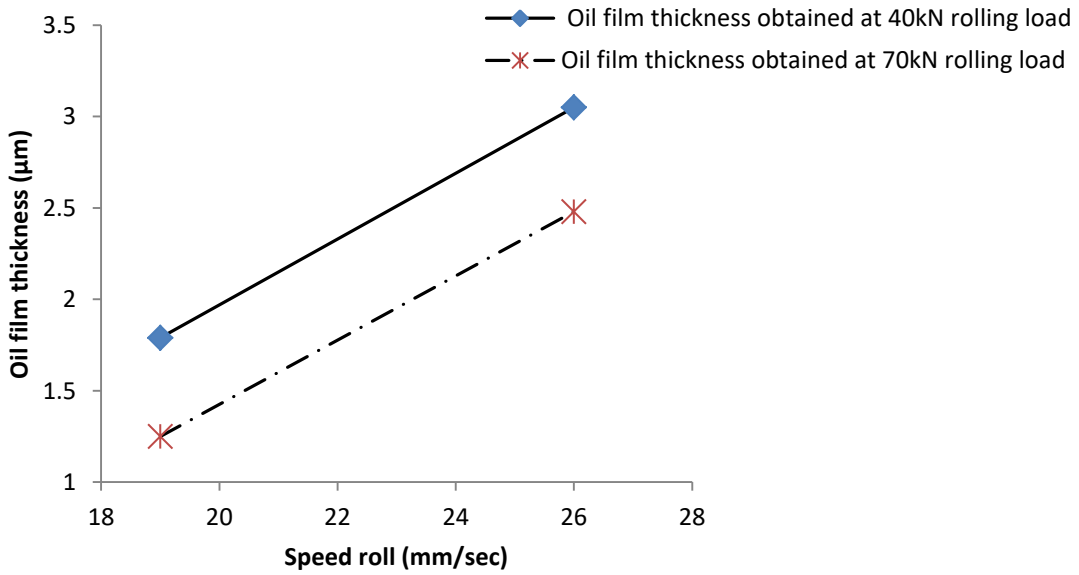

Figure 7-54: Experimental oil film thickness obtained at various roll speeds under 40kN and 70kNplied loads

It is clearly shown in Figure 7-54 that the oil film thickness obtained from the various applied roll speeds is different under the same rolling loads applied to them during the rolling process. As explained in the previously, an increase in roll speed permits more volume of lubricant oil to be drawn into the metal-to-roll interface. This causes a separation of the interface and causes the reduction of the contact length of the roll-bite. This leads to the increase in of the oil film thickness at the roll - bite. As it can be seen in the above figure, the higher the roll speed, the higher the thickness of the oil film on roll-bite.

Furthermore, as previously discussed in Section 7.4.1, low reflection coefficient means that high pressure was applied to the metal-to-roll interface. As the rolling load increases, the pressure on the metal-to-roll interface increases, while it decreases with increasing roll speed. This can be seen clearly from Figure 7-54 where at low rolling load, the pressure is

low and thus the lubricant penetrates more to the interface and results in high oil film thickness value. At high rolling load the lubricant has less chance to penetrate to the metal-to-roll interface due to the high pressure on their surfaces caused by the plastic and elastic deformation of the asperity contact. Thus a low value of the oil film thickness is recorded at the same roll speed due to the high rolling load involved. That explains the variation in the oil film thickness values obtained at the same roll speed under different applied rolling loads. The value of 3.05μm oil film thickness was obtained at 26mm/sec roll speed under the 40kN rolling load while 2.4μm was also obtained under the same roll speed but with 70kN rolling load. Therefore, both rolling load and roll speed have a significant effect on the formation of oil film thickness at the roll - bite during metal rolling operation.

7.5 Comparison with the literature

Dwyer-Joyce and Hunter [66] applied internal ultrasonic sensors fitted in the work roll to measure the oil film thickness formed between the roll and strip interface during the metal rolling operation. As discussed in their study, the experiment was conducted with Gerolub lubricating oil, which is also the lubricating oil employed for conducting the experiments in our research.

Table 7-3, includes the experimental rolling conditions and oil film thickness values obtained from theoretical calculations, from the proposed method developed in this research with experimental procedure explained in Section 7.2.3, as well as those obtained from Dwyer-Joyce and Hunter [66].

Table 7-3: Applied techniques with their rolling conditions observed

Techniques	Experimental Conditions	Oil film thickness (μm)
Hunter [66]	387mm roll diameter, 1666.7mm/s roll speed, 2.8mm strip thickness, 100mm strip width, 490mm strip length, 10% metal reduction, 0.77μm and 1.88μm roll and strip roughness value.	1.72
Pitch-catch	Shown in Table 7-1	2.07
Theory (Equation 2-29)	Shown in Tables 5-3 and 7-1	2.63

Dwyer-Joyce and Hunter [66] carried out the investigation with an industrial rolling mill and IF steel described in Section 5.4. for rolling conditions listed in Table 7-3. The variation of the experimental oil film thickness obtained along the roll-bite distance with the Dwyer-Joyce and Hunter [66] approach is shown in Figure 7-55.

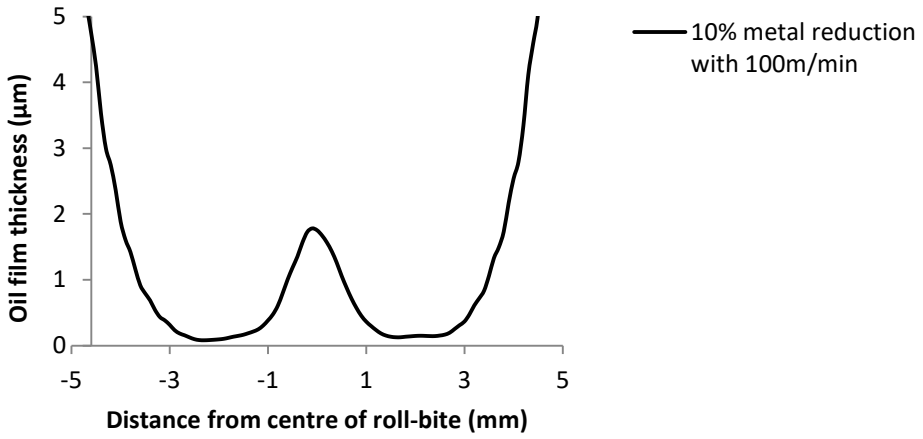

Figure 7-55: Oil film thickness obtained by the internal ultrasonic sensor layout arrangement [66]

As can be seen from Figure 7-55, the variation of the oil film thickness against distance across the roll-bite has the same trend as that obtained with the applied technique in this research shown in Figure 7-13. Both results show a clear double dip, despite the fact that there is a difference in the rolling parameter conditions involved. The comparison between the oil film thickness obtained from this research and the theoretical value is shown in Figure 7-20 of Section 7.4.1.4. The reasons for the differences are also discussed.

As can be seen from the comparison Table 7-3, there is a difference of 16% between the oil film thickness obtained from this research and the oil film value measured by Dwyer-Joyce and Hunter [66]. The differences observed between the two experimental results above are due to the variation in the rolling parameter conditions used during the investigation as shown in Table 7-3.

Furthermore, the higher value of oil film thickness obtained in this research may also have been due to the fact that a pilot mill which operated under lower rolling load was employed in this research; this contrasts with the industrial mill operated under higher rolling load used by Dwyer-Joyce and Hunter [66]. The higher the rolling load, the lower the oil film thickness obtained.

The results strongly imply the measurement reliability of the system: the oil film thickness obtained from both techniques only differed slightly; and both revealed similar double-dip shapes on the graphs. The external ultrasonic technique employed by this research is accurate enough with only a minor deviation in the oil film thickness obtained using the experimental approach when compared with the theoretical approach. It is, however, difficult to compare the accuracy of the oil film thickness values obtained in [66] with the values obtained in our research because of the difference in the rolling parameter conditions.

It can be concluded that the order of magnitude indicates that the oil film thickness obtained in this research work conforms to expectations from the literature. Additionally, the values of oil film thickness obtained are in the same range as those obtained with other experimental measurement techniques reviewed in the literature and shown in Table 2-5, Section 2.6.4. Finally, the experimental results obtained are in good agreement with the results obtained from the theoretical predictions shown in Figure 7-20.

Furthermore, when the film thickness values obtained for various ranges of applied loads and roll speeds were compared with the results obtained from the literature [65, 106], it can be observed that the film thickness was dependent on the sliding speed at the contact. This showed good agreement with the results obtained in the investigation reported in [65, 106], which studied the effect of load and roll speed on the formation of an oil film at metal-to-roll interface. In particular, as the roll speed increased, more oil was trapped by the work roll which then flowed into the interface space during the rotation of the work rolls. Because of this, the oil film thickness of the lubricating oil applied also increased at the metal-to-roll interface during the rolling process (Figure 7-54). Additionally, as the applied rolling loads increased, the film thickness obtained at the metal-to-roll interface decreased (Figure 7-31). Therefore, the comparison of the results obtained from this layout with the results obtained from the theoretical predictions as well as the those from the literature with different measurement techniques have shown that the proposed technique is indeed a promising measurement approach. As explained above, this external sensor layout configuration used in this research has shown that this arrangement does not result in markings on the rolled product surface under large contact pressure when compared with the existing techniques. As such, the experimental methodology is suitable for real-time measurements of oil film thickness in metal-to-roll interface in industrial mills.

7.6 Conclusion

This study was set up to measure the oil film thickness and monitor the effect of rolling parameters on the formation of oil film thickness at the metal-to-roll interface during the rolling process. The measurement was done with the aid of a novel oblique ultrasonic technique. As previously explained, the ultrasonic sensors were located on both sides of the roll at an angle to each other. The sound waves were allowed to propagate through the roll and reflected at metal-to-roll interface during the rolling process. The reflections of the waves were processed and used for the film thickness calculation during the rolling operation. This process of capturing the wave reflection was used to conduct experiments with different rolling conditions. The reflection coefficients of the reflected wave processed were recorded for further uses. The following deductions are drawn from the experiments conducted and reported in this chapter:

- This study has shown the ability to use the ultrasonic reflection to measure the oil film thickness at metal-to-roll interface during the metal rolling process;
- The results in this chapter indicate that the oil film thickness formation is varied under applied rolling loads;
- This study indicates that roll speeds have a significant effect on the formation of oil film thickness at metal-to-roll interface during the rolling process;
- The oil film measurement was carried out without any damage of the roll and strip surfaces;
- Good correlation between normal and oblique oil film thicknesses was obtained.

Chapter 8

Conclusions and Recommendations

8.0 Novelty of the Work

This study has clearly demonstrated the feasibility of using non-invasive sensors on rolling mills, not only for research purpose, but more importantly, the solution found can be reliably transferred to industry.

Although previous work showed that ultrasonic sensors could be embedded into a roll, there were clear limitations, which have been overcome in this work. Rolls only require minor modifications in areas not affecting the rolling process of the strip, especially the surface integrity of the rolled material. Holes drilled into the roll could also affect its integrity with fatigue cracks potentially developing over time. Collapse of the embedded plug is not a problem anymore, with sensors easily and securely mounted onto the roll.

The proposed solution makes use of a pitch-catch ultrasonic measurement technique, as opposed to a pulse-echo method, with a new experimental procedure which has been successfully developed and implemented. Results in terms of interface conditions (oil film thickness, roll bite length and strip thickness) measurements have been verified against theoretical predictions as well as with the pulse-echo technique (for oil film thickness) to demonstrate the robustness of the new procedure.

8.1 Development of External Sensor Arrangement

Metal forming is one of the backbones of many metal industrial developments. Metal forming plays a major part in the provision of employment and development of numerous steel companies that directly and indirectly depend on it. It is therefore pertinent that metal forming analytics and procedure receives attention from the research and development community. Metal rolling is one the major metal forming processes, is the process of reducing the metal thickness through the gap between the two adjacent rolls. This is due to the coefficient friction which develops between the rolls and metal surfaces. Several attempts by different scholars have been made to measure the coefficient of friction at the roll-bite. The excess of the friction experienced at the metal-to-roll interface has a significant

harmful side effect on both roll and rolling metal surfaces. It is also a problem if it is not high enough because the metal will be slippery at roll-bite during the rolling process. Therefore, for the purpose of surface cooling and controlling of the friction at the metal-to-roll interface a lubricant is introduced. The oil thickness of this interface is necessary to achieve the required friction.

8.1.1 Implementation of the Technique

The measurement of the oil film thickness at the metal-to-roll interface is needed to control the friction strength at the metal-to-roll interface and also to reduce the amount of energy wasted during the metal rolling process [18]. This has been a problem due to the harsh nature of cold rolling that makes implementing sensors in industrial applications difficult [5]. Additionally, the negative effect of roll modification on the potential of the rolling process makes instrumentation of cold rolling mills difficult.

In this research, two non-invasive methods, with no need to insert a sensor plug into the roll to measure the oil film and strip thickness at the metal-to-roll interface were developed and studied (Chapter 4). The two methods were based on the external arrangement of the longitudinal and shear wave sensors. In the first method, sensors were mounted on the sensor carrier before coupling with gel into the model roll and its signal transmission was based on the pulse-echo technique. The signals generated from the sensor were transmitted through the sensor carrier and model roll before reflecting from the back surface of the model roll and received by the same sensor. In the second method, the signal transmission process was based on the pitch-catch technique. The sensors were mounted on both sides of the roll at an angle to each other; one of the sensors acts as a pulser while the other one acts like a receiver. The signals generated from the pulser were transmitted through the model roll and reflected back from its surface before being captured by the receiver sensor on the other side of the model roll. The wave reflection obtained from both approaches was studied.

The first method with the sensor carrier was found to perform below expectations due to the interfaces between the sensor carrier and model roll before reaching the back of the model roll (Figure 4-3). In addition, the amplitude of the reflected signal was smaller than the amplitude of the noise obtained on the back surface of the 110mm roll model with the high value of the pressure applied during the signal transmission process (Figure 4-12). The

signal-to-noise ratio was less than 1:1 and the noise totally masked by the shear wave reflection. The technique is a highly attenuated process with high signal energy loss during the transmission operation. Furthermore, the rapid attenuation of the shear wave within the coupling gel at the sensor carrier to model roll interface is another challenge that affects the transmission of the shear waves throughout the sensor carrier to the model roll. Shear waves only propagate very well in an acoustic solid material, while it was not effectively propagated in a liquid or gas medium. Therefore, with the high 20kN pressure applied during this investigation, no reflected wave was received from the back surface of the employed roll model (Figure 4-17).

The second method, which is pitch-catch, was concluded to be the best transmission process technique because a high energy of the reflected signal was received at the back surface of the model roll with little or no pressure applied during the signal transmission (Figure 4-21). This resulted in a high signal-to-noise ratio achieved from both sensors applied through the layout configuration. The process is a less attenuated signal transmission operation. Additionally, in this technique the sensor was mounted directly on the model roll without any interface (Figure 4-18), which was easier for the shear wave to transmit through the roll model (Figure 4-22).

Finally, the oblique reflection technique was selected out of the two mentioned techniques due to the explanation given above. The technique was installed into the pilot roll mill and tested (Chapter 5). The Time-of-Flight of the reflected wave obtained through this technique, was used to determine the strip thickness in both stationary (Figure 5-9) and dynamic (Figure 5-16) modes. It also studied the effect of loads on the Time-of-flight of ultrasonic reflection at the back of the strip during the rolling operation (Figures 5-22 and 5-23). Finally, it was applied to measure the roll-bite length during the metal rolling process (Figure 5-32).

8.1.2 Analysis of the Oblique Reflection Technique

This technique was modelled and analysed with the aid of MatLab scripts written by Li [99] that were modified to suit the purpose of this project. The aim is to compare the reflection coefficients obtained from the ultrasonic signal sent at different incidence angles. The simulations were run for longitudinal waves at incidence angles of 0^{o} and 19^{o} for two different values of rolling loads.

The maximum reflection coefficient value of 0.9 was obtained from the embedded layer at 0^{o} angles of incidence (Figure 6-6). This is followed by reflection coefficient values of 0.82 obtained at 19^{o} angle incidences at the same 2.32μm and 1.27μm embedded thickness layers. Minor changes in the reflection coefficient values of 0.08 were clearly shown as the angle of the incidences as it increased from 0^{o} to 19^{o} respectively.

The experimental validation of this analysis was conducted by transmitting the incidence waves at 19^{o} with pitch-catch and pulse-echo (0^{o} of incidence angle) techniques in a dynamic mode. The investigations were conducted under 70kN and 90kN applied rolling load. The reflected wave of the sent signal at this condition was captured, processed and studied.

A little difference was observed between the reflection coefficient of the reflected signal and the stiffness values obtained from both techniques under the same applied loads respectively. The difference in the results obtained from both techniques is negligible, because they are small values. Due to this reason, pulse-echo mathematical computation approaches were employed to calculate the pitch-catch technique. Also, based on the outcome and the recommendation of a researcher that has already worked on similar research, the longitudinal reflection coefficients obtained at a 19^{o} angle of incidence wave are similar to those obtained at a normal incidence longitudinal wave [98].

8.1.3 Application of the Chosen Technique

Finally, this technique was applied during the cold metal rolling process to measure and study the effect of rolling parameters on the formation of oil film thickness at the metal-to-roll interface.

The followings are the main findings drawn:

- The thicknesses of the rolled strip were successfully measured with dynamic position. The three differences of the strip samples were rolled from the initial thickness of 5mm value in and 4.40mm, 4.04mm and 3.71mm experimental values while the obtained measured values are 4.52mm, 4.28mm and 3.80mm. The accuracy of the measured values of the three samples are; 2.7%, 5.9% and 1.39%, which shows a good agreement with standard measuring devices (Fig. 5-27).
- The technique was applied to the measurement of the roll-bite length during the metal rolling process. The value of the 5.59mm was experimentally obtained while

the computed value was 6.29mm. The accuracy of the obtained value compared with the mathematical prediction value is 12.5%, shows the validity of the technique for the measurement of the roll-bite during the metal rolling process (Fig. 5-33).

- It was apparent from the experimental results obtained that the angle of incidence has a minor effect on the stiffness's value obtained from both ultrasonic measurement techniques. These were in good agreement with that seen from scholars during their investigations.
- The difference in reflection coefficients obtained from the modelling of angles of incidence is more noticeable than the experimental value. The reasons for these differences were not clear.
- The oil film thicknesses at the metal-to-roll interface were successfully measured at the metal-to-roll interface during the metal rolling process. The value of 2.07μm was experimentally obtained while the theoretical value was 2.62μm, but with good correlation between normal and oblique oil film thickness (2.32μm) was obtained. Also, this result was about the same trend with the result obtained by Dwyer-Joyce and Hunter [66]. These points proved the accuracy of the technique for the measurement of oil film thickness.
- The effect of rolling loads on oil film thickness formation was also successfully studied with this technique and a positive reaction was obtained. Three different values of the rolling load values were employed during the investigation with the same roll speed. The oil film thickness value of 2.84μm was obtained at 40kN, which was reduced to 2.32μm at 70kN and finally reduced to 1.27μm at 90kN applied rolling loads respectively. The theoretical values of oil film obtained in these loads are: 3.2μm, 2.46μm and 1.36μm which are close to the experiments values. It proved the authentication of the ultrasonic oblique reflection coefficient as the best method to study the metal-to-roll interface conditions.
- The effects of roll speeds on the oil film thickness were also examined under the two various rolling loads during the metal rolling process. It was observed that the higher the roll speed, the higher the oil film thickness obtained. The value of oil film thickness obtained at 19mm/sec at 40kN was 1.79μm which increased to 3.05μm at 26mm/sec under the same roll load. Likewise, the 1.25 μm oil film obtained at 19mm/sec under 70kN rolling load was increased to 2.48μm at 26mm/sec roll speed. These oil film thicknesses that were obtained are close to the oil film thicknesses

obtained theoretically, which shows that the technique is suitable to study the roll speed effect on the oil film thickness formation.

8.2 Recommendations for Further Work

In this thesis, a non-invarse ultrasonic technique based on the reflection of ultrasound from the external ultrasonic sensor arrangement was developed for measuring at the metal-roll-interface during rolling conditions. The technique shows significant promise as an efficient method to study the metal-to-roll interface during the cold metal rolling process. The following further work set out in this section could be of help to improve and build more confidence in the present possibility of the new experimental layout.

- The outcomes of this study have shown a number of important implications for future practice in industry. The advantage of this research technique is that it provides some evidence of useful measurement parameters at the metal-to-roll interface during cold metal rolling. Therefore, it could be developed further by avoiding the mounting of the sensor direct on the roll to reduce the risk of roll modification. The water based coupling method can be applied; this will give room for continuous measurement during the rolling process. But this could only apply to longitudinal sensors for the measurement of strip thickness only.
- This technique was used to study the small roll diameter interface. This research should be developed further and implemented onto a larger roll and tested. This could be done whilst increasing the applied ultrasonic equipment voltage to avoid signal attenuation that might be caused due to the long part transmission of the signal.
- It was observed in the modelling section of the work that the frequency values have a significant effect on the value of the reflection coefficient at the angle of the incidence applied. Thus, a 2MHz and 3MHz sensor was recommended to be used, and their effect on the angle of incidence transmission signal studied. Drinkwater [97] explained that the reflection coefficient obtained from angle incidence of 0^{o} and 45^{o} are almost the same at 2MHz and 3MHz applied sensor.
- Further experimental investigation is needed by applying this technique to estimate the deflection of the roll during the rolling process.

- The study should be repeated using other external sensor, such as EMAT and laser ultrasound to investigate the metal-to-roll interface conditions during the rolling process.

References

[1] **Valiev, R. Z., Estrin, Y., Horita, Z., Langdon, T. G., Zechetbauer, M. J., & Zhu, Y. T.,** Producing bulk ultrafine-grained materials by severe plastic deformation. Journal of the Minerals, Metals and Materials Society, 2006; 58(4):33-39.

[2] **Schey, J.A.,** Metal deformation processes/friction and lubrication, I.L. Iit Research Inst Chicago, Editor 1970.

[3] **Morfeldt, J., W. Nijs, and S. Silveira,** The impact of climate targets on future steel production–an analysis based on a global energy system model. Journal of Cleaner Production, 2015;103:469-482.

[4] **Kleiner, M., M. Geiger, and A. Klaus.,** Manufacturing of light weight components by metal forming. CIRP Annals-Manufacturing Technology, 2003;52.(2): 521-542.

[5] **Liu, Y.,** Friction at strip-roll interface in cold rolling. Doctoral Thesis, University of Wollongong, 2002.

[6] **Le, H.R. and M.P.F. Sutcliffe,** Measurements of friction in strip drawing under thin film lubrication. Tribology International, 2002; 35(2):123-128.

[7] **Huart, S., Dubar, M., Deltombe, R., Dubois, A., & Dubar, L.,** Asperity deformation, lubricant trapping and iron fines formation mechanism in cold rolling processes. Wear, 2004; 257(5):471-480.

[8] **Dieter, G. E., and Bacon, D. J.,** Mechanical Metallurgy. Vol.3. New York: McGraw-Hill, 1986.

[9] **Pialucha, T.P.,** The Reflection Coefficient from Interface Layers in NDT of Adhesive Joints, Doctoral Thesis, University of London, 1992.

[10] **Roberts, W. L**. Cold rolling of steel. New York: McGraw Dekker, 1978.

[11] **Altan, T., S.-I. Oh, and G. Gegel**, Metal forming fundamentals and applications. American Society for Metals, 1983:353.

[12] **Liu, Y. J., Tieu, A. K., Wang, D. D., & Yuen, W. Y. D.** Friction measurement in cold rolling. Journal of Materials Processing Technology, 2001;111(1):142-145.

[13] **Beddoes, J. and M. Bibby,** Principles of metal manufacturing processes Butterworth-Heinemann, 1999.

[14] **Ďurovský, F., L. Zboray, and Ž. Ferková,** Computation of rolling stand parameters by genetic algorithm. Acta Polytechnica Hungarica, 2008;5(2):14.

[15] **Yun, I., W. Wilson, and K. Ehmann,** Review of chatter studies in cold rolling. International Journal of Machine Tools and Manufacture, 1998;38(12): 1499-1530.

[16] **Louaisil, K., Dubar, M., Deltombe, R., Dubois, A., & Dubar, L.,** Analysis of interface temperature, forward slip and lubricant influence on friction and wear in cold rolling. Wear, 2009;266(1):119-128.

[17] **Pietrzyk, M., Kusiak, J., Majta, J., Hartley, P., Lin, J., & Mori, K.** Proceedings of the 12th International Conference on Metal Forming Akademia Gorniczo-Hutnicza, Krakow, Poland.2008.

[18] **Le, H. R. and M.P.F. Sutcliffe,** The effect of surface deformation on lubrication and oxide-scale fracture in cold metal rolling. Metallurgical and Materials Transactions B, 2004;35(5):919-928.

[19] **Tieu, A.K. and Y.J. Liu,** Friction variation in the cold-rolling process. Tribology International, 2004;37(2):177-183.

[20] **Nilsson, M.,** Tribology in Metal Working, Doctoral Thesis, Uppsala University, 2012.

[21] **Atkins, A.G.,** Hydrodynamic lubrication in cold rolling. International Journal of Mechanical Sciences, 1974;16(1):1-19.

[22] **Šamánek, O., M. Zimmerman, P. Svoboda, & Vrbka, M.,** Influence of surface texturing on lubricant film formation and surface fatigue. Engineering Mechanics, 2010;17(1):27-36.

[23] **Stephenson, D.A.,** Friction in cold strip rolling. Wear, 1983;92(2):293-311.

[24] **Henningsen, P., M. Arentoft, and J. Jeswiet,** Methods and Devices Used to Measure Friction in Rolling. Proceedings of the Institution of Mechanical Engineers, Part B: Journal of Engineering Manufacture, 2006;220(1):49-57.

[25] **Lenard, J. and L. Lai-Seng,** Study of friction in cold strip rolling. Journal of Engineering Materials and Technology, 1984;106:139-146.

[26] **Siebel, E. and W. Lueg,** Investigations into the distribution of pressure at the surface of the Materials in contact with the Rolls. Mitt. K. W. 1933;15:1-14.

[27] **Van Rooyen, G.T. and Backofen, W.A.,** Friction in cold rolling. Journal of the iron and steel Institue, 1957;186:235-244.

[28] **Lenard, J. G., Altan, B., Bay, D., Geiger, K., Kopp, L., Schey, S., & Shaw, S,** Tribology in metal rolling keynote presentation forming group F. CIRP Annals-Manufacturing Technology, 2000;49(2):567-590.

[29] **MacGregor, C. and R. Palm,** Contact Stresses in the Rolling Metals. Journal of Applied Mechanics-Transactions of the ASME 1948;15(3):297-302.

[30] **Wilson, W.R., H.G. Malkani, and P.K. Saha,** Boundary friction measurements using a new sheet metal forming simulator. Proc. NAMRC XIX, 1991:37-42.

[31] **Jeswiet, J., P. Wild, and H. Sefton,** A friction sensor for a sheet metal forming simulator. Transactions-North American Manufacturing Research Institution of SME, 2001:29-34.

[32] **Moore, T., M. Shalaby, and J. Jeswiet,** An Embedded Friction Sensor Based on a Strain-Gauged Diaphragm. Journal of Manufacturing Science and Engineering.2002; 124:523-527.

[33] **Yajure, E.,**. Master's Thesis, Queen's University, Kingston, Ontario, Canada, 2002.

[34] **Henningsen, P., M. Arentoft, and T. Wanheim,** Measurements of normal and frictional forces in a rolling process. Proceedings of the Institution of Mechanical Engineers, Part B: Journal of Engineering Manufacture, 2006. 220(1): p. 59-64.

[35] **Xie, H. B., K. Manabe, and Z. Y. Jiang.** A Novel Approach to Investigate Surface Roughness Evolution in Asymmetric Rolling Based on Three Dimensional Real Surface. Finite Elements in Analysis and Design, 2013;74:1-8.

[36] **Shalaby, M.,** Novel Friction Sensors for Bulk and Sheet Metal Forming. Library and Archives Canada Bibliothèque et Archives Canada. 2005.

[37] **Fudanoki, F., Araki, J., Inoue, S., & Yanai, K.,** Development of model for formation of surface properties in cold rolling of stainless steels and application to the actual mill. Nippon Steel Technical Report, 2010.

[38] **Dick, K. and J.G. Lenard,** The effect of roll roughness and lubricant viscosity on the loads on the mill during cold rolling of steel strips. Journal of Materials Processing Technology, 2005;168(1):16-24.

[39] **Hružík, L., Vašina, M., & Bureček, A.,** Evaluation of bulk modulus of oil system with hydraulic line. In EPJ Web of Conferences. 2013;45:01041.

[40] **Azushima, A., S. Inagaki, and H. Ohta,** Plating Out Oil Film Thickness on Roll and Workpiece During Cold Rolling with O/W Emulsion. Tribology Transactions, 2011;54(2):275-281.

[41] **Button, S. T.,** Numerical and experimental analysis of lubrication in strip cold rolling. Journal of the Brazilian Society of Mechanical Sciences and Engineering, 2011;33(2):189-196.

[42] **Lin, H.-S., N. Marsault, and W.R.D. Wilson**, A Mixed Lubrication Model for Cold Strip Rolling—-Part I: Theoretical. Tribology Transactions, 1998;41(3):317-326.

[43] **Merritt, H.E.,** Hydraulic control systems. John Wiley & Sons. 1967

[44] **Dwyer-Joyce, R.S., B.W. Drinkwater, and Donohoe, C.J.,** The measurement of lubricant-film thickness using ultrasound. Proceedings of the Royal Society A: Mathematical, Physical and Engineering Sciences, 2003;459(2032):957-976.

[45] **Hamrock, B.J. and Anderson, W.J.** NASA Reference Publication 1105. Rolling-element bearings, 1983.

[46] **Cho, B.-H., H.-W. Lee, and J.-S. Oh,** Estimation technique of air content in automatic transmission fluid by measuring effective bulk modulus. Int. J. Automot. Technol, 2002;3(2):57-61.

[47] **Gholizadeh, H.,** Modeling and experimental evaluation of the effective bulk modulus for a mixture of hydraulic oil and air, Doctoral Thesis, University of Saskatchewan 2013.

[48] **Hayward, A.,** How to measure the isothermal compressibility of liquids accurately. Journal of Physics D: Applied Physics, 1971;4(7):938.

[49] **Wilson, D. and C. Bolze,** Isothermal Bulk Modulus of Selected Fluids to 700 F and 10,000 psig. Journal of Basic Engineering, 1964:463-467.

[50] **Wilson, W. and L. Murch,** Refined Model for the Hydrodynamic Lubrication of Strip Rolling. J. Lubric. Technol.(Trans. ASME, F), 1976;98(3):426-432.

[51] **Fleck, N. and K. Johnson,** Towards a new theory of cold rolling thin foil. International Journal of Mechanical Sciences, 1987;29(7):507-524.

[52] **Jiang, Z., A. Tieu, and X. Zhang,** Finite element modelling of mixed film lubrication in cold strip rolling. Journal of Materials Processing Technology, 2004;151(1):242-247.

[53] **Montmitonnet, P.,** Hot and cold strip rolling processes. Computer methods in applied mechanics and engineering, 2006;195(48):6604-6625.

[54] **Button, S.T.,** Numerical and experimental analysis of lubrication in strip cold rolling. Journal of the Brazilian Society of Mechanical Sciences and Engineering, 2011;33(2):189-196.

[55] **Sutcliffe, M. P. F., & Johnson, K. L.,** Lubrication in cold strip rolling in the 'mixed'regime. Proceedings of the Institution of Mechanical Engineers, Part B: Journal of Engineering Manufacture, 1990;204(4):249-261.

[56] **Sutcliffe, M P. F.,** Experimental measurements of lubricant film thickness in cold strip rolling. Proceedings of the Institution of Mechanical Engineers, Part B: Journal of Engineering Manufacture, 1990;204(4):263-273.

[57] **Cuperus, R., W. ten Napel, W. Neumann, and Smits, R. P. J. M.,** Measurements of Film Thickness and Friction in Cold Rolling. Tribology at Work: Proceedings of the 5th International Tribology Conference in Australia, Brisbane 6-9 December 1998.

[58] **Saniei, M. and M. Salimi,** Development of a mixed film lubrication model in cold rolling. Journal of Materials Processing Technology, 2006;177(1):575-581.

[59] **Wilson, W. and Walowit J.,** An isothermal hydrodynamic lubrication theory for strip rolling with front and back tension. In Tribology Convention. 1971:169-172.

[60] **Lenard, J. G.** Metal Forming Science and Practice: A State-of-the-Art Volume in Honour of Professor JA Schey's 80th Birthday. Elsevier, 2002.

[61] **Lenard, J.G.,** Primer on flat rolling. Newnes, 2013.

[62] **Whetzel, J. C., & Rodman, S.** Improved lubrication in cold strip rolling. Iron Steel Eng, 1959; 36:123-132.

[63] **Katayama, Y.,** Status of Research on Refining, Analysis, Testing and Products. Bulletin of The Japan Petroleum Institute, 1967;9:122-128.

[64] **Azushima, A.,** Determination of oil film thickness in rolling from the relationship Between Surface Roughness of Strip and Roll: Investigation into Friction and Lubrication in Cold Rolling. Bulletin of JSME, 1978;21(159):1402-1407.

[65] **Azushima, A. and S. Inagaki,** Measurement and analysis of inlet oil film thickness in cold sheet rolling with oil-in-water emulsion. Tribology Transactions, 2009;52(4): 427-434.

[66] **Dwyer-Joyce, R. S., and A. K. Hunter.,** A novel sensor for lubrication and contact measurement in metal rolling. In 5th World Tribology Congress, WTC *2013*, vol. 4, pp. 3048-3051.

[67] **Rose, J.L.,** Ultrasonic waves in solid media. Cambridge university press, 2004.

[68] **Blitz, J. and G. Simpson,** Ultrasonic methods of non-destructive testing. Vol. 2, Springer Science & Business Media, 1995.

[69] **Gasni D.,** Ultrasonic Reflection for Measurement of Oil Film Thickness and Contact between Dissimilar Material. Doctoral Thesis, University of Sheffield, 2012.

[70] **Miclea C., Tanasoiu C., Amarande L., Miclea C., Plavitu C., Cioangher M., Trupina L., and David C**., Effect of Temperature on the Main Piezoelectric Parameters of a Soft PZT Ceramic, Romanian Journal of Information Science and Technology, 2007, vol. 10, pp. 243-50.

[71] **Park J. and Mackay S.**, Practical data acquisition for instrumentation and control systems: Newnes, 2003.

[72] **Krautkrämer, J. and H. Krautkrämer**, Ultrasonic testing of materials: Springer-Verlag (4th Edition), 1990.

[73] **Schmerr Jr, L.W.,** Fundamentals of ultrasonic nondestructive evaluation: a modeling approach. Springer Science & Business Media, 2013.

[74] **Mills, R.,** Ultrasonic measurement of lubricant films generated at the piston-cylinder interface of internal combustion engines. Doctoral Thesis, university of Sheffield. 2012.

[75] **Zhang, J., B.W. Drinkwater, and R.S. Dwyer-Joyce,** Ultrasonic oil-film thickness measurement: An angular spectrum approach to assess performance limits. The Journal of the Acoustical Society of America, 2007;121(5):2612.

[76] **Yao, C. and C. Wu,** A study of contact interface and wear diagnosis for hand taps using ultrasonic method. Applied Acoustics, 2014;85:46-56.

[77] **Cheeke, J.D.N.**, Fundamentals and applications of ultrasonic waves. CRC press, 2012.

[78] **Allegra, J. and S. Hawley,** Attenuation of sound in suspensions and emulsions: theory and experiments. The Journal of the Acoustical Society of America, 1972;51(5B):1545-1564.

[79] **Adler, L., Rokhlin, S. I., Mattei, C., Blaho, G., & Xie, Q.,** Angle Beam Ultrasonic Spectroscopy System for Quantitative Inspection of Adhesive Bonds, in Review of Progress in Quantitative Nondestructive Evaluation, Springer. 1999:1553-1559.

[80] **Geng, T., Meng, Q., Chen, Z. & Wang, P.,** Ultrasonic monitoring of lubricating conditions of hydrodynamic bearing. in Journal of Physics: Conference Series. 2011.

[81] **Kendall, K. and D. Tabor.** An ultrasonic study of the area of contact between stationary and sliding surfaces. in Proceedings of the Royal Society of London A: Mathematical, Physical and Engineering Sciences. The Royal Society, 1971.

[82] **Vail, J. R., Mills, R. S., Stephen, J. T., Marshall, M. B., & Dwyer-Joyce, R. S.,** An ultrasonic method for measuring fluid penetration rate into threaded contacts. Tribology International, 2013;67:21-26.

[83] **Kasolang, S., Ahmed, D. I., Dwyer-Joyce, R. S., & Yousif, B. F.,** Performance analysis of journal bearings using ultrasonic reflection. Tribology International, 2013;64(0):78-84.

[84] **Dwyer-Joyce, R.S., B.W. Drinkwater, and A.M. Quinn,** The Use of Ultrasound in the Investigation of Rough Surface Interfaces. Journal of Tribology, 20011;123(1):8.

[85] **Dwyer-Joyce, R., T. Reddyhoff, and J. Zhu**, Ultrasonic measurement for film thickness and solid contact in elastohydrodynamic lubrication. Journal of Tribology, 2011;133(3):031501.

[86] **Dwyer-Joyce, R.S., T. Reddyhoff, and B.W. Drinkwater,** Operating Limits for Acoustic Measurement of Rolling Bearing Oil Film Thickness. Tribology Transactions, 2004;47(3):366-375.

[87] **Ginzel E**., Beam Width Analysis, NDT. net, vol. Vol.6 No 9, 2001.

[88] **OLYMPUS**, Ultrasonic Transducers Technical Notes, 2006.

[89] **Okamoto S., Toyama M., And Inoue T.**, Effects of Carbon Content, Rolling Condition and Cooling Rate on the Mechanical Properties of As-rolled High-strength Low Alloy Steel, Transactions of the Iron and Steel Institute of Japan, 1987, vol. 27, pp. 474-477,.

[90] **Carretta, Y., Hunter, A., Boman, R., Ponthot J.-P., Legrand, N., Laugier M., and. Dwyer-Joyce R. S**., Ultrasonic roll bite measurements in cold rolling–Roll stress and deformation, Journal of Materials Processing Technology, 2017.

[91] **Howard, T. P.,** Development of a Novel Bearing Concept for Improved Wind Turbine Gearbox Reliability, Doctoral Thesis, University of Sheffield, 2016.

[92] **Carretta, Y., Hunter, A., Boman, R., Ponthot J.-P., Legrand, N., Laugier M., and. Dwyer-Joyce R. S**., Ultrasonic roll bite measurements in cold rolling: Contact length and strip thickness, Proceeding of the Institution of Mechanical Engineers, Part: Journal of Engineering Tribology, p. 1350650117712314, 2017.

[93] **Pilarski, A. and J. Rose,** Ultrasonic oblique incidence for improved sensitivity in interface weakness determination. NDT International, 1988;21(4):241-246.

[94] **Pilarski, A., J. Rose, and K. Balasubramaniam.** The angular and frequency characteristics of reflectivity from a solid layer embedded between two solids with imperfect boundary conditions. The Journal of the Acoustical Society of America 1990;87(2):532-542.

[95] **Pialucha, T., M. Lowe, and P. Cawley,** Validity of different models of interfaces in adhesion and diffusion bonded joints, in Review of Progress in Quantitative Nondestructive Evaluation. Springer. 1993:1547-1554.

[96] **Lowe, M.J.,** Matrix techniques for modeling ultrasonic waves in multilayered media. IEEE transactions on ultrasonics, ferroelectrics, and frequency control, 1995;42(4):525-542.

[97] **Liaptsis, D., B.W. Drinkwater, and R. Thomas,** The interaction of oblique incidence ultrasound with rough, partially contacting interfaces. Nondestructive Testing and Evaluation, 2006;21(3-4):109-121.

[98] **Nam, T., Lee, T., Kim, C., Jhang, K. Y., & Kim, N.,** Harmonic generation of an obliquely incident ultrasonic wave in solid–solid contact interfaces. Ultrasonics, 2012;52(6):778-783.

[99] **LI, X.,** Development of an Ultrasonic Method to Measure Viscosity in a Bearing Contact. Master's Thesis, Imperial College London, 2013.

[100] **Sharma, K. and R.R. Bhargava,** Propagation of thermoelastic plane waves at an imperfect boundary of thermal conducting viscous liquid/generalized thermoelastic solid. Afrika Matematika, 2014:1-22.

[101] **Rokhlin, S. and D. Marom,** Study of adhesive bonds using low‐frequency obliquely incident ultrasonic waves. The Journal of the Acoustical Society of America, 1986;80(2):585-590.

[102] **Rokhlin, S. and Y. Wang,** Analysis of boundary conditions for elastic wave interaction with an interface between two solids. The Journal of the Acoustical Society of America, 1991;89(2):503-515.

[103] **Chen, J., H. Chen, and E. Pan,** Reflection and transmission coefficients of plane waves in magnetoelectroelastic layered structures. Journal of Vibration and Acoustics, 2008;130(3):031002.

[104] **Thomas, R., B.W. Drinkwater, and D. Liaptsis,** The reflection of ultrasound from partially contacting rough surfaces. The Journal of the Acoustical Society of America, 2005;117(2):638-645.

[105] **Lenard, J.G.,** Tribology in Metal Rolling Keynote Presentation Forming Group F. CIRP Annals - Manufacturing Technology, 2000. 49(2): p. 567-590.

[106] **Thompson, P. M., Jones Jr, W. R., Jansen, M. J., & Prahl, J. M.,** The effect of sliding speed on film thickness and pressure supporting ability of a point contact under zero entrainment velocity conditions. 2000.

APPENDIX 1

MATLAB scripts Adopted to investigate and display the effect of wave incidence angle on the reflection coefficient at an interface .

```
% solid-layer-solid with Global Matrix Technique -- XL
% matrix from Palucha' PhD paper
% layer 1 steel, layer 2 viscous fluid, layer 3 steel
% longitudinal incident waves at angle

clear all

% layer thickness
h = 2.32e-6; % m

% layer 1 properties
% steel
cl1=5900; % m/s
cs1=3235;   % m/s
d1=8700;    % kg/m3
alpha1=cl1;
beta1=cs1;

% layer 2 properties
% honey
d2=870.1;% kg/m3
K2=1.5e9;  %Pa (bulk of modulus
eta2=70.0;   %Pas (viscosity)

% layer 3 properties
% steel
cl3=5900;
cs3=3235;
d3=8700;
alpha3=cl3;
beta3=cs3;

f = 0.1:0.1:10;
angle = 0:1:30;
[X,Y] = meshgrid(f, angle);
fTemp = X(:);
angleTemp = Y(:);

% Z = X .* exp(-X.^2 - Y.^2);
% surf(X,Y,Z)

count=1;

for i=1:length(fTemp); % MHz

    f = fTemp(i);
    angleDeg = angleTemp(i);

    omega=2*pi*f*10^6;

    cl2=(K2/d2)^0.5;
    kappal2=(4*pi*omega*eta2)/(3*K2);
    alpha2=cl2/(1+1i*kappal2/(2*pi)); %complex longitudinal velocity
    cs2=(2* omega*eta2/d2)^0.5;
    kappas2=2*pi;
```

```
    beta2=cs2/(1+1i*kappas2/(2*pi)); %complex shear velocity

    %angleDeg = 10;
    aIL=angleDeg*pi/180;
    sinIL = sin(aIL);

    s = aIL/alpha1; % snell constant

    % layer 1 matrix element
    x21=108; % coordinate in layer 1
    A1 =(1-alpha1^2*s^2)^0.5;
    B1 = (1-beta1^2*s^2)^0.5;
    C1 = 1-2*beta1^2*s^2;
    gl1 = exp((1i*omega*A1*x21)/alpha1);
    gs1 = exp((1i*omega*B1*x21)/beta1);

    % layer 2 matrix elment
    x22=h;
    A2 =(1-alpha2^2*s^2)^0.5;
    B2 = (1-beta2^2*s^2)^0.5;
    C2 = 1-2*beta2^2*s^2;
    gl2 = exp((1i*omega*A2*x22)/alpha2);
    gs2 = exp((1i*omega*B2*x22)/beta2);

    % layer 3 matrix element
    x23=108; % coordinate in layer 1
    A3 =(1-alpha3^2*s^2)^0.5;
    B3 = (1-beta3^2*s^2)^0.5;
    C3 = 1-2*beta3^2*s^2;
    gl3 = exp((1i*omega*A3*x23)/alpha3);
    gs3 = exp((1i*omega*B3*x23)/beta3);

    % Matrix M1 bottom
    M1b=[1i*omega*d1*alpha1*C1,2i*omega*d1*s*beta1^2*B1,
1i*omega*d1*alpha1*C1*gl1, -2i*omega*d1*s*beta1^2*B1*gs1;
        -2i*omega*d1*s*beta1^2*A1,
1i*omega*d1*beta1*C1,2i*omega*d1*s*beta1^2*A1*gl1,
1i*omega*d1*beta1*C1*gs1;
        alpha1*s, -B1, alpha1*s*gl1, B1*gs1;
        -A1, -beta1*s, A1*gl1, -beta1*s*gs1];

    % Matrix M2 top
    M2t=[1i*omega*d2*alpha2*C2*gl2,2i*omega*d2*s*beta2^2*B2*gs2,
1i*omega*d2*alpha2*C2, -2i*omega*d2*s*beta2^2*B2;
        -2i*omega*d2*s*beta2^2*A2*gl2,
1i*omega*d2*beta2*C2*gs2,2i*omega*d2*s*beta2^2*A2, 1i*omega*d2*beta2*C2;
        alpha2*s*gl2, -B2*gs2, alpha2*s, B2;
        -A2*gl2, -beta2*s*gs2, A2, -beta2*s];

    % Matrix M2 bottom
    M2b=[1i*omega*d2*alpha2*C2,2i*omega*d2*s*beta2^2*B2,
1i*omega*d2*alpha2*C2*gl2, -2i*omega*d2*s*beta2^2*B2*gs2;
        -2i*omega*d2*s*beta2^2*A2,
1i*omega*d2*beta2*C2,2i*omega*d2*s*beta2^2*A2*gl2,
1i*omega*d2*beta2*C2*gs2;
        alpha2*s, -B2, alpha2*s*gl2, B2*gs2;
        -A2, -beta2*s, A2*gl2, -beta2*s*gs2];

    % Matrix M3 top
    M3t=[1i*omega*d3*alpha3*C3*gl3,2i*omega*d3*s*beta3^2*B3*gs3,
1i*omega*d3*alpha3*C3, -2i*omega*d3*s*beta3^2*B3;
```

```
        -2i*omega*d3*s*beta3^2*A3*gl3,
1i*omega*d3*beta3*C3*gs3,2i*omega*d3*s*beta3^2*A3, 1i*omega*d3*beta3*C3;
        alpha3*s*gl3, -B3*gs3, alpha3*s, B3;
        -A3*gl3, -beta3*s*gs3, A3, -beta3*s];

    %[L]{x}=[R]{y}
    L =[M1b(1,1),M1b(1,2), -M2t(1,1), -M2t(1,2), -M2t(1,3), -M2t(1,4), 0,
0;
        M1b(2,1),M1b(2,2), -M2t(2,1), -M2t(2,2), -M2t(2,3), -M2t(2,4), 0,
0;
        M1b(3,1),M1b(3,2), -M2t(3,1), -M2t(3,2), -M2t(3,3), -M2t(3,4), 0,
0;
        M1b(4,1),M1b(4,2), -M2t(4,1), -M2t(4,2), -M2t(4,3), -M2t(4,4), 0,
0;
        0, 0, M2b(1,1), M2b(1,2), M2b(1,3), M2b(1,4), -M3t(1,3), -M3t(1,4);
        0, 0, M2b(2,1), M2b(2,2), M2b(2,3), M2b(2,4), -M3t(2,3), -M3t(2,4);
        0, 0, M2b(3,1), M2b(3,2), M2b(3,3), M2b(3,4), -M3t(3,3), -M3t(3,4);
        0, 0, M2b(4,1), M2b(4,2), M2b(4,3), M2b(4,4), -M3t(4,3), -
M3t(4,4)];

    R =[-M1b(1,3), -M1b(1,4), 0, 0, 0, 0, 0, 0;
        -M1b(2,3), -M1b(2,4), 0, 0, 0, 0, 0, 0;
        -M1b(3,3), -M1b(3,4), 0, 0, 0, 0, 0, 0;
        -M1b(4,3), -M1b(4,4), 0, 0, 0, 0, 0, 0;
        0, 0, 0, 0, 0, 0, M3t(1,1), M3t(1,2);
        0, 0, 0, 0, 0, 0, M3t(2,1), M3t(2,2);
        0, 0, 0, 0, 0, 0, M3t(3,1), M3t(3,2);
        0, 0, 0, 0, 0, 0, M3t(4,1), M3t(4,2)];

    y = [1; 0; 0; 0; 0; 0; 0; 0];

    Ry = R*y;

    x = L\Ry;

    Rrl(count)=x(1,1);
    Rrs(count)=x(2,1);
    Rtl(count)=x(7,1);
    Rts(count)=x(8,1);

    Rrlamp(count)=(real(Rrl(count))^2+imag(Rrl(count))^2)^0.5;
    Rrsamp(count)=(real(Rrs(count))^2+imag(Rrs(count))^2)^0.5;
    Rtlamp(count)=(real(Rtl(count))^2+imag(Rtl(count))^2)^0.5;
    Rtsamp(count)=(real(Rts(count))^2+imag(Rts(count))^2)^0.5;

    freq(count)=f;
    count=count+1;
end

    N = size(X,1);
M = size(X,2);

%Rrsamp2 = Rrsamp';
%Rrsamp3 = reshape(Rrsamp2,N,M);

Rrlamp2 = Rrlamp';
Rrlamp3 = reshape(Rrlamp2,N,M);


%2D
```

```
%%
%surf(X,Y, Rrlamp3)
angles = [0;19];
colors = {'b--';'k'; 'r'; 'b-.';'k-.';'r-.'; 'b--';'k--'};
for i = 1:length(angles)
    angleTemp=angles+1;


plot(X(angleTemp(i),:),Rrlamp3(angleTemp(i),:),colors{i},'linewidth',1.5)
    hold on

end

xlabel('Frequency(MHz)','fontsize',20)
ylabel('Reflection Coefficient','fontsize',20)
set(gca, 'fontsize',20)
%ylabel('angle')

%
z= 46.0*10^6;
B=1.5*10^9;

K = B/h;
w = 2*pi*fTemp*10^6;

R = 1./sqrt(1+(2.*K./(z.*w)).^2);
plot(fTemp,R, '-r','linewidth',1.5)

hold off

%legend([num2str(angles); 'f'], 'location', 'southeast')
legend(num2str(angles(1)), num2str(angles(2)), 'spring model' )
```